THE FATE OF TIN MOIETIES IN CHEMICAL REACTION

A THESIS

Submitted for the degree of
DOCTOR OF PHILOSOPHY
in the FACULTY of SCIENCE of
THE CITY UNIVERSITY, LONDON

by

SUSAN MARY GRIMES

Department of Chemistry
The City University
LONDON

August 1982

ABSTRACT

The fate of tin moieties in chemical reaction in both solution and solid state, is followed using thermal analysis, optical and electrical measurements, X-ray crystallography and ^{119}Sn Mössbauer spectroscopy to identify the nature of the tin species on reaction.

Thermal analysis is used to provide evidence for the formation of new compounds, to obtain information on the strength of the tin-ligand bonds, and to construct phase diagrams in some solid state systems. Optical and electrical measurements are used to detect the presence, if any of band to band transitions in some solid state materials prepared in this work. Optical reflectance and photoacoustic spectra of phases in the mixed halide $CsSnBr_3$: $CsSnCl_3$ and mixed metal $CsSnBr_3$: $CsPbBr_3$ systems are compared, and additional information is obtained from photoacoustic spectroscopy on the atomic and band transitions in some transition metal metastannates(IV) and hydroxostannates(IV) Optical electronic spectra are used to follow the formation of a formally tin(IV) species in the Pd : Sn : Cl : I system.

The X-ray crystal structures of five materials are determined viz. $K_3Sn_2(SO_4)_3Br$, $K_3Sn_2(SO_4)_3Cl$, $Sn_7Br_{10}S_2$, $Sn(acetate)_2.2tu$ and $Sn_2Br_4.5tu.2H_2O$. This technique is used to show details of the tin(II) environments in compounds which contain tin in unusual bonding situations.

Transmission Mössbauer spectroscopy is used to identify changes in the use of tin bonding electrons in chemical reactions, and to determine the extent of competition between ligands for the use of tin bonding electrons, and between tin and other metal ions for the use of the ligand bonding electrons. In addition, the validity of the assumption that a direct relationship exists between the Mössbauer data recorded at 80K and room temperature crystallographic data is tested. Results from the application of the surface sensitive ^{119}Sn conversion electron Mössbauer technique to various surface systems including glasses, fabrics and ceramics are reported.

In conclusion, the theories of bonding in tin(II) chemistry are reviewed and the concept of orbital matching to describe tin(II) in both high and low symmetry sites is discussed.

ACKNOWLEDGEMENTS

I would like to express my most sincere gratitude to Professor John Donaldson for his tremendous support and encouragement throughout my three years research. His keen interest and patient guidance have been invaluable and I am indebted to him, not only for introducing me to the broad and very interesting field of tin chemistry, but also, for enabling me to develop my ambition to do further research.

Deepest gratitude is due to my Parents, especially my dear Mother, who cheerfully typed this manuscript, and whose loving care and affection have been a constant joy. Special thanks must also be given to my sisters, Jean and Leonie, who, together with many close friends, have supported me throughout the whole of my research.

I would also like to thank the SERC and the International Tin Research Institute, for a CASE award studentship. Much appreciation and thanks are offered to [redacted], Director of the International Tin Research Institute, and to his colleagues, [redacted] and [redacted] for their many helpful discussions and continual interest.

I am grateful for the research facilities provided by the Departments of Chemistry, at Chelsea College, for the first year of my research and at The City University, for the remaining two years.

Finally, I offer my thanks to the Inorganic technical staff at the Chemistry Department of The City University, for their courtesy and co-operation.

THE FATE OF TIN MOIETIES IN CHEMICAL REACTION

CONTENTS

CHAPTER 1

INTRODUCTION

CHAPTER 1

INTRODUCTION

1.1. Introduction

Any study of the fate of tin moieties in chemical reaction must essentially be concerned with the ways in which the use of the valence shell electrons of the element changes as a result of the reaction and with the physical methods of studying such changes.

The purpose of this introductory chapter is, therefore, to give a brief account of the ways in which tin can use its electrons in bonding, and to describe those techniques used in this work to study any changes in the use of the valence shell electrons of tin on reaction.

This introductory chapter is then followed by four chapters describing work carried out on studies of the fate of tin moieties in chemical reaction. Chapter 2 describes the results of a series of investigations on the changes in the use of tin bonding electrons resulting from chemical reaction, while any changes resulting from solid state effects are discussed in Chapter 3. The use of Mössbauer spectroscopy as an element - specific technique for studying the ways in which tin uses its electrons in bulk and surface interactions is detailed in Chapter 4. The purpose of the final chapter is threefold in that it deals with conclusions drawn from the present work, with a survey of the models used to describe the stereochemical activity of the lone pair in tin(II) chemistry and with a new model which fully describes the bonding of tin(II) in its various compounds and which accounts for all of the structural and

physical properties of these compounds.

1.2 Bonding in Tin Compounds

In the chemistry of tin, a distinction is made between the formal oxidation state of the element in compounds, to describe differences in the usage of the bonding electrons of the element. The outer electronic configuration of tin, $5s^2\ 5p^2$, permits the formation of both tin(IV) and tin (II) compounds. For tin(IV) the formal oxidation state represents the loss or use of all the valence shell electrons in bonding, whereas the tin(II) oxidation state describes situations in which, in formal terms, only the outer p-electrons are being lost or used in bond formation.

1.2.1 Tin(IV) Compounds

The element in its (IV)+ oxidation state can form derivatives in three ways:

(i) By loss of all four valence electrons to form the stannic ion Sn^{4+}.

(ii) By hybridization of the available orbitals in a suitable environment to form four covalent bonds.

(iii) By complex formation, i.e. making use of the empty 5d orbitals which are of similar energy to the 5s and 5p orbitals.

These extreme views of the bonding in tin(IV) materials would suggest a spherical ion for ionic bonding, tetrahedral coordination of the tin atom in covalent bonding and octahedral coordination in most complex ions and adducts. The bonding in tin(IV) compounds is summarized in Table 1.1.

The Bonding in Tin(IV) Compounds

Bond Type	Electronic Configuration	Shape of Ion or Hybrid	Typical Ions or Compounds
	5s 5p 5d		
Tin atom (Ground state)	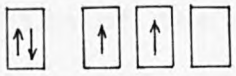	—	—
Stannic Ion	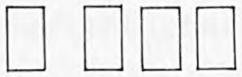	Spherical (radius 0.74Å)	SnO_2 ; $BaSnO_3$.
Covalent	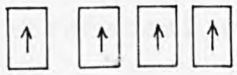 sp^3 hybrid	Tetrahedral	$SnBr_4$: most organotin (IV) compounds
Complex [Tin(IV)]	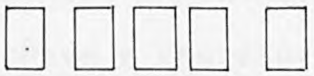 sp^3d hybrid	Trigonal bipyramidal	$(CH_3)_3SnCl$-py.
	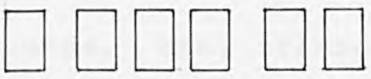 sp^3d^2 hybrid	Octahedral	SnF_6^{2-} ; many complexes of tin(IV) halides with monodentate donors

Table 1.1

The Sn^{4+} ion (radius $\sim$ 0.74Å) may be regarded as present in the lattices of compounds like tin(IV) oxide[1,2] which has a rutile-type structure, and in various stannates e.g. $BaSnO_3$[3,4]. The strong electronegativity of the oxygen suggests the presence of predominantly ionic bonding, although appreciable covalent character in the metal-oxygen bonds has also been reported[5]. The $5s^0p^0$ configuration of the Sn^{4+} ion should give regular octahedral coordination for tin in ionic lattices, although there are tendencies towards distortion from octahedral to tetrahedral environments due possibly to partial covalent character of the bonding in the lattice.

Hybridization of the available 5s and 5p orbitals of tin produces a suitable situation for the formation of four tetrahedral covalent bonds. The structure and bonding in such compounds as the tin halides and most organotin(IV) compounds[6] can be explained in these terms. The literature of organometallic tin chemistry is now one of the largest for any element, but is however well documented and reviewed[6-9]. Many organotin(IV) compounds have a coordination number 4, giving a tetrahedral arrangement of ligands about the tin.

X-ray crystallography has established [10-12] that the tendency for tin to adopt a stereochemistry of higher coordination numbers is very marked among organotin (IV) compounds. Many triorganotins, R_3SnX, diorganotins, R_2SnX_2, and monoorganotins $RSnX_3$ (R = carbon bonded organic group ; X = inorganic substituent) which were previously thought to be simple tetrahedral molecules, have been

found to achieve these more complex structures in the solid state, and sometimes in solution, by intramolecular or intermolecular association. Although the compounds, Me_3SnOH, Me_2SnF_2, and $MeSn(NO_3)_3$ (Figure 1.1) might be expected to have tetrahedral structures, they do in fact have trigonal bipyramidal, octahedral and pentagonal bipyramidal coordination respectively[13]. Such environments in the solid state arise as a result of bridging ligand groups namely, the hydroxyl groups in Me_3SnOH, the fluoride groups in Me_2SnF_2 and the nitrate groups in $MeSn(NO_3)_3$.

Finally tin(IV) compounds make extensive use of the tin 5d orbitals. Thus, for example, in complexes such as $(CH_3)_3SnCl.py$[14], (py = pyridine), the five coordinate tin atom is sp^3d hybridized in a trigonal bipyramidal environment. Similarly in octahedral molecules or ions such as $SnCl_4.2py$[15] and SnF_6^{2-} in the mixed oxidation compound Sn_3F_8[16,17], the 5d orbitals of similar energy to the 5s and 5p orbitals are utilized to form sp^3d^2 hybrid orbitals for largely covalent bonds.

1.2.2 Tin(II) Compounds

In a review of the bonding in tin(II) materials, Donaldson[18] discussed four possible methods of bond formation:

(i) Loss of two p-electrons to form Sn^{2+} ions.

(ii) Use of these electrons to form covalent bonds.

(iii) Complex formation using the empty 5p and possibly 5d orbitals to form hybrid acceptor orbitals.

(iv) Combination with an acceptor species using the lone pair electrons.

Coordination number 4 - tetrahedral

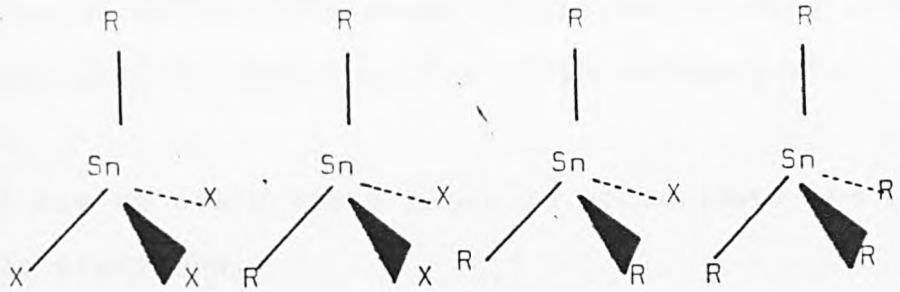

Coordination number 5 - trigonal bipyramidal

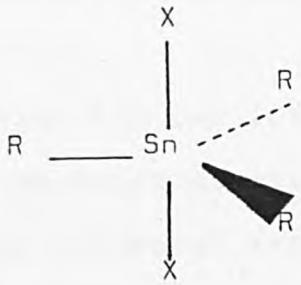

e.g. Me_3SnOH

Coordination number 6 - octahedral

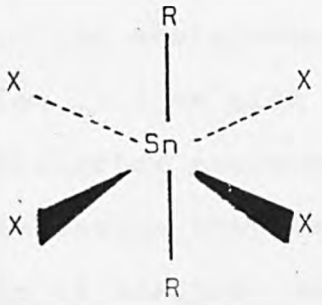

e.g. Me_2SnF_2

Coordination number 7 - pentagonal bipyramidal

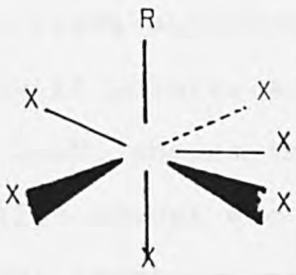

e.g. $MeSn(NO_3)_3$

Figure 1.1 Stereochemistries of Organotin(IV) Compounds

In view of the recent work[19] these four categories should now be extended to cover the effects of direct population of solid state bands by the non-bonding lone pair electrons, by addition of a fifth category of bonding:

(v) Use of solid state bands to accommodate the $5s^2$ lone pair electrons.

These five aspects of bonding will now be discussed in more detail to provide examples of the ways in which tin in its lower oxidation state can use its electrons in bonding.

The ease with which tin can lose its two p-electrons to leave an ion with an outer electronic configuration of $5s^2$ is shown by the values of its first and second ionization potentials (7.63eV and 14.63eV respectively). The $5s^2$ configuration consists of a non-bonding pair of electrons beyond a completed shell and this has a considerable effect on the stereochemistry of compounds containing the Sn^{2+} ion . Ions with this configuration are often found in distorted environments in solid state compounds and for this reason they can be regarded as non-spherical with a bulge of electron density arising from the presence of the non-bonding electron pairs. The distortion would then be due to the bulge of electron density preventing the close approach of ligands along the directions in which it points. A crystal structure determination [20] of $SnSO_4$ showed that in spite of similar X-ray diffraction powder and unit cell data, $BaSO_4$ and $SnSO_4$ were not isostructural. The tin(II)

sulphate structure can be regarded as a badly distorted barite lattice with twelve Sn-O distances of between 2.25Å and 3.34Å , but three of the oxygen atoms are in fact much closer to tin than the others giving a trigonal pyramidal environment of nearest neighbour oxygen atoms. The oxygen atoms in directions opposite to the three short bonds cannot approach the Sn^{2+} ion any closer because of the bulge of electron density on the ion.

The use of the two p-electrons in covalent bond formation, involving essentially sp^2 hybridization is most likely to be of importance in the vapour state. The existence of angular structures of the tin(II) halides in the vapour state support this assumption.

Compounds formed by sp^2 hybridization have empty p-orbitals. A tin(II) compound with appreciable covalent character will therefore act as a monofunctional acceptor to give either an adduct or a complex ion based on sp^3 hybridization. Higher coordination could be attained using the d-orbitals, but of the available orbitals, this is less likely because of the large 5s-5d energy difference.

Tin(II) chloride dihydrate[21,22] provides a good example of adduct formation based on sp^3 hybridization. Crystal structure determinations on $SnCl_2.2H_2O$ have shown that only one water molecule is directly bonded to the tin, using the empty p-orbital. In this compound the tin(II) moiety acts as an acceptor towards one ligand water molecule. The second molecule is not bonded to the tin to give a higher coordination, but forms hydrogen bonds with the water molecule already bonded to the tin,

giving a two dimensional network of hydrogen bonds. The structure consists of double layers of the aquo complex $Cl_2Sn(OH)_2$ parallel to (100) with intervening layers of the second water molecule.

The stable predominant species in solution of monodentate anionic ligands are the triligand-stannate (II) species. Most complex tin(II) chlorides, for example, contain discrete pyramidal $SnCl_3^-$ units e.g. in the monoclinic form of $CsSnCl_3$ (23).

Tin, in its efforts to form bonds to ligands is usually found in a distorted environment. The most common tin(II) environment is shown to consist of a trigonal pyramidal arrangement (Figure 1.2a) of three nearest neighbour tin-ligand bonds with three longer essentially non-bonding contacts completing a distorted octahedral coordination about the tin. These longer contacts arise because close approach of the ligands to the tin is prevented by the lone pair orbitals. The main structural feature found in all distorted four coordinate environments is the existence of two long bonds of considerably greater length than those normally found in tin(II) compounds (Figure 1.2b).

In its (II)+ oxidation state, tin not only has the ability to act as an acceptor but also as a donor species. In its role as an acceptor the empty p-orbitals are used whilst as a donor the non-bonding lone pair electrons are used. The lone pair orbital in acting as a donor towards a powerful acceptor species such as a metal, uses all four electrons in bonding, causing the tin to

Trigonal Pyramidal Tin(II) Coordination

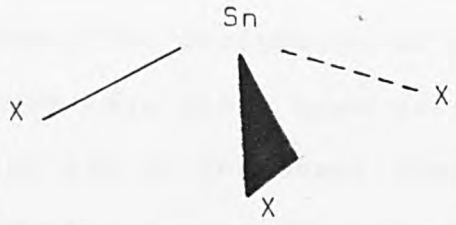

Figure 1.2a

Square Pyramidal Tin(II) Coordination

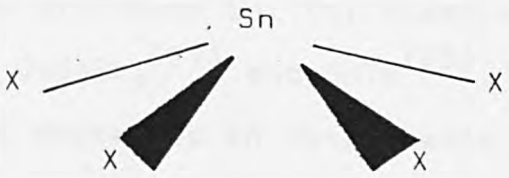

Figure 1.2b

become formally in the (IV)+ oxidation state. This feature of tin(II) bonding is apparent in those Sn-metal complexes with Pt-metal acceptors[24] or Pd-metal acceptors[25,26].

The four methods described have for some time provided the basis for discussion of bonding in tin(II) compounds. These have since been extended to account for the way in which tin in the small number of regular undistorted structures uses its valence shell electrons. In those structures in which no distortion occurs the tin atom is in a high symmetry environment, lying at the centre of an octahedron. Such an environment for tin arises because the distorting effect of the non-bonding electrons is reduced by populating an empty low energy solid state band, thus giving rise to optical colouration and electrical conductivity. Regular octahedral environments for tin are found in, for example, the perovskite structure of $CsSnBr_3$[27] and SnTe[28].

The work described in this thesis deals with most aspects of the bonding of tin(II) but does highlight the difficulty associated with the existing models for bonding in tin(II) compounds. The distorting effects of the non-bonding electrons as lone pairs which have such an influence on the chemistry, structure and reactivity of tin(II) compounds is a well known feature of a main group element in its lower oxidation state. A number of theoretical approaches have been used to explain these effects, but no single approach has successfully explained all aspects of the bonding in these compounds. In certain

ways the currently available theories provide a very convenient pictorial representation of the lone pair distorted environment of tin in its (II)+ oxidation state compounds but fall far short of providing an adequate description of the details of the use of the tin valence electrons in bonding in the solid state. This problem is discussed in greater detail in Chapter 5.

1.3 Techniques

The following techniques were used in this work to study changes in the use of tin electrons in bonding on reaction.

1.3.1 Thermal Analysis

1.3.2 Mössbauer Spectroscopy

1.3.3 X-ray Diffraction

1.3.4 Solid State Measurements

The basis and general background theories applicable to those techniques are described in this introductory chapter.

1.3.1 Thermal Analysis

The term thermal analysis is used to describe those techniques in which some physical parameter of a system under study is determined as a function of temperature and in which the physical parameter is recorded as a dynamic function of temperature. The principal techniques of thermal analysis are dynamic thermogravimetry (TG), differential thermal analysis (DTA) and differential scanning calorimetry (DSC). Two of these techniques (TG and DTA) were used in the present work and are

described in detail in this introduction.

Differential thermal analysis (DTA) is a technique which involves the heating or cooling of a test sample and an inert reference sample under identical conditions and the recording of any temperature difference which develops between them. This differential temperature is then plotted either against time, or against temperature at some fixed point within the apparatus. Any physical or chemical changes occurring to the test sample which involves the evolution of heat will cause its temperature to rise temporarily above that of the reference sample. This exothermic reaction is recorded as a peak on the DTA plot. Conversely, a process which is accompanied by the absorption of heat will cause the temperature of the test sample to lag behind that of the reference material, giving rise to an endothermic process which is also characterised as a peak on the DTA plot (Figure 1.3).

However, even under conditions where no physical or chemical process is occurring a small and steady differential temperature normally develops between the test and reference materials. With care being taken to avoid errors due to sample mass and packing density, the differential temperature will be due to differences in the heat capacities and thermal conductivities of the two materials. It therefore follows that DTA can be used to study transitions in which no heat is evolved or absorbed by the sample, as is the case in certain

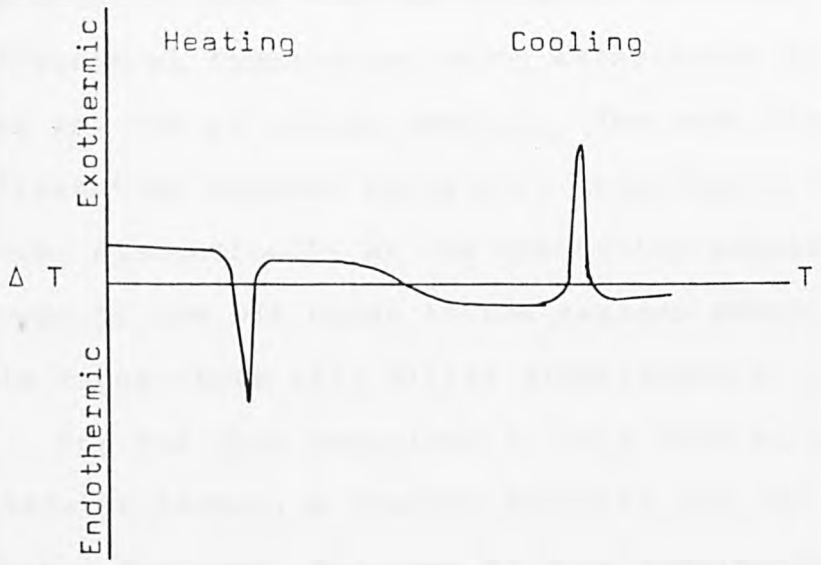

Figure 1.3 Typical curves of melting and resolidification processes.

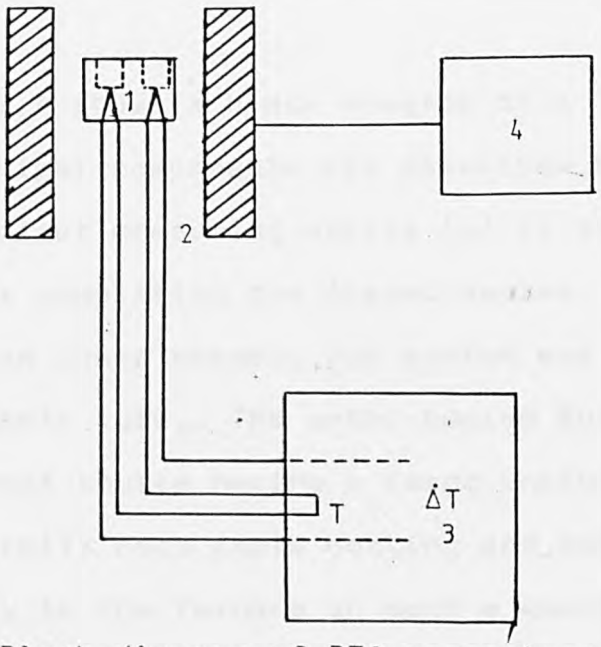

Figure 1.4 Block diagram of DTA apparatus:
1. Sample holder-measuring system: 2. Furnace:
3. Temperature programmer: 4. Recorder.

solid-solid phase changes. The difference in the heat capacity of the sample before and after the transition has occurred will then be reflected in a new steady differential temperature being established between the test and the reference samples. The base line of the differential thermal curve will accordingly show a sudden discontinuity at the transition temperature, the slopes of the DTA curve in the regions above and below this temperature will differ significantly.

For the work described in this thesis, unless otherwise stated, a Stanton Redcroft STA 780 simultaneous Thermal Analyser, designed to give simultaneous TG records (i.e.weight versus time or temperature) and DTA curves (i.e.ΔT-t curves,where ΔT is the temperature difference between the sample and an inert reference material) was used. This simultaneous unit eliminates problems of correlating TG and DTA data for the same substance.

Figure 1.4 shows a block diagram of a DTA apparatus and its principal components are described briefly here. The sample holder measuring system (a) is the heart of the apparatus comprising the thermocouples, sample containers, an inner ceramic cup system and an outer hangdown ceramic tube. The water cooled furnace (b) provides a heat source having a large uniform temperature zone, and permits both rapid heating and cooling. To supply energy to the furnace in such a manner as to ensure a reproducible rate of change of temperature, a temperature programmer (c) is attached. A Linseis

four-pen chart recorder (d) is the recording system used which provides the simultaneous temperature, TG, DTA and derivative thermogravimetric (DTG) traces.

A brief description is now given on the interpretation and presentation of the data using such an instrument. Part of a simple and idealized DTA curve is shown in Figure 1.5. On raising the temperature of the furnace a small but steady temperature difference develops between the test and reference materials. The DTA curve continues in an approximately rectilinear manner, until the test material undergoes some physical or chemical change (AB). At B, the curve begins to deviate from the base line due to an exothermic process occurring within the test sample. This point B represents the onset temperature of the reaction, or phase transition. The exothermic peak temperature C, corresponds to the maximum rate of heat evolution detected by the differential thermocouples. The exothermic process giving rise to peak BCD becomes complete at some temperature between points C and D. No furtner evolution of heat is detectable above D, so the curve returns to a new baseline DE.

The onset of an endothermic process is indicated by the downwards deflection of the baseline at E, giving rise to an endothermic peak EFG. Completion of this process and the formation of a new thermally stable phase, is confirmed by the horizontal portion of the curve GH. Figure 1.6 shows examples of DTA traces

Figure. 1.5 A hypothetical DTA trace showing an exothermic peak, an endothermic peak and the change in off-set temperature of the baseline resulting from these processes.

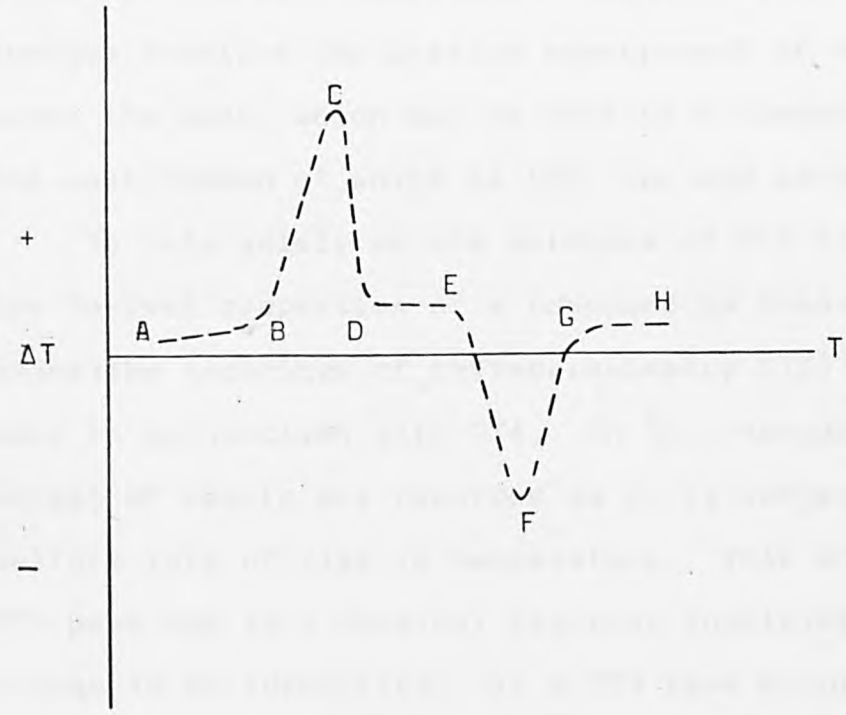

obtained from materials studied in this work which will be discussed in later chapters. Seldom is the DTA peak as sharp as that observed for the melting point of SnF_2 or the phase transition in $CsSnCl_3$ discussed later in this work, there is a tendency for overlapping peaks which makes interpretation difficult. The area under a DTA peak is proportional to the total enthalpy change giving rise to that peak, whilst the area under a melting endotherm is proportional to the latent heat of fusion of the test substance. Determination of such changes involves the precise measurement of the area under the peak, which may be done by a number of methods, the most common of which is the 'cut and weigh' method.

To rely solely on the evidence of DTA to elucidate the thermal properties of a compound is inadvisable, hence the technique of thermogravimetry (TG) is commonly used in conjunction with DTA. In TG, changes in the weight of sample are recorded as it is subjected to a uniform rate of rise in temperature. This enables any DTA peak due to a chemical reaction involving a weight change to be identified. If a DTA peak occurs at a temperature where TG shows that the sample weight remains constant, it follows that either a chemical reaction, or a phase transition, must have occurred.

The thermal analysis technique of thermogravimetry is one in which the change in sample mass is recorded as a function of temperature. Three modes of TG may be described:

(i) Isothermal or static thermogravimetry, in which the sample mass is recorded as a function of time at constant temperature.

(ii) Quasistatic thermogravimetry, in which the sample is heated to constant mass at each of a series of increasing temperatures.

(iii) Dynamic thermogravimetry in which the sample is heated in an environment whose temperature is changing in a predetermined manner, preferably at a linear rate.

All of the studies carried out in this work make use of the dynamic TG mode.

The mass-change versus temperature curves produced in TG provide information on the thermal stability and composition of the initial sample, and of any intermediate compound that may be formed and on the composition of any residue. To yield useful information the sample must therefore evolve a volatile product, which can originate by various physical and chemical processes. Much of the information obtained from the TG curve, except for mass-change, is of an empirical nature in that the transition temperatures are dependent on the instrumental and sample parameters.

The characteristics of a single stage mass-loss curve are illustrated in Figure 1.6a. Two temperatures may be selected as characteristic of any single-stage monoisothermal reaction: T_i, the initial temperature or procedural decomposition temperature (pdt), which is the temperature at which the cumulative mass-change reaches

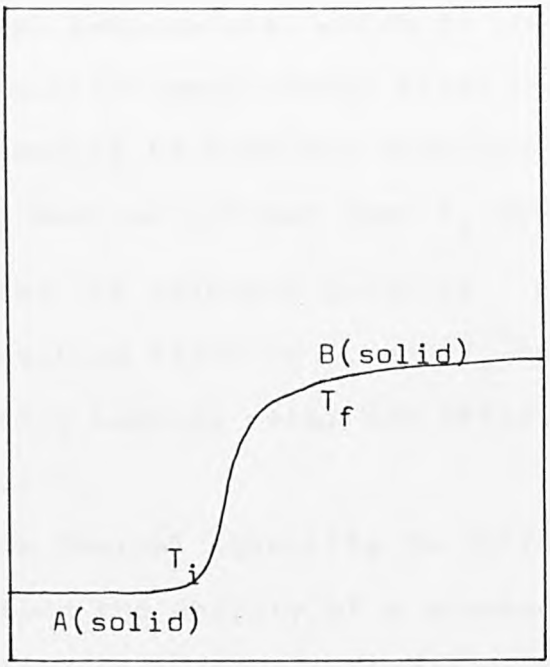

Temp
A(solid)⟶B(solid) + C(gas)

(a)

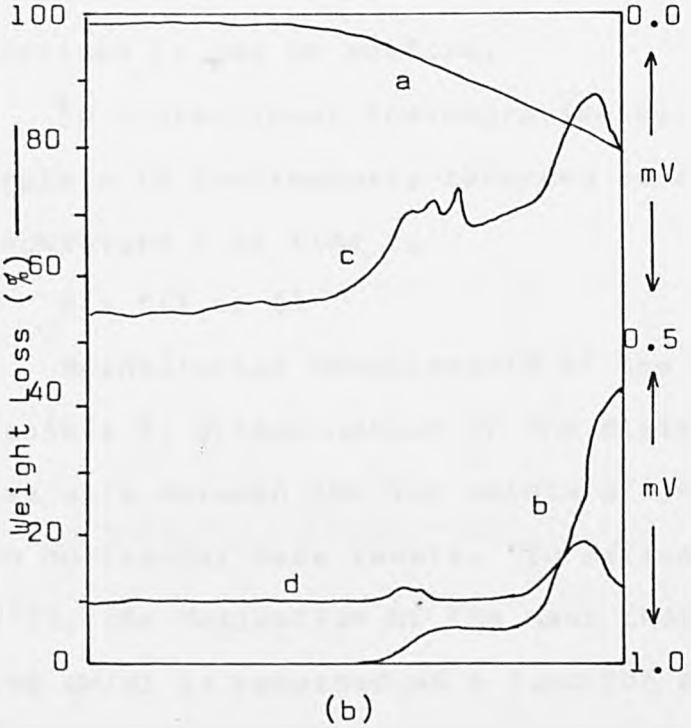

(b)

Figure 1.6 (a) Characteristics of a single stage reaction TG curve

(b) Water Loss from $Sn_2Cl_4.5tu.2H_2O$

a magnitude that the thermobalance can detect; and T_f, the final temperature, which is the temperature at which the cumulative mass-change first reaches its maximum value corresponding to complete reaction. At a linear heating rate T_f must be greater than T_i and the difference $T_f - T_i$ is called the reaction interval. For an endothermic decomposition reaction T_i and T_f both increase with increasing heating rate, the effect being greater for T_f than for T_i.

The thermal stability is defined as a general term indicating the ability of a substance to maintain constant properties on heating. From a practical point of view thermal stability needs to be considered in terms of the environment to be imposed on the material and the functions it has to perform.

In conventional thermogravimetry, the mass of a sample m is continuously recorded as a function of temperature T or time t.

$$m = f(T \text{ or } t)$$

Quantitative measurements of the mass changes are possible by determination of the distance on the curve mass axis between the two points of interest or between two horizontal mass levels. In derivative thermogravimetry (DTG), the derivative of the mass change with respect to time dm/dt is recorded as a function of temperature or time.

$$\frac{dm}{dt} = f(T \text{ or } t)$$

The curve obtained is the first derivative of the mass-change curve. A series of peaks are now obtained, instead of a step-wise weight loss curve. The areas under the DTG peaks are proportional to the total mass-change of the sample. The DTG curve, whether derived mathematically or recorded directly contains no more information than does the integral TG curve obtained under the same experimental conditions, it simply displays it differently.

The advantages of the DTG have been summarized by Erdey et al[29].

(i) The curves may be obtained in conjunction with TG and DTA measurements.

(ii) The curves for DTA and DTG are comparable but the results of the former method indicate even those changes of state that are not accompanied by loss in mass. The curves by the latter method are more reproducible.

(iii) While the curves for DTA extend over a wider temperature interval due to subsequent warming of the material after reaction, the DTG measurements indicate exactly the temperatures of the beginning, the maximum rate and the end of the change.

(iv) In TG, when changes which follow each other very closely cannot be distinguished because of overlapping weight loss curves, the DTG curves of the same changes are usually indicated by sharp maxima so that the TG curves can then be divided into stages.

(v) The DTG curves are exactly proportional to the derivatives of the TG curves, therefore, the area under the curves give the change in mass precisely. Accordingly DTG can give the exact quantitative analyses.

(vi) The DTG method can be used for the investigation of materials which for some reason or another cannot be analysed by DTA.

Applications of TG and DTA Techniques

The applications of TG to a particular problem is possible if a mass-change is observed on the application of heat. Some of the applications of TG are summarized in Table 1.2.

The TG technique provides a means, not only of determining weight loss (Figure 1.6b) but also as a method of identifying the similarity of materials, an example of which is found in Chapter 2 in confirming the products of the phases from the $SnCl_2$: glycylglycine system were identical. Figure 1.6b shows the initial loss of water from $Sn_2Cl_4.5tu.2H_2O$, (tu=thiourea), with a second stage weight loss occurring at≈163°. Further details of the decomposition of this complex are given in Chapter 2.

The manner in which a tin(II) compound decomposes thermally affords a useful indication of the donor strength of the anionic species towards tin. Some tin(II) compounds with strong donor species melt without decomposition, although disproportionation to tin metal and a tin(IV) material may occur at higher temperatures. The tin(II) halides which melt without decomposition at

Table used to convert (mV) to (^{o}C) on a 0-1.0mV scale

for interpretation of temp. data of thermal work in Chapters 2&3.

Taken from (BS 4937:Pt 2:1973) REFERENCE JUNCTION AT 0°C (Correct to nearest whole number)

MILLI VOLTS	0,00	0,10	0,20	0,30	0,40	0,50	0,60	0,70	0,80	0,90	01	02	03	04	05	06	07	08	09
0,00	0	18	35								2	4	5	7	9	10	12	14	15
				51	66						1	3	4	6	7	9	10	12	13
						80	94	107	120	133	1	3	4	6	7	9	10	11	12
1,00	145	157	169	181	192	204	215	226	237	248	1	2	3	5	6	7	8	9	10
2,00	258	269	279	290	300	310	320	331	341	350	1	2	3	4	5	6	7	8	9
3,00	360	370	380	390	399	409	419	428	438	447	1	2	3	4	5	6	7	8	9
4,00	456	466	475	484	494	503	512	521	530	539	1	2	3	4	5	6	6	7	8
5,00	548	557	566	575	584	593	602	610	619	628	1	2	3	4	4	5	6	7	8
6,00	637	645	654	662	671	680	688	697	705	713	1	2	3	3	4	5	6	7	8
7,00	722	730	739	747	755	763	772	780	788	796	1	2	2	3	4	5	6	7	7
8,00	804	812	820	828	836	844	852	860	868	876		2	2	3	4	5	6	6	7
9,00	884	892	900	908	915	923	931	939	946	954	1	2	2	3	4	5	5	6	7
10,00	962	969	977	985	992	1000	1007	1015	1022	1030	1	2	2	3	4	5	5	6	7
11,00	1037	1045	1052	1060	1067	1075	1082	1089	1096	1104	1	1	2	3	4	4	5	6	7
12,00	1111	1119	1126	1133	1140	1148	1155	1162	1169	1177	1	1	2	3	4	4	5	6	7
13,00	1184	1191	1198	1206	1213	1220	1227	1234	1241	1248	1	1	2	3	4	4	5	6	6
14,00	1256	1263	1270	1277	1284	1291	1298	1305	1313	1320	1	1	2	3	4	4	5	6	6
15,00	1327	1334	1341	1348	1355	1362	1369	1376	1383	1391	1	1	2	3	4	4	5	6	6
16,00	1398	1405	1412	1419	1426	1433	1440	1447	1454	1461	1	1	2	3	4	4	5	6	6
17,00	1468	1476	1483	1490	1497	1504	1511	1518	1525	1532	1	1	2	3	4	4	5	6	6
18,00	1540	1547	1554	1561	1568	1575	1583	1590	1597	1604	1	1	2	3	4	4	5	6	6
19,00	1611	1619	1626	1633	1640	1648	1655	1662	1670	1677	1	1	2	3	4	4	5	6	7

Symbols used in this work to denote thermal effects:
(a)Temperature trace; (b) TG trace; (c)DTA trace; (d)DTG trace.

Table 1.2

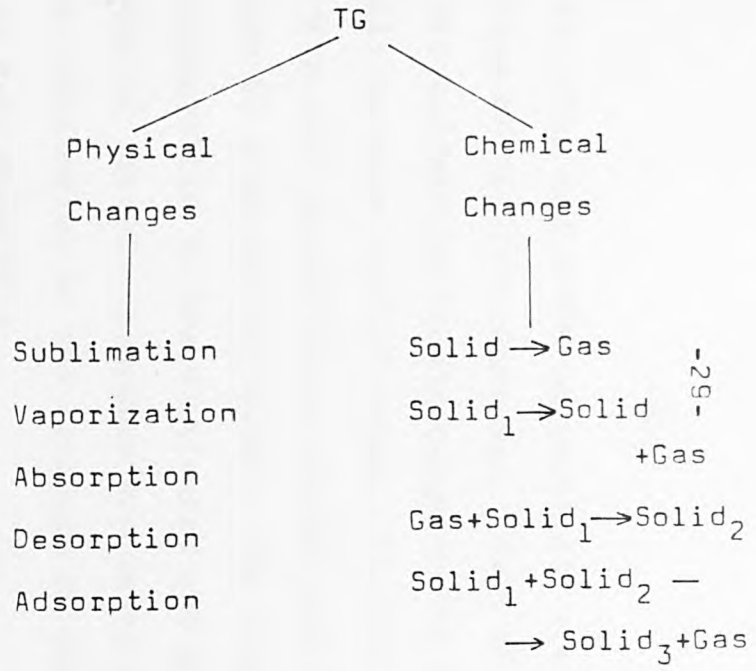

219, 247, 226, and 320°C respectively are examples of this class of tin(II) compounds. Many of those tin(II) materials containing strong oxygen-donor species decompose thermally to give tin(II) oxide. Tin(II) materials containing weak oxygen-donor species and oxidizing anions decompose to give tin(IV) oxide. The stages involved in the decomposition of those thiourea and glycylglycine complexes of tin(II) compounds discussed in Chapter 2, provide information on the strength of the tin-ligand bonds in such materials.

The applications of DTA in this work, largely fall into one of two categories, which will now be discussed under the following headings:- (a) Phase transitions and (b) Phase diagrams.

(a) Phase Transitions: The determination of melting and boiling points has traditionally been used as a method of identification of organic compounds. DTA has the advantage that in the case of melting points, both the temperature and the latent heat of fusion can be determined in a single experiment. The conventional methods of melting point rely on observation of the sample, and the recorded melting point therefore depends to a certain extent on the judgement of the operator. It is well known that impurities in the sample alters the melting point, so melting occurs over a wider range of temperature. DTA can be used to measure both the melting point and mole fraction of impurity present.

Phase transitions observed for materials in the present study are of three types, a solid-liquid, a liquid-

vapour, and a solid-solid transition. A solid-liquid transition arises when the sample is either melting or freezing. The melting and resolidification of tin(II) fluoride is studied in more detail in Chapter 3, but in Figure 1.6c, it provides a good example of such a transition. Examples of liquid vapour transitions i.e. boiling points, in this work, are few, although in the study of the thermal properties of some organotin(IV) halide adducts of glycylglycine discussed in Chapter 2, the parent compound $BuSnCl_3$ was shown to have a boiling point at about 94°C. Its boiling endotherm is shown in Figure 1.6d, the change in baseline is due to evaporation of the sample. Finally, there are solid-solid transitions which may result from one of two transitions either involving a change in crystal structure, which is accompanied by evolution or absorption of heat, or involving the conversion of one phase to another each of which has different heat capacity. An example taken from this work of a solid-solid transition of the former type is shown in Figure 1.6e, where $CsSnCl_3$ undergoes a transition at about 90°C.

(b) Phase Diagrams: DTA is a widely used technique for the determination of phase transitions in multicomponent systems and in the construction of phase diagrams. Before investigating the reaction between two solids, it is first necessary to determine how the individual materials behave on heating. This is because DTA of the reaction mixture will initially produce a curve showing a combination of all exothermic and endothermic effects

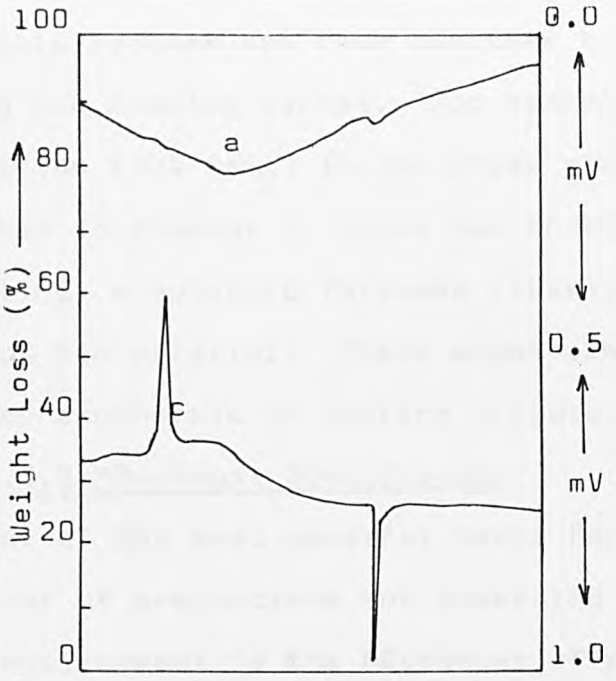

(c)

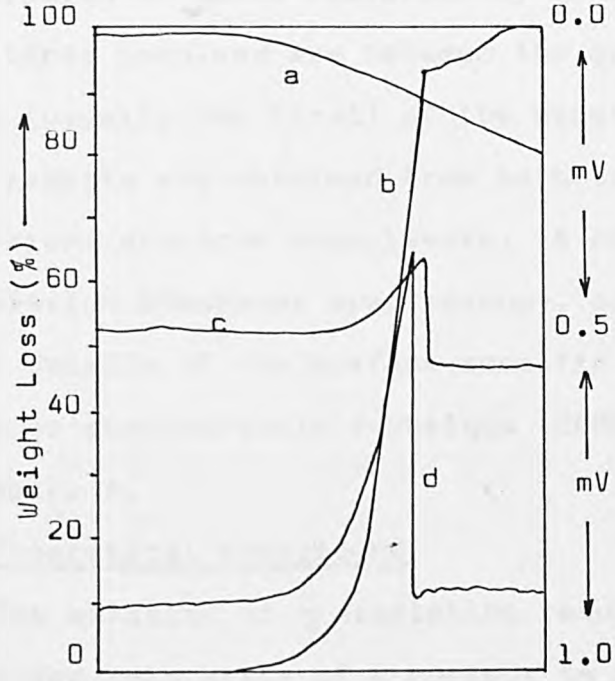

(d)

Figure 1.6 (c) Melting point and resolidification of SnF_2

(d) Boiling endotherm of $BuSnCl_3$

resulting from each of the materials present. In studying solids obtained from molten systems, in this work, this problem has been overcome by carrying out heating and cooling cycles. For example, a material of composition (70% SnF_2) in the phase study CsBr: SnF_2 described in Chapter 3, shows two endothermic peaks on heating, a eutectic followed closely by the melting point of the material. These endothermic peaks become as expected exothermic on cooling (Figure 1.6f).

1.3.2 Mössbauer Spectroscopy

One of the most powerful tools for investigating the behaviour of s-electrons and observing the symmetry of their environment is the Mössbauer effect. The Mössbauer effect[30] is the recoiless emission and resonant reabsorption of gamma radiation by an atomic nucleus. The transitions involved are between the ground and excited states (usually the first) of the atomic nucleus. In this study results are obtained from both transmission and conversion- electron experiments. A discussion of transmission Mössbauer spectroscopy, only, is given here, whilst details of the surface-specific conversion electron Mössbauer spectroscopic technique (CEMS) will be presented in Chapter 4.

Theoretical background

The emission of γ-radiation results from the decay of an excited spin state of a nucleus to the ground state. In a solid the recoil of the emitting nucleus is taken up by the whole crystalline lattice and the γ-ray quantum may be resonantly reabsorbed by another, identical nucleus. Thus,

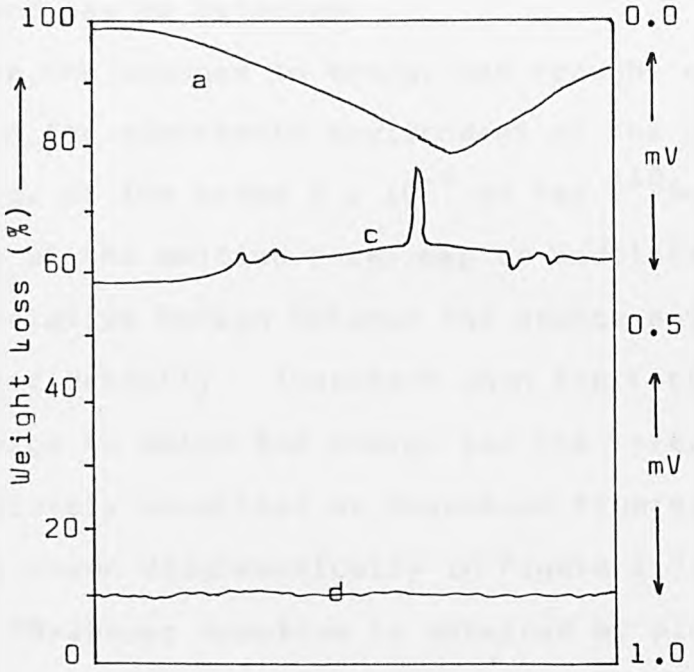

(e)

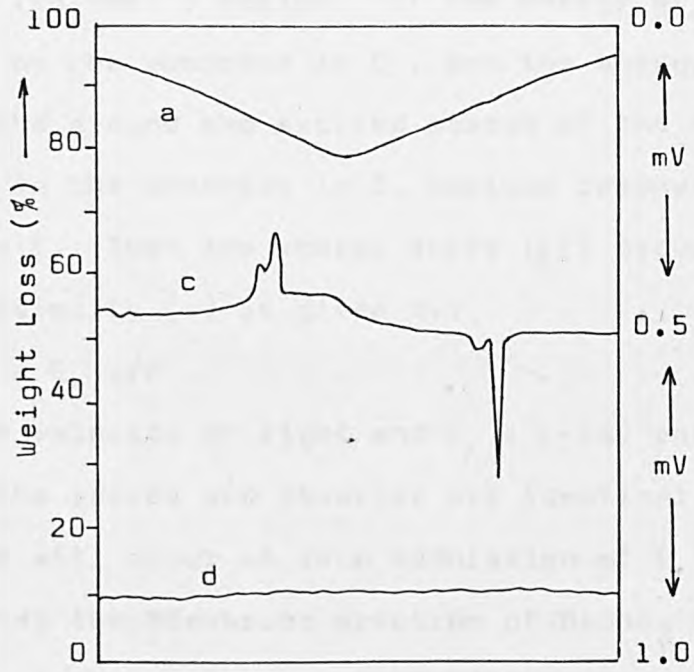

(f)

Figure 1.6 (e) Phase transition of $CsSnCl_3$

(f) Phase: 70%SnF_2:30%CsBr

if the difference in energy between the ground and excited states of the absorber nucleus is the same as that of the emitter the γ-ray will be absorbed, if not, it will pass through and may be detected.

Since the changes in energy gap brought about by changes in the electronic environment of the nucleus are small (e.g. of the order 5×10^{-8} eV for ^{119}Sn), the frequency of the emitted γ-rays may be modulated by supplying a small relative motion between the source and absorber - the Doppler Velocity. Therefore when the γ-ray has the exact energy to match the energy gap the γ-ray is absorbed and immediately re-mitted as resonance fluorescence. This effect is shown diagramatically in Figure 1.7.

The Mössbauer spectrum is obtained by plotting the % transmission (number of counts) of the γ-rays transmitted by the sample at each instant as the relative Doppler velocity (in mms^{-1}) varies. If the energy of the γ-rays incident on the absorber is E_γ, and the energy separation between the ground and excited states of the nuclei embedded in the absorber is E, maximum resonance will occur when $E_\gamma = E$. Then the energy shift (ΔE) produced by the Doppler Velocity (v) is given by:

$$-\Delta E = E_\gamma \, v/c$$

where c = velocity of light and E_γ = γ-ray energy.

If the source and absorber are identical maximum resonance will occur at zero modulation of E_γ. Figure 1.8 illustrates the Mössbauer spectrum of $BaSnO_3$ using a $Ba^{119}SnO_3$ source. The spectral line possesses a finite

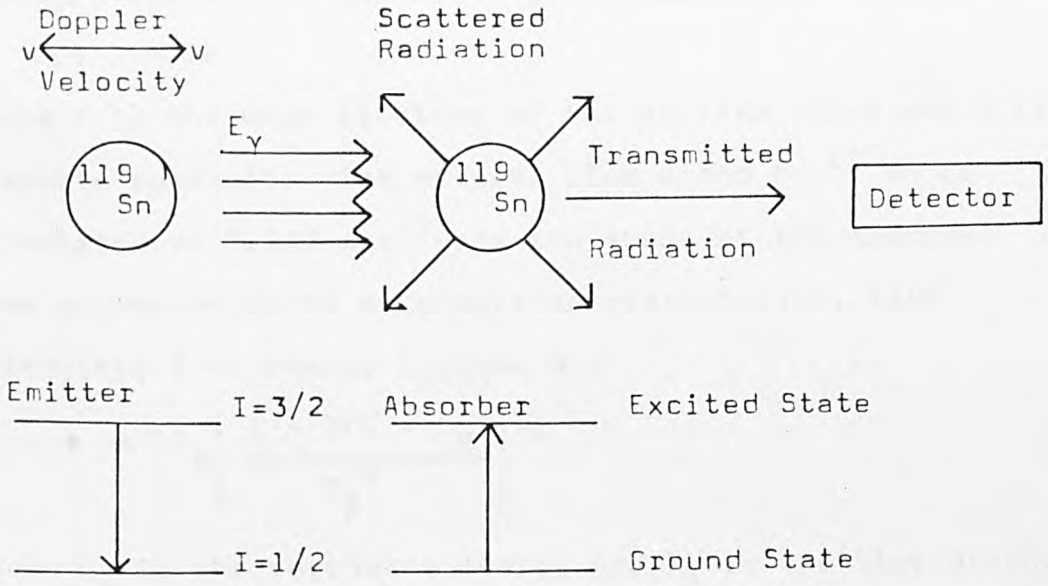

Figure 1.7 Fundamental features of the Mössbauer Effect.

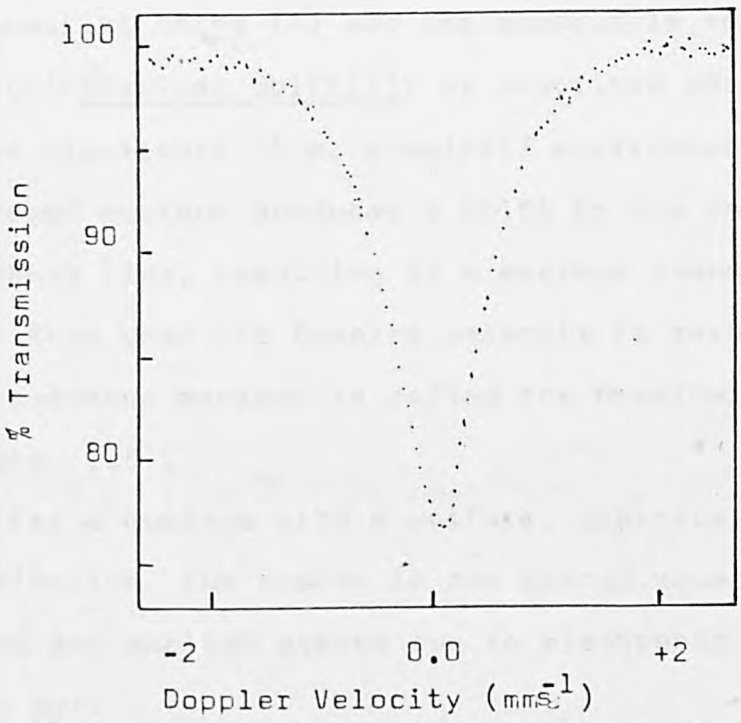

Figure 1.8 Mössbauer spectrum of $BaSnO_3$ using a $Ba\ ^{119}Sn\ O_3$ source.

width, Γ, due to the Heissenberg Uncertainty Principle:

$$\Gamma\tau = h/2\pi$$

where τ is the mean lifetime of the excited state and h is Planck's constant. The natural line width of ^{119}Sn is calculated as 0.646 mms^{-1} and the shape of the spectral line approximates to a Lorentzian distribution, with intensity, I at energy E given by:

$$I = E_R\left[\frac{1 + 2(E - E_R)}{\Gamma_{\frac{1}{2}}^2}\right]^{-1}$$

where E_R is the resonance energy and $\Gamma_{\frac{1}{2}}$ is the line width at half height.

Measurable Parameters

Those parameters reported in this work to explain the ways in which tin uses its outer electrons in bonding, are the chemical shift (δ) and the quadrupole splitting (Δ).

(a) Chemical Shift(δ): As described above, a change in the electronic (i.e. chemical) environment of the Mössbauer nucleus produces a shift in the position of the resonance line, resulting in a maximum resonance at a point other than when the Doppler velocity is zero. This shift in the resonance maximum is called the chemical isomer shift(δ) (Figure 1.9).

For a nucleus with a uniform, spherical, charge distribution, the change in the energy separation of the ground and excited states due to electronic interaction is given by:

$$\Delta E = 4/5\ \pi Z\ e^2\ R^2\ .\ \Delta R/R\ |\psi_s\ (0)|^2$$

where Ze is the nuclear charge, R the radius of the charge distribution, ΔR the difference between the nuclear radii in

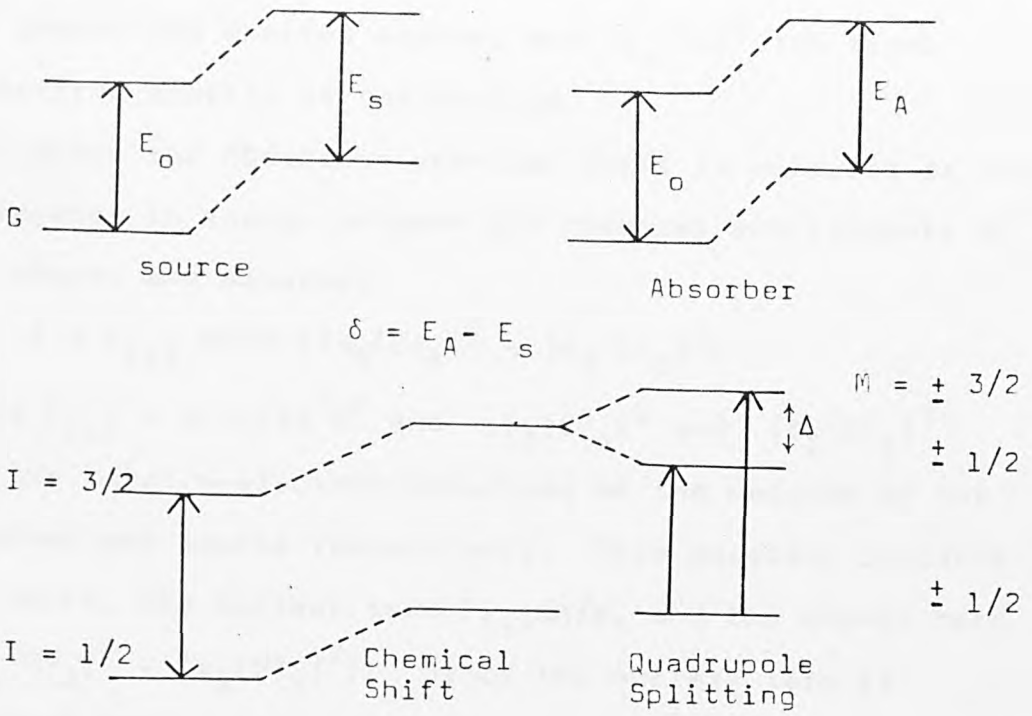

Figure 1.9 Origin of chemical shift and quadrupole splitting.

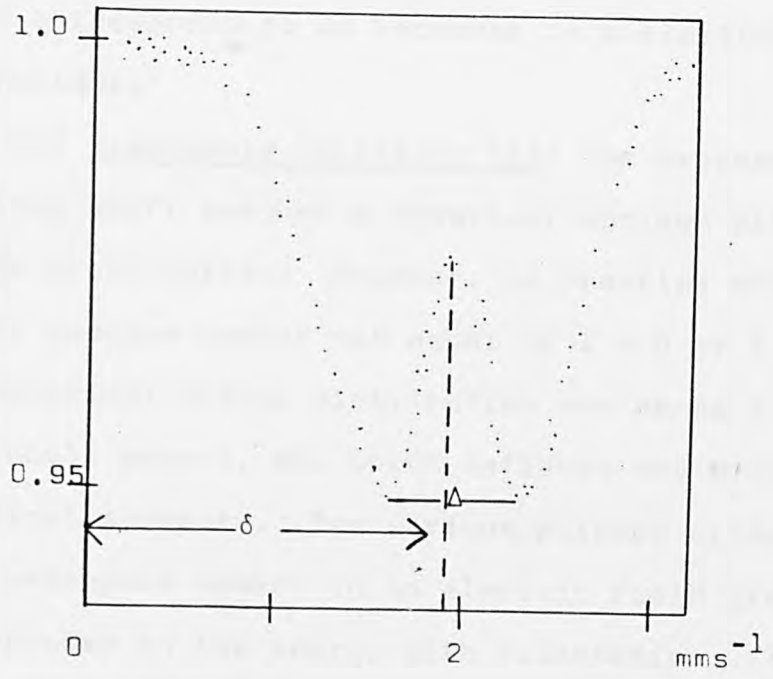

Figure 1.10 Mössbauer spectrum of α-SnF_2 using a $BaSnO_3$ source showing chemical shift and quadrupole splitting

the ground and excited states, and $|\psi_s(0)|^2$ the total s-electron density at the nucleus.

Since the Mössbauer chemical shift is measured as the difference in energy between the chemical environments of the source and absorber.

$$\delta = F_{(z)}\ \Delta R/R\ \{|\psi_S(0)_A|^2 - |\psi_S(0)_S|^2\}$$

where $F_{(z)} = 4/5\,\pi Ze^2R^2$ and $|\psi_S(0)_A|^2$ and $|\psi_S(0)_S|^2$ are the total s-electron densities at the nucleus of the absorber and source respectively. This equation contains two parts, the nuclear term $F_{(z)}\Delta R/R$, and the atomic term $\{|\psi_S(0)_A|^2 - |\psi_S(0)_S|^2\}$. Since the nuclear term is constant for a given transition, the chemical shift gives a measure of the change in s-electron density of the nucleus. For ^{119}Sn $\Delta R/R$ is positive [31], thus a positive chemical shift corresponds to an increase in s-electron density at the nucleus.

(b) Quadrupole Splitting (Δ): The expression for the chemical shift assumes a spherical nucleus with a uniform charge distribution. However, in practice any nucleus with a spin quantum number not equal to I = 0 or I = 1/2 has a non-spherical charge distribution and hence a nuclear quadrupole moment, eQ, which reflects the deviation from spherical symmetry. The various allowed orientations of the quadrupole moment in an electric field gradient leads to differences in the energy with orientation. The quadrupole splitting arises from the interaction between the different possible orientations of the nuclear quadrupole moment (eQ)

with the electric field gradient (eq) at the Mössbauer nucleus. Tin-119 has transitions between the nuclear spin states I=1/2 and I = 3/2, therefore the spectral line is split into two (Figure 1.10) with an energy difference of:

$$\Delta = \left| \frac{e^2 qQ}{2} \right| \left[1+\frac{\eta^2}{3}\right]^{\frac{1}{2}}$$

where η is an asymmetry parameter related to the electric field gradient. The centroid of the doublet corresponds to the chemical shift without a quadrupole interaction.

The extent of the quadrupole splitting is therefore a measure of the asymmetry of the s-electron density at the nucleus due to a non-uniform electric field gradient.

Applications in the Chemistry of Tin Compounds

The interpretation of the Mössbauer spectra of tin compounds is based on qualitative rather than quantitative arguments, with the results discussed in terms of trends in the change in s-electron density and not in absolute values.

Ideally Sn(IV) and Sn(II) may be considered to have the outer electronic configurations $4d^{10}5s^0$ and $4d^{10}5s^2$, respectively, with α-Sn intermediate with the configuration $4d^{10}5s^1$ thus providing a convenient distinction between Sn(IV) and Sn(II) compounds. In practice, α-Sn is taken as the reference material and arbitrary zero. Then, as $\Delta R/R$ is positive, positive values of δ refer to Sn(II) materials and negative values to Sn(IV) as illustrated in Figure 1.11. An increase in positive values of δ indicates an increase in the ionic character of the bonding, conversely an increase in negativity suggests a stronger covalent character.

Alloys

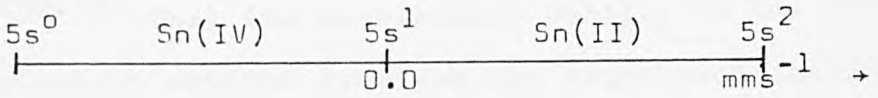

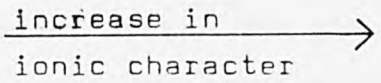

Figure 1.11 Interpretation of δ in relation to Tin Compounds.

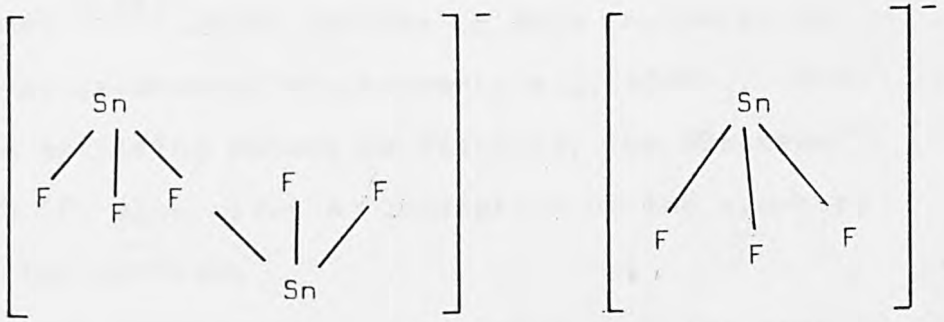

(a) (b)

Figure 1.12 The structures of (a) $Sn_2F_5^-$ ion, (b) SnF_3^- ion.

The splitting of the Mössbauer spectral line is due to quadrupole coupling, which is governed largely by the electric field gradient at the nucleus. It has been suggested[32,33] that the 5p-electron density in the non-bonding lone-pair orbital provides the major contribution to the electric field gradient, and hence the quadrupole splitting in tin(II) materials. Therefore, the larger the quadrupole splitting, the greater the asymmetry of the electronic environment around the tin nucleus. This can be demonstrated by comparing the corresponding pentafluoro-distannate(II) and trifluorostannate(II) complexes ($CsSn_2F_5$ Δ = 2.08 mms^{-1}; $CsSnF_3$, Δ = 1.86 mms^{-1})[34], the larger quadrupole splitting reflecting the lower symmetry of the tin site in the $Sn_2F_5^-$ ion (Figure 1.12). Similarly, compounds of higher symmetry have smaller quadrupole splittings. Caesium trichlorostannate(II) has a distorted octahedral tin environment and a quadrupole splitting of only 0.9 mms^{-1}[35] which reduces to zero in compounds with regular octahedral environments e.g. $CsSnBr_3$. When quadrupole splitting cannot be resolved, the Mössbauer line width (Γ) also gives an indication of the symmetry about the tin nucleus.

Mössbauer spectroscopy is a useful tool for readily distinguishing between tin(II) and tin(IV) materials, and for obtaining information about the character and symmetry of the bonding about the tin nucleus.

In the later part of this work the Mössbauer curve-fitting programs PARLOR[36] and MFIT[37] were used to fit the spectra.

1.3.3 X-ray Diffraction

X-ray diffraction may be used for the study of any crystalline material. An X-ray diffraction pattern can be detected when a monochromatic X-ray beam strikes a small single crystal which is usually turned on a spindle. The crystal behaves as a three dimensional diffraction grating since unit cells with dimensions of the order 5 to 50Å are regularly stacked in each direction. The pattern may be recorded as an array of spots on a photographic film, or by counting the x-radiation. The spot patterns arise from diffraction of the X-ray beam (wavelength λ) from stacks of parallel planes (spacing d) when the incidence angle (θ) is such that Bragg's Law $n\lambda = 2d\sin\theta$ is obeyed.

Crystal powder data were obtained in this work using both 11.6 Debye-Scherrer cameras and a Philips PW1010 X-ray diffractometer. X-ray single crystal data were obtained using four-circle diffractometers at both Queen Mary College, London, and Padua University, Italy.

The following account is given of the general theory of crystal structure determination, providing a background knowledge of the technique involved, for further discussion of the structure determinations carried out in Chapters 2, 3 and 4.

General Theory of Crystal Structure Determination

A crystal diffracts X-radiation in discrete directions. By measuring the intensities of these reflections it is possible to deduce the distribution of electron density within the crystallographic unit cell.

The Structure Factor

The most important quantity derived from the intensity data is the structure factor modulus $|F(hkl)|$ which is related to the experimentally observed intensities by

$$|F(hkl)| \propto \sqrt{I(hkl)obs}$$

The structure factor may be related to the atomic positions in the crystal by the expression

$$F(hkl) = \sum_j f_j(hkl) \exp 2\pi i (hx_j+ky_j+lz_j) \qquad (1)$$

where f_j is the atomic scattering factor, and x_j, y_j, z_j, are the coordinates of the jth atom and the summation is carried out over all atoms.

The above equation is however, true only for stationary atoms. In a real crystal, thermal vibrations[38] cause the atoms to vibrate so that the electron density cloud is distributed over a larger volume than assumed in the ideal stationary case and the scattering power of the atom is reduced. For isotropic vibrations the atomic scattering factor is modified by a function

$$T(hkl) = \exp\left[-B \sin^2\theta/\lambda^2\right]$$

where $B = 8\pi^2 U$ and is known as the isotropic temperature factor and U is $\overline{U}$ the mean-square amplitude of vibration in any direction. However in practice, vibrations are generally anisotropic so that

$$T(hkl) = \exp -(b_{11}h^2+ b_{22}k^2+ b_{33}l^2+ 2b_{12}hk + 2b_{13}hl +2b_{23}kl)$$

where $b_{11}= 2\pi^2 a^{*2}U_{11}$, $b_{12}= 2\pi^2 a^{*2}U_{12}$, etc. U_{11} is the vibration component in the 100 direction parallel to a*, with units of $\AA^2$, b_{ij} are called the anisotropic temperature factors.

The following pages are
in reverse order.

$$I_{obs}(hkl) \propto LpA(hkl)F_T^2(hkl)$$

which allows one to obtain from the observed intensities $I_{obs}(hkl)$, the value of $|F(hkl)|^2_{obs}$ from

$$|F_T(hkl)|^2_{obs} = I_{obs}(hkl)\,(Lp)^{-1}A^*(hkl)$$

where $A^*(hkl) = 1/A(hkl)$.

The structure factor thus obtained experimentally is on a relative scale, but its phase and absolute values can only be obtained from calculated data in the process of crystal structure determination.

Fourier Series[40]

Since a crystal is periodic in three dimensions its electron density (ρ) can be represented by a three dimensional Fourier Series:

$$\rho(x,y,z) = \frac{1}{V}\sum_{hkl}\sum\sum|F(hkl)|\exp[-2\pi i(hx + ky + lz)]$$

where x,y,z are the fractional atomic coordinates within the unit cell. Also $F(hkl) = |F(hkl)|\exp[i\alpha(hkl)]$.

As only $|F(hkl)|$ is experimentally measured, it is necessary to determine the phase angles, $\alpha(hkl)$ before the structure can be determined. In this work the general method used to solve this problem was to find the positioms of the heavy atoms in the cell by a Patterson synthesis and then to assume the sign of $F(hkl)_{obs}$ was the same as that of the calculated structure factor, $F(hkl)_{calc}$.

Patterson Function and the Heavy Atom Method[41,42]

In order to overcome the phase problem, Patterson[41] defined a Fourier series using the experimentally obtained $F^2(hkl)$ values and therefore not involving the phase of the structure factor.

Thus equation (1) becomes:

$$F_T(hkl) = \sum_j f_j(hkl)T_j(hkl) \exp 2\pi i(hx_j + ky_j + lz_j)$$

Data Reduction

The observed reflection intensities are influenced by the time over which the crystal plane will give diffraction (Lorentz factor), polarisation of the X-ray beam, and the absorption of X-radiation by the crystal. Therefore the measured intensities can be corrected by data reduction to give the modulus of the structure factor.

The Lorentz factor is a correction made to allow for the time spent by each plane in passing through the Bragg condition and depends upon the method of recording the reflections. For data collected on a diffractometer the Lorentz correction (L) is $(\sin 2\theta)^{-1}$. The polarisation factor (p) corrects for the partial plane polarisation of the X-ray beam on reflection of the lattice planes and is given by, $p = \frac{1}{2}(1 + \cos^2 2\theta)$.

When a beam of monochromatic X-radiation passes through a crystal of thickness t, it is found that the intensity, I, of the transmitted radiation is related to the intensity, I_0, of the incident radiation by $I = I_0 \exp(-\mu t)$ where μ, the linear absorption coefficient, is a constant and may be calculated [39]. If the thickness of the crystal is less than the optimum thickness, $t_{opt} = 2/\mu$, then the absorption correction is not necessary and may be neglected in all but the most precise determinations.

The final intensity equation is therefore:

$$P(U,V,W) = \frac{1}{V} \sum_h \sum_k \sum_l |F(hkl)|^2 \cos 2\pi(hU + kV + lW)$$

This function represents the product of the electron densities separated by U,V,W, and therefore has a significant value at (U,V,W) when the atoms are separated by U,V, and W in the unit cell. The Patterson function therefore represents all interatomic vectors reduced to a common origin. The magnitude of the Patterson peak is proportional to the product of the atomic numbers of the two atoms giving rise to the peak, so that vectors between the heaviest atoms produce the most intense peaks [42].

If the space group is known, the general positions allow the vectors to be calculated by vector subtraction and correlated with the peaks on the Patterson function, written as a map or a peak interpolation. With the heavy atom positions known, the phase of each reflection can be approximated to that due to the heavy atoms alone so as to obtain an electron density map from which more accurate heavy atom positions and the approximate positions of the lighter atoms can be obtained.

Difference Fourier

In practice when the heavy atom positions are known a difference Fourier is used to locate the light atom positions, thus providing a more accurate determination of atom positions by eliminating Fourier series termination errors which are caused by limitations in the amount of data available. The difference synthesis is found by subtracting the calculated electron densities from those observed:

$$\Delta\rho(xyz) = \frac{1}{V} \sum_h \sum_k \sum_l \left[F(hkl)_{obs} - F(hkl)_{calc}\right] \exp -2\pi i(hx + ky + lz)$$

The resultant difference map then shows only the residual electron density.

Reliability factor

The atomic positions x,y,z and the temperature factors B_j (or b_{ij} for anisotropic factors) are refined by a method of least squares to obtain the best fit between $F(hkl)_{obs}$ and $F(hkl)_{calc}$. The correctness of the structure is measured in terms of a residual, R, where:

$$R = \sum \left| \frac{|F|_o - |F|_c}{|F|_o} \right|$$

which tends to a minimum as a better fit between observed and calculated structure factors is achieved.

Various weighting schemes are used to account for the differences in accuracy of intensity measurements, and to reduce the residual by this means.

Computer Programs used in X-Ray Crystallography

(a) SHELX-76[43]

SHELX-76 is an integrated program for performing crystallographic calculations simply and efficiently. The calculations are valid for all space groups, and there is no limit on the number of reflections. Its facilities include (i) data reduction, including numerical absorption correction with crystal plots; (ii) rejection of systematic absences, least-squares determination of inter-batch scale factor, averaging equivalent reflections; (iii) full matrix, least-squares refinements; (iv) rigid group location on refinement; (v) various Fourier syntheses with peaks search; (vi) structure factor lists.

(b) POWDER and POWREF[44]

These programs fit and refine respectively, data from powder cameras. They may be used separately or as a combined POWREF-POWDER run.

(c) XRAY -72[45]

XRAY-72 is a manual report for the use of a library of crystallographic programs designed to perform the calculations needed to solve the structure of crystals by diffraction techniques.

(d) CELLPLOT[46] and PLUTO[47]

The programs CELLPLOT and PLUTO are used for plotting molecular and crystal structures.

1.3.4 Solid State Measurements

The study of the properties of materials in the solid state lies on the borderline between chemistry and physics so use can be made of the techniques of both structural inorganic chemistry and solid state physics.

Solid state chemistry can be defined as the study of reactions in solids and of the factors which may affect the reactivity of the solids with liquids, gases and other solids. On the other hand solid-state physics can be considered the study of the physical properties of materials and the relationship between those properties and the structure of the materials.

In the present work information was obtained on the fate of tin moieties in solid state reactions from measurement of electrical and optical properties. An account is given here of the theories of the methods used in making these measurements.

Band Theory of Solids

Most of the work on the electronic processes of solids has been carried out by physicists and hence band structures are usually discussed from a physics viewpoint using zone theory and tending to give little consideration to the origins of the bands interms of structure or of atomic or molecular orbitals.

The band theory of solids considers the motion of electrons in an infinite, periodic, three-dimensional field. Fermi-Dirac statistics are used to deal with the large number of electrons involved and to take into account the discrete energy levels required by quantization and the Pauli Principle.

This leads to the concept that electrons occupy bands which are formed in crystals by orbital overlap when the nuclei are within a certain minimum distance, the maximum number of electrons that can be accommodated in the band being determined by the Pauli Principle, taking into aecount the number of energy levels forming the band. Electrical conduction occurs by the movement of electrons (or positive electron holes) within the bands of the crystal. The dependence of this conductivity on the band structure of a crystal gives rise to three classes of solids:

(a) Metal, or conductors, which have high electrical conductivities (of the order 10^4 -10^6 ohm.$^{-1}$cm.$^{-1}$) at room temperature and in which conductivity decreases with temperature.

(b) Insulators, which have low conductivities lying in the range 10^{-14} to 10^{-22} ohm.$^{-1}$cm.$^{-1}$ at room temperature.

(c) Semiconductors, with conductivities intermediate between those of metals and insulators and in which conductivity increases with increasing temperature.

As the inner core orbitals of atoms contain their full complements of electrons, the inner core bands around the nuclei within crystals are also completely filled prohibiting the movement of electrons within the band. The higher, valence bands, on the other hand, may be filled or only partially filled depending upon the number of valence electrons available.

In conductors there is either a partially filled valence band or an empty band which overlaps a filled valence band (Figure 1.13a). The band structure of sodium is shown in Figure 1.14. Electrons in the upper levels of the valence band are then able to move freely within the band under the influence of an external field hindered only by collisions with impurities, lattice defects and phonons which slow the electrons and cause electrical resistance. In an insulator the energy difference between the highest filled valence band and the lowest empty conduction band is such that the forbidden band gap is inaccessible to thermal electrons (Figure 1.13b) e.g.diamond, E_g =5.4 eV. If the band gap is such that some electrons have sufficient thermal energy (kT) to move across the gap then the crystal is an intrinsic semiconductor (Figure 1.13c) e.g.α-Sn, E_g= 0.08 eV. At 0 K an intrinsic semiconductor should behave like an insulator.

A number of insulators become semiconducting when they are non-stoicheiometric or when they are impure, these are extrinsic semiconductors.

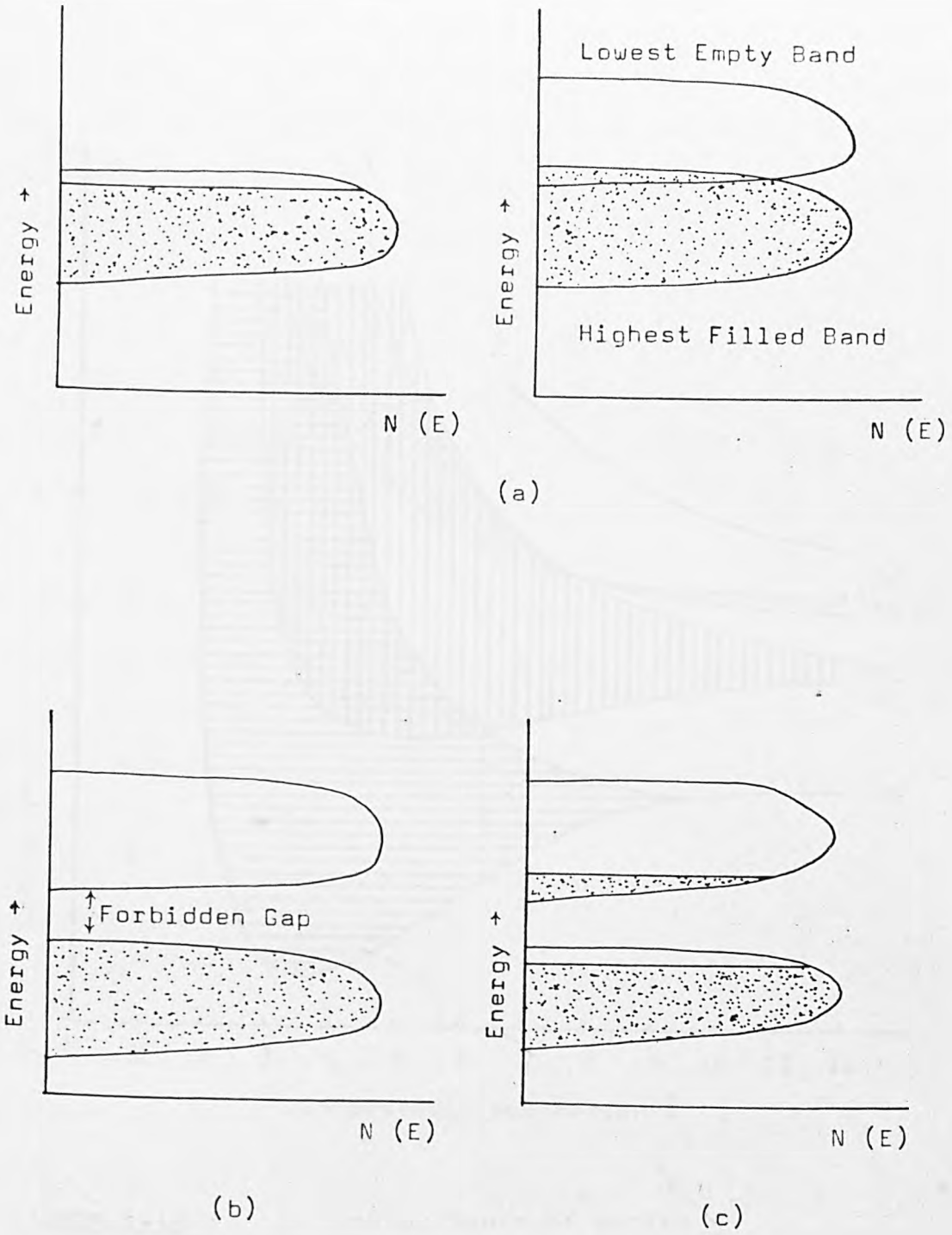

Figure 1.13 Energy band diagrams: (a)conductor, (b) insulator, (c) intrinsic semiconductor

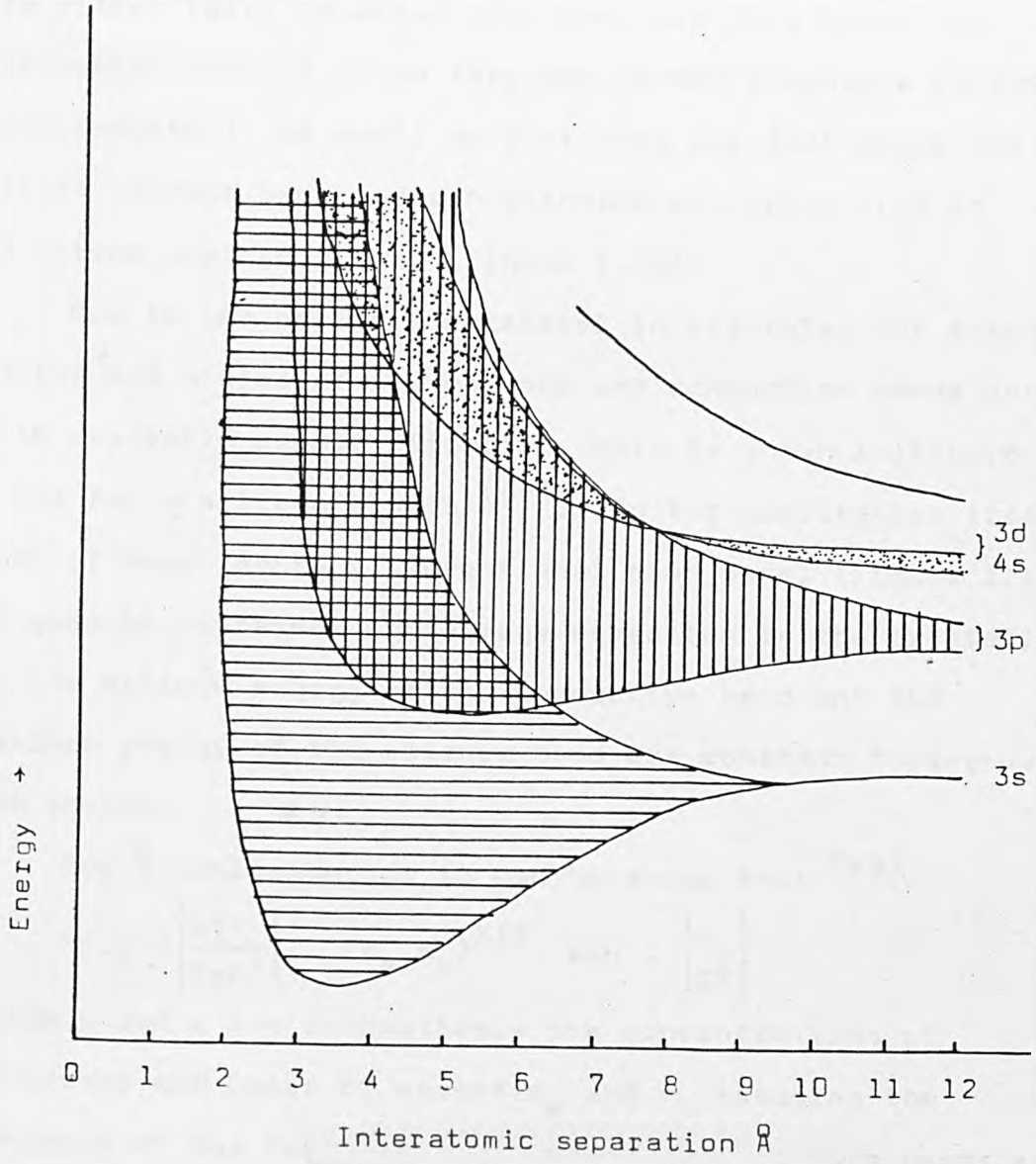

Figure 1.14 Energy bands of sodium

The defects or impurities produce localized energy levels which lie within the forbidden energy region. These levels are either full, in which case they lie just below the conduction band to which they may donate electrons (n-type semiconductor), or empty so that they lie just above the filled valence band and can withdraw electrons from it (a p-type semiconductor) (Figure 1.15).

Due to the periodic potential in crystals, the energy maxima and minima of the valence and conduction bands vary with crystallographic direction, this is shown in Figure 1.16a for a silicon crystal[48]. In the qualitative treatment of band theory a conventional band model (Figure 1.16b) is used to represent an average direction in the crystal, so the minimum energy of the conduction band and the maximum energy of the valence band are constant throughout the crystal.

For a semiconductor it can be shown that [49]

$$np = 4\left[\frac{kT}{2\pi\hbar^2}\right]^3 (m_e\ m_h)^{3/2} \exp - \left[\frac{E_g}{kT}\right]$$

where n and p are respectively the concentrations of electrons and holes of masses m_e and m_h assuming the distance of the Fermi level from the edge of both bands is large compared to kT. Conductivity is proportional to the carrier concentration, so for an intrinsic semiconductor (i.e. if n=p) then:

$$\sigma = A(T)^3 \exp - \left[\frac{E_g}{2kT}\right]$$

where the exponential term is dominant i.e.log σ=-Eg/2kT + C (C=Constant) so Eg may be determined by variable temperature conductivity measurements. The width of the forbidden band

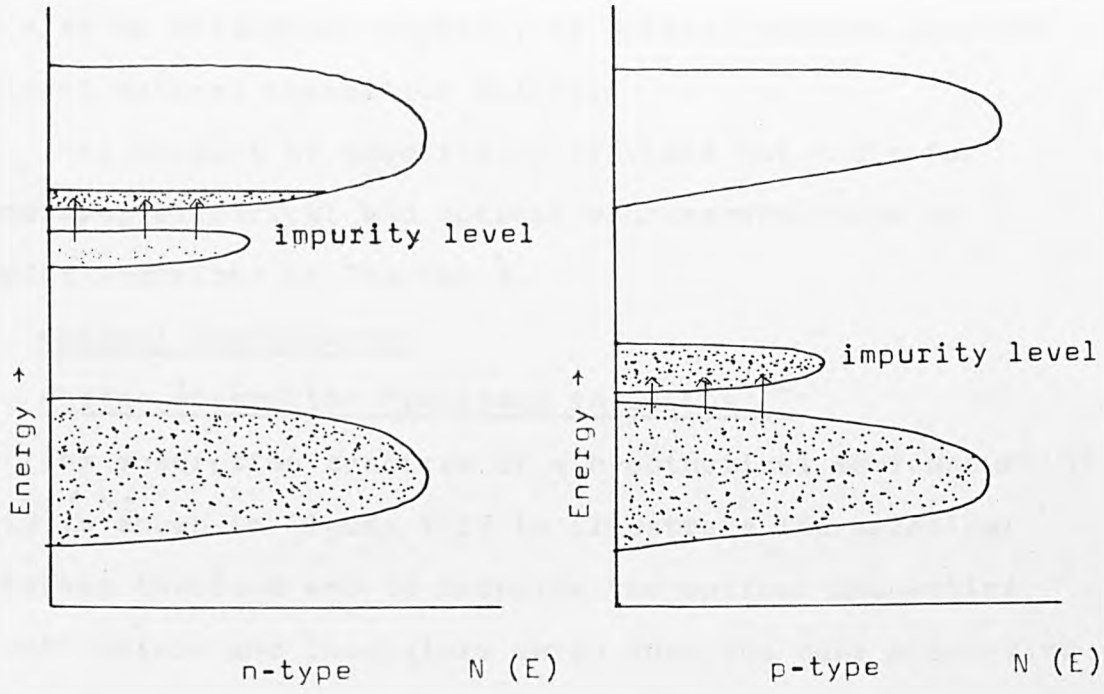

Figure 1.15 Extrinsic Semiconductor

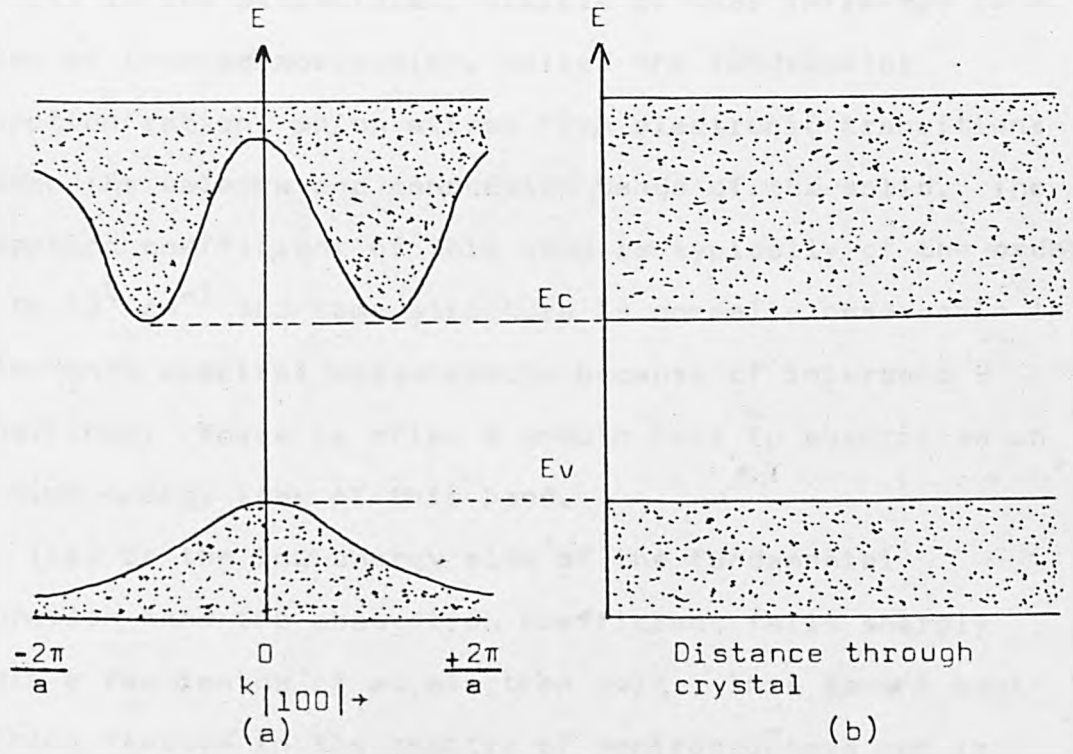

Figure 1.16 (a) Variation of energy levels with direction in a Si crystal; (b) representation in terms of a conventional band model

can also be determined directly by optical methods provided a direct optical transition exists.

This account of band theory provides the basis for discussing electrical and optical measurements made on samples described in Chapter 3.

Optical Spectroscopy

Photon Absorption Processes in Solids[50]

The absorption spectrum of a hypothetical semiconducting solid is shown in Figure 1.17 to illustrate the principal processes involved and to describe the optical properties of both metals and insulators which show the same properties although to different degrees. The energies involved extend from the ultraviolet to the far infra-red, the main features are:

(i) In the ultraviolet, visible or near infra-red is a region of intense absorption, called the fundamental absorption region, which arises from electronic transitions between the valence and conduction bands of the solid. The absorption coefficient of this band is typically of the order 10^5 to 10^6 cm^{-1} and some structure is normally observable in reflectance spectral measurements because of interband transitions. There is often a smooth fall in absorption on the high energy side of this band.

(ii) On the low energy side of the fundamental absorption band the absorption coefficient falls sharply within a few tenths of an electron volt. This is the most striking feature in the spectra of semiconductors and is known as the absorption edge and corresponds to the minimum energy at which interband transitions can occur and

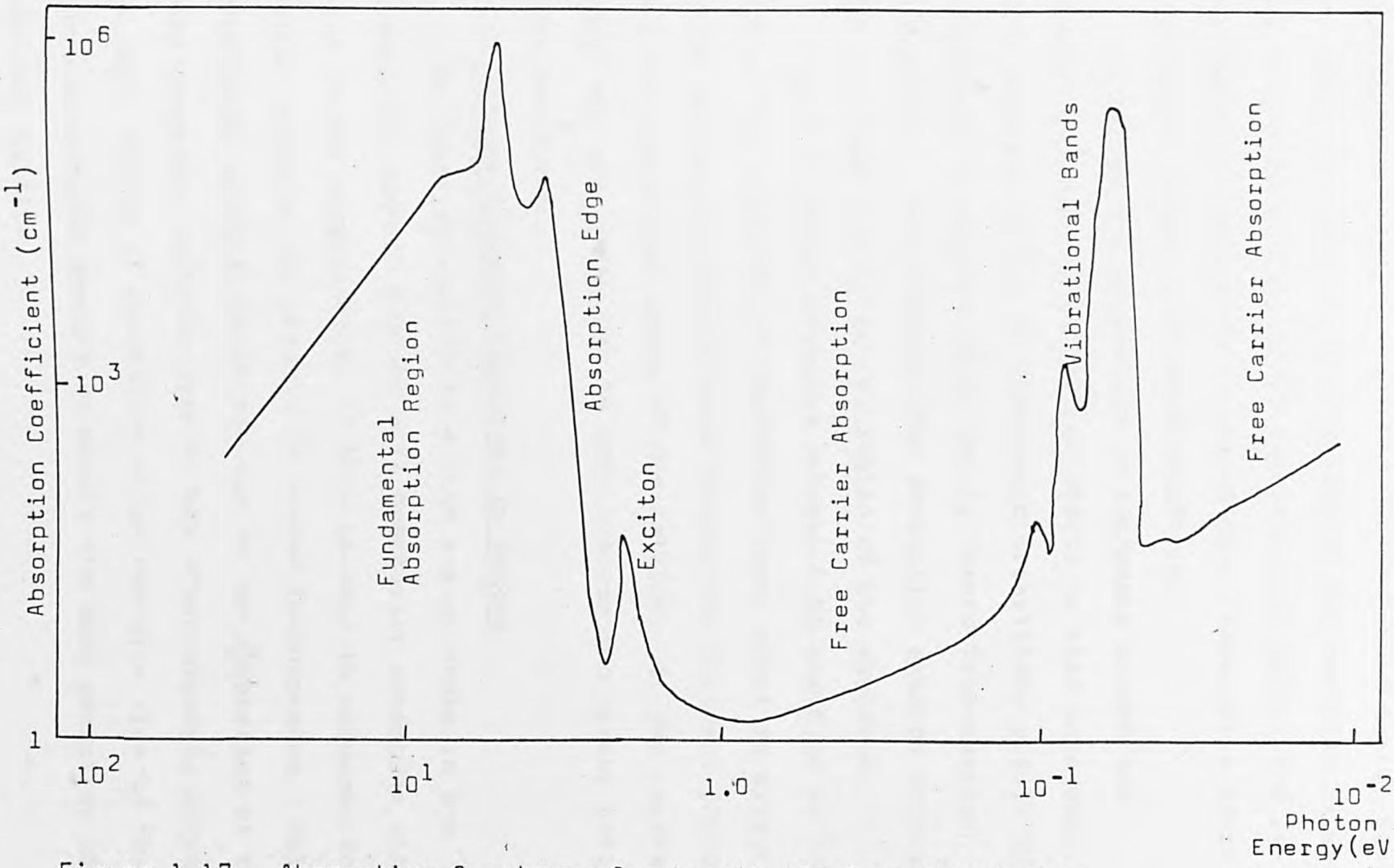

Figure 1.17 Absorption Spectrum of a hypothetical semiconductor.

represents the optical width of the forbidden energy gap(E_g). Any structure found in this region of the spectrum is usually due to excitons, i.e. bound electron-hole pairs, and is particularly noticeable in insulators, (especially ionic insulators) rather than semiconductors.

(iii) As the wavelength is increased beyond the absorption edge the absorption starts to rise once more. This increase is due to electronic transitions within the conduction or valence bands and is termed free-carrier absorption. This free-carrier absorption extends throughout the microwave and infra-red region of the spectrum.

(iv) At photon energies between 0.02 and 0.05 eV (200-500 cm^{-1}), a new set of absorption peaks start to appear. These are due to interactions between the incident photons and the vibrational modes of the lattice. If the crystal is ionic the absorption may be very intense and strong reflection can occur.

Optical Emission Processes in Solids

An electron excited to a high energy state in the conduction band of a solid will eventually recombine with a hole in the valence band, if this process is accompanied by photon emission the process is termed luminescence. Unlike absorption spectra, which are due to the properties of the bulk material, emission spectra are often strongly affected by small traces of impurities which can give rise to their own luminescence spectra or modify the band structure of the host lattice.

The process of luminescence occurs in two steps: the excitation of electrons to higher energy states and the

subsequent reemission of energy by the excited electrons in the form of electromagnetic radiation on the low energy side of the absorption band. When the excitation process involves light from the visible or near visible region of the spectrum this is known as photoluminescence.

There are two basic types of luminescence: luminescence from the excited state of a molecule or ion to its ground state, and interband luminescence.

(a) Excited State Luminescence: When luminescence occurs at a luminescent centre the emission process may be described by the configuration coordinate model of Seitz and Mott[51,52] (Figure 1.18a). This model describes the overall geometrical configuration of the nuclei surrounding the luminescent centre and explains the Stokes Shift i.e. the red shift of a luminescent band relative to the corresponding absorption band. In the case of absorption spectra the Franck-Condon principle means that the electronic transitions occur at energies corresponding to the energy difference between the electronic states at ground state internuclear distances (AB). However for luminescence to occur the lifetime of the emitting state must be long compared with that of a molecular vibration if significant emission is to be observed, hence the excited electron equilibrates prior to emission (CD) at a lower energy than that of the absorption band.

In addition to photon emission the excited electrons can lose energy by non-radiative thermal de-excitation, as the temperature of the luminescent material increases more

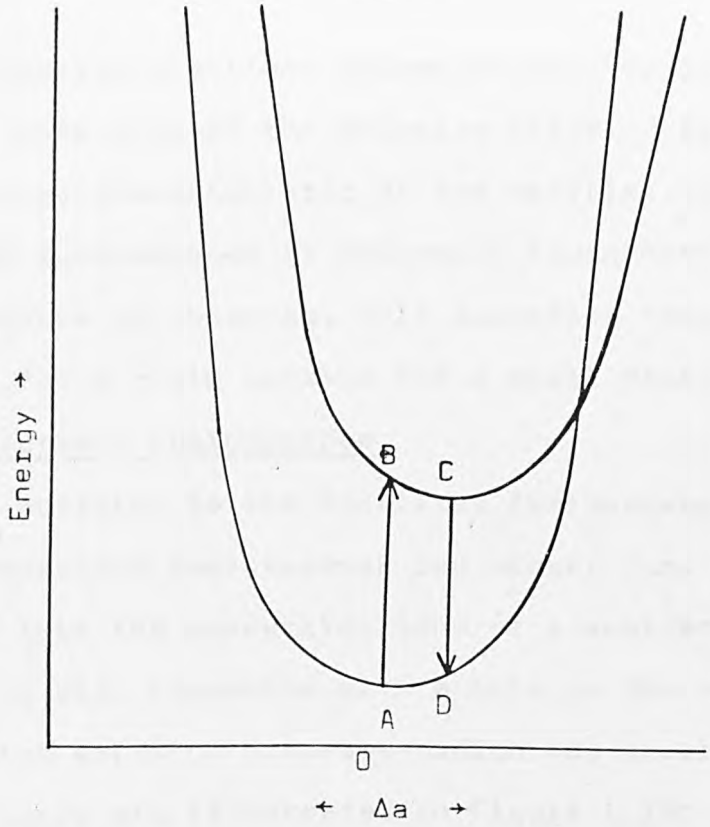

Figure 1.18a Configuration coordinate diagram of luminescence showing the origin of the Stokes shift.

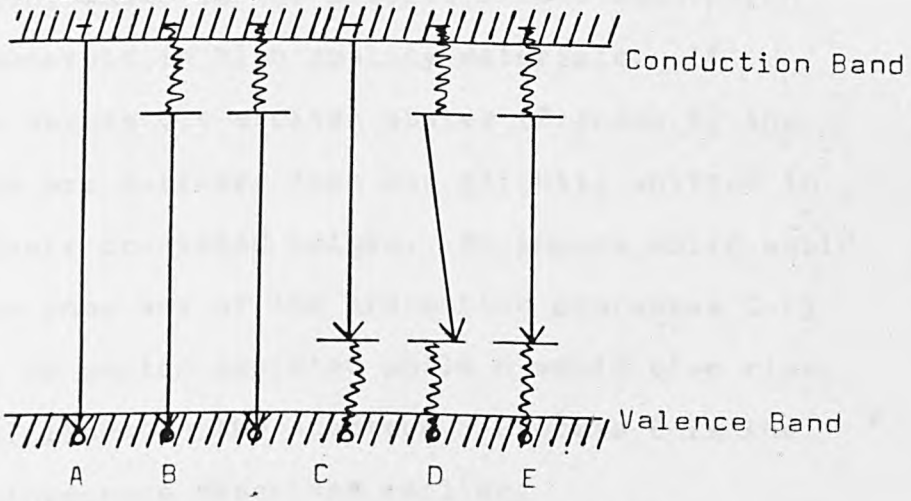

Figure 1.18b Photon emission processes in solids.

A. Conduction band to valence band;

B. Recombination via exciton levels;

C. Donor level to valence band, Conduction band to acceptor level;

D. Donor level to acceptor level;

E. Recombination via impurity excited states.

of the excited electrons become de-excited in this manner and the intensity of the emission falls. At a critical temperature characteristic of the material and emission band the luminescence is thermally "quenched" and no luminescence is observed, this quenching temperature is highest for a rigid lattice and a small Stokes Shift.

Interband Luminescence

In addition to the localized luminescence described above interband luminescence can occur, i.e. an electron excited into the conduction band of a semiconductor or insulator will recombine with a hole in the valence band. The photon emission processes which may occur in interband luminescence are illustrated in Figure 1.18b using the band model of Richl and Shön [53,54] and Johnson[55].

Process A shows direct interband recombination with photon emission, which is the reverse of the absorption edge and is observed in high quality materials. If recombination occurs via exciton states (Process B) the observed bands are narrower than and slightly shifted in energy from their predicted values. An impure solid would be expected to show any of the transition processes C-E; process C may be photon assisted while D would give rise to a series of lines in the spectrum. Process E is the localized luminescence described earlier.

When an electron is excited into the conduction band, any excess vibrational energy will be lost before emission occurs so that the electrons will lie in a band kT wide at the bottom of the conduction band (and the electron holes will lie within kT of the top of the valence band) and give

rise to an emission band of width kT as opposed to the narrow lines expected from well defined localized levels. As in the case of localized emission non-radiative de-excitation increases with increasing temperature.

Photoacoustic Spectroscopy

An alternative method of studying the optical properties of solids is photoacoustic spectroscopy (PAS)[56] which provides a complementary technique giving similar information to that obtained from the conventional techniques described earlier.

Over the years several techniques have been developed to permit optical investigation of highly light scattering materials, such as powders, amorphous solids, gels, smears, suspensions and opaque substances. The most common of these are diffuse reflectance[57], attenuated total reflectance[58], internal reflectance spectroscopy[58] and Raman scattering[59]. Using these techniques however, attempts to measure a very weak absorption in such materials, which involve the measurement of a very small change in intensity of a strong essentially unattenuated transmitted signal, can prove difficult. It is the unique inherent insensitivity of PAS to radiation scattered or reflected from the sample surface that makes PAS extremely attractive for the study of highly light scattering and/or opaque materials. For this reason PAS is becoming progressively more important for the study of optical absorption spectra of solid, semi-solid and liquid samples.

PAS differs from conventional techniques, in that, even though the incident energy is in the form of optical photons,

the interaction of these photons with the material under investigation is studied not through subsequent detection and analysis of some of the photons, but through a direct measure of the energy absorbed by the material as a result of its interaction with the photon.

The theory relating to the generation of a photoacoustic signal in a condensed phase sample has been derived by Rosencwaig et al[60]. In brief, the photoacoustic signal is generated when a light absorbing substance is exposed to modulated incident radiation. A fraction of the radiation falling upon the sample is absorbed and results in excitation, the type of which being dependent upon the energy of the incident radiation. Non-radiative de-excitation processes which normally occur give rise to the generation of thermal energy within the sample. In a solid this heat energy appears as vibrational energy of ions or atoms. If the incident radiation is modulated then the generation of thermal energy within the sample will also be periodic and a thermal wave will be produced having the same frequency as this modulation. Energy is transferred by the thermal wave towards the sample boundary, where a periodic temperature change is generated.

The photoacoustic signal is a function of two types of processes occuring in the sample: the absorption of electromagnetic radiation specified by the absorption coefficient β and the thermal propagation in the sample specified by the thermal diffusivity, x. For the highly absorbing samples the optical absorption length $l_\beta = 1/\beta$ is an important parameter and may be taken as the depth into the sample at which essentially all of the incident radiation has

been absorbed. The thermal wave produced in the sample is heavily damped and may be considered as fully damped out within a distance $2\pi\mu_s$, where μ_s is the thermal diffusion length[60]. It is normally assumed that only those thermal waves originating from a depth less than or equal to μ_s will make an appreciable contribution to the photoacoustic signal measured. The thermal diffusion length is a function of the thermal diffusivity, and the modulation frequency of the incident radiation, ω

$$\mu_s = \sqrt{\left(\frac{2x}{\omega}\right)}$$

This important relationship means that for a sample of given thermal diffusivity the depth examined, μ_s, may be varied by adjusting the modulation frequency, ω.

The observed photoacoustic signal is a complex quantity having a magnitude and phase relative to the modulation of incident radiation. As well as being a function of the absorption coefficient, modulation frequency and thermal characteristics of the sample, the photoacoustic signal is directly proportional to the incident power of radiation and also depends upon characteristics of the gas in contact with the sample surface, the nature of the sample surface and the properties of the backing material upon which the sample is positioned.

The relative magnitudes of the quantities l_β and μ_s critically affect the nature of the photoacoustic spectrum obtained for a particular sample and this is depicted schematically in Figure 1.19. For samples which are optically transparent(Figure 1.19a) the photoacoustic signal is always proportional to the value of β. Remembering that only

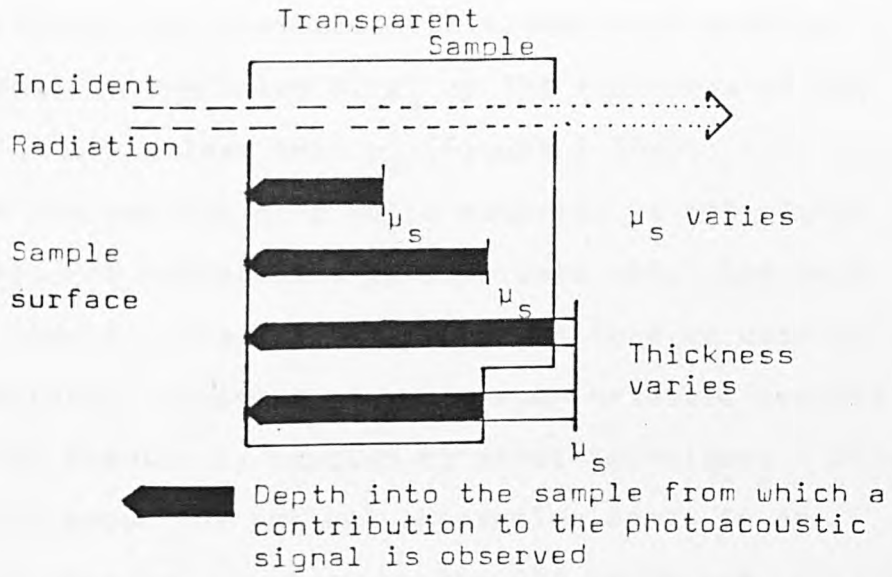

Figure 1.19a Illustration of the interrelationship between the thickness of an optically transparent sample and the thermal diffusion length(μ_s)

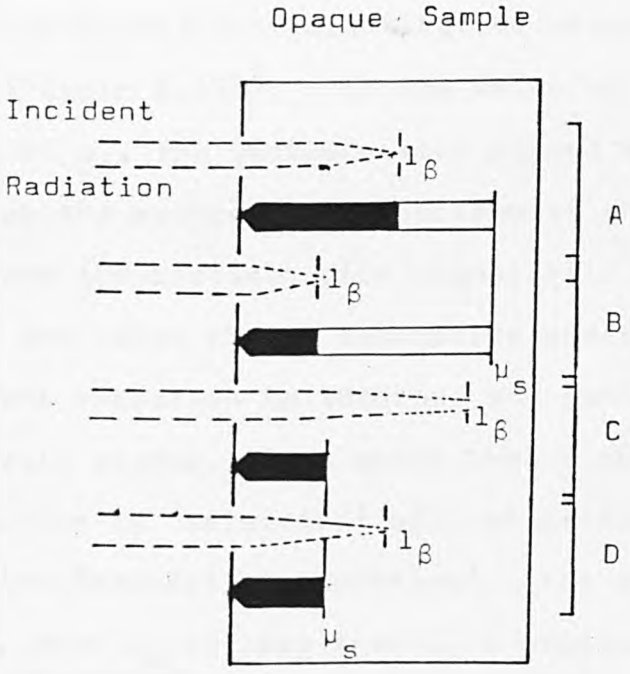

Figure 1.19b Illustration of Photoacoustic saturation for an opaque sample (A,B). Removal of saturation by reduction of μ_s(C,D).

absorbing species at distances less than μ_s into the sample can contribute, the photoacoustic signal will also be proportional to the value of μ_s or the thickness of the sample if this is less than μ_s (Figure 1.19a).

When the surface of a solid material is not highly reflective, PAS can provide optical data about the bulk material itself. The PAS technique can thus be used to study insulator, semiconductor and even metallic systems that cannot readily be studied by other techniques. Direct information about the optical absorption bands in an insulating material is given by the PAS technique, whilst for semiconductors both direct and indirect band transitions can be observed.

For an optically opaque sample an added complication arises if qualitative or quantitative measurements are required (Figure 1.19b). If the value of l_β is less than the value of μ_s, the photoacoustic signal obtained will depend upon the source power spectrum at the wavelength of interest and the photoacoustic signal will not be proportional to the value of the absorption coefficient, as all the incident radiation is absorbed and contributes to the photoacoustic signal. This means that a photoacoustic spectrum which is 'saturated' will be produced, a condition known as 'photoacoustic saturation'. For the converse situation, when μ_s is less than l_β a dependency of the photoacoustic signal upon the absorption coefficient of the sample will be observed, as only the radiation absorbed within the first thermal diffusion length will contribute to the photoacoustic signal measured. The latter two cases

are related and, in theory, may be interconverted by a suitable selection of the modulation frequency. Therefore, for many opaque samples the effects of spectral saturation may be removed by increasing the signal modulation frequency although this reduces the signal magnitude and degrades the signal-to-noise ratio. Clearly, there is a maximum modulation frequency which is realistic for use in practice.

An alternative approach which may be adopted to avoid spectral saturation, especially for extremely strongly absorbing samples, is to disperse the sample over a very weak absorber such as silica gel or magnesium oxide. This may be achieved by grinding the sample and diluent or by evaporating a solution of the sample on to the diluent. In both cases the effect is to reduce the effective thickness of the absorbing sample so that it is less than l_β.

In PAS, the sample under study is placed in a closed cell or chamber. In the case of liquids or gases, the sample generally fills the entire chamber, whilst in the case of solids, such as those studied in this work, the sample is ground to a fine powder which fills only a portion of the chamber and the rest of the chamber is filled with a non-absorbing gas such as air. In addition the chamber contains a sensitive microphone. The sample is illuminated with monochromatic light which passes through an electro-mechanical chopper. Figure 1.20 depicts a schematic representation of the photoacoustic spectrometer, an edt Research OAS and Optoacoustic Spectrometer, used in this work.

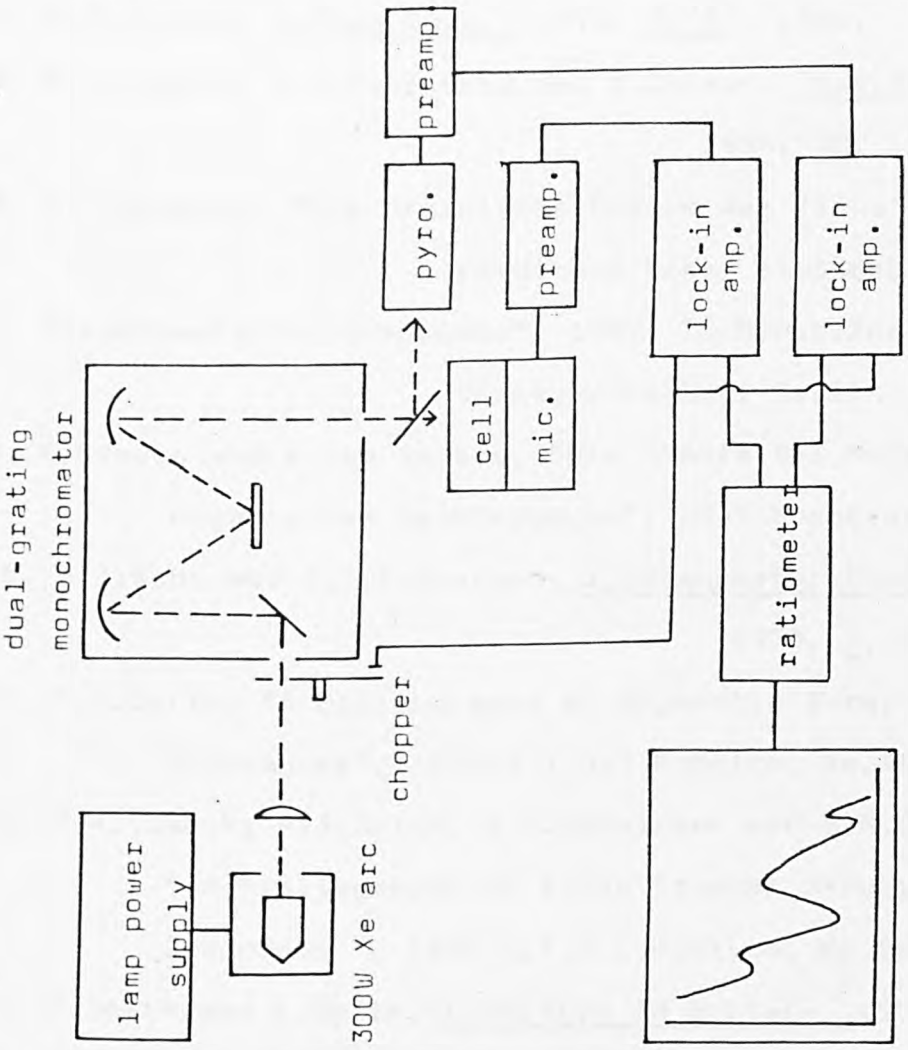

Figure 1.20 Block Diagram of Photoacoustic Spectrometer

REFERENCES

1. W.H.Baur, Acta Cryst., 1956, 9, 515.

2. W.H.Baur, and A.A.Khan, Acta Cryst., 1970, B27, 2133.

3. G.Wagner and H.Binder, Z.Anorg.Chem., 1959, 298, 12.

4. R.Weiss and R.Faivre, Compt.Rend., 1959, 248, 106.

5. M.F.C.Ladd, J.Chem.Phys., 1974, 60(5), 1954.

6. R.K.Ingham, S.D.Rosenberg and H.Gilman, Chem.Rev., 1960, 60, 459.

7. W.P.Neumann, "Die Organische Chemue des Zinns",1967, Ferdinand Enke, Stuttgart.

8. "Organometallic Compounds", 1967, Ed.M.Dub,2nd ed.vol.II, Springer-Verlag, Berlin.

9. E.Krause and A.Von Grosse, "Die Chemie der Metall-organischen Verbindungen", 1937,Borntraeger,Berlin.

10. B.Y.K.Ho and J.J.Zuckerman, J.Organometal.Chem., 1973, 1, 235.

11. P.J.Smith, "A Bibliography of Organotin X-ray Crystal Structures", 1975,I.T.R.I.Publicn. No.484, London.

12. P.A.Cusack, P.J.Smith, J.D.Donaldson and S.M.Grimes, " A Bibliography of X-ray Crystal Structures of Tin Compounds ", 1980,I.T.R.I.Publicn. No.588, London.

13. P.Smith and L.Smith, Chemistry In Britain, 1975, 11(6), 208.

14. R.Hulme, J.Chem.Soc., 1963, 1524.

15. I.R.Beattie, M.Milne, M.Webster, H.E.Blayden. P.J.Jones, R.C.G.Killean and J.L.Lawrence, J.Chem.Soc.(A)., 1969, 482.

16. M.F.A.Dove, R.King and T.J.King, Chem.Comm., 1973, 944.

17. B.Frlec, D.Ganter and I.Leban, Vestn.Slav. Kem.Drus., 1979, 26, 421.

18. J.D.Donaldson, Progress in Inorganic Chemistry, 1967, 8, 287.

19. J.D.Donaldson and S.M.Grimes, in press.

20. J.D.Donaldson and D.C.Puxley, Acta Cryst., 1972, B28, 864.

21. B.Kamenar and D.Grdenic, J.Chem. Soc., 1961, 3954.

22. K.Kitahama and H.Kiriyama, Bull.Chem.Soc.Jap., 1977, 50, 3167; 1973, 46, 1389.

23. F.R.Poulsen and S.E.Rasmussen, Acta Chem.Scand., 1970, 24, 150.

24. J.F.Young, R.D.Gillard and G.Wilkinson, J.Chem.Soc., 1964, 5176.

25. M.A.Khattak and R.J.Magee, Chem.Comm., 1965, 400.

26. J.A.W.Dalziel, J.D.Donaldson and B.W.Woodget, Talanta, 1969, 16, 1477.

27. J.D.Donaldson, J.Silver, S.Hadjiminolis and S.D.Ross, J.Chem.Soc.Dalton, 1975, 1500.

28. H.Krebs, K.Grun and D.Kallen, Z.Anorg.Chem., 1961, 312, 307.

29. L.Erdey, F.Paulik and J.Paulik, Nature, 1954, 174, 885.

30. R.L.Mössbauer, Z.Phys., 1958, 151, 124; Naturwiss, 1958, 45, 538.

31. J.P.Boquet, Y.Y.Chu, O.C.Kistner, M.L.Perlman and G.T.Emery, Phys.Rev.Lett., 1966, 17, 809.

32. T.C.Gibb, B.A.Goodman and N.N.Greenwood, J.C.S.Chem.Comm., 1970, 774.

33. J.D.Donaldson, E.J.Filmore and M.J.Tricker, J.Chem.Soc.(A)., 1971, 1109.

34. J.D.Donaldson and B.J.Senior, J.Chem.Soc.(A)., 1966, 1798.

35. J.Barrett, S.R.A.Bird, J.D.Donaldson and J.Silver, J.Chem.Soc.(A)., 1971, 305.

36. Z.Arifin, Ph.D Thesis, London. 1981.

37. M.Moerup, Private Communication.

38. M.J.Beurger, "Crystal Structure Analysis", 1969, 231, Wiley, New York.

39. "International Tables for X-ray Crystallography",1962, Kynoch Press, Birmingham.

40. G.H.Stout and L.H.Jensen, "X-ray Structure Determination", 1968, MacMillan, London.

41. A.L.Patterson, Phys. Rev., 1934, 46, 372: Z.Krist., 1935, 90, 517.

42. H.Lipson and W.Cochran, "The Crystalline State", 1966 Vol.3. Bell.

43. G.M.Sheldrick, "Program for Crystal Structure Determination",University of Cambridge, 1975.

44. D.Puxley, Ph.D. Thesis, London. 1972.

45. "The X-ray System-Version of June 1972", Technical report TR-192 of the Computer Science Centre, University of Maryland, U.S.A.

46. D.C.Puxley and J.D.Donaldson, Acta Cryst., 1973, A29, 91.

47. W.D.S.Motherwell, "Pluto: Plotting Molecular and Crystal Structures", University of Cambridge,1979.

48. W.Kleinman and J.C.Phillips, Phys.Rev., 1960,118, 1164.

49. C.Kittel, "Introduction to Solid State Physics". 4th Ed., 1971, John Wiley, London.

50. R.J.Elliot and A.F.Gibson, "An Introduction to Solid State Physics", 1974, Macmillan, London.

51. F.Seitz, Phys.Rev., 1949, 76, 1376.

52. N.F.Mott, Proc. Roy. Soc.(Lond), 1939,A171, 27.

53. M.Shön, Ann.Physik., 1948, 3, 333; 343.

54. NRichl and M.Shön, Z.Physik., 1939, 114, 682.

55. R.P.Johnson, J.Opt.Soc.Am., 1939, 29, 283; 387.

56. A.Rosencwaig,"Photoacoustics and Photoacoustic Spectroscopy", Vol.57, Chem.Anal.,1980, Wiley and Sons, New York.

57. W.W.Wendkandt and H.G.Hecht, "Reflectance Spectroscopy", 1966, Wiley, New York.

58. P.A.Wilks and T.Hirschfield, Appl.Spectrosc. Rev. 1968, 1, 99.

59. G.B.Wright, "Light Scattering of Solids", 1969, Springer-Verlag, Berlin and New York.

60. A.Rosencwaig and A.Gersno, J.Appl.Phys., 1976, 47,64.

CHAPTER 2

Complex Formation in Tin Chemistry

CHAPTER 2

Complex Formation in Tin Chemistry

Complex formation is a well-known feature of the chemistry of tin in both the (II)+ and (IV)+ oxidation states and the results described in this chapter are concerned with the fate of tin moieties in chemical reaction that result in the formation of complexes.

In view of the availability of an empty 5p-orbital in molecular tin(II) compounds it is expected that tin(II) halides should act primarily as monofunctional acceptors and compounds of the type SnX_2L where L is a monodentate ligand should be the stable complexes. In the formation of anionic complexes tin(II) is certainly a monofunctional acceptor. Studies[1-3] on the ions present in complex tin(II) halide solutions have shown that the stable and predominant species is the triligandstannate(II), SnX_3^- ion. In the presence of a powerful acceptor the sterically active lone pair on the tin in tin(II) moieties may act as a σ - donor species. The present work was undertaken to investigate the fate of tin(II) moieties in chemical reactions in which tin(II) may act as an acceptor or a donor species.

In section 2.1 the results are presented for the reaction of tin(II) chloride and glycylglycine in solution. Such a reaction could lead to the elimination of HCl to give a glycylglycinate, or to the formation of an adduct of $SnCl_2$ with the glycylglycine. Reactions leading to complex formation between tin(II) chloride and donor molecules of biological interest are described in section 2.2, whilst the

work in section 2.3 is an extension of the work carried out by Nicholson[4] on the nature of the bonding in adducts containing more than one ligand per tin moiety.

The work described in section 2.4 is concerned with chemical reactions that could lead to the production of more than one tin(II) site in the same product lattice and the nature of tin(II) bonding in these compounds. The results of the use of tin(II) electron pairs as donor species in a system containing Pd acceptor molecules are considered in section 2.5. The effects of competition between tin(II) and another metal species viz. In(III) for bond formation to either fluorine or chlorine are detailed in section 2.6.

Unlike tin(II) species where an empty 5p - orbital is available, tin(IV) can only form complexes by use of empty 5d orbitals. The last two sections of this chapter describe studies of complex formation between tin moieties and glycylglycine or sugar derivative molecules.

2.1 Tin(II) Chloride Glycylglycine System

Very few derivatives of tin(II) with biological molecules are known. A series of compounds prepared from some tin(II) halide sulphur-containing amino acid systems has recently been reported[5], but the only known derivative of an oxygen containing amino acid is diglycinatotin(II)[6].

The products obtained by reacting tin(II) chloride with the molecules, glycylglycine, cytosine, adenine, inosine, adenosine and cytidine in methanol have been studied and all of the biological molecules (L) except glycylglycine appear to form only adducts of the type shown:

$$SnCl_2 + nL \rightarrow SnCl_2L_n$$

The adducts with adenine, adenosine, cytosine, cytidine and inosine are described in the next section. This section deals with the preparation and identification of the products obtained from the $SnCl_2$:glycylglycine system in methanol.

2.1.1 Preparative Studies

The products obtained from solutions of tin(II) chloride and glycylglycine in dry methanol were studied for different reaction times under an atmosphere of oxygen-free nitrogen, and for different molar ratios of the reactants. Details of the varying conditions are given in Table 2.1. It can be seen that the product obtained by refluxing a solution containing tin(II) chloride with either equimolar proportions or a two-fold molar excess of glycylglycine for short periods of time (20-90 minutes) is always the adduct tin(II) chloride bis glycylglycine, $SnCl_2 . 2(C_4H_8N_2O_3)$.

The presence of glycylglycine in larger than two-fold excess leads to impure products and finally to the precipitation only of the excess of glycylglycine at for example 4:1 excess. The use of both 2:1 and 3:2 tin(II) chloride: glycylglycine ratios leads on refluxing, to an oil, from which, the only solid product obtained is also $SnCl_2 . 2(C_4H_8N_2O_3)$.

The product obtained by refluxing equimolar quantities of tin(II) chloride and glycylglycine under an oxygen-free nitrogen atmosphere in dry methanol for much longer periods (>10 hours) can however lead to the formation of either $SnCl_2 . 2(C_4H_8N_2O_3)$ or the ternary compound $ClSn(C_4H_7N_2O_3)$.

The analytical data for these products are given in Table 2.2.

2.1.2 Chemical Analysis

To determine the products of the tin(II) chloride: glycylglycine reaction, the materials were analysed by estimating the percentage of tin, chlorine, carbon, hydrogen and nitrogen separately.

Stannous tin was determined by the Donaldson and Moser method[7], while chlorine was estimated by potentiometric titrimetry. Carbon, hydrogen and nitrogen assays were carried out in the microanalytical sections of The City University, London, and the Laboratorio di Chimica Organica, Milano.

Table 2.2 contains the complete analytical data for the materials which have been prepared. The percentage values reported for tin and chlorine are an average of three separate determinations.

X-ray diffractometer data were collected for the products formed over a reaction time of less than 10 hours, and confirm the existence of a single isolated product of formula $SnCl_2 . 2L$ (L = glycylglycine) (Table 2.3).

2.1.3 Thermal Analysis

Thermal analysis of the series of products obtained from reaction of tin(II) chloride with glycylglycine has provided a useful means of comparison of materials formed under differing reaction conditions. The products were heated to $\simeq 600^{o}C$ under a nitrogen atmosphere, and their thermal decomposition processes traced.

All of the adducts gave an identical trace (Figure 2.1)

Summary of Reaction Conditions used

in the Study of the $SnCl_2$: glycylglycine System

Reactants	Reaction Time	Product
$SnCl_2$:H_2glygly	20 minutes	$SnCl_2.2C_4H_8N_2O_3$
	30 minutes	"
	45 minutes	"
	60 minutes	"
$SnCl_2$:$2H_2$glygly	40 minutes	"
	90 minutes	"
$SnCl_2$:$4H_2$glygly	45 minutes	glycylglycine
	50 minutes	"
$2SnCl_2$:H_2glygly	45 minutes	$SnCl_2.2C_4H_8N_2O_3$
$3SnCl_2$:$2H_2$glygly	45 minutes	"
$SnCl_2$:H_2glygly	>10 hours	"
$SnCl_2$:H_2glygly	>10 hours	$ClSnC_4H_7N_2O_3$

Table 2.1

Analytical Data for the Complexes

(%: calculated values in parentheses)

	Sn	Cl	C	H	N
$ClSnC_4H_7N_2O_3$	42.5	11.5	16.7	2.40	10.0
	(41.63)	(12.45)	(16.83)	(2.45)	(9.82)
$SnCl_2.2C_4H_8N_2O_3$	26.6	15.7	20.5	3.51	11.6
	(26.16)	(15.65)	(21.15)	(3.52)	(12.34)

Table 2.2

X-ray Powder Data for $SnCl_2 \cdot 2C_4H_8N_2O_3$

$SnCl_2$	$SnCl_2 \cdot 2C_4H_8N_2O_3$		glycylglycine
d(Å)	d(Å)		d(Å)
8.42 s	9.41 s	3.59 w	10.40 w
5.51 v.s	8.51 v.s	3.53 w	9.21 w
4.23 v.w	8.97 s	3.48 w	7.89 s
4.08 w	8.55 m	3.33 v.w	5.98 m
3.82 m	8.24 w	3.30 w	5.91 s
3.65 s	5.44 w	3.26 v.w	4.21 v.s
3.55 w	5.21 m	3.22 m	4.06 m
3.40 m	4.87 v.w	3.07 w	3.83 v.s
2.82 m	4.77 m	2.98 m	3.66 v.s
2.75 w	4.67 w	2.92 m	3.22 v.v.s
2.71 m	4.51 v.w	2.86 v.w	3.05 m
2.64 w	4.39 m		3.01 m
	4.19 m		2.93 m
	4.11 w		2.58 v.s
	4.07 w		2.52 w
	3.95 m		2.39 w
	3.86 w		2.35 m
	3.69 w		
	3.65 m		

v.v.s: very very strong; v.s: very strong;

s: strong; m: medium;

w: weak; v.w: very weak;

Table 2.3

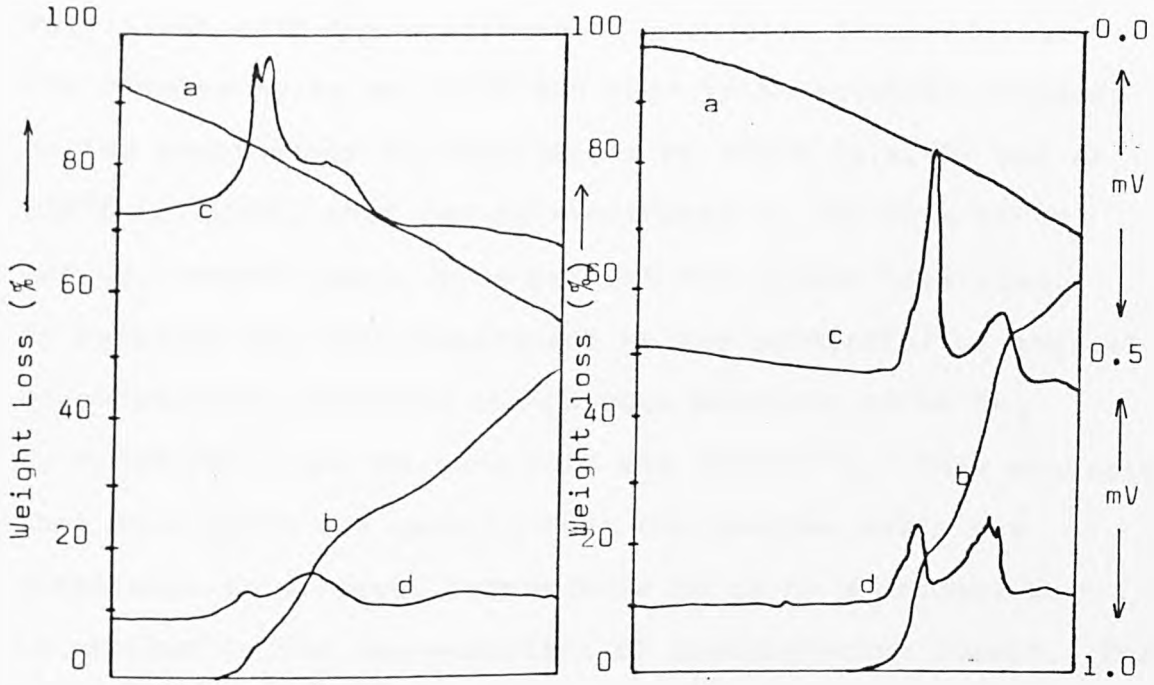

Figure 2.1 TG/DTA trace of $SnCl_2.2L$

Figure 2.2 TG/DTA trace of glycylglycine

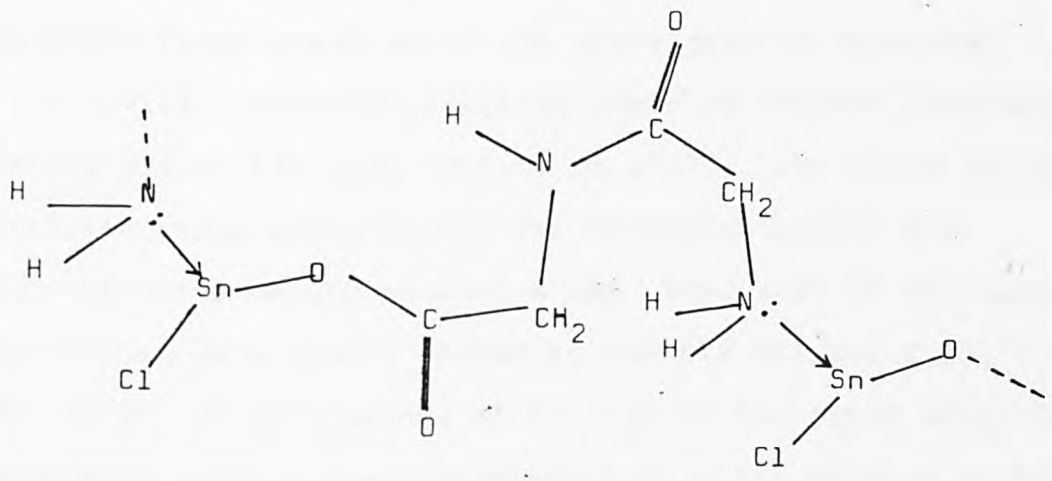

Figure 2.3 Polymeric structure of $ClSn(C_4H_7N_2O_3)$

consistent with the elemental analyses. The thermal decomposition process of the adduct $SnCl_2.\ 2(C_4H_8N_2O_3)$ is consistent with the existence of weak Sn-N interactions. The complex melts at 192°C and this is immediately followed by two endothermic decompositions at 204°C (c.a.6%) and at 230°C (c.a.20%) that can be attributed to the loss of NH_3 and CO_2 respectively, from both of the ligand molecules. An infrared gas cell experiment on the product(s) of thermal decomposition confirmed the gaseous products to be NH_3 (ν = 3585cm^{-1}) and CO_2(ν = 2340 and 2360cm^{-1}). This suggests that Sn-N bonds are weak in that the complex melts and decomposes in a narrow temperature range by a process that is similar to the decomposition of glycylglycine itself. The initial weight loss (c.a.18%) in the decomposition process of glycylglycine occurs at 215°C and this is followed by a second weight loss (c.a.30%) at 243°C. Above ≃ 340°C the decomposition process is continuous which is consistent with the final break up of the glycylglycine molecule.

Tin(II) chloride glycylglycinate decomposes thermally losing 37% of its total weight at 204°C. The first decomposition stage accounts for the decomposition of the glycylglycine moiety in such a way that some of the carboxylate oxygens remain bonded to the tin (Figure 2.3). The weight of the residue at the end of the first stage is consistent with a reaction product of a 1:1 mixture of SnO and $SnCl_2$. This first stage of decomposition is followed by slow loss of $SnCl_2$ at higher temperature.

2.1.4 Infrared Spectra

The infrared spectra of the products of the $SnCl_2$:

glycylglycine system were obtained as mulls of nujol and hexachlorobutadiene in the region 4000-2500cm^{-1} using a Perkin Elmer 580 infrared spectrometer.

The main features of the ir spectra of $ClSn(C_4H_7N_2O_3)$ and $SnCl_2.\ 2(C_4H_8N_2O_3)$ are given in Table 2.4. The spectrum for the chloride glycylglycinate shows changes in the regions of the $-NH_2$ and $-CO_2$ vibrations of glycylglycine on bond formation. The shifts in frequency and the appearance of new bands in the 3000-3400cm^{-1} region of the spectrum are characteristic of the formation of a bond between the N of the $-NH_2$ group and the acceptor metal[8]. There are also significant changes in the symmetric and asymmetric vibrations of the $-CO_2$ group that are consistent with the formation of Sn-O bonds with the carboxylic acid moiety in an ester type bond[9]. There is very little difference in the frequencies of the $\upsilon_{C=O}$ vibrations in the spectra of $ClSn(C_4H_7N_2O_3)$ and glycylglycine compared with those in the carboxylate CO region. This suggests that there is no bond formation between the peptide oxygen atom and the tin.

The appearance of new and broadened bands in the infrared spectra at 612 and 555cm^{-1} are also in agreement with the formation of Sn-O and/or Sn-N bonds. The infrared data are thus consistent with tin(II), in $ClSn(C_4H_7N_2O_3)$, achieving its usual pyramidal three coordination [3] with the formation of Sn-Cl, Sn-O and Sn-N bonds perhaps in a polymeric structure of the type shown in Figure 2.3.

In contrast to the data for $ClSn(C_4H_7N_2O_3)$ the infrared spectrum for the adduct can only be consistent with the

Infrared Data for the Complexes

$ClSnC_4H_7N_2O_3$ (cm^{-1})	$SnCl_2.2(C_4H_8N_2O_3)$ (cm^{-1})	Assignment
3320	3360	)
3250	3295	) υ_{NH_2}
3100	3135	)
1678	1678	)
1663	1662	) $\upsilon_{C=O}$
1622	1605	υ_{asCO_2}
1557	1558	δNH
1384	1410	υ_{CO_2}

Table 2.4

^{119}Sn Mössbauer Data for the Complexes and Related Compounds

Compound	δ(mms^{-1})*	Δ(mms^{-1})	Ref.
$ClSn(C_4H_7N_2O_3)$	3.42	1.76	a
$SnCl_2.2(C_4H_8N_2O_3)$	3.31	1.65	a
$SnCl_2$	4.12	0	10
$Sn(CH_3CO_2)_2$	3.21	1.77	11
$SnCl_2$.2 morpholine	2.81	2.24	12

a. this work; * Relative to $BaSnO_3$ at 80K

Table 2.5

formation of Sn-N(amino) bonds. The significant differences between the spectra of the adduct and the free ligand are in the ν_{NH_2} region in which $SnCl_2.2(C_4H_8N_2O_3)$ shows peaks at 3360, 3295 and 3135cm^{-1}. There are no differences between the spectrum of the adduct and the free ligand in the ν_{CO} (1678 and 1662cm^{-1}), δNH(1558cm^{-1}), $\nu_{as\ CO_2}$(1605cm^{-1}) and $\nu_{sym\ CO_2}$ (1410cm^{-1}) regions.

2.1.5 ^{119}Sn Mössbauer Spectra

The ^{119}Sn Mössbauer data for the tin(II) chloride glycylglycine phases are compared in Table 2.5, with those for other compounds with Sn-O, Sn-Cl and Sn-N bonds. The values of the chemical isomer shift and quadrupole splitting parameters for $ClSn(C_4H_7N_2O_3)$ are much closer to those of $Sn(CH_3CO_2)_2$ than $SnCl_2$. This suggests that a strong Sn-O bond is formed when glycylglycine reacts with tin(II). This is consistent with the thermal decomposition data that suggest the residue of pyrolysis is a mixture of SnO and $SnCl_2$.

The shift for $SnCl_2.2(C_4H_8N_2O_3)$ is lower than that for $SnCl_2$, and this is consistent with complex formation. Two main types of tin(II) chloride adduct are possible *viz*., (1) the formation of a trigonal pyramidal tin(II) moiety by coordination to only one donor atom of the ligand or (2) the formation of a distorted four pyramidal moiety by coordination to two donor atoms of the ligand. There is no evidence from thermal or ir data to suggest the presence of two different types of glycylglycine. This means that the two glycylglycine ligands must be in similar environments and that the tin adopts a four pyramidal

coordination with two strong Sn-Cl and two weak Sn-N interactions. The higher shift of 3.31mms^{-1}, in comparison to a typical $SnCl_2$ adduct with nitrogen donor molecules such as $SnCl_2$.2 morpholine, is also consistent with the presence of only weak Sn-N interactions in $SnCl_2.2(C_4H_8N_2O_3)$.

The relatively large quadrupole splittings found in $ClSn(C_4H_7N_2O_3)$ and $SnCl_2.2(C_4H_8N_2O_3)$ are expected in view of the low symmetry environments containing a lone pair, with bonds from Sn(II) to a mixture of different atoms.

2.1.6 Summary

This study of the tin(II) chloride and glycylglycine system has shown that it is possible to obtain two distinct products resulting from different types of reaction of tin(II) chloride moieties. The main product of reaction is the adduct $SnCl_2.2(C_4H_8N_2O_3)$ in which tin(II) chloride acts as the acceptor species, but it is also possible to obtain the product $ClSn(C_4H_7N_2O_3)$ that results on HCl elimination from a reaction between $SnCl_2$ and the glycylglycine.

2.2 Tin(II) Chloride Adducts with Purine and Pyrimidine Bases and Nucleosides

In section 2.1 reference was made to the fact that tin(II) chloride forms adducts of the type $SnCl_2.L_n$ with molecules of biological interest, other than glycylglycine. Tin(II) chloride is known to form adducts with a wide variety of oxygen and nitrogen donor molecules[12-16] but there are no detailed reports of complex formation with purine and pyrimidine bases or nucleosides. Moreover, relatively few complexes of tin(II) chloride with multidentate ligands have

been studied. The work described in this section deals with the formation of adducts between tin(II) chloride and purine and pyrimidine bases or nucleosides that could act as multidentate ligands.

2.2.1 Preparation of Complexes

All of the complexes described in this work were prepared by refluxing a solution containing $SnCl_2$ in dry methanol with either an equimolar proportion of ligand (Figure 2.4a-c) or a two-fold excess of ligand (Figure 2.4. d,e) under an atmosphere of oxygen-free nitrogen for 3-10 hours. The products were filtered under nitrogen, washed with dry methanol and dried under vacuum.

2.2.2 Analysis of Complexes

Tin analyses of the products were carried out both by a tin(IV) oxide gravimetric procedure and by the Donaldson and Moser method[7]. Chlorine was determined by potentiometric titration and by titration with mercuric perchlorate following the destruction of organic matter by the oxygen flask method. Carbon, hydrogen and nitrogen assays were determined at the Laboratorio di Chimica Organica, (Milan).

For these complexes thermogravimetry was only used to determine the weight loss at low temperatures ($<150^{o}C$) attributable to methanol. No attempt was made to study the decomposition of the complexes at higher temperatures. The complete set of analytical data is given in Table 2.6 with only the average of three separate determinations quoted.

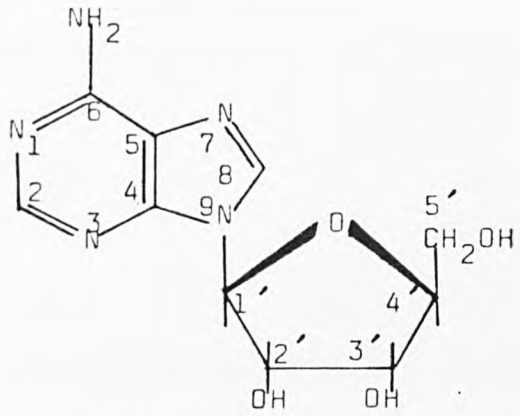

(a) Adenosine

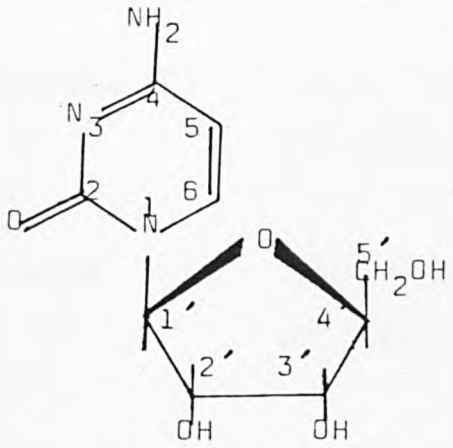

(b) Cytidine

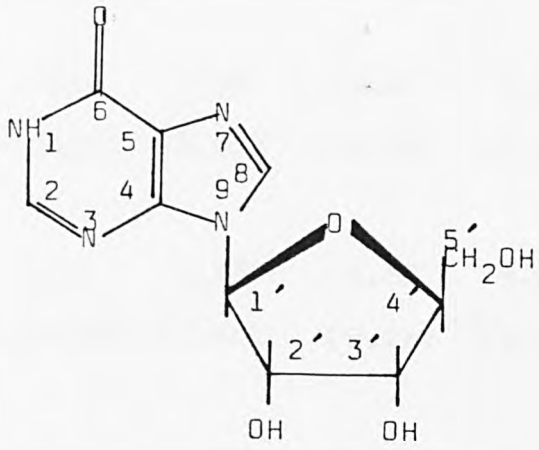

(c) Inosine

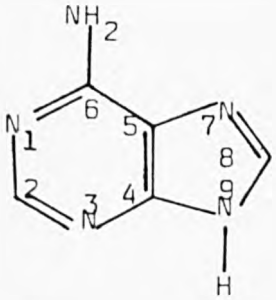

(d) Adenine

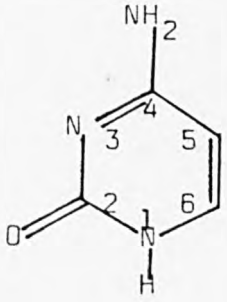

(e) Cytosine

Figure 2.4 Ligands of purine and pyrimidine bases and nucleosides

Analytical Data for the Complexes

$SnCl_2.L_n.CH_3OH$

(%: calculated in parentheses)

$SnCl_2.L_n.CH_3OH$		Sn	Cl	C	H	N	CH_3OH
L=	n=						
adenine	2	23.7	13.7	26.9	2.71	28.9	7.0
		(24.13)	(14.40)	(26.85)	(2.86)	(28.47)	(6.5)
cytosine	2	26.3	16.1	24.9	2.80	18.8	8.0
		(26.74)	(15.98)	(24.35)	(3.18)	(18.93)	(7.2)
adenosine	1	25.1	14.4	26.8	3.30	14.4	6.0
		(24.28)	(14.50)	(27.02)	(3.05)	(14.32)	(6.5)
cytidine	1	25.6	16.1	26.2	3.40	9.60	8.0
		(25.53)	(15.25)	(25.83)	(3.68)	(9.04)	(6.9)
inosine	1	24.1	15.0	27.5	3.06	11.6	6.5
		(24.23)	(14.47)	(26.97)	(3.29)	(11.43)	(6.5)

Table 2.6

2.2.3 Infrared data for the Complexes

The infrared spectra for the complexes were recorded using a Perkin Elmer 580 infrared spectrometer. Table 2.7 contains the more important ir frequencies for these tin(II) chloride complexes.

Small changes are observed in the ν_{NH_2} vibrations and in the vibrations of the purine and pyrimidine rings for all the complexes in comparison with the data for the free ligands. These changes appear to occur as a result of inductive effects in the systems irrespective of the site of coordination to the tin[17]. The most significant change observed in the adenine complex in comparison with the free ligand species is the loss of the δ_{N-H} frequency associated with the atom N(9) of the free ligand (Figure 2.4). This suggests the coordination of adenine to tin(II) chloride occurs at N(9), which is the usual coordination site for unblocked adenine type ligands to metal moieties[18]. The spectra of the adenine complex also contain a new band at 280cm^{-1} assignable to the Sn-Cl vibration.

The ligand cytosine usually forms complexes to metal species at the heterocyclic N(3) atom. Coordination at this site usually results in formation of strong bands in the C=O stretching region of the spectrum[18]. The appearance of the band at 1722cm^{-1} in the $SnCl_2(cytosine)_2 . CH_3OH$ complex and the fact that the δ_{N-H} in plane and out of plane frequencies associated with N(1) are not changed in going from the ligand to the complex is consistent with coordination at N(3). The value of $\nu_{C=O}$ of 1722cm^{-1} is higher than the value in the free ligand in contrast to the lower

Infrared Data for the Complexes

$SnCl_2.L_n.\ CH_3OH$

Adenine (=Ade)	$SnCl_2(Ade)_2\ CH_3OH$	Assignment
3350 w	3320 w	
3282 m	3160 w	ν_{NH_2} as.
3262		
3100 m,bd		
1672 s	1682	δNH_2 in plane purine ring
1605 s	1605 m	
1540 w		
870 m		δ(N(9)-H)
	280 w	ν_{Sn-Cl}

Cytosine (=Cyt)	$SnCl_2(Cyt)_2CH_3OH$	Assignment
3367 s	3340 m,bd	ν_{NH_2} as.
3160 s	3180 m.bd	
1700 v	1722 s	$\nu_{C=O}$
1660 s	1677 s	$\delta(NH_2)$
1635 w		
1615 w		
1538 m	1542 m	δ(N(1)-H) in plane
1275 s	1275 s	δ (C-NH_2)
823 m	823 m	δ (N(1)-H) out of plane
	330 m	ν_{Sn-Cl}

Table 2.7

Infrared Data for Complexes (cont.)

Adenosine (=Ads)	$SnCl_2.Ads.CH_3OH$	Assignments
3320 s	3320 m	
3125 s	3140 m	ν_{NH_2} as
	3100 w	
1670 s	1685 s	$\delta(NH_2)$ in plane vibrations of the purine nucleus
1605 s 1575 m	1605 m	
	1092 s,bd	ν_{C-O} in C-OH | Sn
	320	ν_{Sn-Cl}

Cytidine (=Cyd)	$SnCl_2$. $Cyd.CH_3OH$	Assignments
3448 s	3340 s	
3340 s	3180 m	ν_{NH_2} as
3270 w		
3220 s,bd		
1660 s	1670 s	$\delta(NH_2)$
1645 s	1625 s	$\nu_{C=O}$
1607 s		
1530 s		
1498 s		
1290 s	1290 s	$\nu_{(C-NH_2)}$
	1090 s,bd	ν_{C-O} in C-OH | Sn
	320 w	ν_{Sn-Cl}

Table 2.7

Infrared Data for the Complexes (cont.)

Inosine (=Ino)	$SnCl_2$. Ino.MeOH	Assignments
3540 s		ν_{NH_2}
3300 s	3330 m	ν_{NH_2}
	3140 m	
1690 s,bd	1690 s,bd	$\nu_{C=O}$
1598 s		
	1575 s	
1550 s	1552	δ(N(1)-H)
	1080 m,bd	ν_{C-O} in C-OH (Sn)
	320	ν_{Sn-Cl}

w. weak; m. medium; s. strong; bd. broad;

Table 2.7

values found in other metal complexes of the type M (cytosine)$_2$ X$_2$ compounds[18] which all have $\nu_{C=O}$ values lower than 1703cm^{-1} in cytosine. Values of $\nu_{C=O}$ higher than the cytosine value are however, found in hydrated M (cytosine)$_2$ X$_2$ compounds and interpreted in terms of hydrogen bonding of cytosine to solvate molecules which in turn are coordinated to the metal ion[19]. It is possible that the band at 1722cm^{-1} arises because of the presence of solvated methanol, but it is unlikely that the methanol could be coordinated to the tin. The band at 330cm^{-1} in the cytosine complex is assigned to ν_{Sn-Cl}.

The adenosine ligand can be regarded as an adenine molecule with the favoured N(9) donor atom position blocked so that coordination must occur either through other nitrogen atoms of the nucleoside or through oxygen atoms of the carbohydrate groups. The only major changes in the spectra of the adenosine complex in comparison with the free ligand are in the C-O stretching region of the carbohydrate group.

The changes in the heterocyclic ring system on complex formation are typical of those found when bonding to a metal occurs at any atom in the molecule, including at the carbohydrate oxygen atom[20]. The ir data therefore suggest that at least one of the carbohydrate hydroxyl groups is bonded to the tin. The data do not however, exclude the possibility of donation either by both oxygens in the carbohydrate hydroxyl groups or from one of these oxygen atoms and N(7) from the pyrimidine ring. The band at 320cm^{-1} in the adenosine complex is assigned to ν_{Sn-Cl}. The major changes in the spectra of the tin(II) chloride complexes with cytidine

and inosine are also in the ν_{CO} stretching region of the carbohydrate group and the bonding to the tin is presumably similar to that in the adenosine complex. Bands in the cytidine and inosine complexes at 320cm^{-1} are again assigned to Sn-Cl vibrations.

2.2.4. ^{119}Sn Mössbauer Spectra

^{119}Sn Mössbauer data for the complexes (1-5) are compared with those for related compounds in Table 2.8.

The chemical isomer shifts for the new complexes lie in the narrow range 3.40 - 3.55mms^{-1} and are lower than that for $SnCl_2$. This is consistent with complex formation involving the replacement of a bridging chloride in the trigonal pyramidal coordination of tin(II) chloride with stronger tin(II) to donor atom bonds. The ir data for the complexes $SnCl_2.L.CH_3OH$ (3-5) show that the tin atoms are bonded to oxygen atoms of the carbohydrate groups in the ligands. The data for the $SnCl_2.L_2CH_3OH$ complexes (1-2), however, show that the tin is bonded to ligand N-atoms. It is known that there are two main types of tin(II) chloride adduct possible, involving formation of either a trigonal pyramidal tin(II) moiety by coordination to only one donor atom eg. the tin environment in $SnCl_2.2H_2O$[21], or a distorted four pyramidal moiety such as the tin(II) environment in $SnCl_2$. 1.4 dioxan[22].

The difference in chemical shift values of the complexes is a measure of the disruption of the tin bonding electrons in tin(II) chloride on complex formation. This in turn, gives an indication of the donor strength of the ligands in complexes such as the nucleoside complexes

^{119}Sn Mössbauer Data for the Complexes

$SnCl_2.L_n.CH_3OH$

Compound	$\delta(mms^{-1})$	$\Delta(mms^{-1})$	Ref.
1. $SnCl_2.(Cyt)_2CH_3OH$	3.43	1.45	a
2. $SnCl_2.(Ade)_2CH_3OH$	3.40	1.60	a
3. $SnCl_2.(Ads)\ CH_3OH$	3.50	1.54	a
4. $SnCl_2.(Cyd)\ CH_3OH$	3.39	1.57	a
5. $SnCl_2.(Ino)\ CH_3OH$	3.55	1.54	a
6. $SnCl_2.$	4.12	0	b
7. $SnCl_2.2H_2O$,	3.68	1.21	b
8. $SnCl_2$.1.4 dioxan	3.76	1.61	b
9. $SnCl_2$.py	3.29	0.98	c
10. $SnCl_2$.piperazine	2.87	2.17	d
11. $SnCl_2$.2 morpholine	2.81	2.24	d
12. $SnCl_2$.2 piperidine	2.81	2.21	d

a. This work; b. Ref. 15; c. Ref. 13; d. Ref 12,16;

Table 2.8

described here.

Comparison of the Mössbauer chemical shift data for the nucleoside complexes (3-5), with those of the oxygen-containing $SnCl_2$ adducts (7,8) in Table 2.8 shows that the Sn-O bonds formed in the $SnCl_2$ nucleoside complexes must be somewhat shorter than those found in $SnCl_2.2H_2O$[21] or $SnCl_2$. 1.4 dioxan[22]. The tin-oxygen bonds of 2.32Å in the dihydrate and 2.54Å in the 1.4 dioxan complex are considerably longer than the typical Sn-O bond length[23], representing a weak donor-acceptor interaction. It can be assumed therefore that this somewhat shorter Sn-O bond in the nucleoside complexes is still a relatively weak bond. The chemical isomer shifts for the adenine and cytosine complexes (1,2) are higher than those found in typical $SnCl_2$ adducts with nitrogen-donor molecules such as $SnCl_2$.py or $SnCl_2$.2 Morpholine, suggesting that the Sn-N interactions in these $SnCl_2$ nucleoside complexes are relatively weak.

The Mössbauer quadrupole splitting values for compounds 1 - 5 are in the range 1.45 - 1.60mms^{-1} and would be consistent with low symmetry tin environments containing a lone-pair of electrons and a weak tin-ligand interaction.

2.2.5 Summary

The fate of the tin(II) moiety, $SnCl_2$, in chemical reaction with such donor molecules as adenine, adenosine, cytosine, cytidine and inosine has been studied. Two types of complexes are identified: $SnCl_2.L,CH_3OH$ (L= adenosine, cytidine and inosine) and $SnCl_2.L_2.CH_3OH$ (L = adenine and cytosine). The ^{119}Sn Mössbauer shift data for the complexes suggest that the bonds between tin(II) chloride and

the donor atoms of the ligands are relatively weak.

2.3 Adducts of Tin(II) Compounds containing Nitrogen, Oxygen and Sulphur Donor atoms

Covalent SnX_2 compounds have an empty p-orbital, of similar energy to those used in bonding, and should act primarily as monofunctional acceptors towards suitable donor molecules. Although many of the adducts that have been reported are 1 : 1 complexes, a number of polyligand species have also been prepared[4]. It has been suggested[24] that the second ligand in materials of type SnX_2. 2L, is in fact present only for lattice packing purposes. However, in the crystal structure of $SnSO_4$.2tu (tu = thiourea)[25], the thiourea moieties are bonded to the tin by two sulphur atoms at distances 2.62 and 2.86Å. The difference between the two bond lengths is not quite large enough to justify the assumption that one of the thiourea ligands is a lattice ligand and is not bonded to the tin. In view of this observation a study of the thermal decompositions of a number of thiourea adducts have been studied to obtain information on the bonding of the ligand to the tin species and have been compared with the data for 4 adducts *viz*. $SnCl_2$. $2H_2O$: $SnCl_2$. 2 pyridine : $SnCl_2$.2DMSO and $SnCl_2$. 2 piperidine, for information on the fate of the tin and ligand moieties on pyrolysis.

2.3.1 Thermal Analysis of Adducts of Tin(II) Compounds with donor atoms

In order to understand the modes of decomposition of the adducts (Table 2.9) it is necessary to consider the effects of temperature on the free ligands. Four of the

Thermal Decomposition Data for Adducts of Tin(II) Compounds with Donor Atoms

Complex	Temp.(°C)	Weight Loss (%)	
$Sn(ac)_2(tu)_2$	145	0	Melting
	145	30	
	169	16	
	360	15	
$Sn(form.)_2tu$	120	0	Melting
	133	35	
	210	13	
$SnSO_4.\ 2tu$	94	2	
	169	22	
	226	13	
	350	13	
$2SnSO_4.5tu.\ 2H_2O$	140	0	Melting
	142	15	Loss of SO_2
	169	35	
	258	7	
	390	23	
$SnCl_2.\ tu$	169	0	Melting
	192	20	
	258	10	
	310	35	

Table 2.9

Complex	Temp.(°C)	Weight Loss (%)	
$2SnCl_2.5tu.\ 2H_2O$	66	4	Loss $2H_2O$.
	120	0	Melting
	169	40	
	258	11	
	350	18	
$SnBr_2.\ tu$	145	0	Melting
	169	2	
	192	10	
	285	25	
	390	52	
$2SnBr_2.5tu.\ 2H_2O$	80	4	Loss $2H_2O$.
	133	0	Melting
	169	26	
	279	22	
	370	35	
$SnCl_2.\ 2H_2O$	51	8	
	145	9	
	248	0	
	360	74	
$SnCl_2.\ 2py.$	49	22	Loss 1 py.
	150	46	
	324	44	

Table 2.9 (continued)

Complex	Temp.(°C)	Weight Loss (%)	
$SnCl_2$. 2DMSO	66	0	Melting
	78	22	Loss of 1 L
	192	45	
	266	6	
$SnCl_2$. 2piperidine	169	0	Melting
	197	24	Loss of 1 L
	341	48	

Table 2.9 (continued)

ligands studied, vaporize without decomposition at their boiling points *viz*. H_2O (100°C), DMSO (189°C), pyridine (115°C) and piperidine (106°C). Thiourea, on the other hand undergoes a multistage decomposition, and its pyrolysis was studied for comparison with the adducts. Thiourea melts at 178°C, and this process is accompanied by a sharp endothermic peak on the DTA trace. Ammonium thiocyanate sublimes off at a temperature slightly higher than the melting point and then decomposes to form ammonia, hydrogen cyanide and sulphur.

Thiourea tin(II) acetate:- Stannous acetate is known[26] to melt at 182.5 - 183°C and to boil at 239 - 241°C. When it is heated under an atmosphere of oxygen free nitrogen, in a flask, the material decomposes giving a black residue (tin(II) oxide) and a white sublimate (stannous acetate). The complex, thioureatin(II) acetate melts at 145°C, at which temperature there is indication of the onset of decomposition. The initial loss of 45% weight is a two stage decomposition, that can be explained in terms of the complete breakdown of the ligand and the volatilization of part of the stannous acetate leaving a residue which was identified by Mössbauer spectroscopy as being stannous oxide. The formation of this residue indicates that the Sn-O bonds to the acetate moiety are stronger than the Sn-S bonds to thiourea molecules.

Thiourea tin(II) formate:- Stannous formate[27] decomposes without melting at 198-200°C. When it is heated under an atmosphere of oxygen free nitrogen, in a closed flask, the material decomposes giving a black residue and a white sublimate. Unlike its parent compound, the complex melts at

120°C and then undergoes an apparent one-stage weight loss decomposition of ≈ 35% although the DTA and DTG peaks suggest the decomposition process is more complex. This decomposition step, like that of the acetate complex, can be explained in terms of the complete degradation of the ligand and volatilization of trioxymethylene. Analysis of the final product , as SnO indicates the fate of the tin in the complex formation, in which the Sn-O bonds to the formate group are stronger than the Sn-S bonds to the thiourea molecules.

Dithioureatin(II) sulphate and Pentathioureatin(II) sulphate:

The decomposition of both the penta- and di-thiourea tin(II) sulphate derivatives were studied. The main products of the pyrolysis of stannous sulphate at 379°C are known[28] to be SnO_2 and SO_2. A significant difference between the two types of complex is that the pentathiourea derivative melts before decomposition while the dithiourea derivative does not. The three stage decomposition of $SnSO_4$. 2tu can be explained in terms of the breakdown of the sulphate group, to give SO_2 and the reaction of the remaining tin moiety with the thiourea to give a yellow residue of stannic sulphide. The weight loss at ≈ 300°C is considered to be due to the removal of SO_2. The complex $2SnSO_4$.5tu, after melting at 140°C, immediately loses 15% of its weight. This weight loss is accompanied by a very sharp endothermic DTA peak, which corresponds to the removal of SO_2. The loss of SO_2 at such a low temperature in comparison to its removal in $SnSO_4$. 2tu at ≈ 300°C and $SnSO_4$ at 379°C, suggests that

$2SnSO_4 5tu$ has reacted in such a way during melting, as to alter the tin environment, thus enabling SO_2 to be readily evolved. The complex continues to break down losing three molecules of thiourea during a process of volatilization of ammonium thiocyanate. The final breakdown of the thiourea group follows a reaction of the tin moiety with the thiourea, to give a yellow residue of the stannic sulphide. This residue of SnS_2, after decomposition of both complexes, is sufficient evidence to assume that tin(II) in the stannous sulphate thiourea derivatives forms Sn-S bonds to two thiourea moieties.

Thioureatin(II) chloride and Pentathioureaditin(II) tetra-chloride dihydrate: Stannous chloride melts sharply at 248°C and then decomposes losing 100% weight. Complex formation with one molecule of thiourea lowers the melting point of $SnCl_2$ to 169°C. The subsequent three-stage decomposition which begins at 192°C involves the breakdown of part of the $SnCl_2$ and thiourea, while the remaining tin(II) chloride volatilizes off at ≈ 310°C leaving a black residue which is known to be stannous sulphide. The pentathiourea dihydrate loses its two molecules of water at 66°C and then melts at 120°C, after which the complex breaks down losing four molecules of thiourea by volatilization of NH_4CNS. The decomposition process that follows is like that of the monothiourea derivative, in which there is partial breakdown of the tin chloride moiety and thiourea leaving the remaining $SnCl_2$ to volatilize off at ≈ 350°C, and give a final residue of tin(II) sulphide. The final residue of stannous sulphide for both the mono and pentathiourea derivatives, suggests

there is a strong tin-to-sulphur bond to one thiourea molecule.

Thioureatin(II) bromide and Pentathioureatin(II) tetrabromide dihydrate: The parent material, stannous bromide melts at 226°C and then decomposes. Like the chloro-complexes the two derivatives melt before decomposition. Each of the compounds, on melting, must undergo a chemical reaction thus altering the environment of the tin. The monothiourea derivative melts at 145°C and then decomposes in three stages. Like its chloro-analogue, the first stage and the second stage of decomposition involve the break up of the thiourea moiety. The subsequent decomposition is unlike that of the chloro-complex in that the decomposition goes almost to completion with the products volatilizing off as tin(II) bromide before the tin can form stannous sulphide. After the initial loss of water from the pentathiourea bromide derivative the complex melts at ≃ 120°C. The subsequent decomposition involves the volatilization of NH_4CNS and the complete breakdown of the thiourea moieties. As with the monothiourea complex the final stages of decomposition are accounted for by the volatilization of $SnBr_2$ before the formation of the stannous sulphide. This preference for the tin to remain bonded to bromine suggests that the tin atom is only weakly bonded to the thiourea molecule via the sulphur atom.

Tin(II) Chloride Dihydrate: Tin(II)chloride dihydrate melts at 51°C and loses one molecule of water. This melting is effectively the dissolution of the tin(II) chloride in its own water of crystallization. The second molecule of

water boils off at ≃ 150°C, after which the material solidifies and then melts at 248°C. Finally stannous chloride volatilizes off at ≃ 360°C. The removal of the two molecules of water at different stages suggests that only one water molecule is strongly bonded to the tin.

Tin(II) Chloride Bipyridine: The compound melts at 49°C and proceeds to decompose in three major stages of weight loss. The first weight loss of 24% material at 49°C is followed by a further loss of≃24% at 150°C. Both these weight losses are due to the removal of the ligands leaving tin(II) chloride which volatilizes off at 324°C. The separate removal of the ligands implies that only one of the pyridine molecules is strongly bonded to the tin.

Tin(II) Chloride. 2Dimethylsulphoxide: The complex melts at 66°C and loses one ligand of DMSO at 78°C. The subsequent decomposition of the material is a multistage process. It is clear however, that only one DMSO molecule is strongly bonded to tin and the removal of this second ligand is not as simple as observed in the dihydrate and bipyridine complexes described earlier. The complicated loss of the second DMSO molecule is the result of a reaction to give a tin(IV) species. The fate of the tin on reaction was identified by recording a Mössbauer spectrum of the product collected after loss of the first ligand.

Tin(II) Chloride 2Piperidine: The complex melts at 169°C, and at 197°C begins to lose the first molecule of piperidine. The removal of the second ligand at ≃ 340°C is not simple, but the thermal decomposition shows the Sn-N bonds are relatively strong.

2.3.2 Summary

The thermal decompositions of four adducts of tin(II) chloride containing molecules of water, pyridine, DMSO and piperidine have been studied. Although the complexity of the decompositions varies, there is sufficient evidence from this thermal analytical study, to conclude that there is a difference in the mode of bonding between tin and the two ligands in $SnCl_2$. 2L type complexes All the materials lose the ligands in separate stages, with the removal of the first occurring at low temperature. The early loss of the first ligand during decomposition strongly suggests that this ligand does not contribute to the bonding in the lattice network but is solely used for lattice packing purposes. This is consistent with the crystal structure determination on $SnCl_2$. $2H_2O$[21] which shows that only one molecule of water is directly bonded to the tin (Sn-O = 2.32Å). The second water molecule forms hydrogen bonds with the water bonded to the tin, giving a two dimensional network of hydrogen bonds. The difficult removal of the second ligand from the complexes $SnCl_2$. 2DMSO and $SnCl_2$. 2piperidine must arise because of the strength of the Sn-L bond, relative to the Sn-Cl bonds.

The results obtained from the thermal analytical study of the series of thiourea adduct complexes of tin(II) compounds provides information on the mode and strength of the bonding in such compounds. The type of product from thermal decomposition is an important indication of the strength of the bond. It is found that the decompositions fall into four classes based on their products of decomposition viz: the carboxylate derivatives which give SnO, the

sulphate complexes which give SnS_2, the chloride species which give SnS and $SnCl_2$ and the bromide derivatives which lose tin as stannous bromide before stannous sulphide can be formed.

The thermal data are consistent with the known structural data published previously on $SnSO_4$. 2tu[25], and described for the first time in Chapter 4 on Sn(acetate)$_2$. 2tu and Sn_2Br_4. 5tu $2H_2O$. In the $SnSO_4$. 2tu structure, the tin is bonded to two oxygens (Sn-O : 2.24Å, 2.41Å) and two sulphur atoms (Sn-S : 2.62Å, 2.86Å). The most covalent bond is the Sn-S distance of 2.62Å and the decomposition results in the formation of a tin sulphide residue. It is interesting that the oxidation of the tin species on pyrolysis results in the formation of SnS_2 and not an oxysulphide. The formation of SnS_2 as a product of pyrolysis of the pentathiourea derivative implies that the tin environment is similar to that in $SnSO_4$. 2tu, and that the fifth thiourea ligand in $2SnSO_4$.5tu must only be used for lattice packing purposes. The complex Sn(ac)$_2$. 2tu has been found to have two Sn-O bonds of ≃ 2.18Å, whilst the shortest Sn-S bonds in the structure are about 2.87Å, which are considered ionic in character[23]. During pyrolysis the tin moiety retains its (II)+ oxidation state and forms tin(II) oxide as a product. The Sn-L bonds in the acetate are weak therefore during decomposition the bonds break, and the complex continues to decompose like stannous acetate. In the same way the formation of stannous oxide as a product of pyrolysis of Sn(formate)$_2$. tu results from the destruction of the Sn-L bonds and the subsequent decomposition of the complex as stannous formate.

In $2SnBr_2.5tu,2H_2O$ there are unusually short Sn-Br bonds of 2.65Å. which are strongly covalent in character. The strength of these bonds is retained during pyrolysis, and the tin moiety volatilizes off as stannous bromide, in preference to strengthening Sn-S bonds. The similar decomposition pattern for the monothiourea derivative, seems to suggest the tin in $SnBr_2$. tu also has strong bonds to the bromine atoms. It can be inferred from the thermal decomposition traces of the $SnCl_2$ complexes that the Sn-Cl bonds, although strong, are relatively weaker than the Sn-Br bonds in the corresponding bromo-derivatives, due to the formation of both $SnCl_2$ and SnS as products of pyrolysis.

In conclusion, therefore, the product of the thermal decomposition of a tin(II) compound seems to depend upon the strength of the covalent bond formed between the metal and the anion. In the case of the adducts there are three types of decomposition viz., (1) in which the tin-ligand bond is weak, and the material decomposes by loss of the ligand and subsequent decomposition of normal tin(II) compounds; (2) in which the Sn-L bond is relatively strong and the ligand reacts with the tin moiety to give a tin(II) species; and finally (3) in which the Sn-L bond is relatively strong and there is reaction between the tin(II) moiety and the ligand to give a tin(IV) species.

2.4 Tin(II) : Mixed Anion Systems

A number of papers have been published on tin(II) systems, in which there is more than one anion present. The majority of these papers are concerned with the mixed tin(II) halides[29-32]. In early work Karantassis[29] described the synthesis of tin(II) iodide chloride and tin(II) iodide bromide by the reaction of iodine on solutions of tin(II) chloride and tin(II) bromide in their parent hydrohalic acids. The results of a study of phases from solutions containing tin(II) and halide ions have been reported[33] together with a description of a number of new ternary tin(II) halides.

Fewer papers have been concerned with oxyacid or carboxylic acid systems. It has been shown that the replacement of one, but not both acetate groups from tin(II) acetate to give compounds of the type $Sn(CH_3COO)(NO_3)$[34] and $Sn(CH_3COO)(C_9H_6NO)$[35] is possible. There are some reports of the preparation of mixed tin(II) halide - tin(II) oxyacid salts[36,37] although the exact nature of the materials is not known. The most recent reports on such mixed anion salts includes details of a potassium tin(II) sulphate thiocyanate[38] and potassium tin(II) chloride- and bromide- sulphates[39] of type $K_3Sn_2(SO_4)_3X$ (X = Cl.Br).

In the present work three mixed anion systems have been studied *viz*: (1) SnF_2 - CsBr (2) Sn: K: SO_4: X (where X = Cl,Br) and (3) Pd: Sn: Cl: I. Systems (1) and (2) are described in the following subsections whilst the study of the third system is detailed in section 2.5.

2.4.1 Preparation and Identification of New Phases from the SnF_2 : CsBr system

Products obtained from the aqueous SnF_2 : CsBr system in the composition range 6:1 to 1:6, have been studied and identified by chemical analysis, X-ray diffraction measurements, and Mössbauer spectroscopy. The phases were obtained by mixing a solution of caesium bromide and a solution of tin(II) fluoride in the appropriate molar proportions, in the minimum amount of water. The products crystallized out under nitrogen, as fine white or yellow acicular crystals, the colour of which was dependent on the proportion of CsBr in solution.

Chemical analyses, X-ray and Mössbauer data were obtained for all the products, and the data show that only four phases were isolated. $CsSn_3BrF_6$ was the first phase precipitated from a 6:1,5:1 and 4:1 composition of SnF_2: CsBr. $CsSn_2BrF_4$ was isolated from a 3:1,2:1 and 1:1 composition of SnF_2: CsBr, with only a mixture of starting materials being isolated from the 1:2 SnF_2 : CsBr phase. A yellow crystalline material was obtained with an excess of CsBr(1:3, 1:4 SnF_2:CsBr) which analysed close to CsBr. $CsSnBrF_2$. In view of the results obtained [40] with perovskite $CsSnBr_3$: $CsSnX_3$ systems the phase CsBr.$CsSnBrF_2$, need not contain stoichiometric proportions of elements. It was assumed that the black crystalline product from the solution containing a large excess of CsBr, was the well-known perovskite $CsSnBr_3$ [41].

The analytical data for the tin and bromine contents only, are given in Table 2.10, for the three isolated phases, $CsSn_3BrF_6$; $CsSn_2BrF_4$; and CsBr.$CsSnBrF_2$. Tin analysis was

Analytical Data for New Phases

isolated from the SnF_2 -CsBr system

(% calculated in parentheses)

Compound	Sn(%)	Br(%)
$CsSn_3BrF_6$	51.2	11.9
	(52.2)	(11.71)
$CsSn_2BrF_4$	45.1	15.5
	(45.19)	(15.21)
$CsBr.CsSnBrF_2$	21.2	27.7
	(20.45)	(27.52)

Table 2.10

^{119}Sn Mössbauer Parameters

	$*\delta mms^{-1}$	Δmms^{-1}	Ref
$CsSn_3BrF_6$	3.46	1.53	a
$CsSn_2BrF_4$	3.43	1.44	a
$CsBr.CsSnBrF_2$	2.93	1.81	a
$SnBr_2$	3.98	0	b
SnF_2	3.65	1.80	c
$CsSnF_3$	2.98	2.00	c
$CsSn_2F_5$	3.12	2.06	c
$CsSnBr_3$	3.98	0	c

* - Relative to $BaSnO_3$

a = This work b = Ref(43) c = Ref(40, 44)

Table 2.11

carried out using the method of Donaldson and Moser[7] and bromine content was determined by the oxygen flask method. The percentage values given for Sn and Br are an average of three separate determinations. Table 2.12 contains the X-ray diffraction data for the three materials, and comparison with the data for the parent materials and related complexes eg. $CsSnF_3$ and $CsSn_2F_5$[42], confirm the existence of three new phases.

The Mössbauer parameters measured at 80K, for the three compounds are given in Table 2.11, together with data for related caesium tin(II) complexes, tin(II) fluoride and tin(II) bromide for comparison. The two complexes isolated from an excess of SnF_2 in solution, have similar chemical shift, and quadrupole splitting values. The chemical shift values indicate there is only one tin site. There is no evidence of a peak corresponding to tin in a bromide environment ($SnBr_2$; $CsSnBr_3$ $\delta = 3.98 mms^{-1}$). In view of the low shift values ($CsSn_3BrF_6$, $\delta = 3.46 mms^{-1}$, $CsSn_2BrF_4$ $\delta = 3.43 mms^{-1}$) it must be inferred that there is no distinct tin-bromine site and that every tin atom must form strong bonds to fluorine. There are two possible structures for the complexes, one in which bromine takes part in the bonding and the other in which the bromine atoms lie in the SnF_2 lattice network and are used for packing purposes only. If the latter were true, the shift values would be expected to be similar to that of SnF_2 ($\delta = 3.65 mms^{-1}$) The observed lowering of shift however, which is consistent with complex formation, makes the preferred arrangement to be one in which the bromine takes part in the bonding,

X-ray Diffraction Data for the New Complexes

$CsSn_3BrF_6$	$CsSn_2BrF_4$	$CsBr.\ CsSnBrF_2$
d spacing (Å)	d spacing (Å)	d spacing (Å)
4.67 w	6.66 w	3.97 m
3.78 m	4.67 w	3.82 s
3.39 vs	3.77 w	3.74 m
3.30 vs	3.40 s	3.46 vs
3.21 w	3.31 s	3.41 m
3.16 m	3.15 w	3.36 m
3.12 s	3.11 w	3.28 w
2.86 m	2.86 vw	3.15 vs
2.84 w	2.83 vw	3.05 vs
2.56 w	2.55 m	2.94 vs
2.55 s	2.15 vw	2.76 w
2.22 vw	2.08 vw	2.58 w
2.19 vw	1.87 vw	2.48 vw
2.15 vw	1.77 m	2.39 w
2.08 vw	1.76 m	2.36 vw
1.99 w	1.69 w	2.31 vw
1.87 w		2.29 vw
1.86 w		2.10 vw
1.84 vw		2.07 vw
1.82 vw		2.02 w
1.77 w		1.92 vw
1.75 w		1.87 vw
1.69 m		1.84 vw
1.66 w		1.76 vw
1.65 m		1.73 vw

Table 2.12

although it is only weakly bonded to the tin.

$CsSn_3BrF_6$

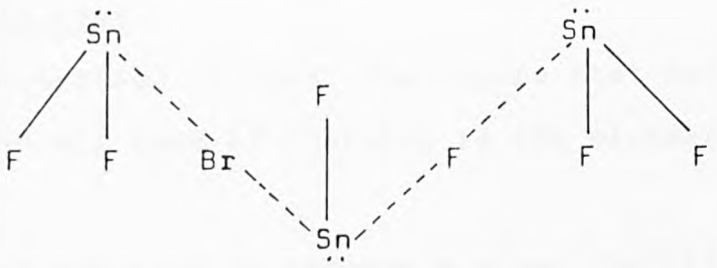

$CsSn_2BrF_4$

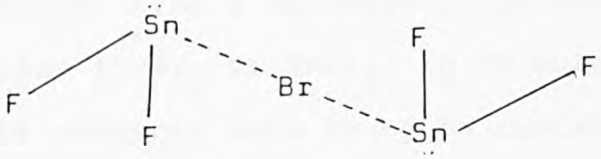

In both structures the tin atom would lie in a trigonal pyramidal environment, with bonds to fluorine, and bridging bromide ions. The species formulated as $CsBr.CsSnBrF_2$, is one in which tin is present as an ion like $[SnF_3]^-$, ($CsBr.CsSnBrF_2$, δ=2.93mms^{-1}, Δ=1.81mms^{-1}, $CsSnF_3$, δ=2.98mms^{-1}, Δ=2.00mms^{-1}). Hence the tin could well exist as $[SnF_2Br]^-$ but with short Sn-F bonds, and the excess caesium bromide is making up the lattice.

In conclusion, therefore, it has been found tin remains strongly bonded to fluorine and this ability to remain so, only breaks down as the ideal structure of the perovskite lattice is approached as in $CsSnBr_3$.

2.4.2 Structure Determination of $K_3Sn_2(SO_4)_3X$

(where X = Cl, Br)

Finagle's Third Law:

In any collection of data, the figure most obviously correct, beyond all need of checking is the mistake.

An attempt was made to prepare a mixed tin(II) halide-acetate complex, from a solution of potassium acetate and tin(II) halide ($SnBr_2$ or $SnCl_2$) in 2M sulphuric acid but the products obtained were found to contain SO_4^{2-} and halide but no acetate. The complexes isolated were in fact, the chloro- and bromo- potassium tin(II) sulphates $K_3Sn_2(SO_4)_3X$ (where X = Cl, Br). Moser et al[39] had previously reported the preparation of these complexes using tin(II) sulphate as a starting material, and described their attempts to determine their crystal structures. Although they suggested that the chloro-and bromo-compounds had structures closely related to chloroapatites, with SO_4^{2-} replacing PO_4^{3-}, the structure factor calculations on their predicted model gave an R value of 0.30. Improved data sets were collected for both the chloro- and bromo- complexes in this work to obtain better structural data.

Preparation of the Crystal

The appropriate tin(II) halide was dissolved in a solution of potassium acetate in the molar ratio 1 : 5, and the mixture was heated in the minimum amount of 2M sulphuric acid. Colourless acicular crystals formed when the solutions were cooled. The products were filtered off and dried in a desiccator over KOH pellets. Crystals from both the halide

systems were used to obtain cell data and were found to be isostructural. (Table 2.13)

Determination of the Space Group and Cell Dimensions

The crystal data were obtained from Weissenberg and single crystal precession data, and refined on the basis of the powder diffraction pattern. Details of the data for the chloro- and bromo-complexes are given in Table 2.14 Single crystal intensity data were collected at Queen Mary's College, London, using a four-circle diffractometer.

On the basis of the systematic absences, the crystals were assigned to the space group $P6_3$ or its centrosymmetric alternative $P6_{3/m}$ (Nos. 173 and 176 respectively in the International Tables of X-ray crystallography[45]).

Location of Atomic Positions

The X-ray crystallographic programs used throughout the crystal structure determination are described in Chapter 1.

The atomic positions were located as a result of a heavy atom Patterson synthesis. The equivalent positions in the space group $P6_3$ are:-

$X, \quad Y, \quad Z; \quad \bar{Y}, \quad X-Y, \quad Z; \quad Y-Z, \quad \bar{X}, \quad Z;$

$\bar{X}, \quad \bar{Y}, \quad \frac{1}{2}+Z; \quad Y, \quad Y-X, \quad \frac{1}{2}+Z; \quad X-Y, \quad X, \quad \frac{1}{2}+Z;$

with two sets of twofold special positions at :-

0, 0, 0; 0, 0, 1/2:

1/3 2/3 0; 1/3 2/3 1/2:

The six sets of general positions give peaks in the Patterson vector map at:-

$X + Y, \quad 2Y - X, \quad 0$

$2X - Y, \quad X + Y, \quad 0$

Crystal Data for the Complexes

$K_3 Sn_2(SO_4)_3 X$

	$K_3Sn_2(SO_4)_3Br$	$K_3Sn_2(SO_4)_3Cl$
	yellow needles	white needles
Crystal Class	Hexagonal	Hexagonal
Cell Dimensions (Å)	a = b = 10.18	a = b = 10.18
	c = 7.54	c = 7.54
Cell Volume $(Å)^3$	677.17	677.17
Molecular Weight (g)	722.3	678.2
Z	2	2
Dc $)gcm^{-3})$	3.54	3.32
F(000)	672	636

Table 2.13

X-ray Diffraction Data for the Complexes $K_3Sn_2(SO_4)_3X$ (X = Cl, Br)

$K_3Sn_2(SO_4)_3Cl$ d spacing (Å)	$K_3Sn_2(SO_4)_3Br$ d spacing (Å)
5.83 m	8.89 m
4.26 w	5.73 m
3.81 s	4.26 w
3.37 m	3.83 m
3.07 vvs	3.79 s
2.95 vs	3.40 w
2.52 m	3.36 w
2.46 w	3.05 vvs
2.33 w	2.95 vs
2.26 w	2.52 m
2.21 w	2.47 w
2.12 s	2.34 w
2.01 s	2.27 w
1.96 s	
1.93 ms	
1.91 m	
1.89 m	
1.56 ms	

w. = weak

m. = medium

m.s= medium strong

s = strong

v.s= very strong

v.v.s = very, very strong

Table 2.14

2X,	2Y,	0.5
X - Y,	X,	0.5
Y,	Y - X,	0.5

The Patterson synthesis for both complexes, gave the most intense peak at 2/3, 1/3, 1/2, with the symmetry related position 2/3, 1/3, 0, appearing as a weaker vector peak. The weaker peaks appeared at:-

	X/A	Y/B	Z/C
2	0.0000	0.0000	0.5000
3	0.0000	0.0000	0.5000
4	0.6667	0.3333	0.0000
5	0.7483	0.0109	0.5000
6	0.7536	0.2849	0.0000
7	0.7358	0.0046	0.2533
8	0.4046	0.0525	0.2527
9	0.5000	0.0000	0.5000
10	0.4035	0.3348	0.2343
11	0.1113	0.4246	0.0000
12	0.8583	0.2227	0.0000
13	0.1518	0.0477	0.5000
14	0.0443	0.3768	0.0000
15	0.2802	0.0940	0.1451

for the bromide complex, and at:-

	X/A	Y/B	Z/C
2	0.0142	0.2628	0.5000
3	0.7540	0.2695	0.0000
4	0.0000	0.5000	0.5000
5	0.0000	0.0000	0.5000
6	0.6667	0.3333	0.0000

	X/A	Y/B	Z/C
7	0.0705	0.4097	0.2388
8	0.8519	0.2266	0.0000
9	0.4262	0.2926	0.0000
10	0.9252	0.3303	0.2551
11	0.9529	0.1245	0.5000
12	0.2740	0.0236	0.2532
13	0.6556	0.0292	0.0000

for the chloride complex. Although the Patterson maps are different, the highest peak is the same. It was therefore assumed that the four tin atoms being the heaviest atoms in the structure, could well be accommodated in two sets of two-fold special positions based on 1/3, 2/3, Z, (with Z = 0 and Z = $\frac{1}{2}$). However, the lowest residual achieved for refinement of these positions for tin in both structures, was 0.658. In the published structure Moser also assumed these positions for tin, and the structure calculations on the final model gave an R value of 0.300. These observations cast doubt on the assumption that the highest Patterson peak is due to Sn-Sn vectors. If the vectors for the tin atom, are not in highest position on the vector map they must be at one of the highest remaining peak positions. The next highest peak in the Patterson map for the bromo-complex arises from the special position 0, 0, 0. The corresponding peak in the Patterson map for the chloro- complex is the fourth highest. Placing the halide at 0, 0, 0, accounts for these differences in the Patterson maps. The second and fifth highest peaks in the chloro- and bromo- derivatives respectively, arise from an atom in the same six-fold

general position which, it was now assumed, were due to the tin atom. Refinement of this new tin position at 1/4 1/4,1/4, with a site occupancy of four-sixths, reduced the residual to 0.518, for the bromo-complex, and 0.530 for the chloro-complex. In view of the fact that the two compounds are isostructural, the complete refinement of only the bromo-complex is described, although refinement of the chloro-complex has been carried out and the final atomic positions are given.

A three dimensional difference Fourier map with phasing based on the refined tin position gave a large peak with coordinates at 0, 0, 0. The coordinates of this two-fold special position discussed earlier could only be assigned to the bromine atom. A further lowering in residual to 0.447 was achieved with bromine atom in this special position. A peak of electron density of 27 electrons appeared as the next highest and had the coordinates of the special position 2/3, 1/3, 0. The appearance of this peak confirms that the position highest in the Patterson map is that of a lighter atom than tin. With four potassium atoms in the positions associated with the 2 two-fold sites based on 1/3, 2/3, 0 and 1/3, 2/3, 1/2 with another lighter atom such as Br, at 0, 0, 0, it can be expected that a combination of K-Br vectors on top of K-K vectors will give rise to the most intense peak at 2/3, 1/3, 1/2. Two sets of potassium atoms were therefore considered to fully occupy the two-fold sites, with K1 in the position 2/3, 1/3, 0 and K2 at 2/3, 1/3, 1/2. Refinement of the K1 position lowered the residual to 0.357 and gave a large peak with coordinates at:-

X = -.5922, Y = .0337 Z = .2708

which were assigned to a sulphur atom. After location of the atoms Sn, Br, S, K1 and K2 at:-

	X	Y	Z
Sn	-0.2575	0.0121	0.2874
Br	0.0000	0.0000	0.5000
S	-0.5922	0.0337	0.2708
K1	0.6667	0.3333	0.0233
K2	0.6667	0.3333	0.5056

the residual fell to 0.236. A three dimensional difference Fourier map, with phasing based on these refined positions, gave three further map peaks, at distances of ≈2.40Å from tin, and 1.45Å from sulphur which were identified as the nearest neighbour oxygen atoms. A further Fourier synthesis enabled the location of the remaining oxygen atom. All four oxygen atom positions were refined using four cycles of full matrix least squares to a residual of R = 0.155, with the oxygen atoms at:-

	X	Y	Z
O1	-0.4290	0.1108	0.2705
O2	-0.6502	-0.1225	0.2740
O3	-0.6471	0.0791	0.4329
O4	-0.6180	0.0912	0.1015

During this refinement a Fourier difference synthesis map peak corresponding to about eight electrons appeared at:-

X = -.2567, Y = .0140, Z = .2012,

a position 0.62Å from tin. Since the tin atom lies in a six-fold general position with only two-thirds site occupancy, it was considered that the remaining potassium,

requiring a site of one-third occupancy could ideally share the general position partially occupied by the tin atom.

A refinement on all atoms, with anisotropic temperature factors for tin and sulphur, gave a residual of 0.062. A final residual of 0.0566 was obtained when all weak reflections for which |Fo < 2Fc| or |Fc < 2Fo| were omitted, and the temperature factors for six atoms made anisotropic. The final atomic positions in $K_3Sn_2(SO_4)_3Br$ were located at:-

Sn1	0.7445	0.0092	0.2848
S1	0.4106	0.0356	0.2601
Br1	0.0000	0.0000	0.5000
K1	0.6667	0.3333	0.0081
K2	0.6667	0.3333	0.5160
K3	0.7411	0.0213	0.2069
O1	0.5745	0.1135	0.2535
O2	0.3488	0.8753	0.2798
O3	0.3514	0.0800	0.4163
O4	0.3789	0.0892	0.0968

Refinement of the data for the isostructural chloro-complex gave a final residual of 0.086. The ten atoms were located in the following positions:-

Sn1	0.7505	0.0060	0.3021
S1	0.4100	0.0352	0.2637
Cl1	0.0000	0.0000	0.5000
K1	0.6667	0.3333	0.0130
K2	0.6667	0.3333	0.5183
K3	0.7552	0.0295	0.2223

O1	0.5701	0.1126	0.2868
O2	0.3502	0.8758	0.2634
O3	0.3567	0.0853	0.4284
O4	0.3790	0.0939	0.0850

Structural Description and Discussion

The structure is composed of a three-dimensional network of tin atoms and bridging sulphate groups, with discrete potassium and bromine ions sited in holes within the tin-sulphate network. Figures 2.5 and 2.6 show projections of the network parallel to the b and c axes respectively.

The tin atoms occupy only four-sixths of the available symmetry related positions for cations in the network, and the remaining two-sixths are taken up by two-sixths of the available potassium atoms. The remaining potassium and bromine atoms lie in special positions and are discrete ions.

Each sulphate group has an almost tetrahedral sulphur environment and forms bonds to the cations Sn/K3 through three of its oxygen atoms with each Sn/K3 atom being bonded to oxygen atoms from three different sulphate groups within the network. Along the b direction the tin atom lies between the bromine atoms forming one bond (3.11Å) and another (3.41Å) similar to the sum of the Sn-Br contact. This difference in Sn-Br distances creates the space for the stereochemically active non-bonding electron pair (Figure 2.7). The projection in the c direction shows the bromine ions to be surrounded by six tin atoms, in an irregular octahedral arrangement. There are three different potassium atoms, K1, K2 and K3. Both K1 and K2 atoms lie in 6-coordinate environments of oxygen atoms, with K-O distances of 2.68, 2.69 and 2.82Å,

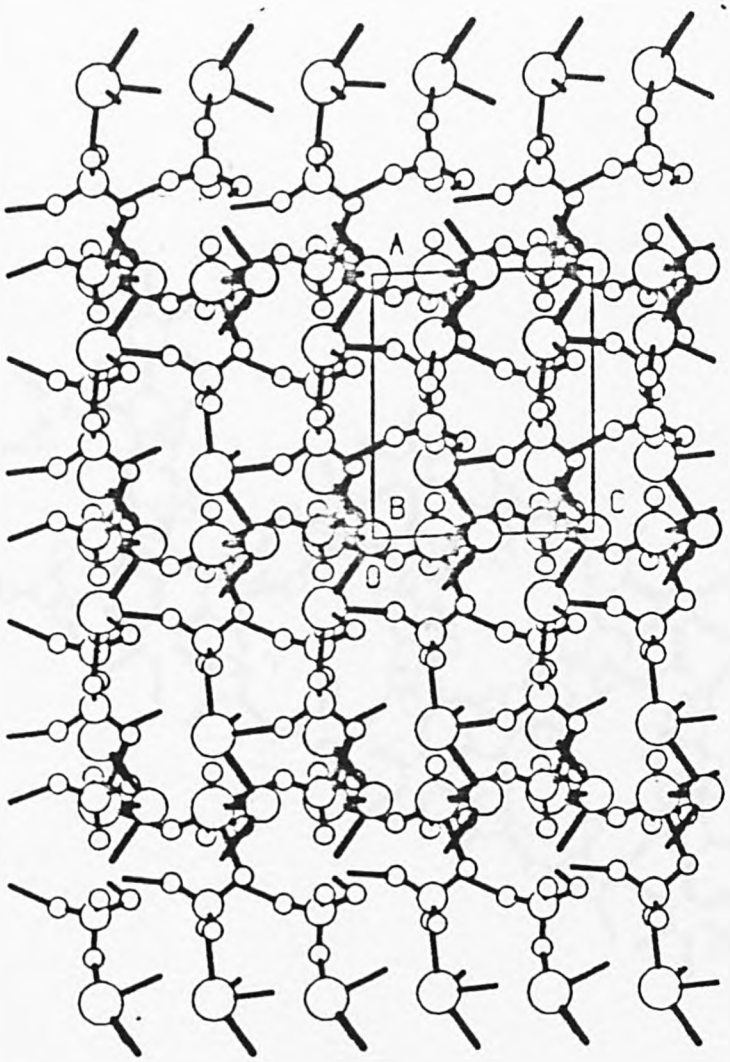

Figure 2.5 Structure of $K_3Sn_2(SO_4)_3Br$ viewed along the b direction (No potassium atoms included in figure)

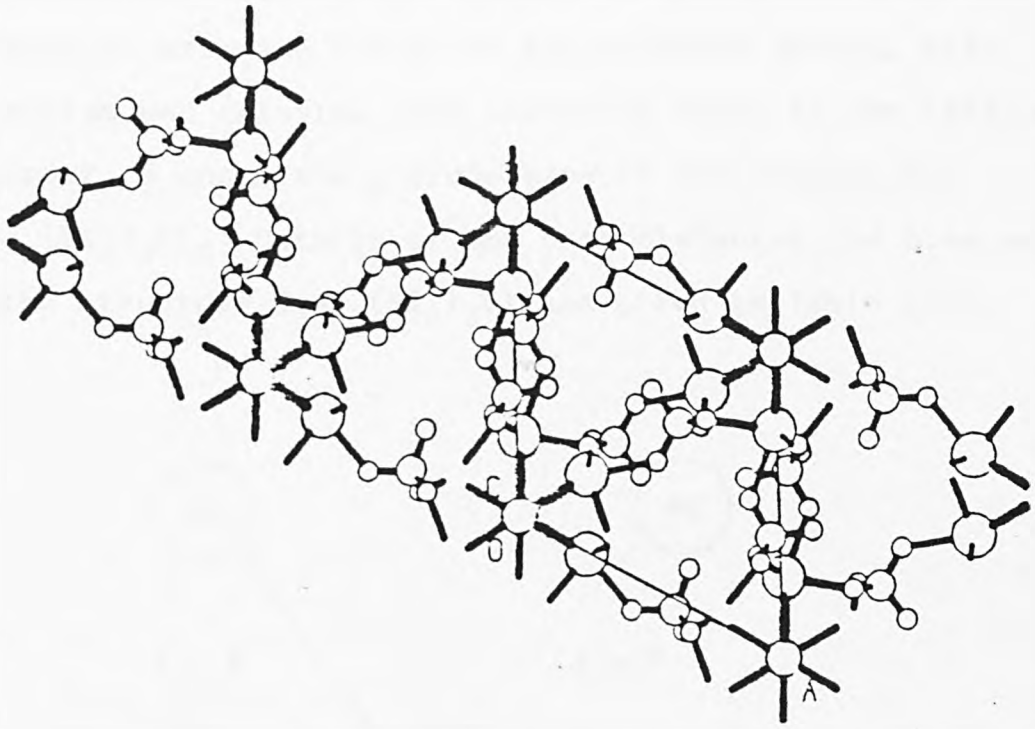

Figure 2.6 Structure of $K_3Sn_2(SO_4)_3Br$ viewed along the c direction (No potassium atoms included in figure)

and 2.78, 2.86 and 3.04Å for K1 and K2 respectively. The environment of K3, on the other hand, is unusual and is described in terms of partial occupation of the tin(II) site. As expected, the bond distances to both oxygen and bromine atoms are similar to those associated with the tin(II) site. Details of the bond distances and bond angles in the structure $K_3Sn_2(SO_4)_3$ Br are given in Table 2.15.

It is assumed that the chloro-sulphate complex, being isostructural with $K_3Sn_2(SO_4)_3Br$, is also a three dimensional network of bridging tin atoms and sulphate groups, with potassium and chlorine ions occupying holes in the lattice. Figure 2. 8 shows the b projection of the network for $K_3Sn_2(SO_4)_3Cl$. Details of the bond distances and bond angles in the structure $K_3Sn_2(SO_4)_3Cl$ are given in Table 2.16.

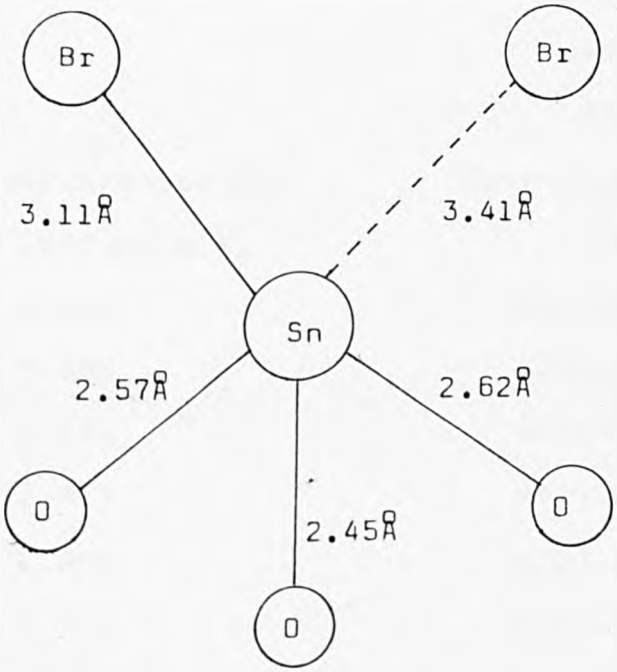

Figure 2.7

Bond Distances and Bond Angles

In $K_3Sn_2(SO_4)_3Br$

Tin Coordination - Sn(1)

Bond Distances(Å)		Bond Angles(°)	
Sn(1) -O(1)	2.453	O(1) -Sn(1)-O(3)	82.02
Sn(1) -O(3)	2.556	O(1) -Sn(1)-O(4)	86.85
Sn(1) -O(4)	2.618	O(1) -Sn(1)-O(4)′	73.38
Sn(1) -O(4)′	2.864	O(1) -Sn(1)-O(3)′	81.22
Sn(1) -O(3)′	2.935		
Sn(1) -Br(1)	3.107		

Sulphur Coordination -S

Bond Distances(Å)		Bond Angles(°)	
S(1)- O(1)	1.446	O(1) -S(1) -O(2)	110.9
S(1)- O(2)	1.433	O(1) -S(1) -O(3)	113.0
S(1)- O(3)	1.492	O(1) -S(1) -O(4)	100.2
S(1)- O(4)	1.447	O(2) -S(1) -O(3)	104.4
		O(2) -S(1) -O(4)	117.6
		O(3) -S(1) -O(4)	110.9

Potassium Coordination-K(1)		Potassium Coordination-K(2)	
Bond Distances(Å)		Bond Distances(Å)	
K(1)- O(1)	2.686	K(2)-O(1)	2.776
K(1)- O(1)′	2.686	K(2)-O(1)′	2.776
K(1)- O(2)	2.677	K(2)-O(2)	2.856
K(1)- O(2)′	2.677	K(2)-O(2)′	2.856
K(1)- O(3)	2.815	K(2)-O(3)	3.040
K(1)- O(3)′	2.815	K(2)-O(3)′	3.040

Potassium Coordination-K(3)- unusual, as K(3) shares Sn site.

Table 2.15

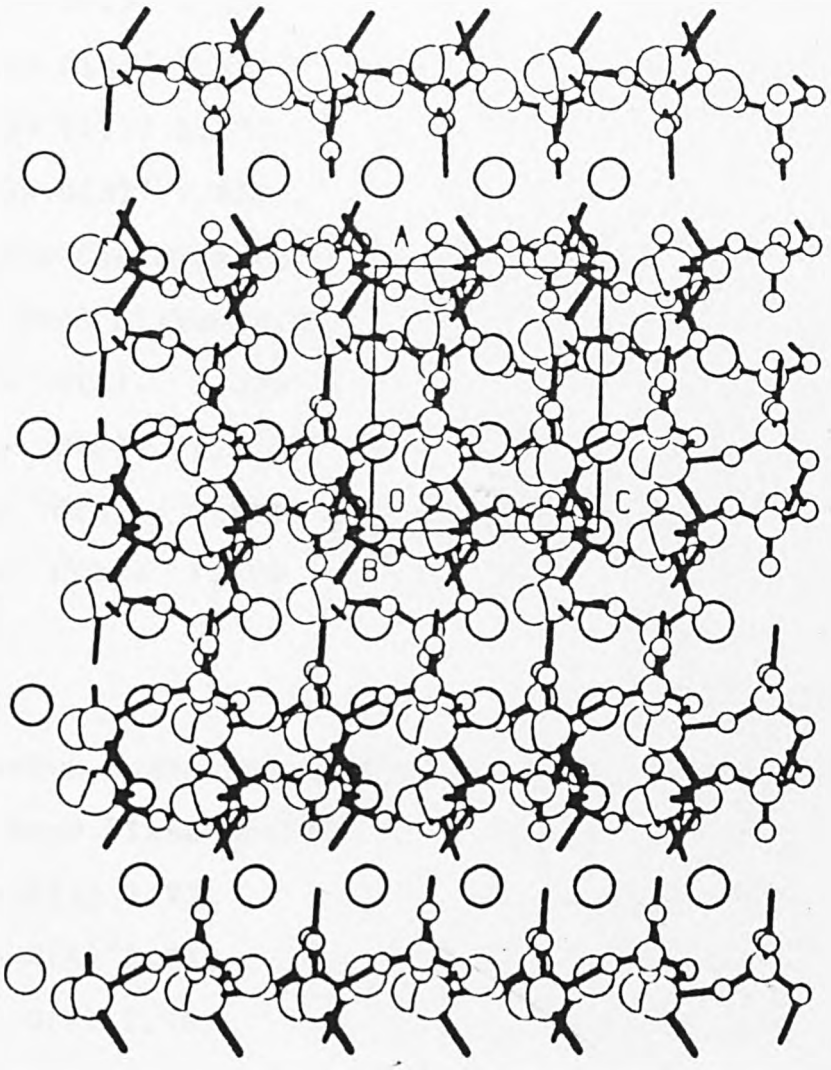

Figure 2.8 Structure of $K_3Sn_2(SO_4)_3Cl$ viewed along the b direction (All atoms included in the figure)

Bond Distances : Bond Angles

In $K_3Sn_2(SO_4)_3Cl$

Tin Coordination - Sn(1)

Bond Distances(Å)		Bond Angles(°)	
Sn(1)- O(4)	2.446	O(1)- Sn(1)- O(3)	78.30
Sn(1)- O(3)	2.547	O(1)- Sn(1)- O(4)	82.18
Sn(1)- O(1)	2.561	O(1)- Sn(1)- O(3)′	82.07
Sn(1)- O(4)′	2.961	O(1)- Sn(1)- O(4)′	73.80
Sn(1)- Cl(1)	2.973		
Sn(1)- O(3)′	2.994		

Sulphur Coordination- S

Bond Distances(Å)		Bond Angles(°)	
S(1)- O(1)-	1.425	O(1)- S(1)- O(2)	110.5
S(1)- O(2)-	1.420	O(1)- S(1)- O(3)	102.3
S(1)- O(3)-	1.541	O(1)- S(1)- O(4)	106.7
S(1)- O(4)-	1.568	O(2)- S(1)- O(3)	111.0
		O(2)- S(1)- O(4)	112.4
		O(3)- S(1)- O(4)	113.2

Potassium Coordination-K(1)

Bond Distances(Å)	
K(1)- O(4)	2.771
K(1)- O(4)′	2.771
K(1)- O(2)	2.783
K(1)- O(2)′	2.783
K(1)- O(1)	2.840
K(1)- O(1)′	2.840

Potassium Coordination-K(2)

Bond Distances (Å)	
K(2)- O(1)	2.618
K(2)- O(1)′	2.618
K(2)- O(2)	2.759
K(2)- O(2)′	2.759
K(2)- O(3)	2.972
K(3) O(3)′	2.972

Potassium Coordination- K(3)- unusual, as K(3) shares Sn site

Table 2.16

2.5 Palladium: Tin: Chloride: Iodide System

The most widely used inorganic reagents for the analysis of palladium, are tin(II) compounds[46,47]. Colour reactions between palladium and tin(II) donor species in the presence of chloride, bromide and phosphate have been reported. Khattak and Magee[48] suggested that the colour of the complex formed in the Pd(II) : Sn(II) : Cl^- system was due to the formation of the binuclear anion $[Pd_2Cl_2(SnCl_3)_4]^{4-}$ in which each palladium atom has a square-planar environment with two bonds to $SnCl_3^-$ donors and two to bridging chlorine atoms. The use of the mixed halide complex formed in the Pd(II) : Sn(II) : Br^- : I^- system for the spectrophotometric determination of palladium has been reported[49]. At the end of this paper it was suggested that the purple complex formed, with an absorbance at 555nm, was of the type:

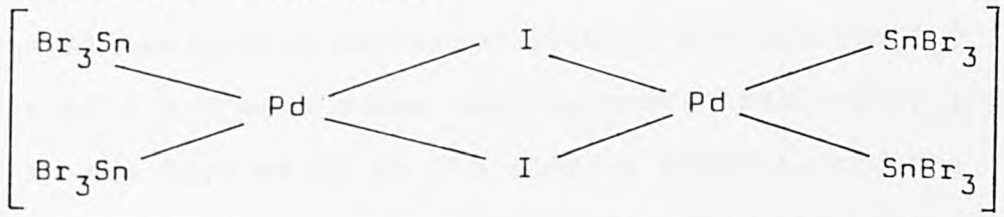

However no confirmatory evidence on the nature of the product was given. The Mössbauer spectra of the complexes prepared by Woodget[50] have the following parameters:-

Mössbauer Parameters (mms^{-1})

Complex	δ	Δ
$Pd_2I_2[SnBr_3]_4$	-0.4	2.9
$Pd_2Br_2[SnBr_3]_4$	-0.6	3.3
$Pd_2Cl_2[SnCl_3]_4$	-0.6	1.2

δ- relative to α- Sn

The small negative values for the chemical shift suggest that the lone pair of the SnX_3^- groups must have been used in bond formation to the palladium, to give effectively, a tin(IV) species. Changing the halide from bromide to chloride has little effect on the shift values. The closeness of these values implies therefore that the M-M bond dominates the use of the tin electrons, thus making it difficult to detect the different halogen. In view of this, any study involving the presence of mixed halogen in such complexes using Mössbauer spectroscopy would be difficult.

The aim of this work is to investigate the presence of more than one halide by studying the changes in absorption spectra with halide content. The system examined was $PdCl_2$: $SnCl_2$: KI, with a variation in the concentration of iodide.

To solutions of 1 : 1 (V/V) mixture of 2M-HCl and methanol containing palladium ($PdCl_2$) and tin ($SnCl_2$) in the ratio of 1 : 5 were added varying concentrations of iodide ion in the form of KI in 20% aqueous ethanol, and the absorption spectrum for each addition was recorded. All absorption measurements were made using a Perkin-Elmer 402 ultraviolet visible spectrophotometer in the range 390-850nm. Table 2.17 contains details of the absorption maxima (λ max) for each concentration of KI added to a solution of Pd : Sn : Cl^- containing 1.129×10^{-6} M Pd; together with details of λmax for PdI_2 : SnI_2 : KI for comparison.

The results show that on addition of a small concentration of I^- (as moles of KI) to the complex, there is a change in λmax from 413 to 440 nm. At a concentration of

Absorption data for the Pd(II): Sn(II): Cl: I System

Molar Concentration of KI ($\times 10^5$)	Moles of KI / Moles of Pd	λmax (nm)
Blank*	Blank*	413
0.45	4	442
0.54	5	445
0.82	7	444
0.91	8	442
1.82	16	444
2.73	24	447
3.64	32	485
4.54	40	485
9.09	80	490
18.18	160	490
27.27	240	490
36.36	320	490
45.45	400	490
PdI_2: SnI_2: KI		≃ 485

Blank : solution of $PdCl_2$: $SnCl_2$ (1:5) in methanol: HCl.

Table 2.17

0.45×10^{-5} MKI, there is evidence of a stable complex being formed. However, further addition of KI at 3.64×10^{-5} MKI moves λmax to ≃ 490 nm a value which corresponds to the absorption maximum for the PdI_2 :SnI_2 : I^- complex. There appears to be no further change in λmax on addition of a large excess of KI implying that the complex formed is very stable.

In order to replace the chlorides on the tin in:

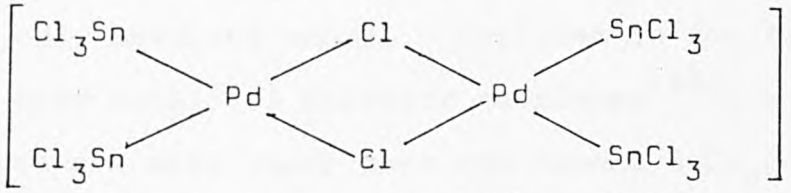

it is necessary to add six iodides ($6MI^-$) per palladium atom as a minimum. The results however, show that for an addition of between 4 and 24MKI the same absorption maximum at ≃ 445 nm is achieved, and only when a 32- fold excess of I^- has been added is a λmax associated with a complex of the type:

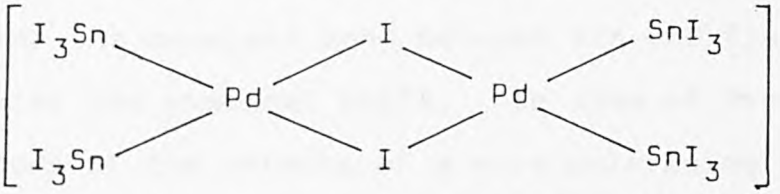

obtained. Since this is so, it must be assumed that the first process is not a replacement of the chlorines bonded to the tin but is more likely to be replacement of the bridging chlorines on palladium. This prediction would therefore be consistent with the A-type acceptor character of tin, and the B-type acceptor character of palladium.

2.6 Tin(II) : Mixed Cation System

Studies have been reported[51,52] on the Mössbauer effect in some metal (I) and non--transition and transition metal (II) derivatives of complex tin(II) fluoride ions.

There is no evidence in these cases for any significant competition between the tin and the other metal ions for bonding to fluorine. The Mössbauer data obtained for such compounds *viz*: $M^{I}SnF_3$ [44], $M^{I}Sn_2F_5$ [44], $M^{II}(SnF_3)_2$ [51], $M^{II}(SnF_3)_2(H_2O)_6$ [52] and $M^{II}(Sn_2F_5)_2(H_2O)_2$ [52], confirm the formation of strong Sn-F bonds. The very low shift values for these compounds, (Table 2.18), being lower than that for SnF_2 are an indication of the presence of strongly covalent bonds. Included in the table are data for some metal (I) chloride complexes[43], whose shift values are also lower than the parent $SnCl_2$, although the overall covalency in the Sn-Cl bonds is not so great. In both the metal (I) and metal (II) complex tin(II) fluoride series there is a small but significant variation in the chemical shift with the polarising power of the metal. The greater the pull on the fluorine by the metal ion, the weaker the covalent bond between tin and fluorine, and the greater the chemical shift. In view of these observations a study of the effects of a more polarising ion eg. In^{3+}, seemed to be worthwhile. The purpose of the work presented in this section is therefore to use Mössbauer spectroscopy to determine the extent of any competition between In(III) and Sn(II) for bonding to fluoride or chloride ions.

Solid products were isolated from aqueous solution and melts containing 1 : 3 and 1 : 6 molar ratios of indium halide with the appropriate tin(II) halide. The products were identified by chemical analysis and X-ray diffraction data as $In(SnF_3)_3$ and $In(Sn_2F_5)_3$ from the InF_3 : SnF_2 system and $In(SnCl_3)_3$ and $In(Sn_2Cl_5)_3$ from

^{119}Sn Mössbauer Parameters of Some known Tin(II) ; Mixed Cation Systems

(see also Table 2.19)

Compound	δ mms^{-1}	Δ mms^{-1}
SnF_2	3.65	1.80
$NaSnF_3$	3.12	1.84
$KSnF_3$	3.07	1.92
$Sr(SnF_3)_2$	3.24	1.75
$Ba(SnF_3)_2$	3.13	1.87
$NaSn_2F_5$	3.32	1.86
KSn_2F_5	3.26	1.96
$Sr(Sn_2F_5)_2$	3.39	2.06
$Ba(Sn_2F_5)_2$	3.36	1.69
$Fe(SnF_3)_2.6H_2O$	2.88	1.84
$Co(SnF_3)_2.6H_2O$	3.10	1.76
$Fe(Sn_2F_5)_2.2H_2O$	2.99	1.88
$Co(Sn_2F_5)_2.2H_2O$	3.19	1.89
$SnCl_2$	4.12	0
$KSnCl_3$	3.76	0.77
$KSn_2Cl_5.H_2O$	3.78	0.88

Table 2.18

the $InCl_3$: $SnCl_2$ system. The X-ray data were compared with the indium and tin halides and were shown not to be mixtures of the parent compounds.

The Mössbauer parameters for the four materials, recorded at 80K are given in Table 2.19 together with the known data for some complex tin(II) fluorides and chlorides. In the absence of serious competition with Sn(II) for bonding to fluorine or chlorine, complex formation results in the formation of trihalostannate(II) or pentahalodistannate(II) ions with an isomer shift value much lower than that of the tin(II) halide (section 1.3 2). Comparison of the data for the known fluoro- and chloro- stannates(II) with the data for their parent halides, is consistent with a lowering of shift due to complex formation. In the case of indium-tin halides, however, there is no appreciable change in chemical shift from that of the parent halides. This would be reflected in longer Sn-X bonds in the indium tin derivatives, (see Chapter 4). These results are interpreted in terms of increased competition for fluorine and chlorine bonding electrons by indium.

^{119}Sn Mössbauer for the In Complexes

Compound	δmms^{-1}	Δmms^{-1}
SnF_2	3.65	1.80
$In(SnF_3)_3$	3.50	1.69
$In(Sn_2F_5)_3$	3.55	1.64
$CsSnF_3$	2.98	2.00
$CsSn_2F_5$	3.12	2.03
$SnCl_2$	4.12	c.a.0
$In(SnCl_3)_3$	4.11	c.a.0
$In(Sn_2Cl_5)_3$	4.11	c.a.0
$CsSnCl_3$	3.64	0.90
$CsSn_2Cl_5$	3.77	1.00

Table 2.19

2.7 Synthesis of and Studies on Organotin(IV) Adducts with Glycylglycine

The preparation and characterisation by infrared and ^{119}Sn Mössbauer spectroscopy of some organotin(IV) derivatives of glycylglycine, adenosine and nucleosides has recently been reported[53-55]. However, no details of thermal studies in such complexes have been given. This section therefore deals with the characterisation of some new compounds R_nSnCl_{4-n}. glycylglycine not only by infrared and ^{119}Sn Mössbauer spectroscopy but also by thermal analysis.

2.7.1 Preparation and Chemical Analysis of the Complexes

The organotin(IV) glycylglycine complexes R_nSnCl_{4-n} glycylglycine (where n = 2, R = Me, Bu, Oct and Ph; and where n = 1, R = Bu, Oct and Ph) were prepared by refluxing 1 : 1 molar quantities of the appropriate organotin(IV) chloride in dry methanol. The products obtained on cooling, were washed with dry methanol and dried under vacuum.

The compounds were analysed for tin gravimetrically as SnO_2 and for Cl by titration with mercuric perchlorate following the destruction of organic matter by the oxygen flask method. Percentages of C,H and N were determined at the Laboratorio di Chimica Organica(Milan). The analytical data for the glycylglycine complexes are given in Table 2.20 as averages of three separate determinations.

2.7.2 Infrared Spectra

The infrared spectra for the complexes were recorded

Analytical Data for H_2glygly adducts with R_nSnCl_{4-n} (%: calculated in parentheses)

	C	H	N	Cl	Sn
$Me_2SnCl_2.H_2$glygly	21.6	4.08	7.60	20.0	33.5
	(20.48)	(4.01)	(7.96)	(20.16)	(33.74)
$Bu_2SnCl_2.H_2$glygly	33.8	6.13	7.33	16.3	27.3
	(33.05)	(6.01)	(6.43)	(16.26)	(27.23)
$Oct_2SnCl_2.H_2$glygly	43.1	7.61	5.70	13.0	21.8
	(43.82)	(7.67)	(5.12)	(12.95)	(21.67)
$Ph_2SnCl_2.H_2$glygly	39.8	4.04	5.98	15.2	25.3
	(40.38)	(3.81)	(5.89)	(14.90)	(24.94)
$BuSnCl_3.H_2$glygly	23.4	4.28	6.71	25.3	29.0
	(23.19)	(4.14)	(6.76)	(25.67)	(28.65)
$OctSnCl_3.H_2$glygly	30.3	5.53	5.74	22.1	25.5
	(30.64)	(5.36)	(5.95)	(22.61)	(25.23)
$PhSnCl_3.H_2$glygly	27.9	2.81	6.57	24.7	27.6
	(27.64)	(2.99)	(6.45)	(24.50)	(27.34)

Table 2.20

using a Perkin Elmer 580 infrared spectrometer.

The bidentate nature of the glycylglycine ligand towards the tin(IV) moieties can be inferred from the infrared data (Table 2.21) for the complexes because (1) the region of the spectra attributable to the animo N-H stretching vibration in the adducts differs from those for matrix-isolated glycylglycine and sodium glycylglycine[9]. (2) the NH_3^+ deformation at 1657cm^{-1} present in glycylglycine and its hydrochloride is absent in the spectra of the adducts.
(3) the absorption at about 1740cm^{-1} can be attributed to the normal carbonyl absorption of the COOH group and
(4) the absorptions due to COOH at 1224cm^{-1} are shifted to lower frequencies in the adducts, and
(5) the free ligand bands at 1678 and 1575cm^{-1} attributable to $\nu_{C=O}$ and δ_{N-H} are not shifted in the adducts. These data suggest that coordination of the ligand to tin is through the amino group and the carboxylic OH group and there is no bond formation between Sn and the C = O group of the peptide.

The bands at 560 and 525cm^{-1} for R = Me, and at 605 and 525cm^{-1} for R = Bu, Oct, were attributed by Pellerito et al[56] to symmetric and anti-symmetric stretchings of a bent C-Sn-C skeleton. The skeleton Sn-C mode for the Ph derivatives is assigned by comparison with literature assignments and does not provide any configurational information. The bands attributable to ν_{SnCl_2} lie in the region that is typical for these vibrations in organotin(IV) chloride and tin(IV) chloride adducts.

Infrared Data for R_2SnCl_2 adducts of H_2glygly

Me_2SnCl_2		Bu_2SnCl_2		Oct_2SnCl_2		Ph_2SnCl_2		Assignments
3350	m,bd	3340	m,bd	3335	m,bd	3340	m,bd	)
3200	m,bd	3230	m,bd	3210	m,bd	3230	m,bd	) ν_{NH}
1735	s	1740	s	1720	s	1740	s	$\nu_{C=O(carbonyl)}$
1677	s	1678	s	1678	s	1678	s	$\nu_{C=O(amide)}$
1575	m	1575	m	1575	m	1575	m	$\delta_{NH(amide)}$
1215	m,bd	1195	m	1215	m,bd	1230	m,bd	ν_{C-O} or δ_{OH}
		605	sh					$\nu_s + \nu_{as(SnC_2)}$
				605	s			$\nu_{(SnC_2)}$
560								$\nu_{(SnC_2)}$
525	s	525	s	525	s			$\nu_s + \nu_{as(SnC_2)}$
265	m	290	s	280	s			ν_{SnCl_n}
						282	w	) $\nu_{as\ SnCl_2}$+
						272	w	) $\nu_s\ (SnCl_2)$+
								$\nu_{as(SnPh_2)}$

s = strong, m = medium, sh = shoulder, w = weak, bd = broad.

Table 2.21

Infrared Data for $RSnCl_3$ adducts of H_2glygly.

$BuSnCl_3$		$OctSnCl_3$		$PhSnCl_3$		Assignments
3340	m,bd	3320	m,bd	3360	m,bd	)
3200	m,bd	3180	m,bd	3180	m,bd	)
3130	m,bd	3110	m,bd			) ν_{NH}
						)
						)
1738	s	1732	s	1730	s	$\nu_{C=O(carbonyl)}$
1678	s	1678	s	1678	s	$\nu_{C=O(amide)}$
1575	m	1575	m	1575	m	$\delta_{NH(amide)}$
1205	w	1200	w	1249	s	ν_{C-O} or δ_{OH}
475	m					ν_{SnC}
270	s	270	s	270	s	ν_{SnCl_n}

Table 2.21 (continued)

2.7.3 ^{119}Sn Mössbauer Spectra

The ^{119}Sn Mössbauer parameters for the organotin(IV) chloride adducts with glycylglycine are given in Table 2.22 The chemical shift values show the expected trends in that the values are lower for the monoalkyl complexes than for the dialkyl complexes which reflects the increase in covalent bonding on replacement of a second chlorine with an alkyl group. All Sn-C bonds have s-electron density, but the aryl group uses more p- and less s- electron density in bonding, in comparison to the alkyl group. Hence the bonding in the phenyl derivative is effectively more ionic in character. The lower chemical shifts values for the diphenyl complexes are consistent with this view.

2.7.4 Thermal Analysis

There have been no reports in the literature giving details of any thermal study on complexes related to those prepared in this work. The aim of the present work is to identify and assign the stages involved in the decomposition processes of the complexes. Two different types of glycyl-glycine complex are examined *viz* monoorganotin derivatives whose parent organotin halides are liquids and diorganotin derivatives with parent organotin halides as solids. In view of the difference in the nature of the compounds, the thermal decomposition processes are discussed separately.

There appears to be no general pattern of decomposition of the complexes of type $R_2SnCl_2.H_2glygly$. (where R=Me,Bu,Oct or Ph). The thermal decomposition patterns are different and characteristic of the specific complex. To help assign

^{119}Sn Mössbauer parameters of Organotin(IV) adducts with glycylglycine

Compound	δ mms^{-1}	Δmms^{-1}
$Me_2SnCl_2.H_2glygly$	1.36	3.58
$Bu_2SnCl_2.H_2glygly$	1.40	3.71
$Oct_2SnCl_2.H_2glygly$	1.48	3.82
$Ph_2SnCl_2.H_2glygly$	0.76	1.80
$BuSnCl_3.H_2glygly$	1.04	2.06
$OctSnCl_3.H_2glygly$	1.09	2.01
$PhSnCl_3.H_2glygly$	1.02	2.18

Table 2.22

the stages involved in the decomposition, the thermal analysis was also carried out on the individual parent materials and on an intimately ground mixture of glycylglycine with the organotin halides. The decomposition of glycylglycine has already been described in section 2.1.3, so the details are only included in the relevant tables below.

Dioctyltindichloride glycylglycine: The dioctyltin dichloride after melting at 48°C volatilizes off at ≃ 107°C in a one stage decomposition process. This weight loss is accompanied by a boiling endotherm on the DTA trace which returns sharply to the baseline. The melting point of the mixture of dioctyltindichloride and glycylglycine is 51°C. The mixture then undergoes two endothermic heat changes losing 100% weight at 120°C. The melting point of the complex at 91°C is considerably higher than that of the parent organotin halide. It is not surprising therefore that the complex is also stable to a higher temperature (220°C) when it loses 83% of its total weight in one step and loses a further 5% weight at 336°C. Figure 2.9 shows traces of the decompositions of the parent compound, the mixture of the parent materials, and the complex.

Compound	Temp.(°C)	Weight Loss (%)	Nature of DTA peaks	No. of DTG peaks	
Oct_2SnCl_2	45	0	Endo		Melting
	107	100	Endo	1	Volatilization
Glycylglycine	215	≃ 18	Endo	1	
	243	≃ 30	Endo	1	
	340	≃ 52			

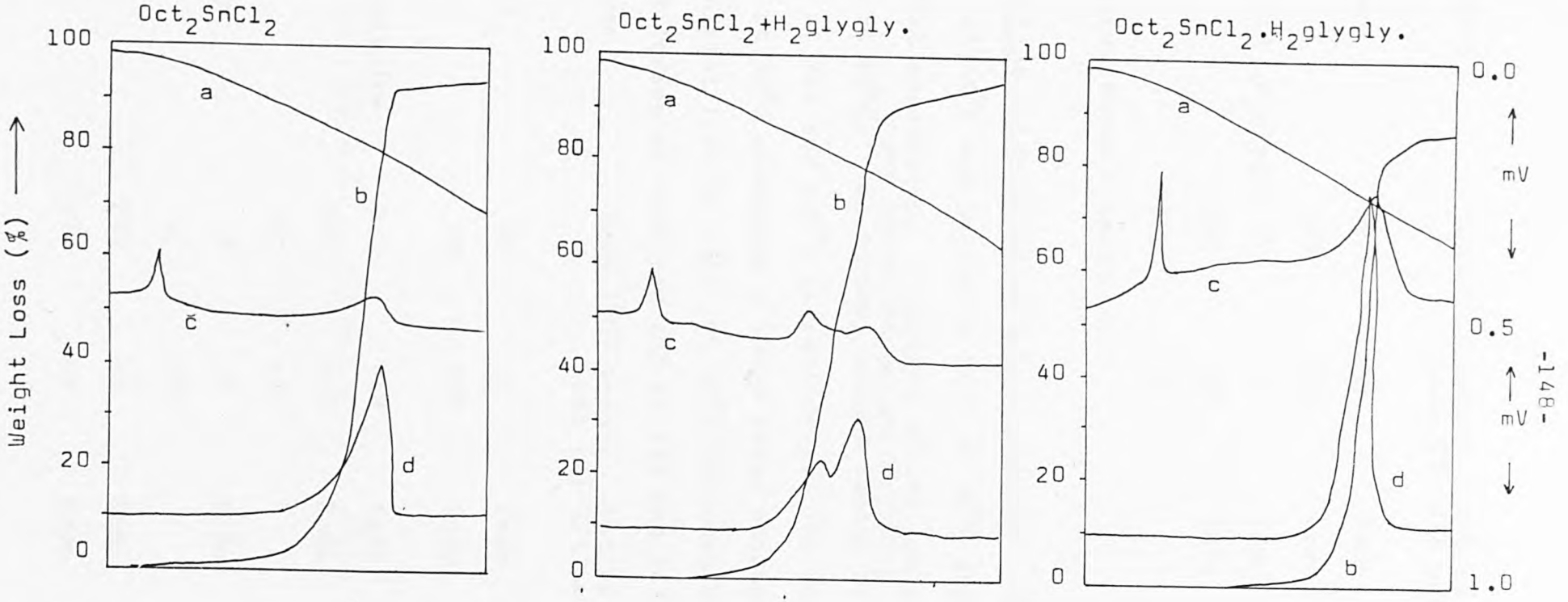

Figure 2.9 Thermal decomposition traces of: Oct_2SnCl_2; $Oct_2SnCl_2+H_2glygly.$; and $Oct_2SnCl_2.H_2glygly.$.

Compound	Temp.(°C)	Weight Loss (%)	Nature of DTA peaks	No.of DTG peaks	
Mixture	51	0	Endo		Melting
	120	100	Endo	2	
$Oct_2SnCl_2.H_2glygly$	91	0	Endo		Melting
	220	≈83	Endo	2	
	336	≈5		1	

Endo (Endothermic reaction)

Dibutyltindichloride glycylglycine: Solid Bu_2SnCl_2 melts at 45°C and begins to boil at 80°C when 100% of the material evaporates. A mixture of the two parent materials melts at 49°C and loses 75% weight at 80°C. Two further weight losses of c.a.6% and 8% occur at 204 and 270°C respectively. The complex which melts at 39°C undergoes a three stage decomposition with the initial loss of ≈70% at 80°C followed by two smaller weight losses of ≈10% and 12% at 175 and 243°C respectively.

Compound	Temp.(°C)	Weight Loss (%)	Nature of DTA peaks	No.of DTG peaks	
Bu_2SnCl_2	45	0	Endo		Melting
	80	100	Endo	1	Volatiliz-ation
Glycylglycine	215	≈18	Endo	1	
	243	≈30	Endo	1	
	340	≈52			
Mixture	49	0	Endo		Melting
	80	≈75			
	204	≈6	Endo	1	
	270	≈8	Endo	1	

Compound	Temp.(°C)	Weight Loss(%)	Nature of DTA peaks	No.of DTG peaks	
$Bu_2SnCl_2.H_2glygly$	39	0	Endo		Melting
	80	≈70		2	
	175	≈10			
	243	≈12	Endo	1	

Dimethyltindichloride glycylglycine: The parent organotin halide melts at 107°C and then volatilizes off losing 100% weight at 145°C. The thermal decomposition of the mixture appears to involve three major weight losses. The first loss of 42% weight occurs at 50°C before the appearance on the DTA trace of a melting endotherm at 107°C. The second weight loss of 28% at 133°C is followed by a final weight loss of 30% at 248°C. Decomposition of the complex occurs in four stages without melting. A two stage weight loss of 10% precedes the major weight loss of 62% at 157°C and a final loss of 30% at 260°C completes the decomposition. In Figure 2. 9 are traces obtained for the decomposition processes of these materials.

Compound	Temp.(°C)	Weight Loss(%)	Nature of DTA peaks	No. of DTG peaks	
Me_2SnCl_2	107	0	Endo		Melting
	145	100	Endo	1	Boiling
Glycylglycine	215	≈18	Endo	1	
	243	≈30	Endo	1	
	340	≈52			
Mixture	50	≈42	Endo	1	
	107	0	Endo		Melting
	133	≈28	Endo	1	
	248	≈30	Endo	1	

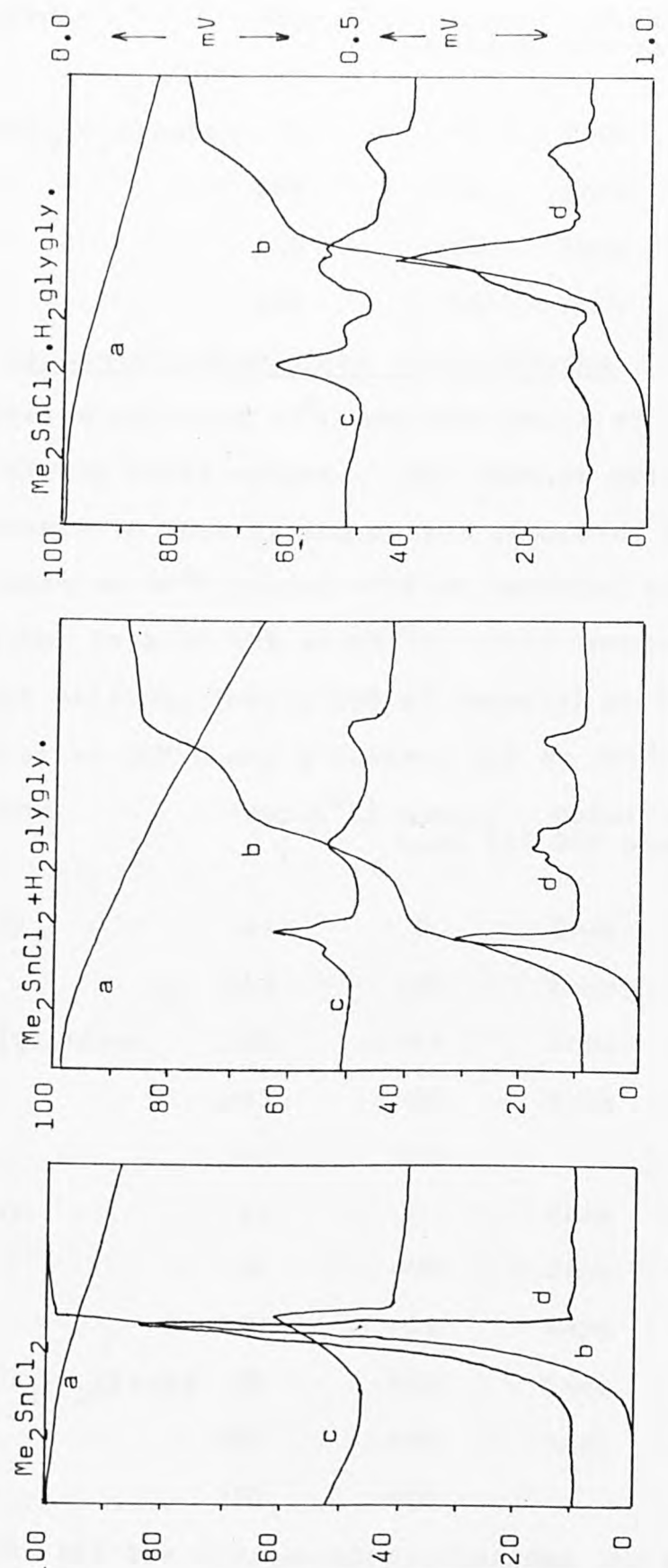

Figure 2.9 Thermal decomposition traces of: Me_2SnCl_2; Me_2SnCl_2+H_2glygly.; and Me_2SnCl_2.H_2glygly..

Compound	Temp.(°C)	Weight Loss(%)	Nature of DTA peaks	No.of DTG peaks
$Me_2SnCl_2.H_2glygly$	51	≈5	Endo	1
	107	≈5	Endo	1
	157	≈62	Endo	2
	260	≈30	Endo	1

Diphenyltindichloride glycylglycine: The diphenyltin dichloride melts at 44°C and then boils at 114°C losing 100% of its total weight. The mixture melts at a temperature comparable to that of the parent compound, and begins to decompose at 80°C losing ≈70% of material in one step then a further loss of 12% at 260°C. This complex also decomposes without melting, losing 10% of material at 50°C, 40% of material at 200°C and a further 20% at 310°C.

Compound	Temp.(°C)	Weight Loss (%)	Nature of DTA peaks	No.of DTG peaks	
Ph_2SnCl_2	44	0	Endo		
	114	100	Endo	2	Merged
glycylglycine	215	≈18	Endo	1	
	243	≈30	Endo	1	
	340	≈52			
Mixture	42	0	Endo		Melting
	80	≈70	Endo	1	
	260	≈12	Endo	1	
$Ph_2SnCl_2.H_2glygly$	50	≈10	Endo	1	
	200	≈40	Endo	1	
	310	≈20			

For all the diorganotindichlorides the melting point is followed by 100% volatilization at a higher temperature.

The differential weight loss during volatilization of the diphenyltindichloride suggests that a two stage process is involved. Such a process would be consistent with the known rearrangement of Ph_2SnCl_2 to give $SnCl_4$ and Ph_3SnCl whose decomposition temperatures are 114°C and 240°C respectively. There is no evidence in the DTG curves, in the region of vaporization of the other diorganotindichlorides of any similar rearrangement occurring.

There is some similarity in the thermal decompositions of those mixtures of R_2SnCl_2 and glycylglycine (where R = Bu, Oct or Ph). In each case, the diorganotindichloride melts and the glycylglycine dissolves in the molten phase. Except for the case of the dioctyltindichloride mixture the melts decompose by volatilization of most of the diorganotin dihalide leaving impure glycylglycine to decompose at a higher temperature. In the case of the dioctyltindichloride the weight loss due to the volatilization of Oct_2SnCl_2 overlaps the weight loss due to the decomposition of glycylglycine. Thermal analysis of the dimethyltindichloride- containing mixture shows that the mixture decomposes without melting by loss of 42% weight at 50°C. This is followed by melting at 107°C and subsequent loss of weight by volatilization of the organotin halide and decomposition of glycylglycine. These results can be explained if part of the dimethyltindichloride undergoes rearrangement to give tetramethyltin and $SnCl_4$, whose boiling points are 78 and 114°C respectively. The broad DTG peak confirms the loss of two materials, over this temperature range, instead of the apparent one stage weight

loss. During the evaporation of $SnCl_4$ there is evidence of a melting endotherm on the DTA trace, due to the remaining part of Me_2SnCl_2 melting and volatilizing off. The final weight loss at 248°C is due to the breakdown of glycylglycine.

The fact that the organotin dihalides volatilize off from molten mixtures at temperatures similar to their boiling points suggests that there is no strong interaction between the organotin moiety and the glycylglycine ligand.

The thermal decomposition of the complexes fall into two classes, following one of two distinct mechanisms: viz. (1) in which the decomposition of the complex follows a process similar to that of the mixture, and (2) in which the decomposition involves a reaction within the lattice which does not occur in the mixture.

Both the dioctyl- and dibutyltinchloride derivatives of glycylglycine decompose following mechanism (1). The complex and mixture of the dibutyltindichloride derivative both melt at approximately the same temperature and decompose in a similar manner, indicating that the bonding in the dibutyl complex is weak. The difference between the decomposition of the complex and mixture of the dioctyl derivative lies in the fact that melting occurs at a low temperature in the mixture; glycylglycine then dissolves, whereas the distinct complex is stable to a higher temperature. This high melting point of the dioctyltindichloride complex does not necessarily mean it is a stronger complex but may possess a higher lattice energy.

Thermal decomposition of those complexes involving

some reaction in the lattice which is absent in the decomposition of the mixtures, is evident in the dimethyl- and diphenyl- derivatives. The thermal process involves the elimination of HCl from the lattice to give a glycyl-glycinate which subsequently gives a different thermal decomposition pattern to those of the mixtures.

The results obtained from the study of the thermal decompositions of the glycylglycine derivatives of some monoorganotin trihalides of type $R\,SnCl_3.H_2glygly$ (R = Bu, Oct, Ph) show that the decomposition reactions are much more complicated than the dihalides. Again the thermal analytical data for the decompositions of the parent materials, of mixtures of the two parent materials, and of the complexes are given.

Monooctyltintrichloride glycylglycine: The parent octyltin-trichloride boils at 87°C losing 100% weight in one step. This volatilization process is accompanied by a DTA endotherm which returns sharply to its baseline. On heating the mixture, a two stage decomposition occurs at 66°C involving the loss of 8% of material. This is followed by a loss of 57% weight at 170°C and 12% at 360°C. In a similar manner, the complex, on heating, loses ≈11% weight in two steps, 62% weight at 192°C and a further 12% at 360°C.

Compound	Temp.(°C)	Weight Loss (%)	Nature of DTA peaks	No.of DTG peaks	
$OctSnCl_3$	87	100	Endo	1	Boiling
Glycylglycine	215	≈18	Endo	1	
	243	≈30	Endo	1	
	340	≈52			

Compound	Temp(^{o}C)	Weight Loss(%)	Nature of DTA peaks	No.of DTG peaks
Mixture	66	≈8		1
	170	≈57	Endo	3
	360	≈12		
$OctSnCl_3.H_2glygly$	27	≈11		
	192	≈62	Endo	3
	360	≈12		

The thermal decomposition traces obtained for the materials are given in Figure 2.9

Monobutyltintrichloride glycylglycine: $BuSnCl_3$ begins to boil at 44^{o}C when it undergoes 100% weight loss. The thermal decomposition of the mixture involves a multistep process. At about 20^{o}C, there is a weight loss of 8%, which is followed by a 10% weight loss at 120^{o}C, a 40% weight loss at 180^{o}C, and a 10% weight at 237^{o}C. A final loss of 12% weight at 250^{o}C completes the decomposition at 250^{o}C. The complex decomposes with an initial loss of 5% of material, at ≈20^{o}C. Two weight losses of 50% at ≈170^{o}C and ≈25% at 250^{o}C complete the decomposition of the $BuSnCl_3.H_2glygly$ complex.

Compound	Temp(^{o}C)	Weight Loss (%)	Nature of DTA peaks	No.of DTG peaks	
$BuSnCl_3$	44	100	Endo	1	Boiling
Glycylglycine	215	≈18	Endo	1	
	243	≈30	Endo	1	
	340	≈52			
Mixture	20	≈8	Endo	1	
	120	≈10	Endo	1	
	180	≈40	Endo	3	
	237	≈10		1	
	250	≈12			

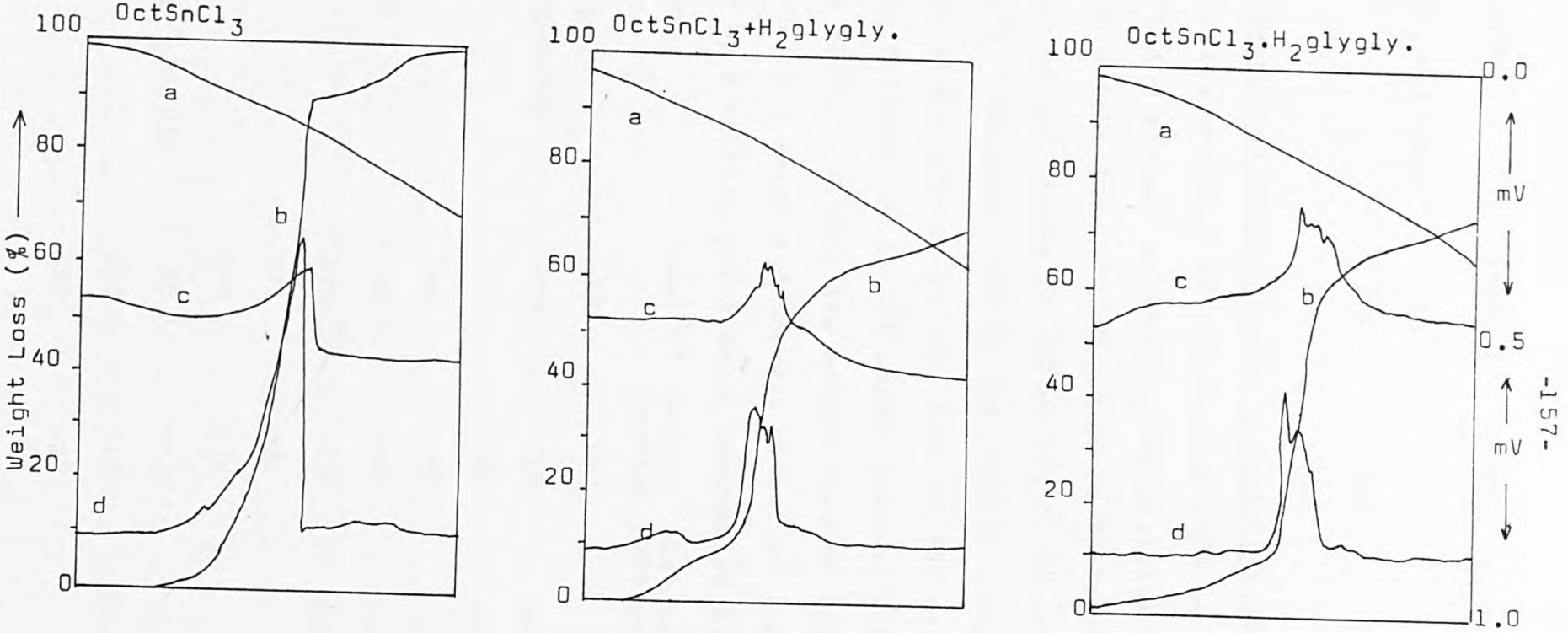

Figure 2.9 Thermal decomposition traces of: $OctSnCl_3$; $OctSnCl_3 + H_2glygly.$; and $OctSnCl_3.H_2glygly.$

Compound	Temp(^{o}C)	Weight Loss(%)	Nature of DTA peaks	No.of DTG peaks
$BuSnCl_3.H_2glygly$	20	≈5		
	170	≈50	Endo	>4
	250	≈25		

Monophenyltintrichloride glycylglycine: Phenyltin trichloride boils at 66^{o}C and loses 100% weight in one step. At 66^{o}C the mixture of $PhSnCl_3$ and glycylglycine undergoes a major weight loss of 50%, which is followed by three further weight losses of 15% at 170^{o}C, 8% at 221^{o}C and 10% at 270^{o}C. Decomposition of the complex occurs in three gradual steps with an initial loss of 43% weight at 66^{o}C. This is followed by an 18% weight loss at 258^{o}C and a further 20% at 310^{o}C. During the weight loss of 18% there is evidence of a sharp endothermic effect on the DTA trace, caused by a melting point being reached at 270^{o}C.

Compound	Temp(^{o}C)	Weight Loss(%)	Nature of DTA peaks	No. of DTG peaks	
$PhSnCl_3$	66	100		2	Boiling
Glycylglycine	215	≈18	Endo	1	
	243	≈30	Endo	1	
	340	≈52			
Mixture	66	≈50	Endo	1	
	170	≈15	Endo	2	
	221	≈8		1	
	270	≈10			
$PhSnCl_3.H_2glygly$	66	≈43		7	
	258	≈18	Endo	1	
	310	≈20		1	

All the parent organotin trihalides, on reaching their boiling points, volatilize off losing 100% weight in one step. There is no evidence from the differential weight losses to indicate decomposition occuring in more than one stage.

Both the octyl- and butyl- complexes decompose at temperatures lower than the boiling points of their parent compounds. The two complexes appear to undergo a three-stage weight loss, although the unusually broad DTG peaks suggest the decompositions are more complicated. These three-stage weight losses are assigned to the initial elimination of HCl, forming the glycylglycinate which then undergoes decomposition to lose the organotin trichloride, followed by the breakdown of the glycylglycine moiety. The mixture of octyltin trichloride and glycylglycine decomposes in a similar manner although the solid phase decomposes at a lower temperature. Although the decomposition of the mixture of $BuSnCl_3$ and glycylglycine appears to be a multi-stage process, combination of certain weight losses gives a trace similar to that obtained for the complex.

Both the complex, $PhSnCl_3.H_2$glygly and the mixture of $PhSnCl_3$ and glycylglycine begin to lose weight at 66°C which is the boiling point of the parent compound $PhSnCl_3$. The complexity of the corresponding DTG peaks strongly suggest that the decompositions of the complex and the mixture of the starting materials are not simple. The initial weight losses indicate it is possible to consider the rearrangements of $PhSnCl_3$ to form tetraphenyltin and $SnCl_4$, followed by the loss of the latter.

2.7.5 Summary

The preparation and characterisation of some organotin(IV) complexes of type $R_2SnCl_2 . H_2glygly$ (R = Me, Bu, Oct, Ph) and $R\ SnCl_3 . H_2glygly$ (R = Bu, Oct, Ph) have been described and a study of complex formation between the tin(IV) moieties and glycylglycine have been made using infrared and ^{119}Sn Mössbauer spectroscopy and thermal analysis. Both the Mössbauer and thermal data suggest the bonding in the diorganotin complexes is relatively weak between the tin(IV) moiety and the ligand. The complexity of the thermal traces obtained for the mono-organotin derivatives of glycylglycine makes it difficult to suggest the nature of the bonding of the compounds. The lack of knowledge on the bonding effects in such compounds, derived from thermal decomposition studies warrants further studies in this field.

2.8 Thermal Analysis of Some Organotin(IV) Sugar Derivatives

The work reported in this section deals with an investigation of the fate of tin during the thermal reactions of some dialkyl tin(IV) sugar derivatives. There are no reports in the literature detailing the mode or modes of decomposition of such compounds.

Only the organotin(IV) derivatives of some simple sugars (monosaccharides) have been studied. Monosaccharides can be divided principally into two categories, those which are polyhydroxyaldehydes (aldoses), which have as their name implies, an aldehydic group, and the polyhydroxyketones (ketoses) with a ketone group present. Of those sugars

studied most are aldoses but the sugars, fructose and sorbose are examples of ketoses.

The results show that the thermal decompositions of the complexes fall into one of three main types (Type A,B,C). Type A are those sugar derivatives which break down in two stages leaving a residue of stannous oxide. Type B sugars pyrolyse in a two-step process to give either stannic oxide, or stannic oxide and carbon as products of decomposition. Finally Type C includes a small number of sugar complexes which melt before decomposition and give either stannous or stannic oxides as residues. Table 2.23 lists the dialkyltin(IV) sugar derivatives into one of the three modes of decomposition.

It appears that the fate of tin during decomposition to give either a tin(II) or tin(IV) species as a product is dependent on the nature of the sugar, i.e. whether it is an aldose or ketose. The dialkyltin derivatives of aldoses give stannous oxide, whilst those derivatives of ketoses give SnO_2. These results are consistent with the reducing properties of aldoses, in which tin(IV) is reduced to tin(II) and the aldehyde groups of aldoses are oxidized to form carboxylic acids, known as aldonic acids. No such reducing properties occur with ketoses. The reactions described above deal with tin species in the solid state. However different criteria apply to the third group of compounds in which melting precedes the decomposition. In a molten system the final tin product depends not only on the nature of the sugar but also on the nature of the molten tin species. Some of the sugar derivatives decompose to

Thermal Behaviour of Some Organotin(IV) Sugar Derivatives

Type A Complex	Type B Complex	Type C Complex	m.p. (°C)	Res*
$Bu_2SnC_6H_{10}O_5$ (rhamnose)	$Bu_2SnC_6H_{10}O_6$ (fructose)	$Oct_2SnC_5H_8O_5$ (ribose)	94	SnO_2
$Bu_2SnC_5H_8O_5$ (arabinose)	$Bu_2SnC_6H_{10}O_6$ (sorbose)	$Oct_2SnC_4H_6O_4$ (erythrose)	107	SnO_2
$Bu_2SnC_5H_8O_5$ (ribose)		$Oct_2SnC_6H_{10}O_6$ (galactose)	97	SnO_2
$Bu_2SnC_6H_{10}O_6$ (glucose)		$Me_2SnC_6H_{10}O_6$ (galactose)	163	SnO_2
$Bu_2SnC_6H_{10}O_6$ (galactose)		$Me_2SnC_6H_{10}O_6$ (glucose)	155	SnO
$Bu_2SnC_4H_6O_4$ (erythrose)				

* Res. = residue

Table 2.23

give the expected tin product, viz.aldoses leading to SnO, and ketoses giving SnO_2, however, this is not always the case. It is found that with, for example, $Oct_2SnC_4H_6O_4$ (erythrose-aldose) and $Oct_2SnC_5H_8O_5$ (ribose-aldose) the final tin product is SnO_2 and not the reduced tin species-SnO.

In conclusion, therefore a study of the decomposition of some dialkyltin sugar derivatives, has given information on the fate of the tin(IV) moiety in the thermal reaction. No details of the specific breakdown of the sugar molecules are given, however sufficient evidence has been obtained viz. heating samples of SnO_2, SnO, SnO + C, SnO_2 + C and SnO_2 + glucose to predict that the sugars break down at an early stage in the decomposition process. There is plenty of scope to examine further the modes of decomposition of these sugars to fully understand the effect of the presence of the tin moiety in the breakdown processes of the sugars.

References

1. C.E.Vanderzee and D.E.Rhodes, J.Amer. Chem. Soc., 1952, 74, 3552.

2. W.B.Schaap, J.A.Davis, and W.H.Nebergall, J.Amer. Chem. Soc., 1954, 76, 5226.

3. J.D.Donaldson, Progress Inorganic Chem., 1967,8, 287.

4. D.G.Nicholson, Ph.D.Thesis (London), 1969.

5. P.A.Cusack, P.J.Smith and J.D.Donaldson, Inorg.Chim.Acta, 1980, 46, L73.

6. W.T.Hall and J.J.Zuckerman, Inorg. Chem., 1977,16, 1239.

7. J.D.Donaldson and W.Moser, Analyst, 1959, 84, 10.

8. L.Pellerito, G.Ruisi, M.T.LoGiudice, J.D.Donaldson and S.M.Grimes, Inorg.Chim.Acta, 1982, 58, 21.

9. B.Y.K.Ho and J.J.Zuckerman, Inorg Chem., 1973, 12, 1552.

10. J.D.Donaldson and B.J.Senior, J.Chem.Soc.A, 1969, 2358.

11. J.D.Donaldson and A.Jelen, J.Chem.Soc.A, 1968, 1448.

12. V.J.Goldanskii, V.V.Khrapov, V.Y.Rochev, T.N.Sumarokova and D.E.Surpina,Doklady Akad.Nauk, SSR, 1968, 183, 364.

13. J.D.Donaldson, D.G.Nicholson and B.J.Senior, J.Chem.Soc.A, 1968, 2928.

14. J.S.Morrison and H.M.Haendler, J.Inorg.Nucl.Chem., 1967, 29, 393.

15. J.D.Donaldson and D.G.Nicholson, J.Chem.Soc.A, 1970, 145.

16. J.D.Donaldson and D.G.Nicholson, Inorg.Nucl.Chem.Letters, 1970, 6, 151.

17. G.L.Heichhorn, P.Clark and E.D.Becker, Biochemistry, 1966, 5, 245.

18. D.J.Hodgson, Progress Inorganic Chem., 1977, 23, 211.

19. M.Goodgame and K.W.Johns, Inorg.Chim.Acta, 1980, 46, 23.

20. L.Pellerito, G.Ruisi, R.Barbieri and M.T.LoGiudice, Inorg.Chim.Acta, 1977, 21, L33.

21. K.Kitahama and H.Kiriyama, Bull.Chem.Soc.Jap., 1977, 50, 3167.

22. E.Hough and D.G.Nicholson, J.C.S.Dalton, 1976, 1782.

23. J.D.Donaldson and S.M.Grimes, in press.

24. J.E.Cassidy, W.Moser, J.D.Donalson, A.Jelen and D.G.Nicholson, J.C.S.Dalton, 1970, 173.

25. J.D.Donaldson, D.G.Nicholson, D.C.Puxley and R.A.Howie, J.C.S.Dalton, 1973 , 1810.

26. W.B.Simpson, Ph.D. Thesis Aberdeen, 1962.

27. J.F.Knifton, Ph.D. Thesis, London, 1965.

28. J.D.Donaldson, Ph.D. Thesis, Aberdeen, 1959.

29. T.Karantassis, Compt.Rend., 1926, 182, 134.

30. W.H.Nebergall, G.Baseggio and J.C.Muhler, J.Am.Chem.Soc., 1954, 76, 5353.

31. P.Pascal, Nouveau Traite de Chemie Minerale. Vol.8. Masson et Cie., Paris. 1963.

32. J.D.Donaldson, D.R.Laughlin and D.C.Puxley, J.C.S.Dalton, 1977, 865.

33. J.D.Donaldson and B.J.Senior, J.C.S.Dalton, 1969, 2358.

34. C.C.Addison and W.B.Simpson, unpublished work.

35. J.S.Morrison, Ph.D.Thesis, Univ. New Hampshire, 1965

36. D.A.Everest, J.Chem.Soc., 1951, 2903.

37. R.Klement and H.Haselbeck, Chem.Ber., 1963, 96, 1022.

38. B.R.Chamberlain and W.Moser, J.Chem.Soc.(A). 1969, 354.

39. R.A.Howie, W.Moser, R.G.Starks, F.W.D.Woodhams and W.Parker, J.C.S.Dalton 1973, 1478.

40. J.D.Donaldson and J.Silver, J.C.S.Dalton 1973, 666.

41. J.Barrett, S.R.A.Bird, J.D.Donaldson and J.Silver, J.Chem.Soc.(A). 1971, 3105.

42. J.D.O'Donoghue, Ph.D. Thesis.London. 1965.

43. S.R.A.Bird, J.D.Donaldson and J.Silver, J.C.S.Dalton, 1972, 1950.

44. J.D.Donaldson and B.J.Senior, J.Chem.Soc., 1966, 1798.

45. International Tables for X-ray Crystallography Birmingham, Kynoch Press, 1962.

46. G.H.Ayres and J.H.Alsop, Anal Chem., 1959, 31, 1135.

47. F.Pantani and G.Piccardi, Anal.Chim, Acta, 1960, 22, 231.

48. M.A.Khattak and R.J.Magee, Anal.Chim.Acta, 1966, 35, 17.

49. J.A.W.Dalziel, J.D.Donaldson and B.W.Woodget, Talanta, 1969, 16, 1477.

50. B.W.Woodget, M.Sc.(London). 1968.

51. J.D.Donaldson, B.J.Senior, J.Chem.Soc.(A). 1967, 1821.

52. J.D.Donaldson and R.Oteng, J.Chem.Soc.(A). 1969, 2696.

53. L.Pellerito, G.Ruisi, N.Bertazzi, M.T.LoGiudice and R.Barbieri, Inorg.Chim.Acta, 1976, 17, L9.

54. L.Pellerito, M.T.LoGiudice, G.Ruisi, N.Bertazzi, R.Barbieri and F.Huber, Inorg.Chim.Acta, 1976, 17, L21.

55. R.Barbieri, L.Pellerito and F.Huber, Inorg.Chim.Acta, 1978, 30, L321.

56. L.Pellerito, G.Ruisi and R.Barbieri, Private Communication.

CHAPTER 3

Solid State Properties of Tin(II) Compounds

CHAPTER 3

Solid State Properties of Tin(II) Compounds

The stereochemistry of most p-block elements in lower oxidation states is dominated by the presence of filled non-bonding lone-pair orbitals. The environments of these elements in many of the compounds of Sn(II), Pb(II), As(III), Sb(III), Bi(III), Se(IV), Te(IV) and Po(IV) are distorted by the presence of the lone pair orbitals[1-5]. There are however, a number of compounds in which these elements are found in regular octahedral sites[6-10]. All of the solid compounds containing ns^2 elements in high-symmetry sites are coloured and many of them show metallic or semi-conducting electrical properties. A key compound in studies of undistorted ns^2 species has been $CsSnBr_3$, which is a black solid with metallic lustre which acts as a metallic conductor over a wide temperature range[6,11]. Its X-ray and ^{119}Sn Mössbauer data are consistent with it having an undistorted cubic perovskite structure. It has been suggested [12] that its Mössbauer data and metallic conducting properties, and therefore colour, can be explained by the population of conduction bands in the solid, by the tin $5s^2$ - electrons. These bands would arise from the mutual overlap of empty bromine t_{2g}, 4d - orbitals which would be at a maximum in the undistorted perovskite lattice. The tin(IV) compound Cs_2SnBr_6 is cubic and has a structure[13] closely related to that of $CsSnBr_3$, and Cs and Br atoms are in the same relative position but in the tin(IV) complex only one half of the perovskite tin sites are occupied. The cell volume for Cs_2SnBr_6 ($\underline{a}$ = 10.8Å) is less than that for the corresponding

number of Cs and Br atoms in $CsSnBr_3$ ($\underline{a}$ = 11.6Å). The tin(IV) complex must therefore contain a lower energy band like $CsSnBr_3$ but in common with similar hexabromo- and hexachlorostannates(IV) is white and insulating. In contrast, the corresponding Te(IV) and Po(IV) derivatives, which are known to be isostructural with the hexahalogenostannates(IV) are intensely coloured. The difference between the Sn(IV) and the Te(IV) or Po(IV)complexes is the presence of $\underline{ns}^2$ non-bonding, lone-pair orbitals on the group-6 elements. The intense colours and conducting properties of the Te(IV) and Po(IV) complexes can be explained, like those of $CsSnBr_3$, by population of bands by the $\underline{ns}^2$ non-bonding electrons. The lack of these properties in Cs_2SnBr_6 would then be accounted for by the absence of a lone-pair in the Sn(IV) outer-electronic configuration. The band structure of $CsSnBr_3$ is best illustrated[14] with reference to the density of states diagram. This band model places the bromine 4d - level just above the $5s^2$ level of the tin where it can be populated thermally to account for the high electrical conductivity of $CsSnBr_3$. The presence of the next highest energy band allows optical transitions to occur between the $5s^2$ level and the conduction band. The properties of $CsSnBr_3$, explained by this approach are : (1) the relatively low ^{119}Sn Mössbauer chemical shift ($3.97 mms^{-1}$) and the electrical conductivity arising from loss of s-electron density to the solid state bands by process A; (2) the optical absorption edge arising from the process B and (3) the two observed photoemission bands arising from the process C.

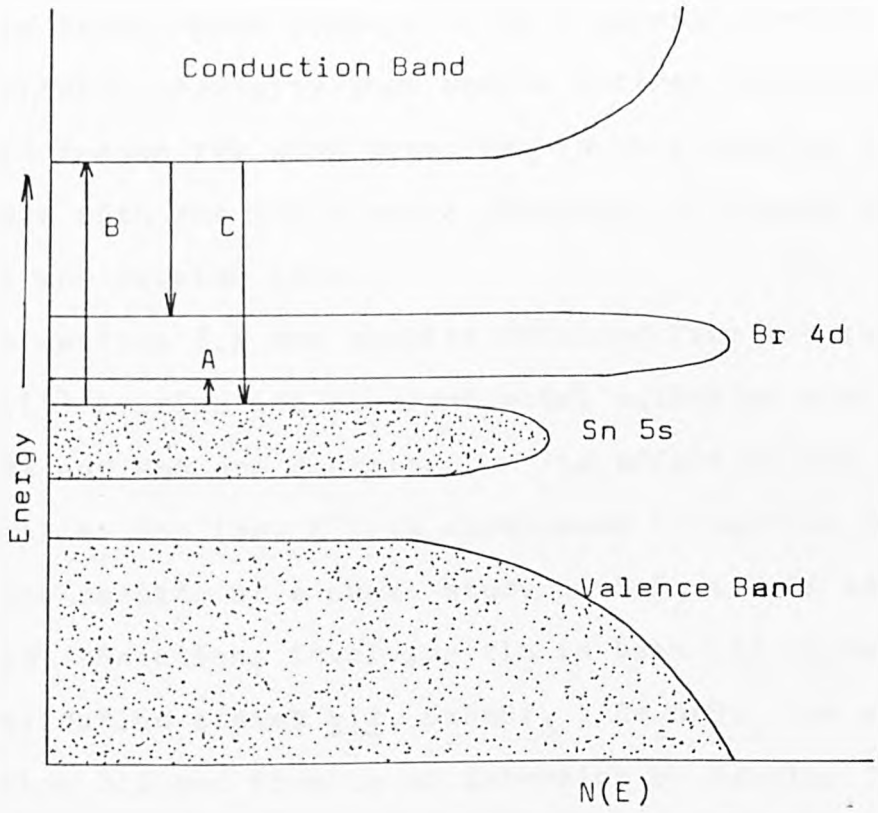

Suggested band structure for $CsSnBr_3$ showing thermal population (A), optical absorption (B) and emission (C).

High symmetry environments in compounds of the lower oxidation states of most p- block elements are found only in their heavier halide and chalcogenide derivatives and where these anions are in close contact. Regular octahedral Sn(II) environments are, for example, found in SnSe[1] SnTe[1] and SnI_2[15] as well as in $CsSnBr_3$ and related halides. The compounds of these elements with oxygen or fluorine environments generally have distorted sites for the element. The removal of the distorting effects of non-bonding electrons as lone pairs by their direct population

of solid state bands appears to be a general feature of main group element chemistry that merits further detailed study. For this reason the work described in this chapter is concerned with the solid state chemistry of phases containing tin(II) and bromide ions.

In section 3.1 the results obtained from the reaction of tin(II) bromide and divalent metal sulphides such as SnS, CdS and PbS are described. The effect of the presence of a smaller ion (eg. F^-) is considered in section 3.2 in which the results of a phase study of SnF_2 : CsBr are detailed. Reactions involving tin in both its higher and lower oxidation states viz. $CsSnBr_3$: Cs_2SnBr_6 are presented in section 3.3 and finally an extension of studies [16] on the two systems $CsSnBr_3$: $CsSnCl_3$ and $CsSnBr_3$: $CsPbBr_3$ are described in section 3.4.

3.1 $SnBr_2$: MS Systems (M = Sn, Cd and Pb)

Although a number of lead(II) chalcogenide halides have been described as a result of phase diagram studies[17,18] until recently very little was known of the corresponding tin(II) compounds. Laughlin[19] carried out a detailed study of the products obtained from cooled melts of the systems SnX_2 - SnZ (X = Cl, Br; Z = S, Se or Te). The new compounds $Sn_7Br_{10}S_2$, Sn_4Br_6Se and Sn_4Br_6Te were identified as the only distinct phases from the $SnBr_2$ - SnZ system. These results have prompted the present study in which the structure of $Sn_7Br_{10}S_2$ has been determined, and in which the work has extended to include a study of phases in $SnBr_2$ - MS systems, where M is a divalent metal other than tin(II).

3.1.1 Structure Determination of $Sn_7Br_{10}S_2$

Previously reported data[20] suggest that $Sn_7Br_{10}S_2$ (hexagonal cell with a = 11.35 and c = 4.40Å and space group $P6_{3/m}$ or $P6_3$) is isostructural with $Pb_7Br_{10}S_2$, which structure although not fully determined is said[21] to be similar to that of Th_7S_{12}[22]. This would mean that two types of tin environment would be present in $Sn_7Br_{10}S_2$: viz a set of six tin atoms on one crystallographic site (site 1) and the seventh on a different special position (site 2).

Two methods of structure determination are adopted and described in this work. One uses the atomic parameters identifiable from the Th_7S_{12} structure, the other involves a complete refinement of the data following Patterson and Fourier syntheses.

Preparation of the Crystal

In a detailed study[19] of the products obtained from cooled melts of all the systems SnX_2- SnZ (X = Cl or Br ; Z = S, Se or Te) one of the new distinct phases identified was that of $Sn_7Br_{10}S_2$. The preparation was repeated add a product was obtained from a cooled melt of $5SnBr_2$: 2SnS under an atmosphere of oxygen-free nitrogen. A yellow needle was taken from the bulk material and was used to obtain the cell data.

Determination of the Space Group and Cell Dimensions

The yellow prismatic crystals used had a maximum thickness of 0.1mm and the following crystal data were obtained from single crystal precession data and refined on the basis of the powder diffraction pattern.

Crystal data for $Sn_7Br_{10}S_2$:

Crystal Class	Hexagonal
Cell Dimensions (Å)	$\underline{a} = \underline{b} = 12.185$
	$\underline{c} = 4.418$
Cell Volume $(Å)^3$	568.08
Molecular Weight	1693.99
Z	1
Dc	$4.95 gcm^{-3}$
F(000)	732
Systematic Absences	00L for L = 2n.

As a result of these data, the crystal was assigned to the space group $P6_3$ or the centrosymmetric alternative $P6_{3/m}$ (No. 173 and 176 respectively in the International Tables for X-ray crystallography[23]).

Collection of Intensity Data

Intensity data were collected using a Philips PW1100 four-circle diffractometer in the range $4 < 2\theta < 50^o$ with monochromatized Mo -Kα radiation. 1176 intensities were recorded and 325 hexagonal reflections with $I \leq 3\sigma(\underline{I})$ were obtained and considered observed. The data were corrected for Lorentz and polarization effects but no absorption corrections were considered necessary due to the small size of the crystal.

Determination using the Th_7S_{12} structure as a Model

To understand the application of this model a description of the Th_7S_{12} structure is now given.

The final structure obtained for Th_7S_{12} is as follows:

Space group : $P6_{3/m}$

Atomic positions : 1 Th(1) in ± $(0,0,\frac{1}{4})$

6 Th(2), 6 S(1) and 6 S(2) in ± $(x,y,\frac{1}{4})$; $(\bar{y},x-y,\frac{1}{4})$; $(y-x,\bar{x},\frac{1}{4})$ with parameters:

	x	y
Th(2)	0.153 ± 0.002	-0.283 ± 0.002
S (1)	0.514 ± 0.010	0.375 ± 0.010
S (2)	0.235 ± 0.010	0 ± 0.010

In order to account for the intensities observed for the Laue-Bragg reflections it was necessary to associate one half Th(1) atom with each of the twofold sites ± $(0,0,\frac{1}{4})$. Along a given sixfold axis, these sites are separated by only 1.99Å. The author's conclusion[22], therefore, was that only every other site along a given sixfold axis can be occupied by Th(1) atoms. Since it was known that the sites $0,0,\frac{1}{4}$ and $0,0,\frac{3}{4}$ were statistically equivalent it was assumed that the sites $0,0,\frac{1}{4}$ were occupied for 50% of the sixfold axes and the sites $0,0,\frac{3}{4}$ for the other 50%.

Figure 3.1 shows the structure, Th_7S_{12} viewed along the sixfold axis. Two of the four Th(1) atoms contained in the figure are shown to be at $0,0,\frac{1}{4}$, and the other two to be at $0,0,\frac{3}{4}$.

Each Th(1) atom is bonded to nine atoms S(2), while each Th(2) atom is bonded to five S(1) atoms and to three S(2) atoms.

Zachariasen's results for the Th_7S_{12} structure showed a statistical distribution of the Th atom over the two sites $0,0,\frac{1}{4}$ and $0,0,\frac{3}{4}$. Laughlin[19] on the other hand, with a data set of 104 reflections for $Sn_7Br_{10}S_2$ suggested that the alternative twofold position of 0,0,0 and $0,0,\frac{1}{2}$, should also be considered because a lower residual was achieved with Sn(2)

The Th_7S_{12} structure viewed along a sixfold axis. Two of the four Th_I atoms shown here are placed at $z=\frac{1}{4}$ and two at $z=\frac{3}{4}$.

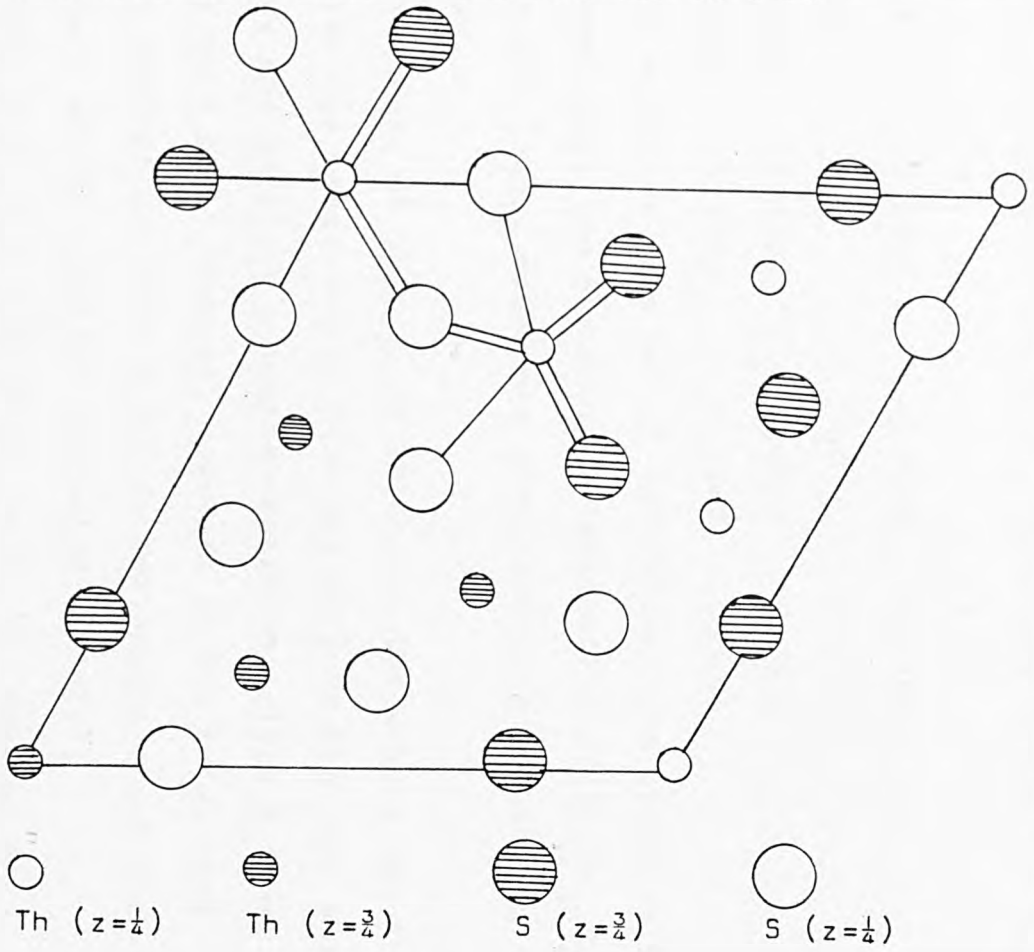

Figure 3.1

in this position. Any structure based on the Th_7S_{12} structure will require a statistical distribution of tin atoms over the positions of a twofold site.

The following atomic parameters, used by Laughlin, in relation to the Th_7S_{12} structure are now considered as possible positions in the Sn_7X_{12} structure (where X = Br/S).

	x	y	z
Sn1	0.1264	-0.2909	0.2465
Sn2	0.0	0.0	0.5
Br(S)1	-0.4863	0.3811	0.2496
Br(S)2	-0.2201	-0.2407	0.2458

With a larger data set of 325 reflections obtained in the present work the structure determination of $Sn_7Br_{10}S_2$ based on the Th_7S_{12} model has been attempted and is now described.

Refinement of Sn_7X_{12}, in which all the anions are the same, with the atoms Sn(1), X(1) and X(2) having full site occupancy and Sn(2) in a special position, gives a final residual of 0.183. However, movement of the Sn(2) atom from its special position $0,0,\frac{1}{2}$ raised doubts about the correctness of the position allocated to Sn(2).

Substituting for X in Sn_7X_{12} with the appropriate number of Br and S atoms, there are three possible distributions of the atoms.

For a statistical distribution of the sulphur atoms through both anion sites a residual of 0.183 is achieved, with movement of the Sn(2) position to -0.9668, -0.0085, -0.2236. With allowances being made for the distribution of sulphur atoms in one anion site (either Br(1) or Br(2)),

the lowest residual attained is of the order 0.20. Again there is movement of the Sn(2) atom from the special position at $z = \frac{1}{2}$ and 0.

With the three possible distributions of atoms a lower residual was achieved on removal of the Sn(2) position, and a peak of electron density equivalent to approximately seven electrons appeared in the Fourier map. The results seemed to suggest the Sn(2) atom was not in the position $0,0,\frac{1}{2}$, as proposed by Laughlin, but at $0,0,\frac{1}{4}$, as predicted by Zachariasen for the Th(1) atom. The three possible distributions of atoms, were tested for the new Sn(2) position and the residual fell to 0.157, for the structure in which both sulphur atoms were in the Br(1) site.

If the material, therefore had the Th_7S_{12} structure, the single tin atom would be distributed between positions $0,0,z$ and $0,0,\frac{1}{2}+z$ that arise by placing an atom on the threefold axis in the cell. In addition the sulphur atoms would be randomly distributed on one or both of the two possible anion sites. However, the high residual obtained from even the best fit to the data casts some doubt on the validity of the assumption that $Sn_7Br_{10}S_2$ has a structure closely related to Th_7S_{12}.

Determination of the Structure from Patterson Synthesis

Location of Atomic Positions: The X-ray crystallographic programs used throughout the crystal structure determination are outlined in Chapter 1.

The atomic positions were located as a result of a heavy atom Patterson synthesis. The equivalent positions in the space group $P6_3$ are:-

$x, y, z;$ $\bar{y}, x-y, z;$ $y-x, \bar{x}, z;$

$\bar{x}, \bar{y}, \frac{1}{2}+z;$ $y, y-x, \frac{1}{2}+z;$ $x-y, x, \frac{1}{2}+z;$

and these positions give peaks in the Patterson vector map at:-

$x+y,$	$2y-x,$	0
$2x-y,$	$x+y,$	0
$2x,$	$2y,$	0.5
$x-y,$	$x,$	0.5
$y,$	$y-x,$	0.5

The Patterson vector density map has the following peaks:-

	HEIGHT	X/A	Y/B	Z/C	Allocation of Vectors
1	999.	0.0000	0.0000	0.0000	
2	999.	-.0000	-.0000	1.0000	
3	312.	.2572	.3633	.0103	Br(1)-Br(1):Br(1)-Br(2)
4	298.	.3617	.1059	.0027	" "
5	298.	.3617	.1059	1.0027	" "
6	260.	.1143	.5056	.5056	" "
7	241.	.5008	.3836	.5154	" "
8	164.	.2230	.2376	.4855	Br(1)-Br(1):Br(2)-Br(2)
9	163.	.2192	.0072	.5206	" "
10	152	.2687	.1583	.4982	Br(1)-Br(2)
11	144.	.2566	.2049	.0336	
12	140.	.1207	.2684	.5025	Br(1)-Br(2)
13	131	0.0000	0.0000	.5000	
14	131.	.1909	.0979	.4951	
15	127.	.0933	.4473	.0156	
16	124.	.2609	.3834	.4959	Sn(1)-Sn(1)
17	123.	.2793	.4386	.4679	

	HEIGHT	X/A	Y/B	Z/C	Allocation of Vectors
18	123.	.0708	.5000	-.0033	
19	123.	.0708	.5000	.9967	
20	122.	.0235	.2483	.9808	
21	122.	.4587	.3530	.9799	
22	120.	.1051	.2034	.5198	Sn(1)-Br(1)
23	119.	.4990	.4292	.0030	
24	119.	.4990	.4292	1.0030	
25	118.	.4653	.1963	.0163	Sn(1)-Sn(1):Br(1)-Br(2)
26	116	.3878	.1202	.4851	
27	86.	.3424	.1914	.9674	Sn(1)-Sn(1):Br(1)-Br(2)
28	61.	.1211	.3023	.0260	Sn(1)-Br(1)
29	30.	.4832	.0200	.4999	Br(2)-Br(2)

None of the bigger vector peaks can be uniquely assigned to Sn-Sn vectors, but the top ten peaks can be accounted for by placing two heavy atoms in the sixfold positions:-

x = .6200, y = .1400, z = .2500,

x = .9800, y = .2200, z = .2500,

These positions are not close enough in the lattice to represent one tin and one Br(S) site so in the initial stage they were assumed to be two sets of Br(S) atoms. The positions were refined using four cycles of full matrix least squares to a residual of R = 0.409, with the bromine atoms at:-

Br(1) x = -.1360, y = .4845, z = .2122,

Br(2) x = .0123, y = .7771, z = -.2487,

A three dimensional difference Fourier map with phasing based on the refined bromine positions gave a large peak with coordinates

x = .1128, y = .8871, z = .2375,

This peak was assigned to a tin atom which had bond distances of the order of 2.85Å to atoms 1 and 2 now confirmed to be bromine atoms. The residual fell on refinement to 0.259. At this stage eighteen of the nineteen atoms in $Sn_7Br_{10}S_2$ had apparently been located, so a further Fourier synthesis was expected to reveal the position of the remaining tin atom. In fact one of the highest peaks in the Fourier map was at a position with coordinates close to $0,0,\frac{1}{4}$.

Refinement of this seventh tin atom position, at $0,0,\frac{1}{4}$, with half occupancy of the twofold site, resulted in a residual of 0.1705. This unexpectedly high R value was explained by the appearance of a Fourier difference synthesis map peak corresponding to about eleven electrons. This peak with coordinates at

x = -.2214, y = .5855, z = -.1048,

lies at a distance of 0.91Å from Sn(1). It is therefore necessary to consider the possibility that the Sn(1) atoms are not distributed over one sixfold site, but are instead distributed over two sixfold general positions (Sn(1)A and Sn(1)B). The relative heights of the peaks assignable to the two tin positions suggest that four atoms were distributed in the Sn(1)A site at

x = .4241, y = .1156, z = .7500,

and the remaining two tin atoms were distributed in the Sn(1)B site at

x = .5948, y = .8320, z = .2936,

This distribution of tin atoms in two rather than one sixfold general position explains why the Sn-Sn vectors appear so low

in the Patterson map.

After location and refinement of the atoms Sn(1)A, Sn(1)B, Sn(2), Br(1) and Br(2) at

Atom	x	y	z	site occupation factor based on 6fold general positions
Sn(1)A	.5761	.8845	.2392	.6667
Sn(1)A	.5939	.8327	.2916	.3333
Sn(2)	.9757	.0370	.2251	.1667
Br(1)	.6200	.1352	.2664	1.0000
Br(2)	.7777	.7618	.2664	1.0000

the residual dropped to 0,164. A refinement made with anisotropic temperature factors on all atoms gave a residual with R = 0.0605. Similar treatment of the data based on the Th_7S_{12} structure described earlier in this section did not improve the residual to an R value of less than 0.14.

There are three possible arrangements of sulphur atom positions in the structure. These may arise either from location of the two S atoms at the Br(1) or the Br(2) site, or from an even distribution of the two sulphur atoms over the two bromine sites.

Refinement of those atomic positions in which both sulphur atoms occupied a Br(1) site, and in which there was an even distribution of the sulphur atoms over the two Br sites resulted in residuals of 0.212 and 0.167 respectively.

However, with the two sulphur atoms occupying a Br(2) site, a residual of 0.067 was achieved. It was therefore considered, that there was not a random distribution of the

sulphur atoms over the two Br sites but a distribution of the S atoms on the Br(2) site only. A total of twenty nine reflections were then removed for which $|Fo|>2|Fc|$ or $|Fc|>2|Fo|$ and a final refinement was made with anisotropic temperature factors on all atoms to give a final residual of 0.0591.

Structural Description and Discussion

The crystal structure of $Sn_7Br_{10}S_2$ shows an unusual set of disordered atomic positions. It is not surprising that the presence of a total of twelve anions in a hexagonal cell results in the occupation of two complete sets of six-fold positions. The data are, however, not consistent with completely random distribution of Br^- and S^{2-} ions within the structure but only with random distribution of these ions on one of the two sets of six-fold positions. The second set of six positions is occupied only by Br^- ions.

The distribution of tin atoms within the cell is very unusual. With a total of seven tin atoms in the hexagonal cell, the expected distribution of cations based on the probable Th_7S_{12} would have been six in a general sixfold site and one randomly distributed on a twofold special position. The situation is, however, much more complicated than this. Attempts to fit the data to a set of six tin atoms in a general site failed and so it was necessary to redistribute the atoms as a set of four distributed in a general six-fold position based on a tin atom (Sn1) at .424, .116, .739 and a set of two distributed in a general sixfold position based on a tin atom (Sn2) at .595, .831,.287. The two sets of positions in which the tin atoms are distributed are only

0.814Å apart. This means that the distribution of tin atoms and vacancies within the two sites cannot be a simple random distribution. There must be some type of cooperative disorder that avoids the positioning of tin atoms in the two sites 0.814Å apart, but instead ensures that the positions associated with these short distances are always tin-vacancy distances.

The environments of the tin atoms (Sn1) and (Sn2) differ, but are typical of environments found in many tin(II) compounds (see Chapter 4). Table 3.1 contains details of bond lengths and angles associated with the Sn1, Sn2 and Sn3 sites. Sn(1) has a pyramidal environment of three short bonds to bromine atoms at distances of 2.83, 2.91 and 3.00Å and Br-Sn-Br angles of 82.89°, 81.48° and 96.74°. Three longer Sn-Br contacts of 3.13, 3.21 and 3.46Å complete the distorted octahedral coordination about Sn(1) (Figure 3.2(a)). The atom Sn(2) on the other hand, lies in the less common four coordinate environment, which consists of two short bonds and two longer Sn-anion distances. The short bonds to sulphur or bromine atoms are 2.76 and 2.85Å, which are typical of Sn-S and Sn-Br bond lengths respectively[24]. Two longer Sn-Br/S distances of 3.04 and 3.05Å complete the square pyramidal coordination and even longer contacts (greater than 3.24Å) complete a distorted octahedral environment about Sn(2) (Figure 3.2 (b)). The environment of the third tin atom is very unusual, with an extremely short Sn-L bond of 2.19Å which is most likely to be a Sn-S rather than a Sn-Br bond. This distance together with six tin-ligand distances (in the range 3.04 -3.52Å) give an irregular coordination about the tin atom Sn(3). Most of these Sn-L contact distances (3.24 -

Bond Lengths and Bond Angles

for

$Sn_7 Br_{10} S_2$

(a) Tin Coordination Sn(I)

Bond Distances (Å)		Bond Angles (°)	
Sn(I) - Br	2.831	Br - Sn(I) - Br	85.9
Sn(I) - Br	2.907	" " "	96.8
Sn(I) - Br	3.002	" " "	83.0
Sn(I) - Br	3.133	" " "	88.3
Sn(I) - Br	3.209	" " "	79.8
Sn(I) - Br	3.461	" " "	82.9
		" " "	81.5
		" " "	78.5

(b) Tin Coordination Sn(2)

Bond Distances (Å)		Bond Angles (°)	
Sn(2) - Br/S	2.764	Br -Sn(2) -Br/S	85.6
Sn(2) - Br/S	2.850	" " "	97.1
Sn(2) - Br/S	3.044	" " "	79.2
Sn(2) - Br	3.050	" " "	81.4
Sn(2) - Br	3.244	" " "	79.1
Sn(2) - Br	3.576	" " "	75.9
		" " "	78.2
		Br -Sn(2)- Br	89.1

Table 3.1

Bond Lengths and Bond Angles

for

$Sn_7 Br_{10} S_2$

(c) Tin Coordination Sn(3)

Bond Distances (Å)		Bond Angles (°)			
Sn(3) - Br/S	2.195	Br/S	- Sn(3)	-Br/S	85.5
Sn(3) - Br/S	3.037	"	"	"	133.4
Sn(3) - Br/S	3.239	"	"	"	100.2
Sn(3) - Br/S	3.271	"	"	"	69.4
Sn(3) - Br/S	3.307	"	"	"	79.8
Sn(3) - Br/S	3.493	"	"	"	79.0
Sn(3) - Br/S	3.523	"	"	"	123.3
		"	"	"	136.5

Table 3.1 (continued)

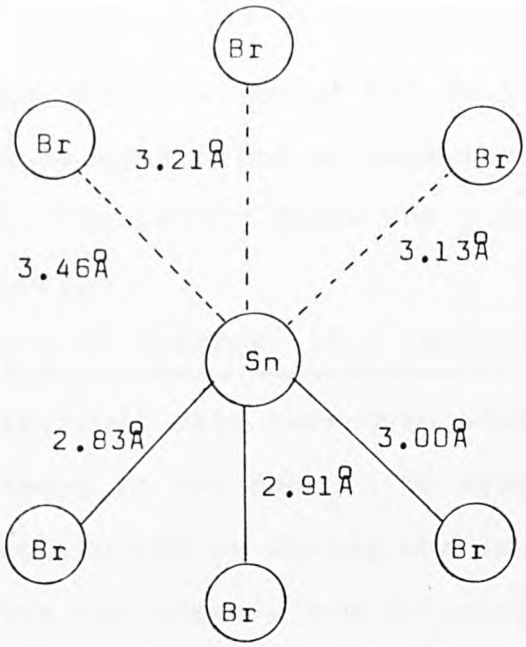

Figure 3.2a
The environment of Sn(1): Trigonal pyramidal

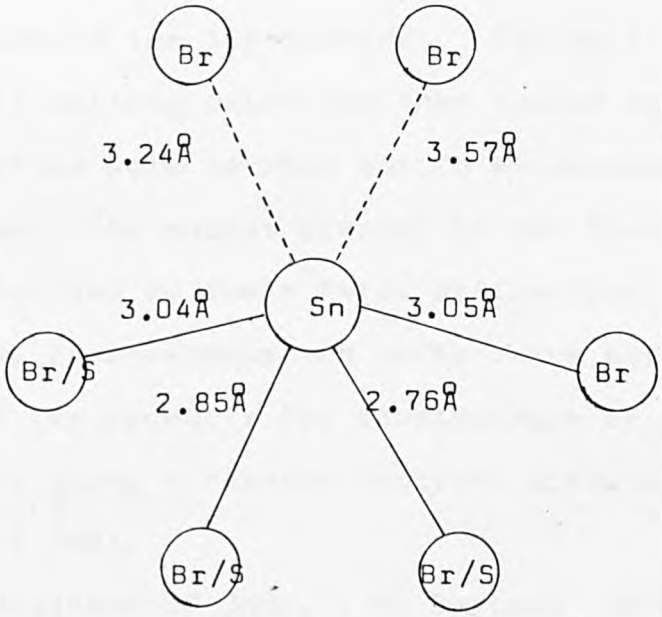

Figure 3.2b
The environment of Sn(2): Square pyramidal

3.52Å) are longer than the sum of the Sn-S and Sn-Br ionic radii, and must be considered as weak interactions rather than Sn-L bonds. Figure 3.2c shows the c projection of the unit cell of $Sn_7Br_{10}S_2$.

3.1.2 $SnBr_2$: MS Systems (M = Cd, Pb)

Thermal analytical data have been used in this work to study ternary phases in the $SnBr_2$: MS systems. Phase diagrams were constructed by mixing the appropriate molar proportions of the two phases, and grinding them to give an intimate mixture. This mixture was then placed in a narrow-necked tube designed to restrict the loss of any volatile products of the reaction between the two components. The temperature of the mixture was than raised to the melting point of stannous bromide to obtain a solution of metal sulphide in the tin bromide. The melt was cooled, heated to its melting point and then cooled again. All of these operations were carried out in an atmosphere of oxygen free nitrogen. The phases present in the final cooled melts were characterized by their X-ray diffraction, ^{119}Sn Mössbauer, conductivity, luminescence and reflectance data. The thermal behaviour of the products for construction of a phase diagram were obtained using a Stanton Redcroft Simultaneous Thermal Analyser (STA 780).

Phase Diagrams of $SnBr_2$: MS Systems (M = Cd, Pb)

The phase diagrams were constructed for the titled systems over a composition range where complete solubility of the metal sulphide in tin(II) bromide can be achieved. These composition ranges were 40 - 100 mole % $SnBr_2$ for the

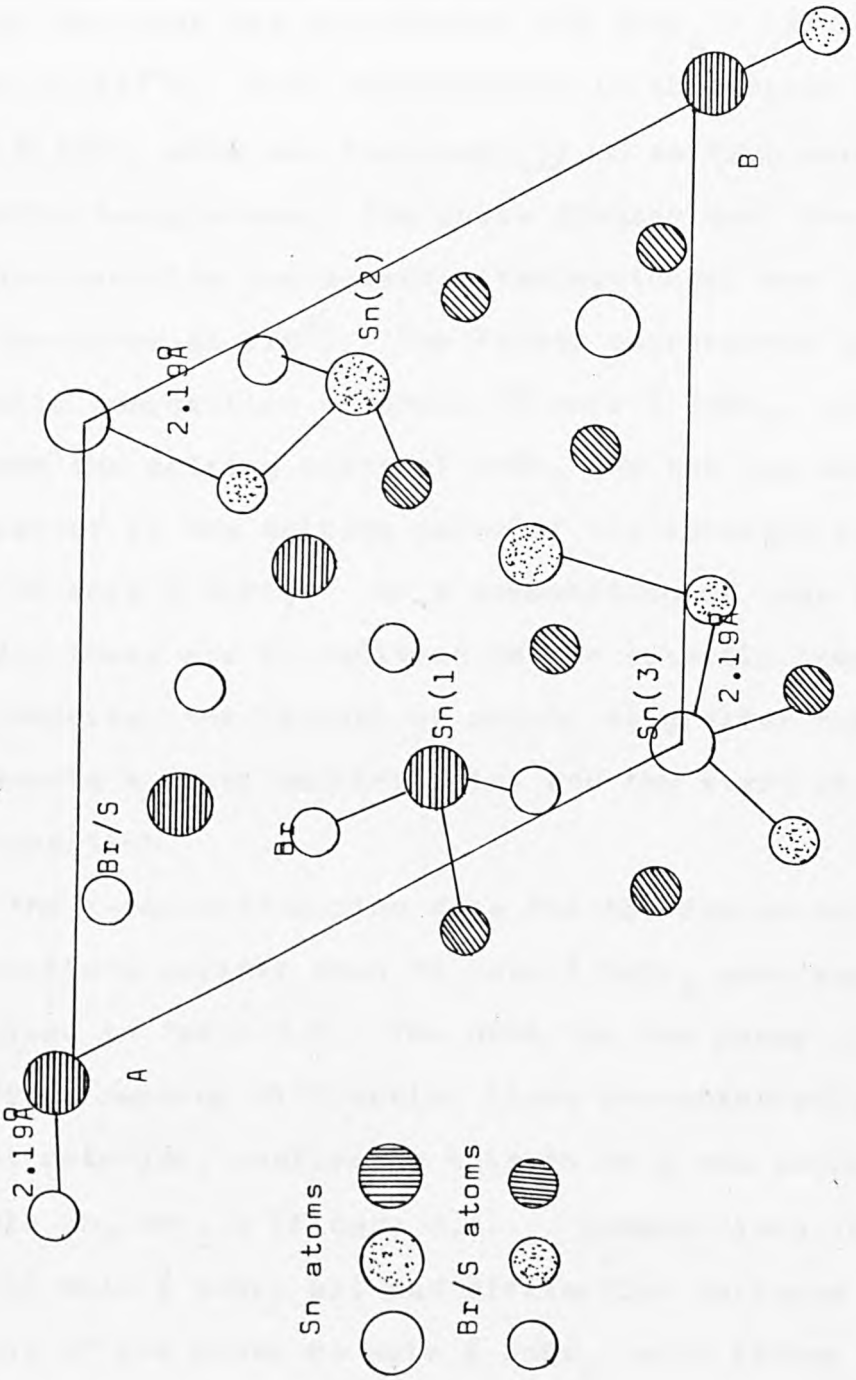

Figure 3.2c Structure of $Sn_7Br_{10}S_2$ viewed along the c axis

CdS system, and 60 - 100 mole % $SnBr_2$ for the PbS system, and the results of the two phase studies are given in Table 3.2.

The phase diagram for the cadmium sulphide system is shown in Figure 3.3. The phase diagram, in the region 40 - 100 mole % $SnBr_2$, shows only one congruently melting phase, and that has composition 85% $SnBr_2$: 15% CdS, which melts at 247°C. Most compositions in the region 70 - 100 mole % $SnBr_2$ show two features *viz.* a melting point and a eutectic temperature. The phase diagram over the region studied exhibits two eutectic temperatures, one at 215°C and the other at 226°C. The former corresponds to a eutectic composition of about 95 mole % $SnBr_2$, which lies between the melting point of $SnBr_2$ and the new phase, whilst the latter is the melting point of the eutectic composition with 65 mole % $SnBr_2$. At a composition of less than 60 mole % $SnBr_2$ there are in addition to the eutectic temperature, two features, the highest of which, at greater than 300°C represents a final melting point and the start of thermal decomposition.

The X-ray diffraction data for the cooled melts with compositions greater than 70 mole % $SnBr_2$ were recorded and are given in Table 3.3. The data for the phase with 85 mole % $SnBr_2$ showed no diffraction lines characteristic of either parent material, confirming this to be a new single phase of formula $Sn_6CdBr_{12}S$ (Figure 3.4). Compositions in the range 70 - 80 mole % $SnBr_2$ all had diffraction patterns similar to that of the phase 85 mole % $SnBr_2$, with strong lines that could now be associated with those of the new $Sn_6CdBr_{12}S$ phase. There are, however, additional lines but these are

Results of Phase Diagram Studies

for the

$SnBr_2$: MS systems

$SnBr_2$: CdS System

Composition	Melting Point	Eutectic Temp.
100% $SnBr_2$	226°C	-
95% $SnBr_2$	226°C	215°C
90% $SnBr_2$	238°C	226°C
85% $SnBr_2$	247°C	-
80% $SnBr_2$	242°C	226°C
75% $SnBr_2$	237°C	226°C
70% $SnBr_2$	226°C	226°C
65% $SnBr_2$	226°C	226°C
60% $SnBr_2$	226°C	226°C
55% $SnBr_2$	237°C	-

$SnBr_2$: PbS System

100% $SnBr_2$	226°C	-
95% $SnBr_2$	238°C	-
90% $SnBr_2$	258°C	236°C
85% $SnBr_2$	263°C	258°C 236°C
80% $SnBr_2$	284°C	258°C
75% $SnBr_2$	281°C	258°C
70% $SnBr_2$	292°C	258°C
65% $SnBr_2$	305°C	258°C
60% $SnBr_2$	310°C	-

Table 3.2

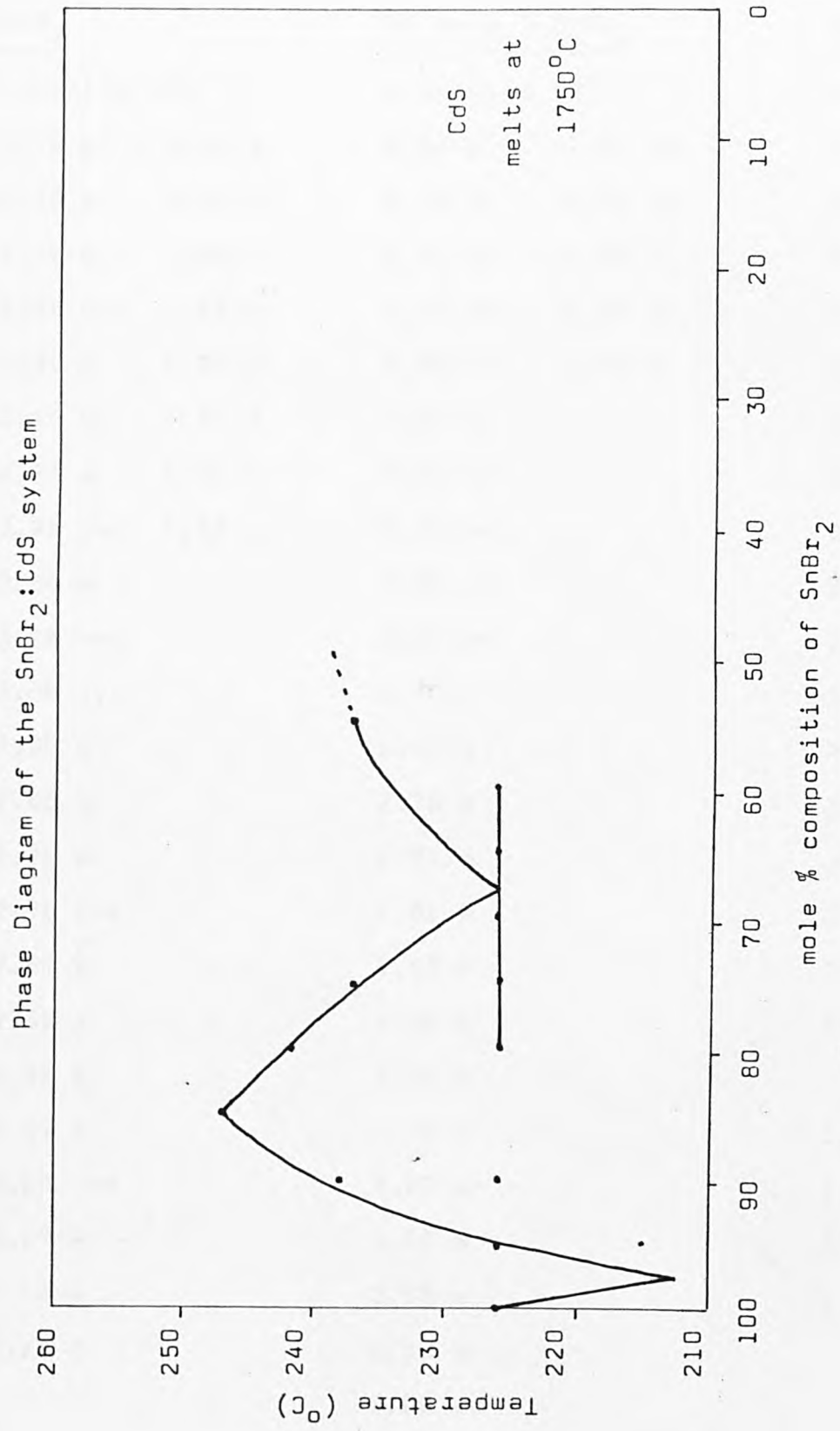
Phase Diagram of the $SnBr_2$:CdS system
CdS
melts at
1750°C
Temperature (°C)
260
250
240
230
220
210
100
90
80
70
60
50
40
30
20
10
0
mole % composition of $SnBr_2$

X-ray Diffraction Data for the cooled melts from the $SnBr_2$: CdS system

$SnBr_2$		95 mole % $SnBr_2$		90 mole % $SnBr_2$
d spacing (Å)		d spacing (Å)		d spacing (Å)
11.79 w	2.04 w	6.61 w	1.97 vw	6.32 vs
10.78 w	2.02 w	6.15 w	1.91 vw	6.15 m
9.21 m	1.98 w	5.31 vw	1.88 w	4.02 m
6.61 vvs	1.95 w	4.48 vw	1.86 w	3.56 vw
5.31 m	1.88 m	4.04 w	1.75 w	3.37 w
4.48 ms	1.85 s	3.92 w		3.14 w
4.23 w	1.80 m	3.56 w		3.07 w
3.92 vvs	1.78 w	3.41 vw		2.96 s
3.56 w		3.30 w		2.75 w
3.29 vvs		3.08 ms		2.51 w
3.08 vvs		2.96 s		2.44 w
2.99 w		2.88 m		2.31 m
2.88 s		2.76 w		2.27 w
2.78 w		2.71 m		2.18 w
2.71 vvs		2.61 m		2.13 w
2.60 s		2.58 m		2.09 w
2.58 s		2.52 m		2.01 vw
2.52 s		2.44 w		1.99 vw
2.47 s		2.32 m		1.91 w
2.19 vvs		2.27 w		1.75 w
2.17 m		2.19 m		1.59 w
2.14 m		2.16 w		1.57 w
2.12 s		2.13 w		
		2.00 vw		

Table 3.3

X-ray Diffraction Data

for the

$SnBr_2$: CdS System

85 mole % $SnBr_2$	80 mole % $SnBr_2$	75 mole % $SnBr_2$
d spacing (Å)	d spacing (Å)	d spacing (Å)
6.37 s	6.32 m	6.32 m
6.15 m	6.15 w	6.15 w
4.02 w	4.02 vw	4.04 w
3.57 vw	3.93 vw	3.95 vw
3.43 w	3.57 vw	3.57 vw
3.15 vw	3.40 w	3.40 w
3.07 w	3.05 m	3.05 m
2.97 s	2.96 s	2.96 s
2.76 m	2.91 m	2.91 m
2.51 w	2.75 m	2.76 m
2.45 w	2.57 vw	2.52 vw
2.31 m	2.52 vw	2.49 vw
2.27 vw	2.44 m	2.45 w
2.20 vw	2.32 m	2.32 w
2.13 vw	2.27 vw	2.27 vw
2.10 vw	2.19 vw	2.19 vw
1.99 w	2.13 vw	2.13 vw
1.91 vw	2.05 w	2.06 w
1.82 vw	1.99 vw	1.99 vw
1.75 vw	1.85 vw	1.90 vw
1.69 vw	1.82 vw	1.89 vw
1.59 vw	1.75 vw	1.82 vw
1.58 vw	1.59 vw	1.75 vw

Table 3.3 (continued)

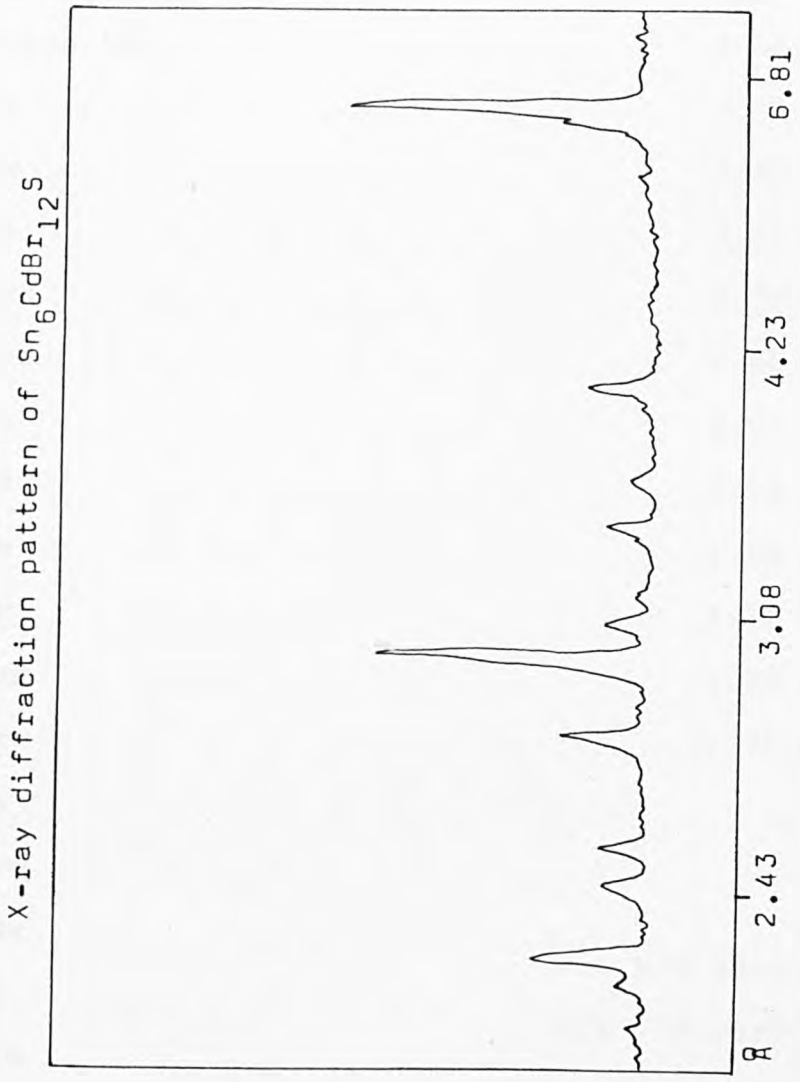

Figure 3.4

X-ray Diffraction Data

for the

$SnBr_2$: CdS System

70 mole % $SnBr_2$	CdS
d spacing (Å)	d spacing (Å)
6.15 w	3.80 w
4.02 w	3.53 m
3.93 m	3.51 m
3.57 vw	3.36 s
3.37 vw	2.96 m
3.05 s	2.47 w
2.96 s	2.06 m
2.90 s	1.89 vw
2.75 w	1.83 vw
2.57 vw	1.76 w
2.51 vw	1.75 w
2.49 w	
2.44 vw	
2.42 vw	
2.32 w	
2.27 vw	
2.19 vw	
2.13 vw	
2.06 m	
2.01 vw	
1.85 vw	
1.82 vw	
1.78 vw	
1.75 vw	

v.v.s = very, very strong

v.s = very strong

s. = strong

m.s = medium strong

m. = medium

w. = weak

v.w = very weak

Table 3.3 (continued)

not characteristic of CdS, which suggests that at least one additional new phase must exist between the composition range 60 and 100 mole % CdS. The data for the cooled melts with 90 mole % $SnBr_2$, contain lines that can be attributed to stannous bromide.

The phase diagram for the lead sulphide system is shown in Figure 3.5 Two phases, those with 90 mole % $SnBr_2$ and 80 mole % $SnBr_2$ are identified as the only congruently melting compounds in this system with melting points of 258°C and 284°C respectively. The phase diagram has two eutectic temperatures over the region studied viz. 236°C at 87.5 mole % $SnBr_2$ and 258°C at 72.5 mole % $SnBr_2$. Cooled melts containing less stannous bromide than the eutectic composition of 72.5 mole % have melting points greater than 290°C, that increase with the lead sulphide concentration.

X-ray diffraction data were recorded for the cooled melts with compositions in the range 60 - 95 mole % $SnBr_2$. Details of the X-ray data are given in Table 3.4. The X-ray patterns for compositions with greater than 90 mole % $SnBr_2$ show lines characteristic of stannous bromide. The data for the material of composition 90 mole % $SnBr_2$ however, are consistent with this being a distinct new phase of formula $Sn_{0.9}Pb_{0.1}Br_{1.8}S_{0.1}$ (Figure 3.6). Further addition of lead sulphide to stannous bromide alters the diffraction pattern of the material, giving a similar but not identical trace. These differences first appear in the X-ray pattern of the cooled melt of composition 85 mole % $SnBr_2$. For the material with 80 mole % $SnBr_2$ the lines are well resolved, showing that a distinct new crystalline phase Sn_4PbBr_8S exists (Figure 3.7).

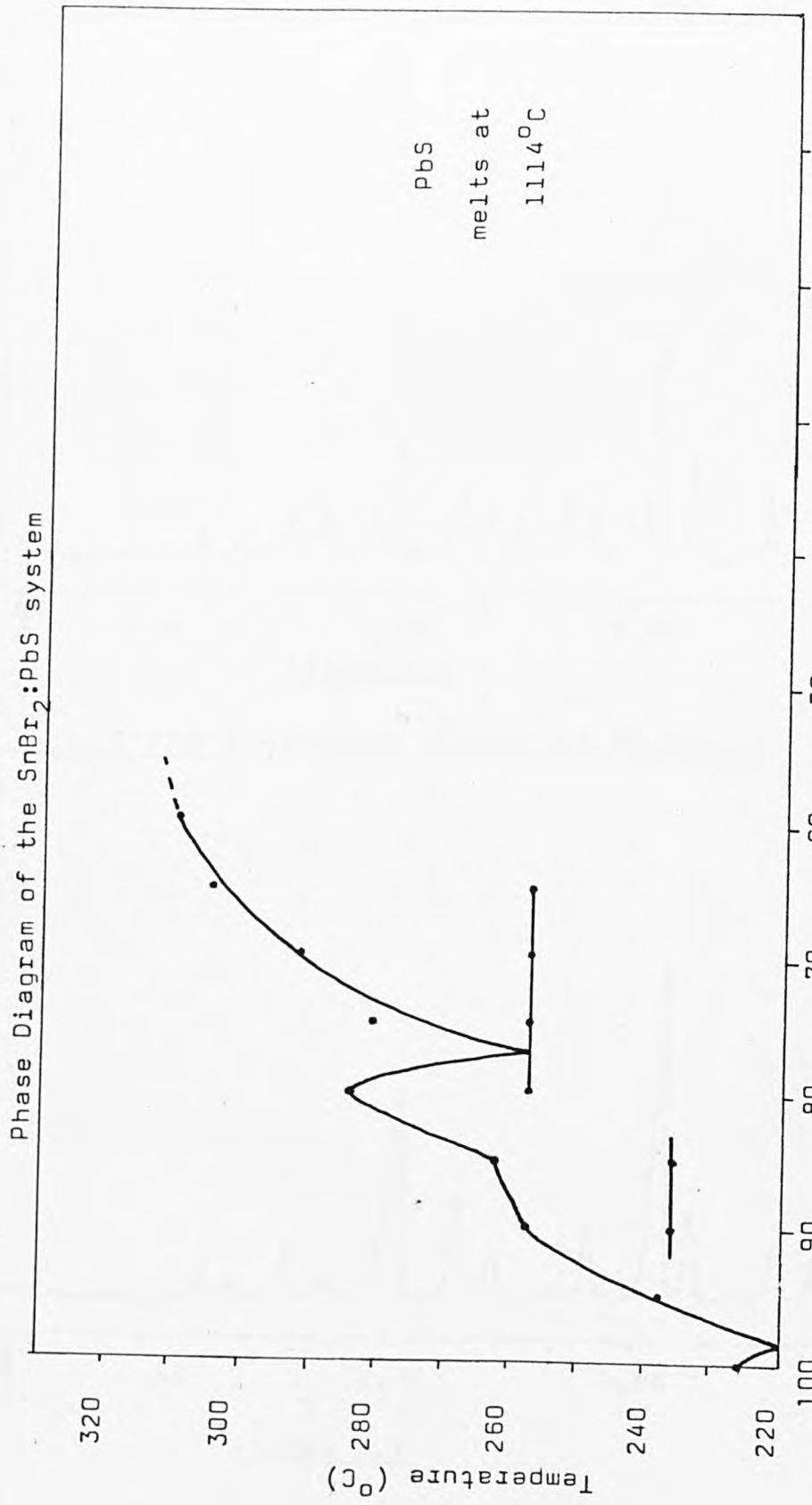
Phase Diagram of the $SnBr_2$:PbS system
PbS
melts at
1114°C
Temperature (°C)
320
300
280
260
240
220
0
10
20
30
40
50
60
70
80
90
100
mole % composition $SnBr_2$

Figure 3.5

X-ray Diffraction pattern of $Sn_{0.9}Pb_{0.1}Br_{1.8}S_{0.1}$

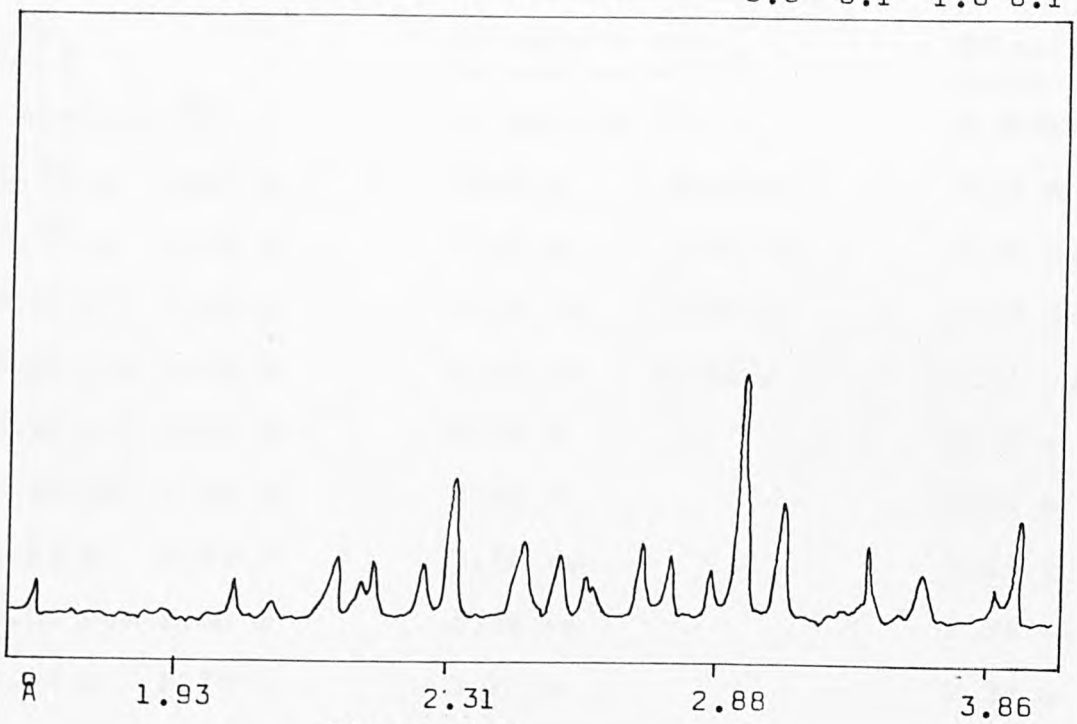

Figure 3.6

X-ray Diffraction pattern of Sn_4PbBr_8S

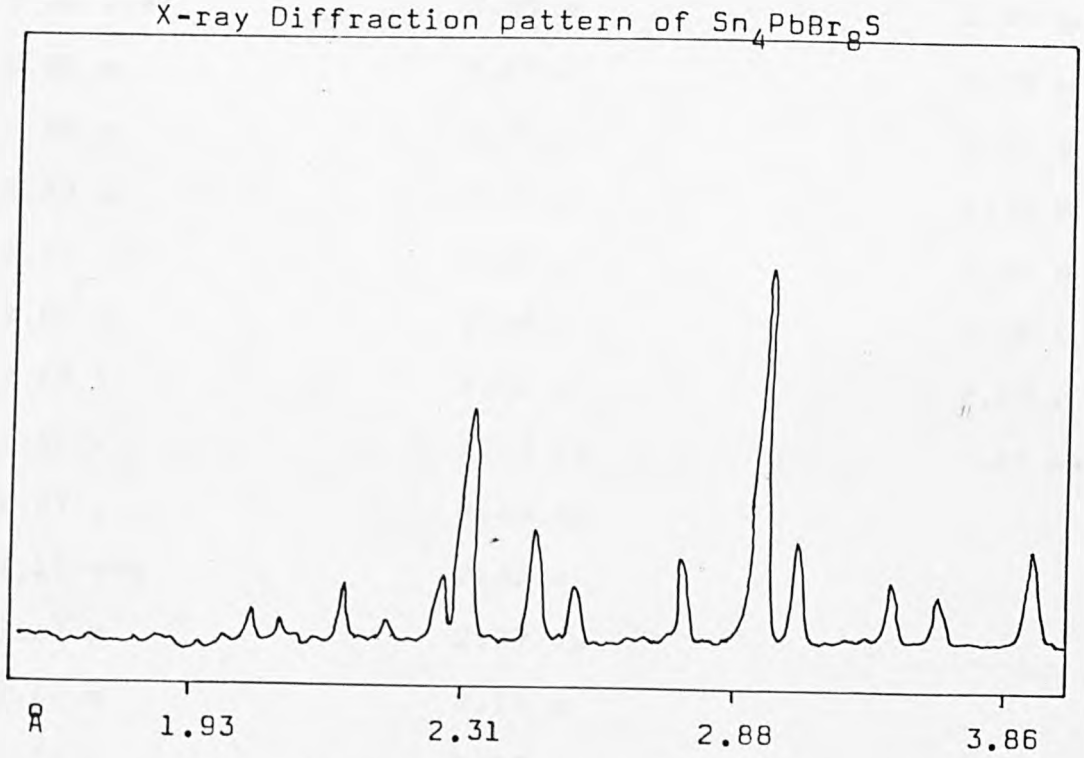

Figure 3.7

X-ray Diffraction Data for the cooled melts from the $SnBr_2$: PbS system

$SnBr_2$		95 mole % $SnBr_2$		90 mole % $SnBr_2$
d spacing (Å)		d spacing (Å)		d spacing (Å)
11.79 w	2.04 w	6.61 m	2.13 m	4.04 m
10.78 w	2.02 w	6.19 w	1.92 vw	3.90 vw
9.21 m	1.98 w	5.31 vw	1.88 w	3.59 vw
6.61 vvs	1.95 w	4.48 vw	1.85 w	3.51 vw
5.31 m	1.92 w	4.04 w		3.39 w
4.48 ms	1.88 m	3.91 m		3.08 m
4.23 w	1.85 s	3.56 vw		2.97 s
3.92 vvs	1.80 m	3.39 vw		2.88 vw
3.56 w	1.78 w	3.29 m		2.76 w
3.29 vvs		3.09 s		2.71 w
3 08 vvs		2.97 s		2.61 w
2.99 w		2.88 m		2.58 w
2.88 s		2.76 w		2.52 w
2.78 w		2.71 s		2.32 m
2.71 vvs		2.59 m		2.27 w
2.60 s		2.58 m		2.19 w
2.58 s		2.51 m		2.13 w
2.52 s		2.47 vw		2.01 vw
2.47 s		2.45 vw		
2.19 vvs		2.33 m		
2.17 m		2.27 vw		
2.14 m		2.19 m		
2.12 s		2.17 m		

Table 3.4

X-ray Diffraction Data

for the

$SnBr_2$: PbS System

85 mole % $SnBr_2$	80 mole % $SnBr_2$	75 mole % $SnBr_2$
d spacing (Å)	d spacing (Å)	d spacing (Å)
6.24 vw	6.15 vw	6.15 w
4.04 w	4.02 w	4.02 m
3.59 w	3.56 vw	3.56 w
3.40 w	3.37 w	3.37 m
3.21 w	3.08 w	3.07 vw
2.98 s	2.97 s	2.96 s
2.88 vw	2.76 w	2.75 m
2.77 m	2.51 vw	2.51 w
2.59 vw	2.44 w	2.44 m
2.52 vw	2.32 m	2.31 m
2.45 w	2.27 w	2.27 w
2.32 w	2.19 vw	2.18 m
2.28 vw	2.13 w	2.13 w
2.19 vw	2.05 vw	2.05 vw
2.13 vw	2.01 vw	2.01 vw
1.76 vw	1.76 vw	1.92 vw
1.59 w	1.62 vw	1.82 vw
	1.59 w	1.75 vw
		1.61 vw
		1.59 w

Table 3.4 (continued)

X-ray Diffraction Data

for the

$SnBr_2$: PbS System

60 mole % $SnBr_2$	PbS
d spacing (Å)	d spacing (Å)
4.87 w	10.28 m
4.19 w	5.94 w
4.09 m	4.21 vw
3.80 m	3.43 vvs
3.41 w	3.19 w
3.30 w	2.97 vvs
3.14 m	2.81 vw
3.11 m	2.62 vw
2.98 s	2.57 vw
2.96 s	2.09 s
2.86 w	1.79 ms
2.85 w	1.71 m
2.78 w	1.48 vw
2.67 s	
2.53 w	
2.45 w	
2.42 w	
2.37 m	
2.34 vw	
2.29 w	
2.23 w	
2.19 vw	
2.12 vw	

v.v.s = very, very strong

v.s = very strong

s. = strong

m.s = medium strong

m. = medium

w. = weak

v.w = very weak

Table 3.4 (continued)

The diffraction pattern for the cooled melt 60 mole % $SnBr_2$, is different from that of lead sulphide implying another distinct phase exists in the composition range with less than 60 mole % $SnBr_2$.

^{119}Sn Mössbauer Spectra

The ^{119}Sn Mössbauer parameters for the two $SnBr_2$: MS (M = Cd, Pb) systems have been recorded at 80K for some of the cooled melts with compositions in the range 95 - 70 mole % $SnBr_2$ for the CdS system, and in the range 95 - 60 mole % $SnBr_2$ for the PbS system. Details of these Mössbauer data are given in Table 3.5. Also included in the table are the data for the tin(II) bromide, tin(II) sulphide and the tin(II) chalcogenide halide $Sn_7Br_{10}S_2$.

In both systems, the melts with composition of 90 mole % $SnBr_2$, have single line spectra which are similar to that of tin(II) bromide. Although X-ray data identify the cooled melt from the lead system as a distinct phase, ($Sn_{0.9}Pb_{0.1}Br_{1.8}S_{0.1}$) the similarity of its Mössbauer data to that of $SnBr_2$, suggests that with the presence of 10% PbS in the lattice there is little change in the average way in which tin uses its electrons in bond formation. The spectra for the distinct phases $Sn_6CdBr_{12}S$ and Sn_4PbBr_8S show the presence of two tin sites. The data are not, however, consistent with the existence of separate Sn-Br and Sn-S environments. In the lead sulphide system, evidence for the two tin sites begins at the composition of 85 mole % $SnBr_2$, however, fitting to two sites does not improve the statistics of the fit of the data points. As the concentration of the metal sulphide is increased, the low shift site shows a

^{119}Sn Mössbauer Data

Compound		δ mms^{-1}	Δ mms^{-1}
$SnBr_2$: CdS			
90 mole % $SnBr_2$		3.95	0
$Sn_6CdBr_{12}S$	site(1)	4.25	0
	site(2)	3.46	0
80 mole % $SnBr_2$		4.23	0
		3.40	0
75 mole % $SnBr_2$		4.23	0
		3.28	0
$SnBr_2$: PbS			
$Sn_{0.9}Pb_{0.1}Br_{1.8}S_{0.1}$		3.94	0
85 mole % $SnBr_2$		3.96	0
Sn_4PbBr_8S	site(1)	4.13	0
	site(2)	3.39	0
60 mole % $SnBr_2$	site(1)	3.87	0
	site(2)	2.80	0
$Sn_7Br_{10}S_2$	site(1)	3.76	0
	site(2)	3.41	0
SnS		3.29	0.93
$SnBr_2$		3.93	0

Table 3.5

steady decrease in shift towards the value for SnS. This is interpreted as being due to the formation of increasing amounts of tin-sulphur type environments with increasing sulphide concentration.

The Mössbauer data for both systems are in fact similar to those of $Sn_7Br_{10}S_2$ (Table 3.5) which also show a two tin site Mössbauer spectrum. Although none of the distinct phases obtained from the cadmium and lead sulphide systems can be isostructural with $Sn_7Br_{10}S_2$, the immediate environment of the tin atoms in $Sn_6CdBr_{12}S$ and Sn_4PbBr_8S are similar.

Optical Properties

Both luminescence and reflectance measurements have been made on some of the cooled melts from both the $SnBr_2$: CdS and $SnBr_2$: PbS systems.

Luminescence spectra recorded for the samples, showed only a broad emission band in the region 520 - 700nm with no other identifiable features in the spectra. This broad emission band could arise from two possible mechanisms *viz*. the involvement of transitions between broad bands or a series of closely spaced transitions between narrow bands. In view of the fact that band to band transitions are known for main group elements in their lower oxidation states in bromide environments, it seems reasonable to suggest that the transitions between broad bands is more likely.

All reflectance spectra were measured using an Hitachi Perkin Elmer EPS - 3T recording spectrophotometer. The spectra of the phases in the $SnBr_2$: CdS system all have one or more absorption edge. The absorption edges appear to move towards lower energies with increasing cadmium sulphide

content and there is evidence of a second edge in the spectra of the materials with composition of 70 and 65 mole % $SnBr_2$ (Table 3.6). The appearance of the second edge suggests the tin(II) bromide in the two mixtures is not absorbing all the visible radiation, hence the absorption edge associated with cadmium sulphide is superimposed. The reflectance spectra for most of the cooled melts from the lead sulphide system show strong absorption over the entire visible region. Lead sulphide has high background absorption and no edge in the visible region. Hence the effect of stannous bromide in the material is one of dilution. Those phases with more than 75 mole % $SnBr_2$ have a small edge superimposed on the high background absorption of lead sulphide, and as a result are black in colour.

Electrical Properties

All electrical measurements were carried out on pelleted samples of most of the cooled melts obtained from the $SnBr_2$: MS system (M = Cd:Pb). Approximately 0.5g of the ground sample was put into a 13mm silver steel die, which was put under vacuum, and an external pressure of 5 tons applied to the die for 5 - 10 minutes. To ensure that an intimate electrical contact was made, tin foil discs (radius 0.5cm) were pressed onto opposite faces of the pellet. In all cases, the pellets were prepared immediately prior to use. Measurements were made by placing the pellet between copper electrodes and recording the resistance in terms of MhO's, using a Wayne Kerr Bridge. The electrical conductivity data for the samples are given in Table 3.7 together with the data for $Sn_7Br_{10}S_2$ for comparison.

Reflectance Data for the cooled melts from $SnBr_2$: MS systems

$SnBr_2$: CdS system

Compound	Absorption Edge (eV)
$SnBr_2$	3.06
90 mole % $SnBr_2$	2.74
$Sn_6CdBr_{12}S$	2.75
80 mole % $SnBr_2$	2.82
75 mole % $SnBr_2$	2.79
70 mole % $SnBr_2$	2.86, 2.33
65 mole % $SnBr_2$	2.86, 2.33
CdS	2.23

$SnBr_2$: PbS system

Compound	Absorption Edge (eV)
$SnBr_2$	3.06
$Sn_{0.9}Pb_{0.1}Br_{1.8}S_{0.1}$	2.67
Sn_4PbBr_8S	2.40
75 mole % $SnBr_2$	2.48
60 mole % $SnBr_2$	no edge
PbS	no edge

Table 3.6

Electrical Conductivity Data

for the Cooled Melts

from the $SnBr_2$: MS Systems (M = Cd,Pb)

Compound	Electrical Conductivity (ohm^{-1} cm^{-1})
$SnBr_2$: CdS System	
95 mole % $SnBr_2$	9.09×10^{-8}
90 mole % $SnBr_2$	1.76×10^{-7}
$Sn_6CdBr_{12}S$	4.60×10^{-8}
80 mole % $SnBr_2$	1.53×10^{-7}
75 mole % $SnBr_2$	3.34×10^{-8}
70 mole % $SnBr_2$	1.22×10^{-7}
65 mole % $SnBr_2$	1.76×10^{-7}
60 mole % $SnBr_2$	1.01×10^{-5}
50 mole % $SnBr_2$	2.81×10^{-5}
CdS	3.00×10^{-4}
$SnBr_2$: PbS System	
95 mole % $SnBr_2$	7.51×10^{-8}
$Sn_{0.9}Pb_{0.1}Br_{1.8}S_{0.1}$	1.57×10^{-8}
85 mole % $SnBr_2$	1.08×10^{-7}
Sn_4PbBr_8S	5.97×10^{-7}
75 mole % $SnBr_2$	2.89×10^{-7}
70 mole % $SnBr_2$	3.61×10^{-7}
65 mole % $SnBr_2$	1.67×10^{-5}
60 mole % $SnBr_2$	3.06×10^{-5}
PbS	5.42×10^{-5}
$SnBr_2$	1.07×10^{-6}
$Sn_7Br_{10}S_2$	7.34×10^{-8}

Table 3.7

The results show that conductivities of all samples measured lie within the range 10^{-4} to 10^{-8} ohm^{-1} cm^{-1}. These compounds can therefore be classified as semiconductors. Although the conducting ability of the phases of mixed composition is considerably less than that of the parent compounds, the conductivities of all of the mixed phases are orders of magnitude less than that of the high symmetry perovskite phase, $CsSnBr_3$, in which the conductivity arises from the direct population of solid state bands by the tin non-bonding electrons. It is therefore unlikely that the conductivities in the halide chalcogenides arise from a similar direct population mechanism.

3.1.3 Summary

This study of the reaction of tin(II) bromide with metal (II) sulphides has shown that the addition of the sulphide to $SnBr_2$ changes the X-ray pattern dramatically and new phases appear with as little as 10 and 20 mole % PbS in the $SnBr_2$ lattice, and 15 mole % CdS in the lattice. If these new compounds have structures similar to that of $Sn_7Br_{10}S_2$, the tin and metal atoms must be accomodated in the lattice in a complicated manner.

The absence of high symmetry tin(II) sites in the crystal structure of $Sn_7Br_{10}S_2$ and of narrow Mössbauer resonance lines in all of the mixed phases are consistent with the suggestion that the conductivity in the materials does not arise from direct population of the solid state bands, but must be associated with impurity levels in the lattices. In spite of the fact that the anionic sub-lattice is made up of relatively large anions, it appears that no empty accessible three-

dimensional bands are formed in the halide chalcogenides. The fate of the tin species in the formation of these phases is unusual in that it is likely to lead to partial occupancy of crystallographic sites, but is normal in that the tin sites that are formed, are of the usual lone pair distorted type.

3.2 Tin(II) Fluoride : Caesium Bromide Molten System

To date, studies of reactions between tin(II) halide and caesium halide species (where the halide is fluoride or bromide) in both molten and aqueous solutions have been of three types viz. (1) the all-fluoride system, SnF_2 : CsF, (2) the all-bromide system, $SnBr_2$: CsBr and (3) the mixed halide system, $CsSnBr_3$: $CsSnF_3$.

The complex tin(II) compounds precipitated from the molten systems MF - SnF_2 (M = Li,Na,K, Rb and Cs) have been shown[25] by X-ray analysis to be identical to those crystallised from the corresponding aqueous systems. The results from the study showed that the predominant species found in aqueous media, viz. SnF_3^- and $Sn_2F_5^-$ are also present in tin(II) fluoride melts. The complete equilibrium diagram of the CsBr : $SnBr_2$ system has been determined[26]. It was found that, in addition to the $CsSnBr_3$ and $CsSn_2Br_5$ phases, that had also been prepared from aqueous solution, a third phase of composition Cs_4SnBr_6 was also present. An investigation into the preparation of the dark grey Cs_4SnBr_6 phase revealed that, like $CsSnBr_3$, it could be prepared readily either from solution or molten systems. The only mixed halide phases reported[27] were those resulting from a study of the molten systems $CsSnBr_3$: $CsSnF_3$. In the $CsSnF_{3-n}Br_n$ system, the materials have lone pair distorted

environments at room temperature for n less than 1.5, and perovskite lattices for n greater than 1.5. This is reflected in the Mössbauer data where the resonance lines show quadrupole splitting for n < 1.5 and decreasingly small line widths for n greater than 1.5. In these systems, there are always sufficient caesium ions to make a $CsSnX_3$ species. The aim of the present work is to study the results from the molten system SnF_2: CsBr in which there may be either an excess or a deficiency of caesium ions for fluorostannate(II) formation.

3.2.1 Phase Diagram for SnF_2 : CsBr system

The thermal analytical technique described in section 3.1.2 was used to construct the phase diagram for the system. The composition range of 15 - 100 mole % SnF_2, in which there was complete solubility of caesium bromide in tin(II) fluoride was studied. The materials for study were prepared by heating the cooled melts of an intimately ground mixture of SnF_2 and CsBr in an atmosphere of oxygen-free nitrogen. The phase diagram for the system is shown in Figure 3.8, whilst the numerical results are given in Table 3.8. X-ray, Mössbauer, reflectance and conductivity measurements were used to characterise the cooled melts.

Although the two starting materials are white, as the concentration of caesium and bromide ions in the sample was increased, the intensity of the colour of the cooled melts changes, from white at 100 mole % SnF_2, to grey and finally black, at 15 mole % SnF_2. The phase diagram shows three congruently melting phases of composition 72.5, 45 and 35 mole % SnF_2 whose melting points are 220°, 213° and 210°C

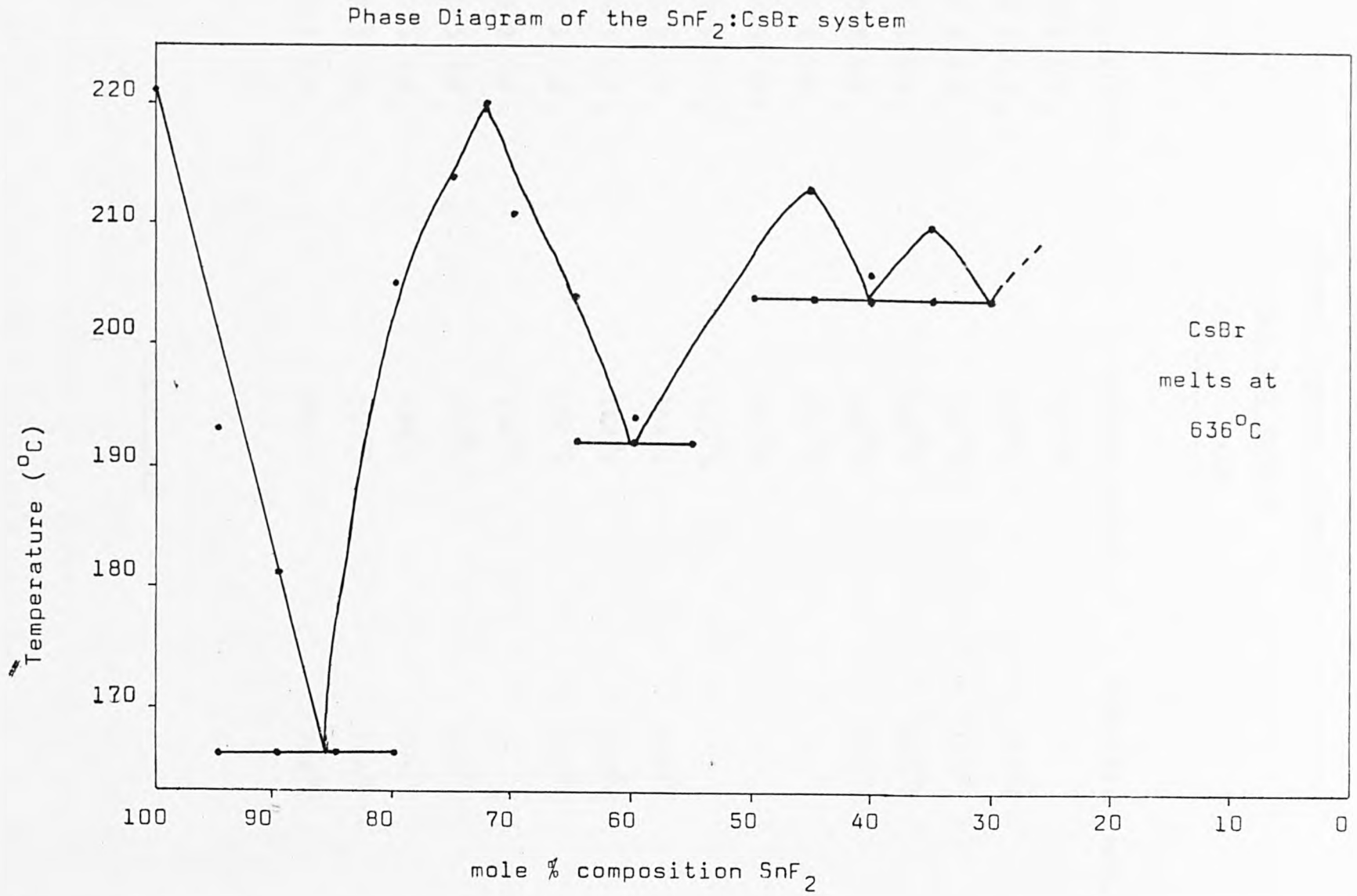
Phase Diagram of the SnF_2:CsBr system
Temperature (^oC)
220
210
200
190
180
170
100
90
80
70
60
50
40
30
20
10
0
mole % composition SnF_2
CsBr
melts at
636^oC

Figure 3.8

Phase Diagram Results for the system SnF_2 : CsBr

Composition	Melting point	Eutectic Temp.
100% SnF_2	221°C	-
95 % SnF_2	193°C	166°C
90 % SnF_2	181°C	166°C
85 % SnF_2	166°C	166°C
80 % SnF_2	205°C	166°C
75 % SnF_2	214°C	-
72.5% SnF_2	220°C	-
70 % SnF_2	211°C	-
65 % SnF_2	204°C	192°C
60 % SnF_2	194°C	192°C
55 % SnF_2	192°C	192°C
50 % SnF_2	204°C	-
45 % SnF_2	213°C	204°C
40 % SnF_2	206°C	204°C
35 % SnF_2	210°C	204°C
30 % SnF_2	204°C	204°C

Table 3.8

respectively. These phases give rise to four eutectic phases with compositions of 85, 55, 40 and 30 mole % SnF_2, with melting points at 166°, 192°, 204° and 204°C respectively. The new phases A, B and C (compositions 72.5, 45, 35 mole % SnF_2 respectively) that have been isolated from the molten SnF_2 : CsBr system, appear to have different compositions to those isolated from the aqueous system studied and described in section 2.4.1. In view of these differences, X-ray diffraction data were recorded (Table 3.9) and used to identify the new phases isolated from the molten system, and to compare them with the known phases obtained from aqueous solution. None of the diffraction patterns for the cooled melts from the SnF_2 : CsBr system, have traces identical to those of the parent compounds, although there is evidence at the high fluoride and the high bromide ends, of lines that can be associated with SnF_2 and CsBr, respectively. The diffraction pattern for SnF_2, changes markedly on addition of as little as 5 mole % CsBr. With up to 15 mole % CsBr there is little change in the complexity of the line-pattern. Comparison of the diffraction patterns of the cooled melts above and below the eutectic composition (85 mole % SnF_2) show the phases to be mixtures of both SnF_2 and the new phase A. The disappearance of any lines that could be associated with a mixture first becomes apparent in the diffraction pattern of the melt, with a composition of 75 mole % SnF_2. In the region 70 - 75 mole % SnF_2 in which phase A has been isolated as shown by a phase diagram study, there is no real change in the diffraction patterns. Comparison of these diffraction data and those characteristic of

X-ray Diffraction Data for the cooled melts from the SnF_2 : CsBr system

SnF_2	95 mole % SnF_2	90 mole % SnF_2
d spacing (Å)	d spacing (Å)	d spacing (Å)
3.53 s	3.71 w	3.77 vw
3.39 m	3.59 s	3.67 vw
3.21 w	3.37 w	3.56 s
3.19 w	3.28 ms	3.53 ms
3.14 w	3.23 ms	3.36 m
2.15 m	3.16 w	3.23 m
2.14 m	2.58 w	3.17 m
1.98 w	2.49 vw	3.15 m
	2.45 vw	3.11 w
	2.40 vw	2.85 vw
CsBr	2.12 vw	2.81 vw
d spacing (Å)	2.06 vw	2.53 w
4.31 m	2.01 w	2.38 vw
3.38 s		2.17 vw
3.05 vs		2.10 vw
2.48 w		
2.38 w		
2.15 m		

Table 3.9

X-ray Diffraction Data

for the cooled melts

from the SnF_2 : CsBr system

72.5 mole % SnF_2	70 mole % SnF_2	65 mole % SnF_2	60 mole % SnF_2
d spacing (Å)	d spacing (Å)	d spacing (Å)	d spacing (Å)
3.77 m	3.77 m	4.11 w	4.07 w
3.71 w	3.71 w	3.79 m	3.77 w
3.52 m	3.52 m	3.71 w	3.68 w
3.40 s	3.40 s	3.53 w	3.49 s
3.39 s	3.33 w	3.45 m	3.44 s
3.33 w	3.19 s	3.40 s	3.37 w
3.19 m	3.13 m	3.33 w	3.24 m
3.13 m	2.98 w	3.20 m	3.19 s
2.97 w	2.86 w	3.13 m	3.17 s
2.86 m	2.84 w	2.90 w	3.16 w
2.84 m	2.79 w	2.87 m	2.88 w
2.76 w	2.56 w	2.84 w	2.75 vw
2.71 w	2.39 vw	2.78 w	2.59 vw
2.56 w	2.34 vw	2.76 w	2.36 vw
2.51 vw	2.18 w	2.56 w	2.05 vw
2.18 w	2.15 vw	2.48 w	
2.15 vw	2.12 w	2.39 w	
2.11 vw	2.11 w	2.19 w	
2.09 vw	2.09 w	2.01 w	
		2.00 w	

Table 3.9 (continued)

X-ray Diffraction Data

for the cooled melts

from the SnF_2 : CsBr system

85 mole % SnF_2	80 mole % SnF_2	75 mole % SnF_2
d spacing (Å)	d spacing (Å)	d spacing (Å)
3.77 w	3.77 w	3.77 m
3.71 vw	3.56 m	3.71 w
3.57 s	3.49 m	3.51 m
3.52 m	3.40 s	3.37 s
3.38 s	3.23 m	3.31 w
3.27 m	3.18 m	3.18 ms
3.24 m	3.11 m	3.12 m
3.19 m	2.98 vw	2.96 vw
3.16 w	2.85 vw	2.86 m
3.12 w	2.82 vw	2.83 w
2.87 w	2.76 vw	2.76 vw
2.83 w	2.55 w	2.56 w
2.76 vw	2.18 w	2.51 vw
2.56 w	2.14 vw	2.18 w
2.18 w	2.11 vw	2.10 vw
2.15 vw	2.09 vw	2.09 w
2.11 vw	2.00 vw	
2.00 w		

Table 3.9 (continued)

X-ray Diffraction Data

for the cooled melts

from the SnF_2 : CsBr system

55 mole % SnF_2	50 mole % SnF_2	45 mole % SnF_2
d spacing (Å)	d spacing (Å)	d spacing (Å)
4.11 w	4.09 w	4.15 w
3.78 m	3.77 s	3.85 s
3.71 w	3.68 w	3.72 w
3.52 vw	3.44 s	3.48 s
3.45 s	3.33 w	3.28 w
3.35 w	3.25 w	3.15 w
3.25 w	3.13 m	3.06 m
3.13 m	3.06 vw	2.96 m
2.90 m	2.89 m	2.92 w
2.83 vw	2.83 vw	2.85 m
2.75 w	2.75 w	2.76 w
2.56 vw	2.57 vw	2.59 m
2.47 w	2.47 w	2.49 w
2.38 w	2.38 w	2.40 w
2.37 w	2.37 w	2.38 w
2.06 w	2.10 vw	2.08 w
2.05 w	2.07 w	2.06 w
2.01 w	2.05 w	2.02 w
	2.01 w	

Table 3.9 (continued)

X-ray Diffraction Data

for the cooled melts

from the SnF_2 : CsBr system

40 mole % SnF_2	35 mole % SnF_2	30 mole % SnF_2
d spacing (Å)	d spacing (Å)	d spacing (Å)
4.46 vw	4.33 w	4.27 w
4.27 vw	4.15 w	4.07 w
4.07 w	3.82 m	3.77 m
3.77 ms	3.72 w	3.44 m
3.68 w	3.48 m	3.33 w
3.44 s	3.28 w	3.24 w
3.34 w	3.15 m	3.12 m
3.25 w	3.06 s	3.03 vs
3.14 w	2.92 w	2.88 w
3.12 m	2.76 w	2.75 w
3.03 s	2.60 w	2.58 vw
2.88 w	2.49 w	2.47 w
2.75 w	2.39 w	2.37 w
2.58 w	2.16 w	2.14 w
2.47 w	2.08 w	2.06 w
2.38 w	2.02 w	2.05 w
2.35 w		
2.14 w	vw = very weak	s = strong
2.06 w	w = weak	vs = very strong
2.05 w	m = medium	
2.01 w	ms = medium strong	

Table 3.9 (continued)

the compound $CsSn_3BrF_6$,isolated from aqueous solution, show no similarities between the molten phase A and the highly crystalline $CsSn_3BrF_6$. The next distinct change in the diffraction pattern occurs below 55 mole % SnF_2 where the traces, once again become well resolved. It can be inferred that the diffraction patterns for the cooled melts with compositions 55 - 70 mole % SnF_2 are mixtures of the lines associated with phase A and the new phase below 55 mole % SnF_2. Although the diffraction pattern for the cooled melt of 50 mole % SnF_2 is well resolved new lines appear in the diffraction pattern for the melt of 45 mole % SnF_2, identifying this as the new phase (phase B in the phase diagram). The diffraction patterns for cooled melts with the compositions of SnF_2 less than 45 % show a marked increase in the intensity of the very strong line (3.05Å) associated with CsBr, so much so that the diffraction pattern for 35 mole % SnF_2, shows an entirely new trace implying that the cooled melt with this composition of SnF_2 must also be a new phase, namely, phase C as shown in the phase diagram. No further new phases could be identified from the X-ray diffraction patterns for the cooled melts. The X-ray diffraction patterns for the three new phases A, B and C are given in Figure 3.9.

3.2.2 ^{119}Sn Mössbauer Spectra

The ^{119}Sn Mössbauer data for some of the cooled melts from the SnF_2 : CsBr system have been recorded at 80K and are given in Table 3.10. The data for SnF_2 and related compounds are included for comparison.

The Mössbauer spectra for the three new phases A, B and

X-ray Diffraction Patterns of New Phases

from the SnF_2:CsBr system

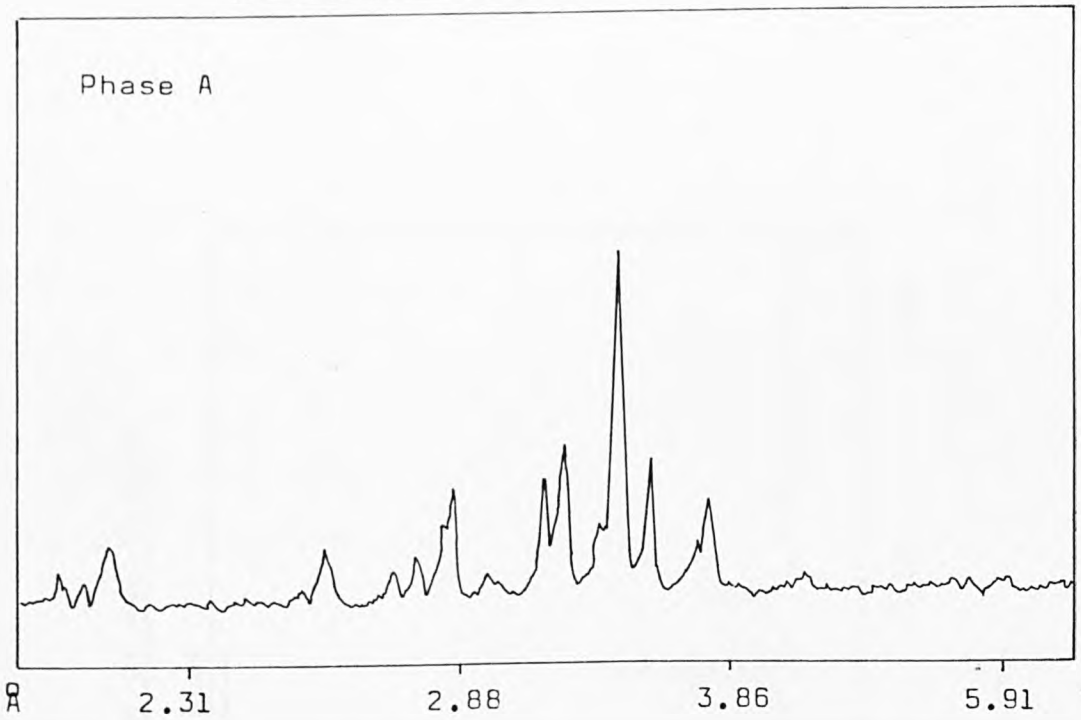

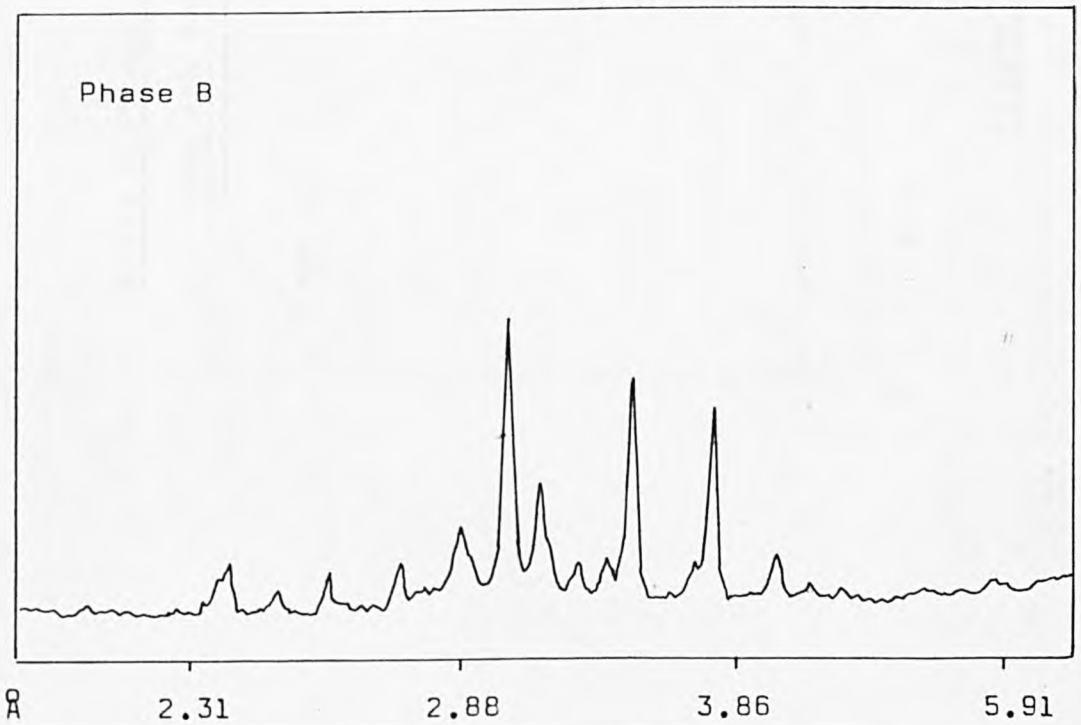

Figure 3.9

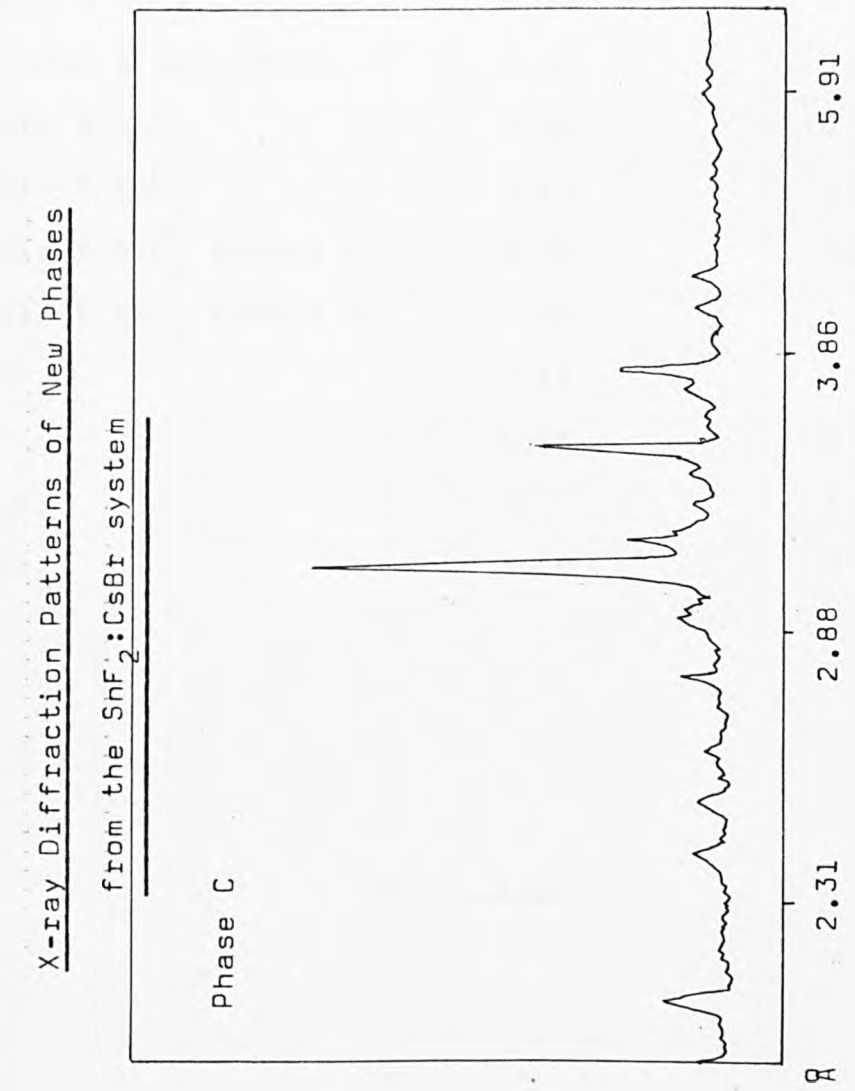

Figure 3.9(continued)

^{119}Sn Mössbauer Spectra

Compound	δmms^{-1}	Δmms^{-1}
SnF_2	3.65	1.80
75 mole % SnF_2	3.39	1.57
72.5 mole % SnF_2(Phase A)	3.43	1.56
70 mole % SnF_2	3.40	1.59
55 mole % SnF_2	3.23	1.69
45 mole % SnF_2 (Phase B)	3.04	1.92
35 mole % SnF_2 (Phase C)	3.04	1.97
Sn_3BrF_5	3.69	1.18
$CsSnF_3$	2.98	2.00
$CsSn_2F_5$	3.12	2.06
$CsSnBr_3$	3.98	0

Table 3.10

C all show quadrupole split Sn(II) doublets, with chemical shift values lower than that of SnF_2 and the mixed anionic compound Sn_3BrF_5. The shifts for the phases A, B and C are lower than for SnF_2, this suggests that halostannate(II) anion involving both fluorine and bromine ions are being formed in the molten system. The alternative structure with polymeric tin(II) fluoride networks and no tin-bromine bonds such as that found in Sn_3BrF_5 is not likely because such an arrangement of bridging fluorine atoms would lead to an increase rather than a decrease in the shift[28]. The phases A, B and C must therefore contain discrete SnX_3^- units or polymeric units such as $Sn_2X_5^-$ or $Sn_3X_7^-$, with the tin atoms bonded to both bromine and fluorine atoms. The compound identified as phase A could be formulated as $CsSn_3BrF_6$ which is the product of 3 : 1 composition. The similarity of its Mössbauer data with that of the melt of 75 mole % SnF_2, permits this assumption.

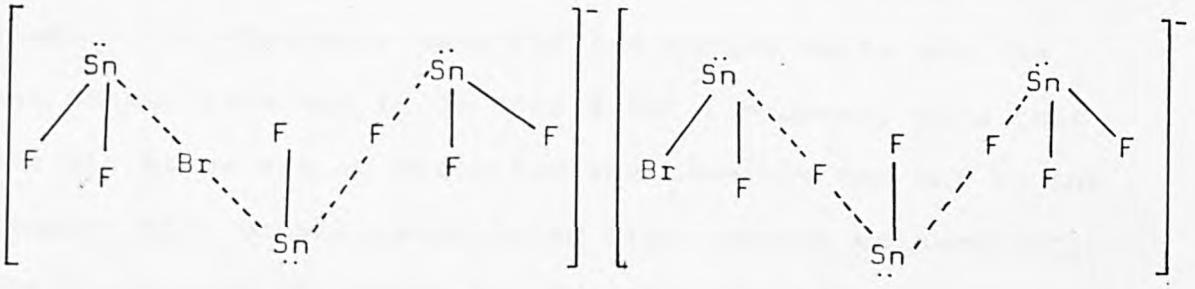

(I)

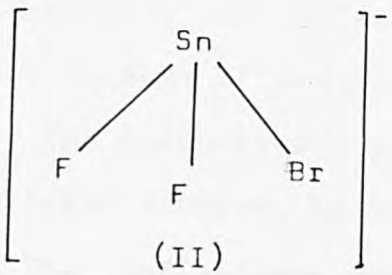

(II)

A complex of this type could have the bromine atom as either a bridging or terminal ligand (I). The still lower chemical shift for phase B implies that the complex formed is like $CsSnF_3$, with one of the fluorine atoms replaced by a bromine atom, giving a discrete trigonal pyramidal unit of the SnF_2Br^- ion (II). The fact that the shift is higher than that found for $CsSnF_3$ is consistent with replacement of one of the fluorine atoms by bromine. The shift for phase C of composition 35 mole % SnF_2, is the same as that for phase B in spite of the increase in bromide content. Phases of the type $MX.MSnX_3$ that contain discrete SnX_3^- species are however known, and it is suggested that phase C should be formulated as $CsBr.\ CsSnF_2Br$.

3.2.3 Electrical and Optical Properties

The cooled melts from the $CsBr.SnF_2$ system can be divided into two types according to their colour. For compositions containing more than 65 mole % SnF_2, the products are white but, the cooled melts with less SnF_2 are black. The Mössbauer data for the cooled melts and the new phases obtained to 35 mole % SnF_2, however, show that the tin atoms are in distorted environments and not in the regular site usually associated with intense colouration. The appearance of colour is, however, related to the amount of CsBr in the products.

Electrical conductivity and reflectance measurements have been carried out on most of the cooled melts from the SnF_2 : CsBr system. The conductivity data (Table 3.11) have been recorded on pelleted samples, by the method described in section 3.1.2. The reflectance measurements were

Electrical Conductivity for the cooled melts from the SnF_2 : CsBr system

Compound	Electrical Conductivity ($ohm^{-1}\ cm^{-1}$)
SnF_2	6.30×10^{-8}
90 mole % SnF_2	1.71×10^{-8}
85 mole % SnF_2	1.76×10^{-7}
75 mole % SnF_2	1.09×10^{-7}
72.5 mole % SnF_2	6.09×10^{-9}
70 mole % SnF_2	5.24×10^{-8}
65 mole % SnF_2	3.15×10^{-8}
60 mole % SnF_2	1.44×10^{-8}
55 mole % SnF_2	8.12×10^{-8}
50 mole % SnF_2	4.31×10^{-9}
45 mole % SnF_2	3.43×10^{-7}
40 mole % SnF_2	9.22×10^{-8}
35 mole % SnF_2	3.02×10^{-8}
30 mole % SnF_2	3.05×10^{-8}
CsBr	1.71×10^{-6}

Table 3.11

obtained on ground samples using the Hitachi Perkin Elmer EPS - 3T recording spectrophotometer, and the data are given in Table 3.12.

The conductivities of all of the cooled melts are similar to that for SnF_2, and are weak semiconductors. The low levels of conductivity for the black phases obtained are surprising but are entirely consistent with the distorted tin(II) environments suggested by Mössbauer data. The colour and the observed optical edges must therefore arise from localised rather than delocalised events. It seems likely that in phases with more than 35% CsBr, there are sufficient numbers of bromine neighbours to some of the tin atoms to permit the transfer of the lone pair electrons into the solid state bromine bands. In the same way the band edge which becomes apparent in the reflectance spectra for the cooled melts with concentrations of CsBr greater than 35 mole %, arises from the transfer of the tin(II) lone pair electrons into the solid state bromide bands.

3.2.4 Summary

Three new phases A, B and C have been obtained from the molten SnF_2 : CsBr system. It is suggested that the formulation of the three phases A, B and C is $CsSn_3BrF_6$, $CsSnBrF_2$ and $CsBr.CsSnBrF_2$ respectively. The fate of the tin moiety in this molten chemical reaction is such that the tin atoms are involved in lone pair distorted halostannate(II) ion formation, with bonds to both fluorine and bromine atoms. The ^{119}Sn Mössbauer data are consistent with tin being in a mixed halide environment. It is suggested that the colours of the phases containing more than 35 mole % CsBr must be

Reflectance Measurements

for the cooled melts

for the

SnF_2 : CsBr system

Composition	Absorption Edge (eV)	% Absorption
90% SnF_2	No edge	-
80% SnF_2	No edge	-
75% SnF_2	1.85	5%
70% SnF_2	1.82	34%
60% SnF_2	1.79	72%
50% SnF_2	1.77	80%
40% SnF_2	1.79	66%
30% SnF_2	1.77	60%

Table 3.12

associated with localised transfer of some tin(II) non-bonding electrons, and the absence of a three-dimensional delocalised band structure. Both the electrical and optical properties of the materials are in agreement with this.

3.3 Mixed Tin(II) : Tin(IV) System

The compound $Cs_2Sn^{IV}Br_6$ is a white material and it has been shown[29] that colour can be introduced into this sytem by formation in aqueous systems of mixed phases with $CsSn^{II}Br_3$ which has a closely related structure. The cubic cell of the tin(IV) compound (a = 10.8Å) contains the same number of Cs and Br atoms but only as many tin atoms as a cell (a = 11.6Å) containing eight formula units of $CsSn^{II}Br_3$. The high symmetry environment for the Sn^{II} in $CsSnBr_3$, is said to arise because the distorting effect of the non-bonding electrons is reduced by their populating an empty low energy band, thus giving rise to the black colour and the metallic conducting properties. There are no such high-energy non-bonding electrons in $Cs_2Sn^{IV}Br_6$ to populate the empty bands which must be present in its structure. However, the tin(IV) compound does form a mixed-lattice compound with $CsSn^{II}Br_3$ which effectively introduces Sn(II) into $Cs_2Sn^{IV}Br_6$ without destroying its cubic unit cell. Mixed-lattice compounds of this type were prepared from solution, it is therefore the aim of the present study to investigate the effect of introducing tin(II) into $Cs_2Sn^{IV}Br_6$ in molten systems.

3.3.1 A Study of the Molten $CsSnBr_3$: Cs_2SnBr_6 system

Dicaesium hexabromostannate(IV) was prepared from tin(IV) bromide and caesium bromide in a solution of 48% hydrobromic acid. The product was stored in vacuo over potassium

hydroxide pellets. Caesium tribromostannate(II) was prepared from a melt of caesium bromide and tin(II) bromide, in an atmosphere of oxygen free nitrogen.

Samples of Cs_2SnBr_6 containing tin(II) were prepared by heating intimately ground mixtures of $Cs_2Sn^{IV}Br_6$ and $CsSn^{II}Br_3$, in narrow necked tubes under a nitrogen atmosphere. An attempt to construct a phase diagram from the heating and cooling curves of the cooled melts (25 - 100 mole % $CsSnBr_3$) failed due to the melting point of $CsSnBr_3$ appearing as the single melting point of all phases in the region studied. Above the melting point (380°C) the materials begin to decompose. It is not possible for a mixture of two components in molten solution to give as a single product, one of its parent materials, for this reason, X-ray diffraction data have been collected and compared for random phases throughout the composition range studied. Although all the diffraction patterns are different, the changes in the patterns occur in the region of d spacings 4.44 - 2.31Å. Figure 3.10 shows this part of the trace for some of the cooled melts from the Sn(II) : Sn(IV) system, whilst the data are given in Table 3.13.

At the high Sn(II) end of the system, comparison of the data for the cooled melts of 85 and 95 mole % Sn(II) with that of $CsSnBr_3$, shows that the strong lines of $CsSnBr_3$ have remained, although, the total number of lines has increased implying that the materials are either mixtures or simply the results of a lowering of symmetry from the cubic lattice. At a composition of 75 mole % Sn(II), the overall intensity of the peaks falls dramatically as a result of considerable

X-ray Diffraction patterns for some cooled melts from the $CsSnBr_3$:Cs_2SnBr_6 system

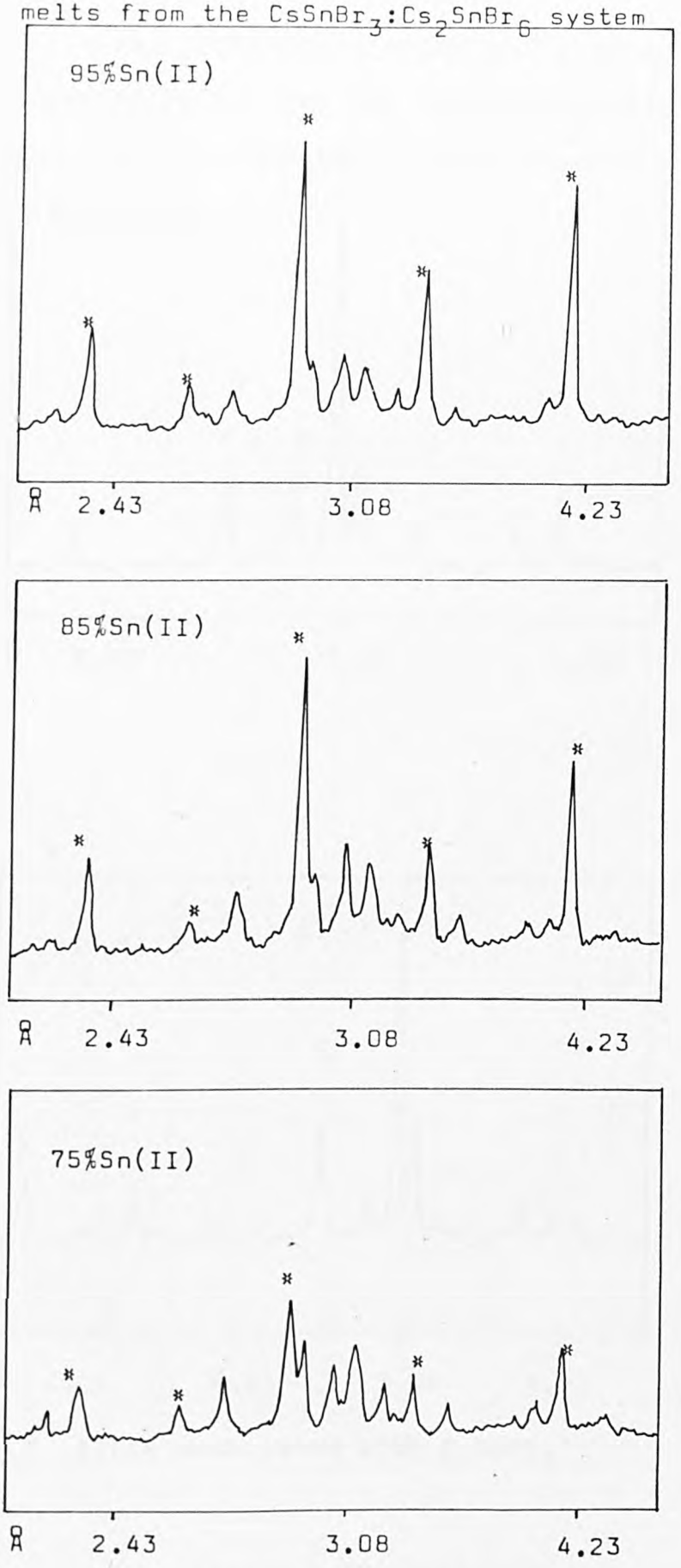

Figure 3.10

X-ray Diffraction patterns for some cooled melts from the $CsSnBr_3$:Cs_2SnBr_6 system

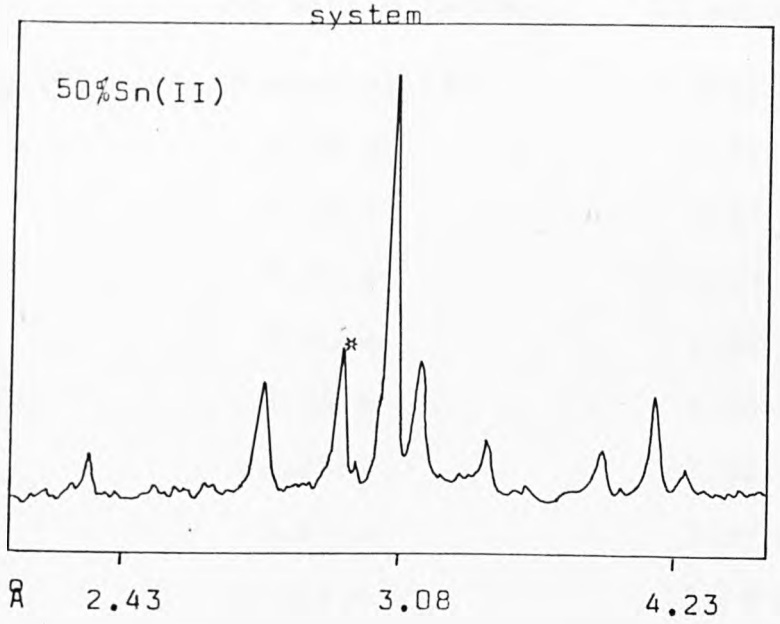

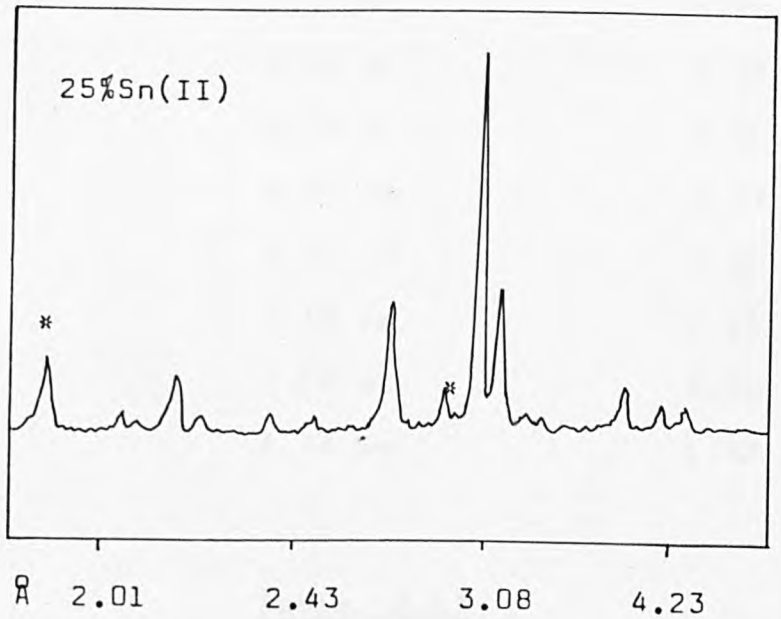

* lines associated with $CsSnBr_3$

Figure 3.10(continued)

X-ray Diffraction Data

for some cooled melts

from the mixed tin(II) : tin(IV) system

$CsSnBr_3$	95 mole % $CsSnBr_3$	85 mole % $CsSnBr_3$
d spacing (Å)	d spacing (Å)	d spacing (Å)
5.83 vw	5.87 w	6.32 w
4.11 vs	4.13 s	5.87 w
3.35 m	3.97 w	4.13 s
2.90 vs	3.51 w	3.98 vw
2.60 m	3.36 m	3.85 vw
2.37 m	3.24 w	3.52 w
2.05 s	3.14 w	3.37 m
1.94 s	3.13 w	3.25 w
	3.06 m	3.14 m
Cs_2SnBr_6	2.96 m	3.06 m
d spacing (Å)	2.91 s	2.95 m
5.21 m	2.72 w	2.91 vs
3.85 m	2.59 w	2.72 w
3.29 w	2.38 m	2.61 w
3.13 vs	2.31 vw	2.37 m
2.72 vs	2.21 vw	2.31 vw
2.49 vw	2.16 vw	2.15 vw
2.22 w	2.06 m	2.06 m
2.09 vw	1.94 vw	1.92 vw
1.92 s		

Table 3.13

X-ray Diffraction Data

for some cooled melts

from the mixed tin(II)-tin(IV) system

75 mole % $CsSnBr_3$	50 mole % $CsSnBr_3$	25 mole % $CsSnBr_3$
d spacing (Å)	d spacing (Å)	d spacing (Å)
6.91 w		
6.32 w	6.32 w	6.32 w
5.83 w	4.31 w	4.33 w
4.44 w	4.11 m	4.13 w
4.11 m	3.85 w	3.86 w
3.97 w	3.36 w	3.37 w
3.83 w	3.13 m	3.30 w
3.51 w	3.05 vs	3.14 m
3.35 m	2.94 vw	3.07 vs
3.23 m	2.91 m	2.92 w
3.12 m	2.71 m	2.72 m
3.04 m	2.37 w	2.49 vw
2.90 s	2.22 vw	2.37 vw
2.72 s	2.15 w	2.22 vw
2.59 m	2.08 vw	2.16 w
2.37 w	2.05 w	2.08 vw
2.30 m	1.92 w	2.06 vw
2.21 w		1.92 m
2.15 w		
2.05 s		
1.92 m		

vs = very strong

vw = very weak m = medium

w = weak s = strong

Table 3.13 (continued)

lattice distortion. A striking feature of the diffraction patterns of the cooled melts with more than 50 mole % Sn(IV), is the presence of a strong peak at 3.05Å, which increases in intensity as the concentration of Sn(IV) is increased. This line although present in all the traces for the cooled melts, cannot be associated with either parent material. It is, however, a characteristic peak of the diffraction pattern of CsBr (see Table 3.9). It appears that in all phases there is the separation of CsBr possibly associated with the loss of tin halide. At the high tin(II) end, the materials are mixtures of tin(II), tin(IV) and possibly some CsBr. Whilst at the high tin(IV) end, the diffraction pattern is simpler, although there is an increase in CsBr content, and the peaks associated with $CsSnBr_3$ are very weak at 25 mole % Sn(II) which suggests that some Sn(II) is in fact, entering suitable vacancies in the tin(IV) lattice.

3.3.2 ^{119}Sn Mössbauer Spectra

The ^{119}Sn Mössbauer data, recorded at 80K for the cooled melts with 75, 50 and 25 mole % Sn(II) are given in Table 3.14, together with the data for the parent compounds. For all phases the spectra obtained, show both a singlet tin(II) and a singlet tin(IV) resonance. The singlet in the tin(II) shift region for all the mixed phases indicates that tin(II) remains, like tin(II) in $CsSnBr_3$, in a high symmetry environment. It is not surprising that the percentage resonance dip for this line is reduced as the amount of tin(IV) increases, the line width of the tin(II) singlet increases and this lowering of symmetry may be associated with the substitution of some tin(IV) in the lattice. At the high tin(IV) end, the Mössbauer spectra show

^{119}Sn Mössbauer data for the cooled melts from $CsSnBr_3$: Cs_2SnBr_6

Compounds		δ mms^{-1}	Δ mms^{-1}	Γ mms^{-1}
$CsSnBr_3$		3.97	0	0.84
75% $CsSnBr_3$	Sn(II)	4.02	0	0.91
	Sn(IV)	0.37	0	1.79
50% $CsSnBr_3$	Sn(II)	4.04	0	1.02
	Sn(IV)	0.53	0.71	
25% $CsSnBr_3$	Sn(II)	4.03	0	0.82
	Sn(IV)	0.56	0.74	
Cs_2SnBr_6	Sn(IV)	0.75	0	

Table 3.14

Sn(IV) in an octahedral site, but as the amount of tin(II) in the lattice is increased, the line becomes much broader, again this would be consistent with substitution of tin(IV) by tin(II).

3.3.3 Electrical Properties

Electrical conductivity measurements have been carried out on pelleted samples of some cooled melts isolated from the $CsSnBr_3$:Cs_2SnBr_6 system. The conductivities of these materials (Table 3.15) lie in the range 10^{-9}-10^{-4} ohm^{-1} cm^{-1} hence they are semiconductors. $CsSnBr_3$ has a conductivity of about 10^{-4} ohm^{-1} cm^{-1} and its ability to conduct electricity is explained in terms of direct population of the empty solid state bands by the ns^2 non-bonding electrons. Cs_2SnBr_6, on the other hand is a white insulator. This lack of conducting ability can be accounted for by the absence of a lone-pair in the Sn(IV) outer electronic configuration. The conductivities of the materials with high tin(II) content, are of the same order of magnitude as the parent $CsSnBr_3$. Reducing the amount of Sn(II) in the lattice does lower the conducting ability of material, although the cooled melts even at the high tin(IV) end are still semi-conducting materials. It appears that the lower conductivity of mixed tin(II) : tin(IV) phases results essentially from the number of tin(II) atoms present, because they supply the donor electrons.

3.3.4 Summary

Unlike the aqueous Sn(II) : Sn(IV) system there is no real evidence for the formation of solid solutions between the two lattices in cooled melts. The increase in the Mössbauer line width on addition of tin(II) into the tin(IV) lattice and

Electrical Conductivity Data for the cooled melts from $CsSn^{II}Br_3$: $Cs_2Sn^{IV}Br_6$ system

Compound	Electrical Conductivity ($ohm^{-1}\ cm^{-1}$)
$CsSnBr_3$	9.00×10^{-4}
95 mole % $CsSnBr_3$	1.76×10^{-4}
85 mole % $CsSnBr_3$	7.63×10^{-4}
75 mole % $CsSnBr_3$	3.78×10^{-8}
50 mole % $CsSnBr_3$	2.50×10^{-7}
25 mole % $CsSnBr_3$	2.96×10^{-9}
Cs_2SnBr_6	insulator

Table 3.15

of tin(IV) into the tin(II) lattice may be associated with some substitutional effects. There is also evidence for the decomposition of CsBr in the cooled melts particularly for the high tin(IV) region. The conductivity of the mixed phases becomes less as the amount of tin(II) in the lattice decreases, this is considered to be a direct result of the reduction in the number of non-bonding electrons available as donors.

3.4 Photoacoustic Spectroscopy of Tin Compounds

The application of photoacoustic spectroscopy(see Section 1.3.4.) to some solid state materials is investigated in this work, and where possible a comparison is made of the data obtained with those from reflectance spectroscopy. The materials studied include the phases from the two systems: $CsSnBr_{3-x}Cl_x$ (x = 0-3)[30] and $CsSn_xPb_{1-x}Br_3$ (x = 0-1)[16], some tin halides and chalcogenides, and a number of transition metal stannates(IV) and hydroxostannates(IV). In the course of the preparation of the phases from the $CsSnBr_{3-x}Cl_x$ system, a differential thermal analytical study was also made of the variation, with Cl content, of temperature of the transition from the monoclinic to the cubic form of $CsSnX_3$.

3.4.1 $CsSnBr_{3-x}Cl_x$ and $CsSn_xPb_{1-x}Br_3$ Systems

All the compounds were prepared as cooled melts of intimately ground mixtures of appropriate starting materials. In the mixed halide system the starting materials were CsBr, $SnBr_2$ and CsCl, whilst in the mixed metal system the starting materials were CsBr, $SnBr_2$ and $PbBr_2$. The photoacoustic spectra were measured on thoroughly ground samples and the positions of the absorption edges measured. The data for the mixed halide and mixed metal systems are given in Tables 3.16

A Comparison of Photoacoustic and Optical Reflectance data for the $CsSnBr_{3-x}Cl_x$ system

Compound	Absorption Edge (PAS - eV)	Absorption Edge (OR - eV)
$CsSnBr_3$	1.77	1.80
$CsSnBr_{2.75}Cl_{0.25}$	1.82	
$CsSnBr_{2.5}Cl_{0.5}$	1.92	1.91
$CsSnBr_{2.25}Cl_{0.75}$	2.00	
$CsSnBr_2Cl$	2.07	2.03
$CsSnBr_{1.75}Cl_{1.25}$	2.14	
$CsSnBr_{1.5}Cl_{1.5}$	2.25	2.19
$CsSnBr_{1.25}Cl_{1.75}$	2.36	
$CsSnBrCl_2$	2.39	
$CsSnCl_3$	2.86	2.85

Table 3.16

and 3.17, respectively, along with the relevant data obtained from optical reflectance spectra[30,16]. Figure 3.11 shows the photoacoustic spectra for the three materials $CsSnBr_3$, $CsSnCl_3$ and $CsPbBr_3$.

A direct comparison can be made between the positions of the edges in the photoacoustic spectra, and those in the optical spectra of the mixed halide system. In both cases. the absorption edges, which are well defined, indicating a series of homogeneous mixtures, move to progessively higher energies with increasing chlorine content. The results from the two techniques are compatible and are therefore in agreement with the suggestion[30] of an"average halide" effect, since a series of edges would be expected from a domain structure. A plot of the position of the absorption edge versus the chloride composition in the $CsSnBr_{3-x}Cl_x$ phases shows some deviation at about $CsSnBr_{3-x}Cl_x$ (where x lies between 1.50 and 1.75) composition which is consistent with the materials of high bromide content having high symmetry phases at room temperature, and those of high chloride content having high symmetry phases at high temperature (Table 3.18).

The positions of the absorption edges, measured by photoacoustic spectroscopy for the mixed metal phases are in agreement with those measured by reflectance spectroscopy. The movement of the edges to progressively higher energies with an increase in the amount of lead in the lattice, is consistent with poorer donation of lone-pair electron density to the band system. The effect on the absorption edge of varying the lead content of the mixed phases is one

Photoacoustic Spectra

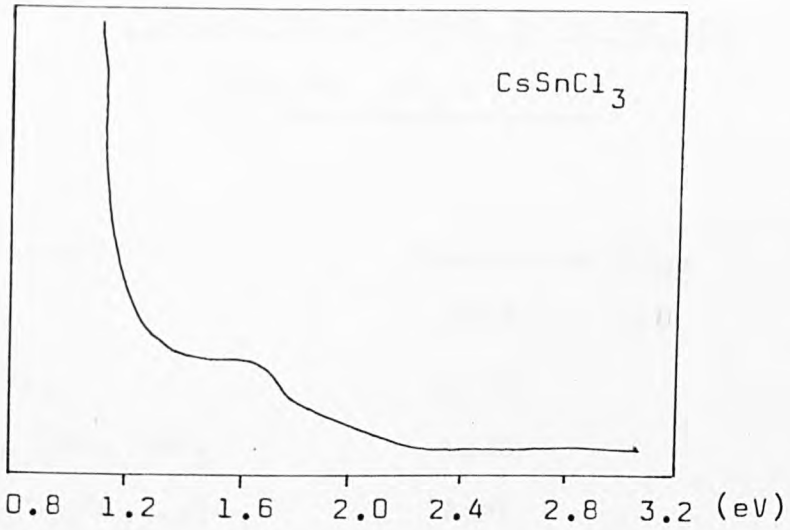

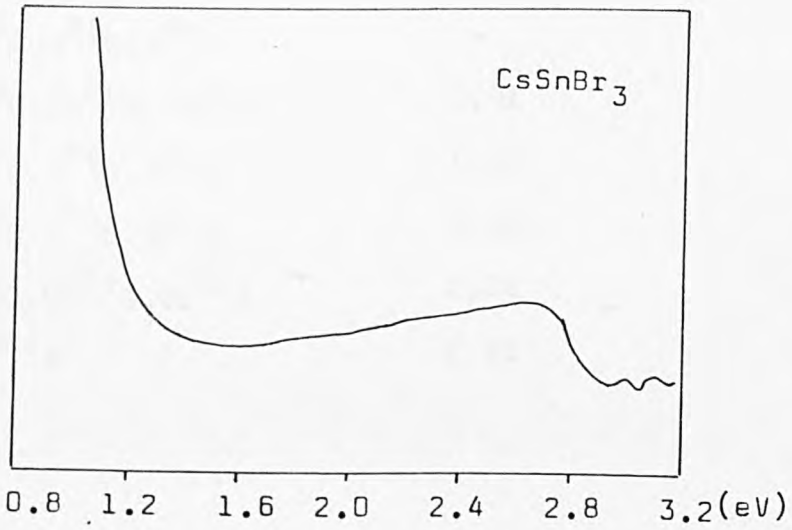

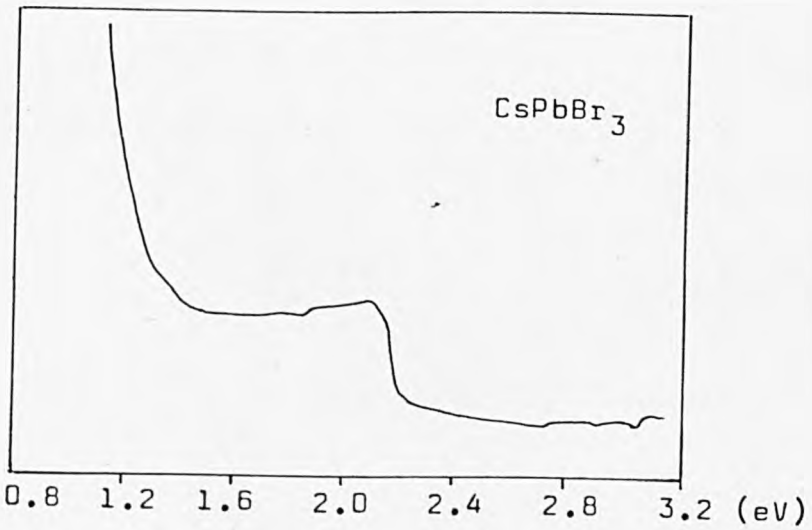

Figure 3.11

A Comparison of Photoacoustic and Optical Reflectance data for the $CsSn_xPb_{1-x}Br_3$ system

Compound	Absorption Edge (PAS - eV)	Absorption Edge (OR - eV)
$CsSnBr_3$	1.77	1.80
$CsSn_{0.8}Pb_{0.2}Br_3$	1.70	-
$CsSn_{0.75}Pb_{0.25}Br_3$	1.81	-
$CsSn_{0.5}Pb_{0.5}Br_3$	1.78	1.85
$CsSn_{0.4}Pb_{0.6}Br_3$	-	1.91
$CsSn_{0.25}Pb_{0.75}Br_3$	1.91	-
$CsSn_{0.2}Pb_{0.8}Br_3$	1.95	1.97
$CsSn_{0.1}Pb_{0.9}Br_3$	1.98	2.08
$CsSn_{0.05}Pb_{0.95}Br_3$	2.02	-
$CsPbBr_3$	2.28	2.33

Table 3.17

Phase Transition Temperature for the $CsSnBr_{3-x}Cl_x$ System

Compound	Transition Temperature(^oC)
$CsSnCl_3$	94
$CsSnBr_{0.5}Cl_{2.5}$	90
$CsSnBrCl_2$	79-80
$CsSnBr_{1.25}Cl_{1.75}$	66
$CsSnBr_{1.5}Cl_{1.5}$	RT

All phases with $x < 1.75$ showed no transition temperature above room temperature.

Table 3.18

in which the band gap widens as replacement of Sn(II) by Pb(II) expands the lattice and increases the average inter-atomic distances, thus reducing the overlap between the 5s and bromine 4d - orbitals.

On two occasions when poor spectra were obtained for the mixed metal series, dilution studies were carried out. Poor spectra may arise as a result of saturation and/or particle size effects. A spectrum becomes saturated because the incident radiation is totally absorbed, and all of this energy contributes to the photoacoustic signal. (see Chapter 1. Figure 1.19b). However, dilution of the sample by grinding with silica in the ratio 1 : 1, was found to be sufficient to reduce the effective thickness of the absorbing sample to less than l_β and therefore improve the spectrum giving a well-defined absorption edge. The spectra for the two samples in the $CsSn_xPb_{1-x}Br_3$ series, before and after dilution studies are shown in Figure 3.12.

3.4.2 Photoacoustic Spectra of Other Tin Compounds

The photoacoustic spectra of some tin(II) halides, chalcogenides, transition metal stannates(IV) and hydroxo-stannates(IV), are now described. The transition metal stannates(IV) and hydroxostannates(IV) provide an interesting example of materials in the solid state exhibiting atomic spectra. Two types of electronic transitions are possible *viz*. (1) the atomic transitions, in which there is transfer of electrons from one orbital to another giving rise to an absorption line, and (2) the band to band transitions in which the orbital level has become a number of levels ie. a band, and the transitions of electrons from one band to another are

Dilution Studies

Photoacoustic Spectra

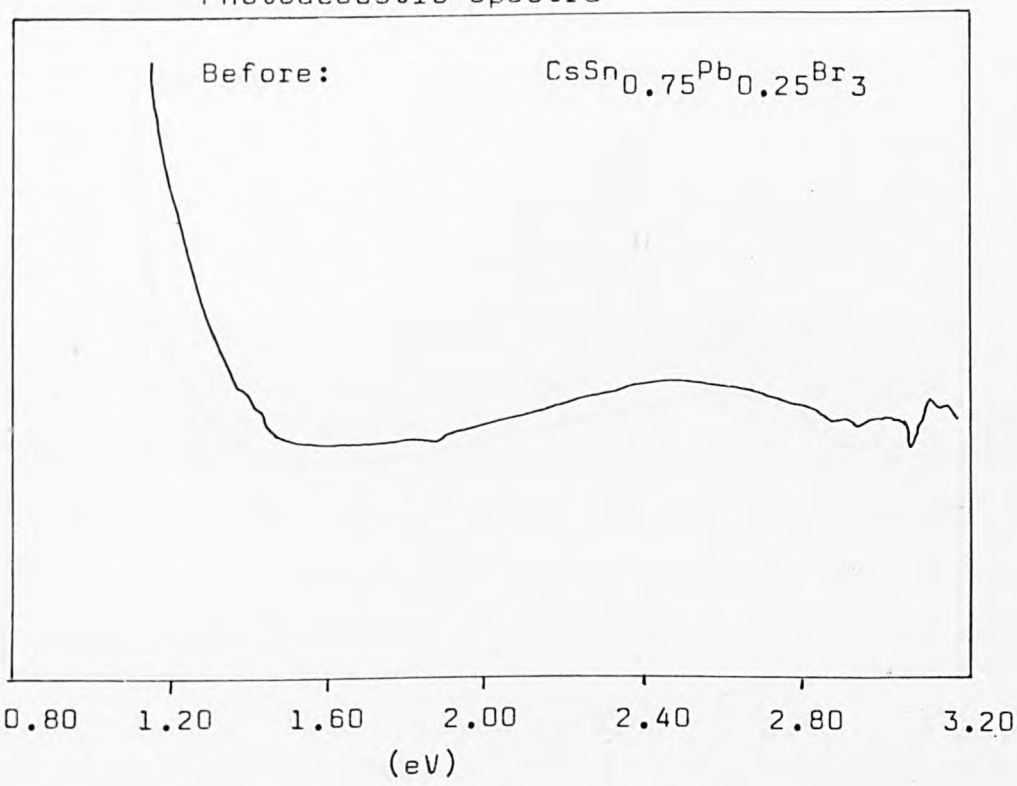

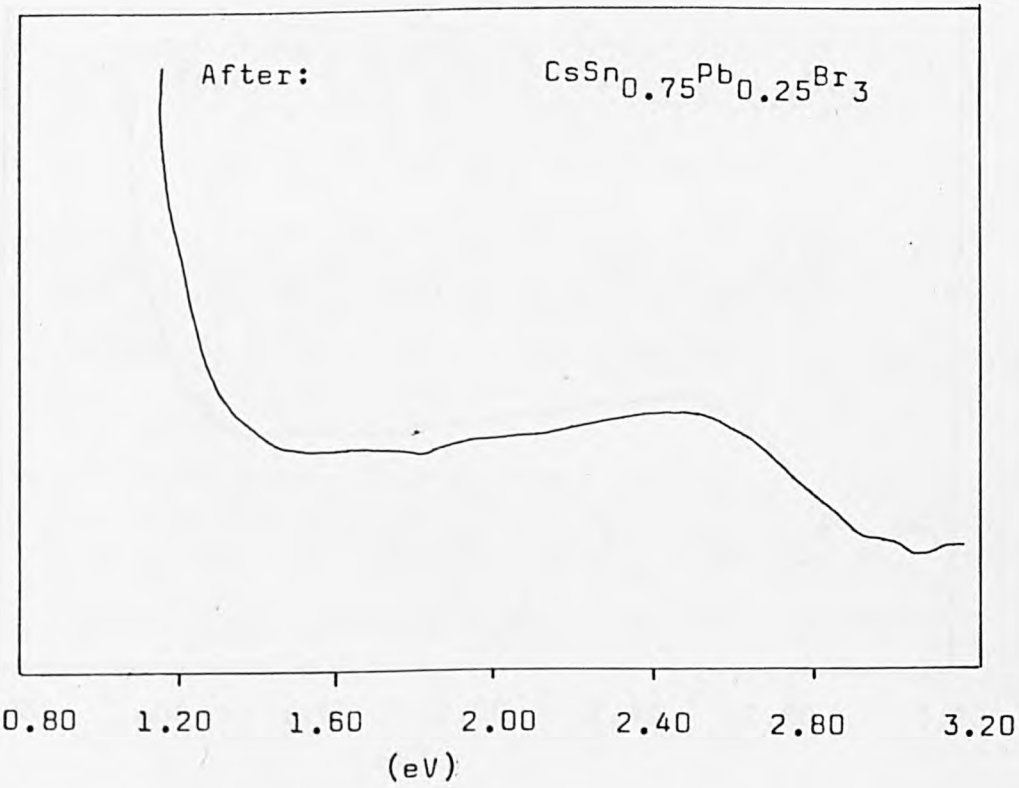

Figure 3.12

Dilution Studies

Photoacoustic Spectra

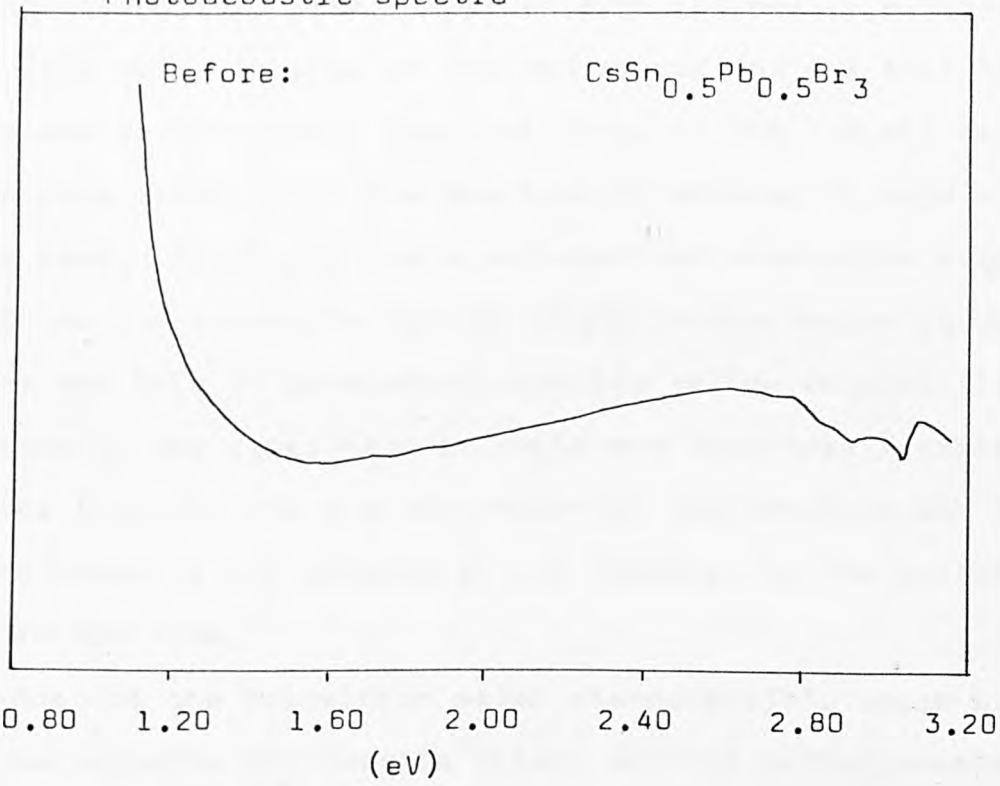

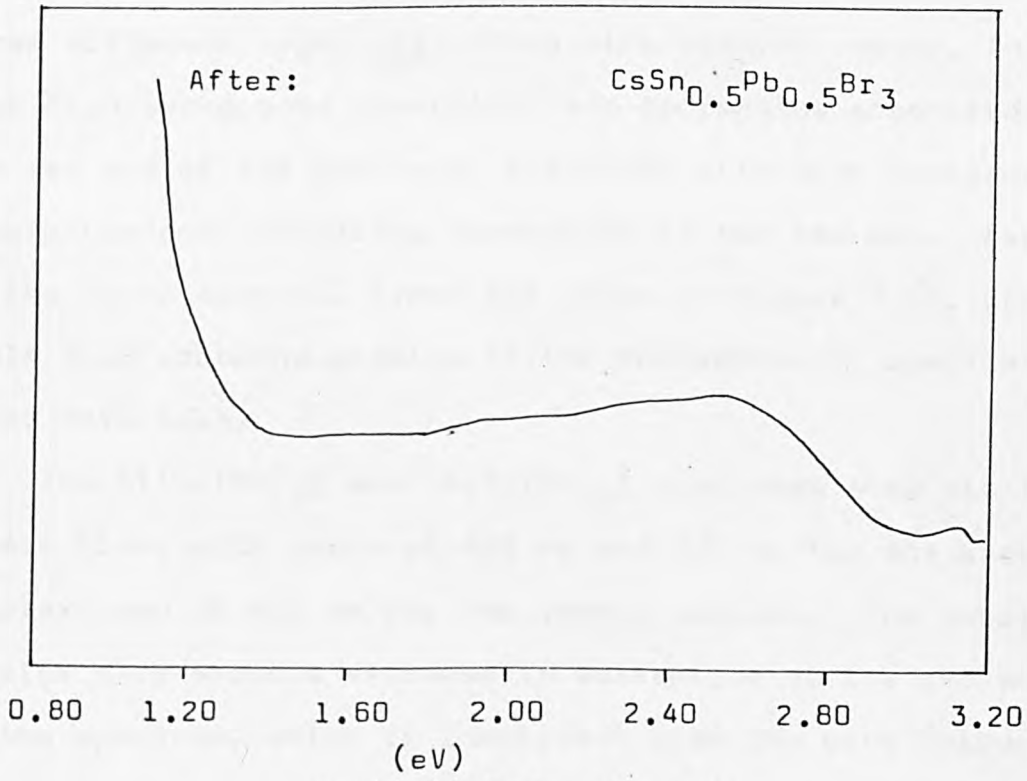

Figure 3.12(continued)

observed, appearing as an edge in the optical spectrum.

The spectrum of red tin oxide shows a very high background absorption, with either an edge (620nm) or a broad line (570 nm). In view of its red colour and the fact that there are no tin atomic spectral lines in the visible region, it is more likely that the spectrum is showing an edge and not a band. $Sn_7Br_{10}S_2$ has a well-defined absorption edge at 450 nm and transmits all the light in the region above 500 nm and this is consistent with its yellow colour. Tin(II) fluoride on the other hand is white and therefore transmits all the light in the visible region of the spectrum and this is confirmed by the absence of any features in the photoacoustic spectrum.

Most of the transition metal stannates(IV), which are used as pigments for ceramic tiles, and the hydroxostannates (IV) have spectra that can be explained in terms of atomic effects of the transition metal atom. These spectra are of three different types <u>viz</u>. those with distinct bands, those with high background absorption and decreasing absorption in the red end of the spectrum, and those with high background absorption and increasing absorption at the red end. Examples of the three spectral types are shown in Figure 3.13, whilst Table 3.19 contains details of the photoacoustic spectra of these materials.

The $Ni[Sn(OH)_6]$ and $Co[Sn(OH)_6]$ complexes show distinct atomic lines with peaks at 405 nm and 620 nm for the nickel complex, and at 530 nm for the cobalt complex. The cobalt complex also shows a decrease in absorption at the red end of the spectrum, which is consistent with its pink colour.

Photoacoustic Spectra

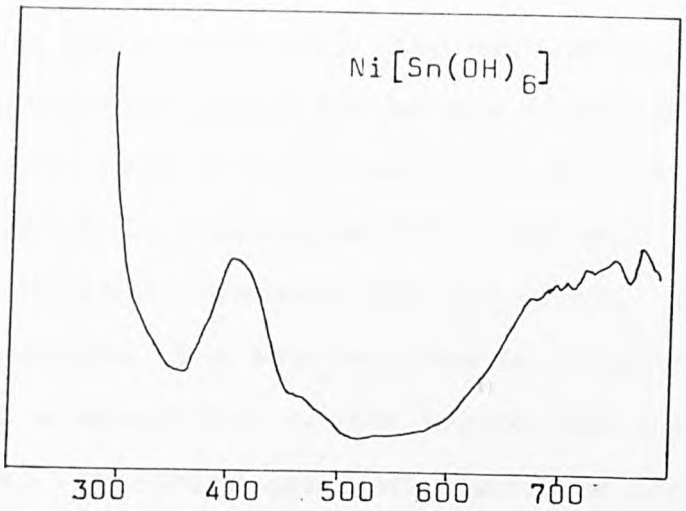

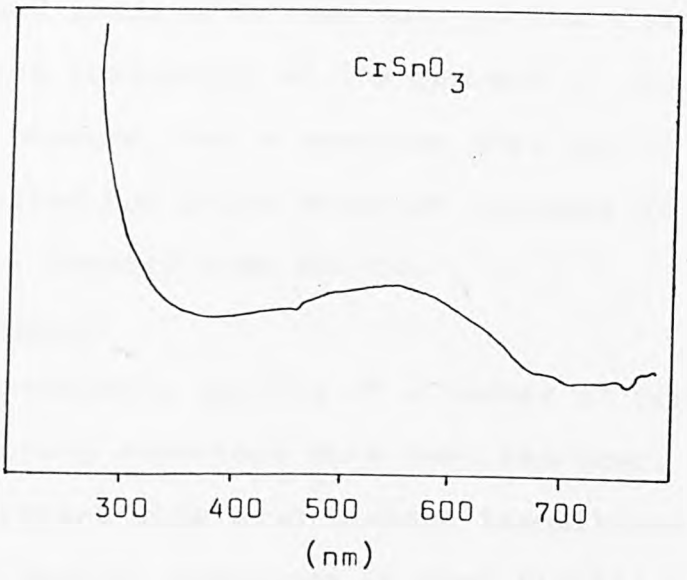

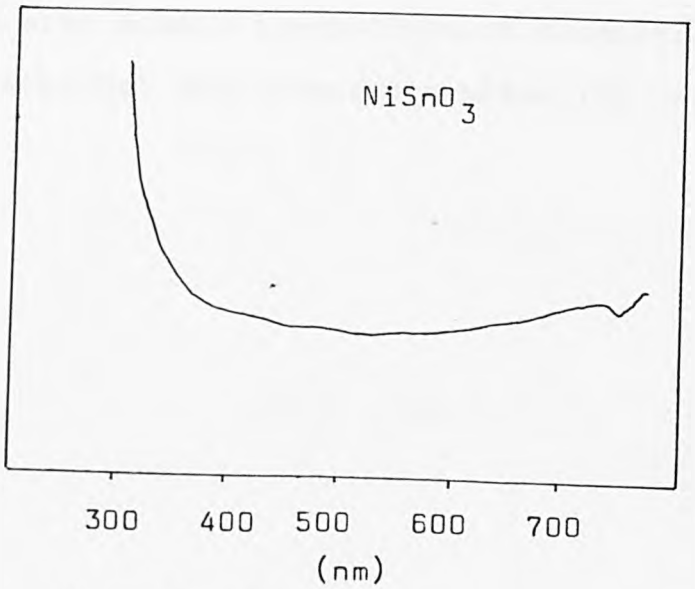

Figure 3.13

Those materials which generally show high absorption and a decrease in absorption above 650 nm are listed in part II of Table 3.19. They have a high background absorption with some evidence for lines in the region 550 - 650 nm. Above 650 nm the materials begin to transmit all the light. In the case of vanadium stannate, the spectrum can be interpreted as showing either a broad line in the region 350 - 460 nm or an edge at 500 nm. The third group of compounds included in part III of Table 3.19 have spectra which show a relatively high background absorption over most of the visible region, with increasing absorption at the red end of the spectrum. $Cu[Sn(OH)_6]$, however, has a spectrum that has no high background absorption but which shows an increase in absorption at wavelengths greater than 620 nm.

3.4.3 Summary

The photoacoustic spectra of a number of tin(II) and tin(IV) containing materials have been recorded. The spectral data are consistent with band-to-band transitions involving the lone pair tin(II) electrons in most tin(II) compounds studied, and with atomic transitions of transition metal ions in the stannates(IV) and hydroxostannates(IV) investigated.

Photoacoustic Spectra for Transition Metal Stannates (IV) and Hydroxostannates(IV)

Part I

Compound	Transmission Range (nm)	Absorption Bands (nm)	Colour
$Ni[Sn(OH)_6]$	450 - 620	405;> 620	green
$Co[Sn(OH)_6]$	370 - 450,>600	530	pink

Part II

Compound	Transmission Range (nm)	Absorption Bands (nm)	Colour
$CoSnO_3$	400 - 600;>700	650	brown
$CrSnO_3$	340 - 500;>670	550	deep red
$CaSnSiO_3$+ 15% $CoSnO_3$	350 - 560;>700	665	blue/grey

Part III

Compound	Transmission Range (nm)	Absorption Range (nm)	Colour
$Cu[Sn(OH)_6]$	380 - 620	>620	pale blue
$CuSnO_3$	360 - 640	>640	green
$NiSnO_3$	360 - 660	>660	green

Table 3.19

References

1. J.D.Donaldson, Progress in Inorganic Chemistry, 1967, 8, 287.
2. A.F.Wells, Structural Inorganic Chemistry, 3rd Edition, Oxford. 1962.
3. D.S.Payne, Q.Rev.Chem.Soc., 1961, 25, 173.
4. T.N.Polynova and M.A.Porai-Koshits, Zh.Strukt. Khim., 1965, 7, 147.
5. C.C.Addison (Editor) M.T.P.International Review of Science, Inorg. Chem. Ser.1 Vol.1, London,1972.
6. J.Barrett, S.R.A.Bird, J.D.Donaldson and J.Silver, J.Chem. Soc.(A), 1971, 3105.
7. J.D.Donaldson, D.R.Laughlin, S.D.Ross and J.Silver, J.Chem. Soc.(A), 1973, 1985.
8. D.S.Urch, J.Chem.Soc., 1964, 5775.
9. T.C.Gibb, R.Greatrex, N.N.Greenwood and A.C.Sarma, J.Chem. Soc.(A), 1970, 212.
10. L.Atkinson and P.Day, J.Chem.Soc.(A), 1969, 2423.
11. D.E.Scaife, P.F.Weller and W.G.Fisher, J.Solid State Chem. 1974, 9, 308.
12. J.D.Donaldson and J.Silver, Inorg.Nucl. Chem.Letters, 1974, 10, 537.
13. G.Markstein and H.Navotny, Z.Krist, 1938, 100, 265.
14. S.J.Clark, C.D.Flint and J.D.Donaldson, J.Phys.Chem.Solids, 1981, 42, 133.
15. R.A.Howie, W.Moser and I.C.Trevena, Acta Cryst., 1972, B28, 2965.
16. S.J.E.Clark, Ph.D.Thesis (London), 1979.

17. A.V.Noveselova, I.N.Odin and B.A.Popovkin, Russ. J. Inorg.Chem., 1969, 14, 1402.

18. A.V.Noveselova, M.K.Toridiya, I.N.Odin and B.A.Popovkin, Izvest. Akad.Nauk.S.S.S.R.,Neorg.Materialy,1971, 7, 437.

19. D.R.Laughlin, Ph.D.Thesis (London). 1974.

20. J.D.Donaldson, D.R.Laughlin and J.Silver, J.C.S.Dalton, 1977, 996.

21. B.Krebs, Z.Anorg.Chem., 1973, 396, 137.

22. W.H.Zachariasen, Acta Cryst., 1949, 2, 288.

23. "International Tables for X-ray Crystallography",Birmingham, Kynoch Press, 1962.

24. J.D.Donaldson and S.M.Grimes, in press.

25. J.D.Donaldson, J.D.O'Donoghue and R.Oteng. J.Chem.Soc., 1965, 3876.

26. R.H.Andrews, Ph.D. Thesis (London). 1977.

27. J.D.Donaldson and J.Silver, J.C.S.Dalton, 1973, 666.

28. J.D.Donaldson, D.R.Laughlin and D.C.Puxley, J.C.S.Dalton, 1977, 865.

29. J.D.Donaldson, J.Silver, S.Hajiminolis and S.D.Ross, J.C.S.Dalton, 1975, 1500.

30. J.Barret, S.R.A.Bird, J.D.Donaldson and J.Silver, J.Chem. Soc.,(A), 1971, 3105.

CHAPTER 4

Conversion Electron and Transmission Mössbauer Spectroscopy in Tin Chemistry

Chapter 4

Conversion Electron and Transmission Mössbauer Spectroscopy in Tin Chemistry

This chapter deals with the study of the fate of tin moieties in chemical reaction using Mössbauer spectroscopy, in both its conversion electron and transmission mode to investigate the effect on the tin at the surface and in the bulk sample.

The present work introduces the more recently developed conversion electron technique which enables studies on the fate of tin moieties in surface reactions to be carried out. In section 4.1 a description of the theoretical background to the technique is outlined. This is followed by details of the known applications of conversion electron Mössbauer spectroscopy to tin chemistry and finally, the results of a number of surface reactions involving tin containing materials are presented. The aim of this part of the work is to examine the method of studying the fate of tin with a view to commercial applications.

The second part of this chapter, section 4.2., deals with a study of the relationship between bond lengths from X-ray diffraction data and transmission Mössbauer parameters. The purpose of this part of the work is to determine whether changes in Mössbauer shift parameters are directly reflected by changes in bond lengths to tin.

4.1 Conversion Electron Mössbauer Spectroscopy

4.1.1 Introduction

The majority of Mössbauer spectroscopic experiments are performed in a transmission geometry and involve the detection of γ- radiation transmitted through thin absorbers. In this mode, data relating to the bulk properties of solids may be obtained. If however, information relating to the surface properties is required, the use of transmission methods is restricted to special absorbers *viz*. microcrystallites and solids such as zeolites or clay minerals. There has been a considerable increase in the interest in the use of back-scattering techniques, over the past fifteen years, to permit the study of the properties of surface and near-surface regions of solids . This back-scattering Mössbauer technique is based on the detection of conversion electrons emitted from the surface following the occurrence of a resonant event in the absorber. These electrons are rapidly attenuated in matter, hence only those electrons produced in regions close to the surface escape the surface and the resulting Mössbauer spectrum is weighted towards the surface regions of the absorber. Although it is possible for most isotopes to be used in conversion electron Mössbauer studies, to date, most of the work reported has involved either ^{57}Fe or ^{119}Sn isotopes.

Two basic types of conversion electron Mössbauer spectroscopic experiments may be performed. The first, integral conversion electron Mössbauer spectrocopy, involves the detection of the total flux of back-scattered electrons without energy resolution. In the second type of experiment the flux of back-scattered electrons is energy resolved and Mössbauer

spectra accumulated using selected bands of electron energies. This technique allows the surface regions of solids to be probed as a function of depth, and is referred to as depth-resolved conversion electron Mössbauer spectroscopy (DCEMS).

A number of reviews describing the developments and applications of Conversion electron Mössbauer spectroscopy (CEMS) to surface studies have appeared in the literature in the past few years[1-6]. Most of the applications of CEMS to date involve the use of the ^{57}Fe isotope. For this reason, the theoretical background of the technique is described in section 4.1.2 with reference to ^{57}Fe studies and where possible to the ^{119}Sn studies. Details of known applications to ^{119}Sn CEMS are given in section 4.1.3.

4.1.2 Theoretical background of CEMS

For many Mössbauer nuclides, the decay of the excited nuclear spin-state is highly internally converted[7]. This process of internal conversion can be explained in terms of the events which occur during the decay of the I = 3/2 excited spin states for ^{57}Fe and ^{119}Sn, summarized in Table 4.1. Following the resonant absorption of the 14.4 keV. γ-photon by Fe-57, only 10% of the excited nuclei decay by emission of a γ-photon. The remaining nuclei undergo internal conversion processes, mainly in the K-shell resulting in the ejection of a 7.3keV conversion electron. The hole in the K-shell is filled by an electron from the L-shell thereby producing a 5.4 keV Auger electron and a 6.3 keV X-ray photon. Internal conversion also occurs in the L- and M-shells but with smaller probability, as the internal conversion coefficient of a particular shell is proportional to the

Summary of major events which occur during the decay of the I =3/2 excited spin states of ^{57}Fe and ^{119}Sn

^{57}Fe	Energy(kev)	Number (per 100) Absorption events	Approx. Max. range
γ-photons	14.4	9	
K-X-rays	6.3	27	
K-conversion electrons	7.3	81	250nm
L-conversion electrons	13.6	9	900nm
M-conversion electrons	14.3	1	
KLL-Auger electrons	5.4	63	
LMM-Auger electrons	0.53		
^{119}Sn			
γ-photons	23.8	17	
X-rays	3.6	9	
L-conversion electrons	19.6	83	2.4μm
LMM-Auger electrons	2.8	74	

Table 4.1

s-electron density of that shell at the nucleus. A similar situation is found for the 23.8keV transition of ^{119}Sn although, in this case, the K-conversion process is energetically forbidden and the majority electrons are 19.6keV L-conversion electrons Figure 4.1.

In view of this phenomenon, it is possible to record Mössbauer spectra in a backscatter geometry by detecting either the back-scattered photons or electrons, rather than the usual detection of transmitted γ-radiation (Figure 4.1).

In a back-scatter geometry, there is no longer the requirement for thin absorbers, thick samples can be easily examined. If the back-scattered photons are detected information pertaining to the bulk of the solid will be obtained. However, the more rapid attenuation of electrons in matter causes the back-scattered conversion electron Mössbauer spectrum to be weighted towards the outermost surface regions of the sample, as only electrons produced close to the absorber surface will escape the surface. Therefore the depth selectivity of a given experiment will depend on the energy spectrum of the electrons produced during the decay of the excited nuclear level of the isotope used, and on the energy of the electrons detected. In the simplest integral CEMS experiment, first performed by Swanson and Spijkerman[8], the back-scattered electrons are efficiently detected with a 2π collection geometry by mounting the sample inside a He/CH_4 flow proportional counter. The electron count-rates are usually significantly smaller than transmission experiments per unit source strengths. Strong sources can however be used without fear of causing

Schematic Representation of the Events Which Occur During Decay of the I=3/2 Excited Spin State of ^{119}Sn

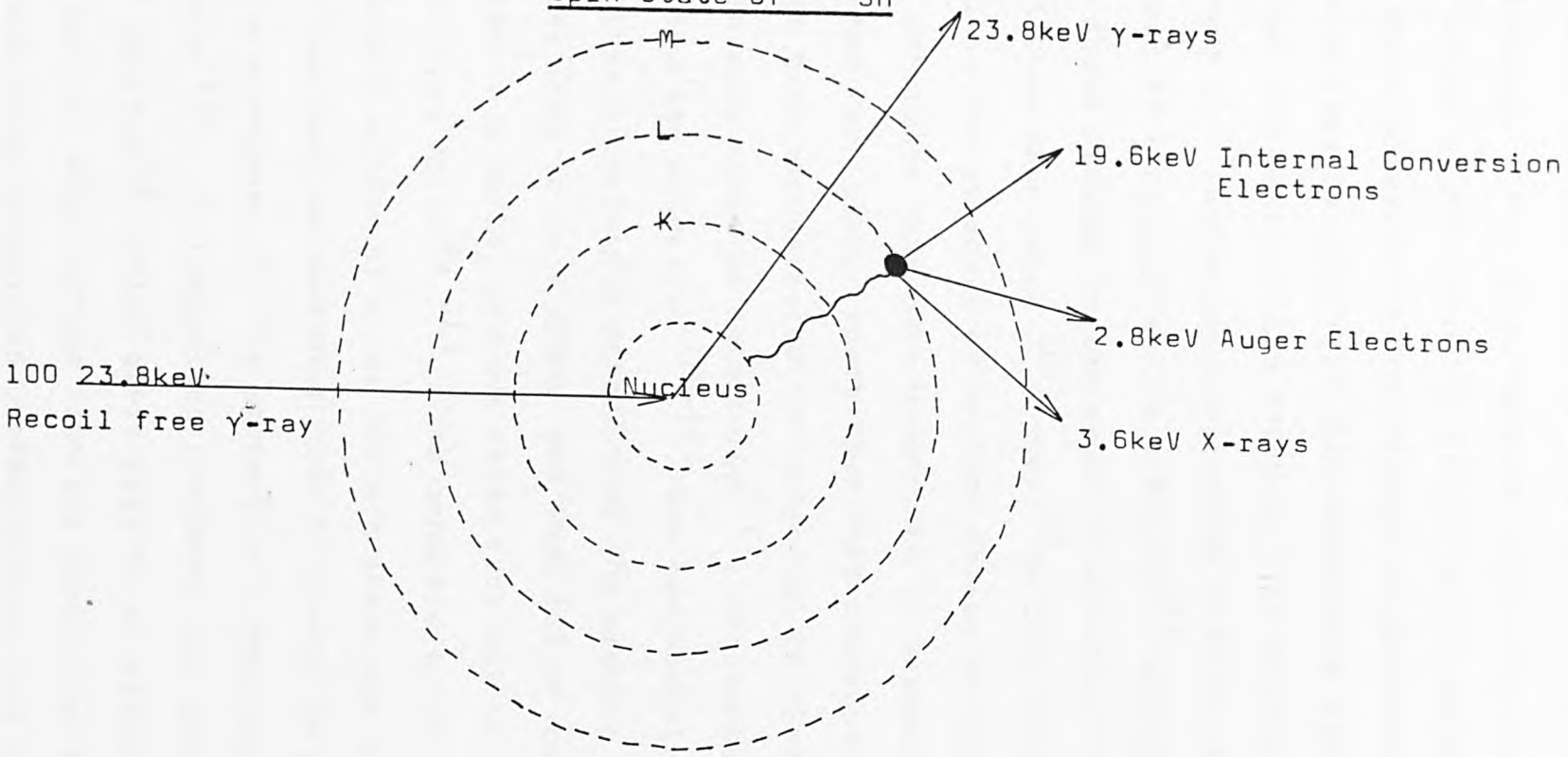

Figure 4.1

saturation effects either in the detector or the counting electronics. For thick samples containing natural abundance of ^{57}Fe the signal to noise ratios are comparable to or less than those obtained in transmission experiments. The background arises largely from photo-electrons ejected from the absorber and walls of the detector. If however samples enriched in ^{57}Fe are used percentage effects of the order of hundreds of a percent may be obtained[9] and data accumulation times reduced to the order of minutes.

It has been shown [10] that ^{57}Fe CEMS is capable of revealing the presence of surface phases on iron foil which would otherwise have gone undetected if transmission methods alone had been used. Apart from this observation, other studies have demonstrated the potential of CEMS as a surface tool in such areas as metallurgy[11], ion-implantation[12-18] corrosion and oxidation [19-22] and geochemistry[23].

Other experiments established the probing depth of ^{57}Fe integral CEMS to be ≃ 300nm and that 66% of the electrons detected in a He/CH_4 counter arise from within 54nm of natural iron foils[8, 21]. The sensitivity of the method is such that c.a.10nm of a new surface phase may be detected and it has been demonstrated that it should be possible to detect a monolayer of ^{57}Fe present on a Mössbauer inert substrate[24]. An unexpected component has been observed in CEM spectra[25] which gives rise to an electron tail. The origin of which arises from the production of so-called γ-ray and X-ray correlated photoelectrons (GPE's and XPE's respectively) produced in surface regions of the absorbers by the Mössbauer spectrum of γ- and X- rays backscattered

from deep within the sample. For ^{57}Fe the XPE's and GPE's contribute about 10% to the total flux of backscattered electrons[26]. The presence of a similar component in ^{119}Sn CEM spectra has also been experimentally confirmed[27].

Now the He/CH_4 detectors do not permit the energy spectrum of the back-scattered electrons to be resolved and in this sense they can be regarded as integral detectors. If however the electrons are energy analysed and spectra accumulated with selected electron energies each of the individual DCEM spectra will be weighted towards a particular depth in the sample therefore providing the possibility of depth profiling the immediate surface regions. A degree of depth profiling may be achieved either with He/CH_4 detectors[9]. or by evaporating inert overlayers onto the sample[28] but more accurate work requires the use of more sophisticated equipment.

4.1.3 ^{119}Sn Conversion Electron Mössbauer Spectroscopy

A number of papers dealing with advances in instrumentation, theoretical aspects and development and application of the CEMS technique have appeared in the literature during recent years[4,5].

A major objective of CEMS studies has been to provide information on the ways in which Mössbauer parameters vary as a function of depth, and for this reason the literature contains many papers dealing with depth-selective applications. The favourable Mössbauer properties of ^{57}Fe γ-radiation and its conversion electrons account for the large number of applications of ^{57}Fe CEMS. However, in the past few years there has been an increase in the reported ^{119}Sn CEMS studies,

some of which are now described.

In a pioneering paper Bonchev, Jordanov and Minkova described the design and use of a magnetic iron-free β-ray spectrometer with intermediate image focussing for use in ^{119}Sn experiments[29]. The spectrometer had an energy resolution of ≈5% and a luminosity of ≈8%. These workers were able to demonstrate that the ^{119}Sn CEM spectra of a brominated tin metal foil consisted of superpositions of peaks arising from α-Sn, SnO_2, $SnBr_2$ and $SnBr_4$. More significantly the area ratios of the spectral components changed with spectrometer settings (i.e. changing electron energy) in a manner which suggested that the overlayer consisted of $SnBr_4$ overlaying $SnBr_2$.

The size of the resonant Mössbauer effects on β-Sn, $CaSnO_3$ and SnO_2 have been measured and compared with theoretical values[27]. The measured percentage effects were 46% 520% and 510% for β-Sn, SnO_2 and $CaSnO_3$ respectively. The anomalously large percentage effect of 950% for SnO_2 measured by Yagnik et al[30] was shown to arise from an inadequate curve fitting procedure caused by neglect of quadrupole line broadening of the resonance.

Bonchev and co-workers[31] have developed an empirical approach to the interpretation of ^{119}Sn data, a method based on the experimental determination of the change in energy distribution of L-conversion electrons emitted from a source which was progressively covered with thin absorbing layers of copper in the range 0.02 - 0.25mgcm^{-2}. The influence of atomic number, crystal structure, and applied electric field on the distribution of ^{119}Sn conversion electrons after passage

through suitable layers, has been investigated[32, 33].

Sano and co-workers[34] have estimated the range of the ^{119}Sn L-conversion electrons to be 1.17 ± 0.20mgcm^{-2} and also used the technique to study the aqueous corrosion of tin[35]. In this latter study the corrosion product formed on tin metal immersed in 6.7 MHNO_3, 5.7 MHCl and 9.0 MH_2SO_4 were determined to be $SnO_2 \cdot nH_2O$; $Sn_4(OH)_2Cl_6$ and $SnSO_4$ respectively. Huffmann and Dunmyre[36], have made detailed ^{119}Sn CEM studies of tinplate. The spectra of tinplate on iron showed contributions from metallic Sn, SnO_2 and $FeSn_2$. The overlayer thicknesses were determined and shown to be in good agreement with the results obtained from standard stripping techniques. A combined ESCA and ^{119}Sn CEMS study[37] has been made of the oxidation of tin. Tin metal was exposed to dry oxygen at 1000^{o}C and it was demonstrated that under these conditions, red SnO was formed at the tin surface. Schunk, Friedt and Llabador[38] have made a depth resolved conversion electron spectroscopic study of a fluorinated tin foil. Depth resolved conversion electron spectra recorded at various energy settings have shown that SnF_4 and SnF_2 were formed at the surface.

The determination of Mössbauer parameters from unresolved spectra with small quadrupole splittings has been studied using SnO_2 and β-Sn absorbers as examples[39]. The apparent linewidths and splittings of the spectra of these materials were found to be sensitive to sample thickness, but the effective linewidths and splittings obtained by back scattering conversion methods were consistent with the values obtained by extrapolation to zero thickness. The

values reported for Γ and Δ were 0.42 ± 0.01 and 0.50 ± 0.02mms^{-1} for SnO_2 and 0.42 ± 0.03 and 0.285 ± 0.017mms^{-1} for β-Sn.

Depth selective Mössbauer experiments have also been carried out on the heterojunctions in thin films of the Sn-Si system[40]. It has been shown that a combination of reflectance high energy electron diffraction and depth selective Mössbauer spectroscopy can give information for the interpretation of the existence of an inverse layer at the metal semiconductor boundary. A new crystalline phase of tin was claimed as a result of CEMS studies of tin evaporated on to the (111) face of Si. The effect on the ^{119}Sn Mössbauer spectra of temperature treatment of tin films on Si was investigated. The cubic lattice phase had an unexpectedly large chemical isomer shift (δ = 4.42mms^{-1}) which after long heating times of the sample at 400^{o}C decreased to 2.75mms^{-1}. It was assumed that the effects resulted from the annealing out of the tin sites with few bonds to neighbouring atoms, to give tin atoms in more strongly bonded sites. A compound semiconductor, tin in silicon carbide, has also been studied by Mössbauer and chanelling experiments [41]. The Mössbauer emission spectra of samples annealed at ≃ 1000^{o}C indicated population of a well defined lattice site. The isomer shift of the Mössbauer spectra showed the electronic structure of the tin atoms to be strongly influenced by the ionicity of the host. CEM and Rutherford backscattering have been used to study laser-implanted tin into silicon[42].

A report has been published describing a conversion electron study of corroded tin plate[43]. The surface layers

of tin plates and tin-coated iron plates corroded by various acids have been studied by means of CEMS. The product identified on samples corroded with HNO_3 was metastannic acid. Maleic, malonic, formic and oxalic acids were used in the corrosion of tin-coated iron plates, the products of which have been identified as tin(IV) oxides by CEMS. Using the CEMS technique as an analytical tool, a system of iron implanted with tin has been investigated(44). Single crystal and polycrystalline samples of α-tin have been implanted at room temperature with 80keV ions of radioactive ^{119m}Sn, ^{119}Sb and ^{119m}Te, whose nuclei decay to the Mossbauer level of ^{119}Sn, and their CEM spectra have been recorded(45). Mössbauer transmission and emission modes have been used to study the oxidation state of tin atoms and the mechanism of their introduction into glass(46).

In recent years the use of ^{119}Sn conversion electron Mössbauer spectroscopy for surface studies has grown. However there is still plenty of scope for further studies on tin containing materials and in Section 4.1.4 details are given of the materials selected for investigation by CEMS in the present work.

4.1.4 Application of ^{119}Sn CEMS

The majority of integral CEMS experiments performed to date have been carried out using a $He/5\%CH_4$ flow proportional counter. A number of designs of such counters have appeared in the literature (47-50). Other workers have used parallel plate avalanche counters(51), channeltrons(52,53) and photo-multipliers(54) to detect the conversion electrons. The backscatter detector used in this work is a gas-flow proportional

counter which was built at Heriot-Watt University, Edinburgh. The counter consists of a single anode and has a working voltage of 1050V. A particular feature of this type of detector shown in Figure 4.2(a) and (b) is its low efficiency for detecting X-rays and γ-photons with this gas mix (95% He/5%CH_4), due to its small sensitive volume. Although, in the past few years there have been reports on both high temperature[55,56] and low temperature (4.2.K) measurements[57], most spectra, including those recorded in this work were obtained at ambient temperatures.

The spectrometer was run in constant acceleration mode, the wave-form being generated by a J & P Mössbauer spectrometer and the spectrum was accumulated in a multichannel analyser using 256 channels. The spectrometer was periodically calibrated with stannic oxide. At the start of the work the source used had an activity of 35mCi. Isomer shifts were determined relative to $BaSnO_3$. Typical data accumulation times for the backscatter spectra were 3 - 12 hours. Spectra of the normal tin compounds were recorded as thin films using chloroform as a mulling agent, whilst direct measurements were made on samples of glasses, ceramics, fabrics and tinplate.

This surface-sensitive technique is now used to obtain further information, if any, about the surface reactions involving tin compounds. There are two types of surface reaction *viz*. those reactions at tin-containing matrix surfaces, and those reactions of tin compounds on matrix surfaces, some of which are listed in Table 4.2. To study fully all such surface reactions is not possible during the time scale of

Figure 4.2a

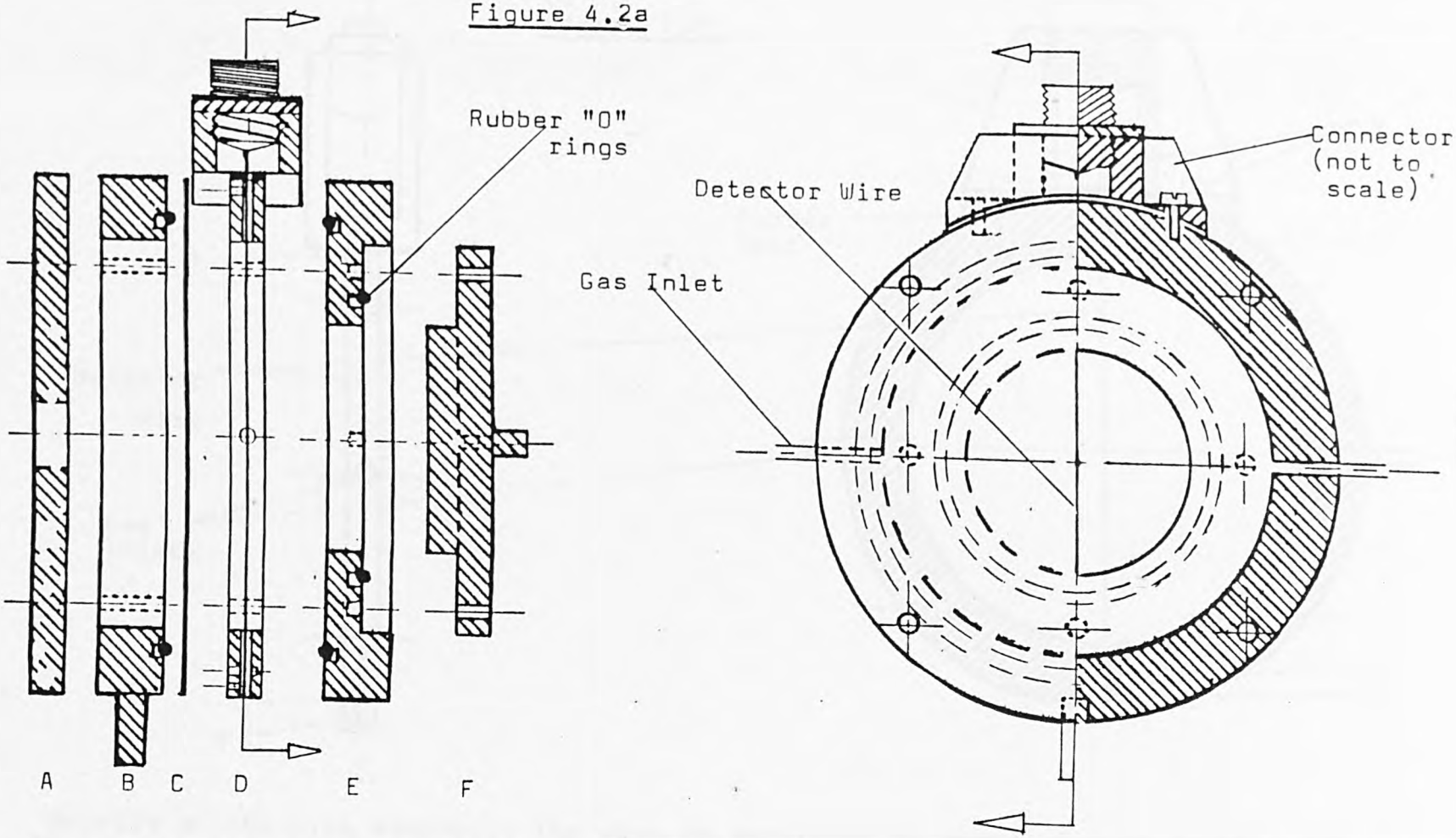

Schematic representation of a CEMS detector: The detector is made up from a lead shield A, a front plate B, an aluminium window C, a wire assembly D, a backplate E and a sample holder F.

Figure 4.2b

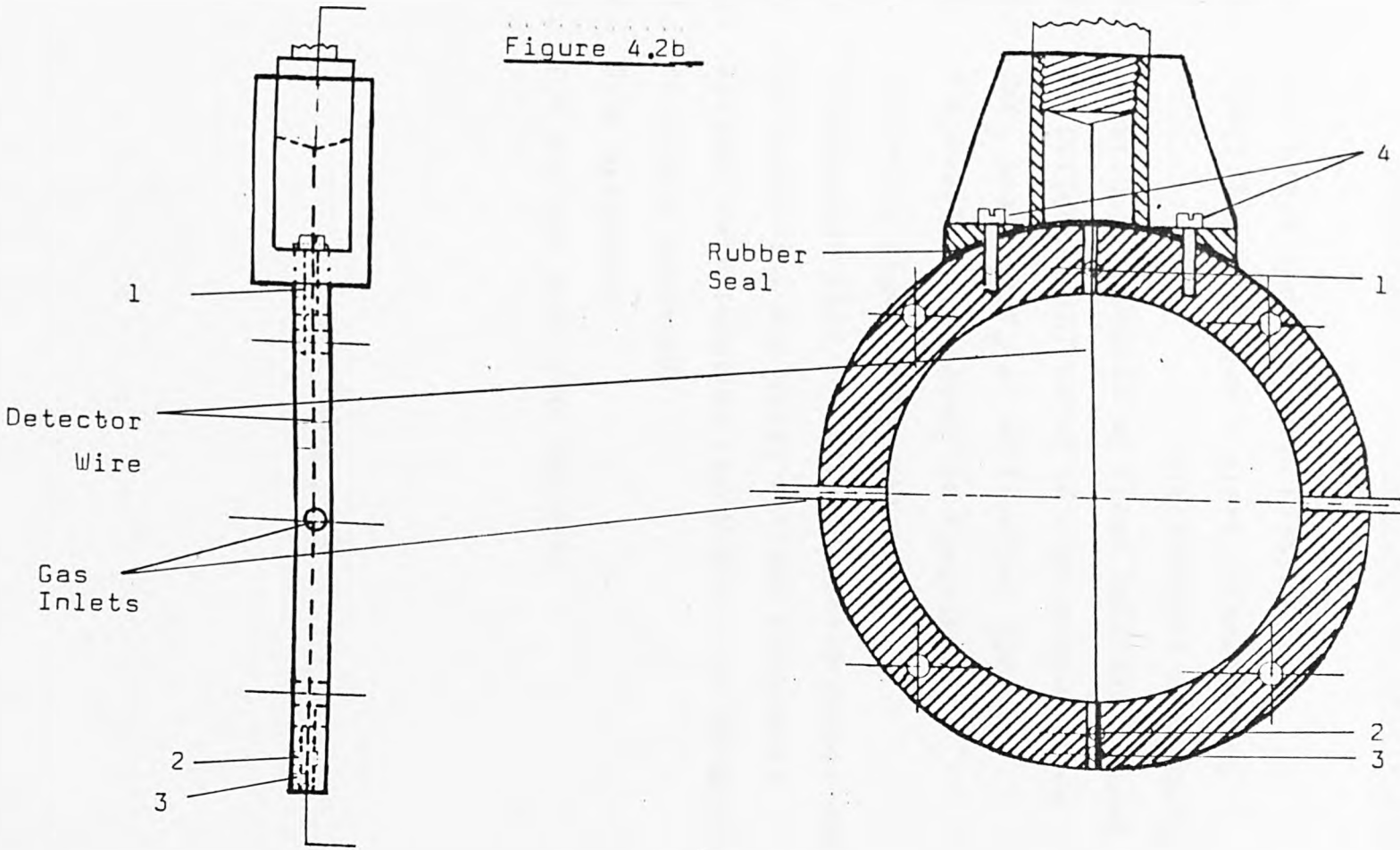

Details of the wire assembly: The wire is tensioned by means of screws 1,2 and 3. The anode is fed through the guide channel and secured by screws 3 and 1 and then tensioned by turning screw 2. The anode is replaced by undoing screws 1 2 3 and 4, holding the connector to the main body.

Reactions of Tin Compounds at Matrix Surfaces

1. Tin plate and tin alloy plating
2. Tin(IV) oxide films - glass strengthening
   electrically conducting films
3. Hexafluorostannates as flame retarder on wool
4. Bis(tributyltin) oxide as wood preservative
5. SnF_2 and Sn_2ZrF_8 as anti-caries agents
6. Triphenyltin compounds as fungicides
7. Tin oxide pigments for ceramics
8. Hydroxystannates in rust inhibiting primer paints
9. Solderability and metal surface treatments
10. Polymer metallisation reactions - tin sensitisors
11. Antitumor compounds
12. Silk weighting
13. Tin and tin compounds deposits

Table 4.2

Reactions at Tin-containing Matrix Surfaces

1. Corrosion
2. Detinning and Desoldering reactions
3. Ion exchange on hydrated tin compounds
4. Heterogeneous catalysis
5. Matrix supported reagents for organic syntheses
6. Metal and compound deposits on tin-containing substances

Table 4.2(continued)

this work, so the aim of the present work is therefore, to examine a variety of tin-containing materials and their surface reactions to determine the scope of the application of the ^{119}Sn Conversion electron Mössbauer spectroscopic technique (CEMS). The work described here is discussed under three headings:

(1) Comparison of conversion electron and transmission Mössbauer data for some tin compounds.

(2) Surface reactions on glasses, ceramics and fabrics.

(3) Applications in some detinning and desoldering projects.

(1) Comparison of conversion electron and transmission Mössbauer data for some tin compounds

A singlet spectrum such as that shown here for SnO_2, which is used to calibrate the instrument, can be accumulated (120,000 counts/channel) in three hours, with 11% effect.

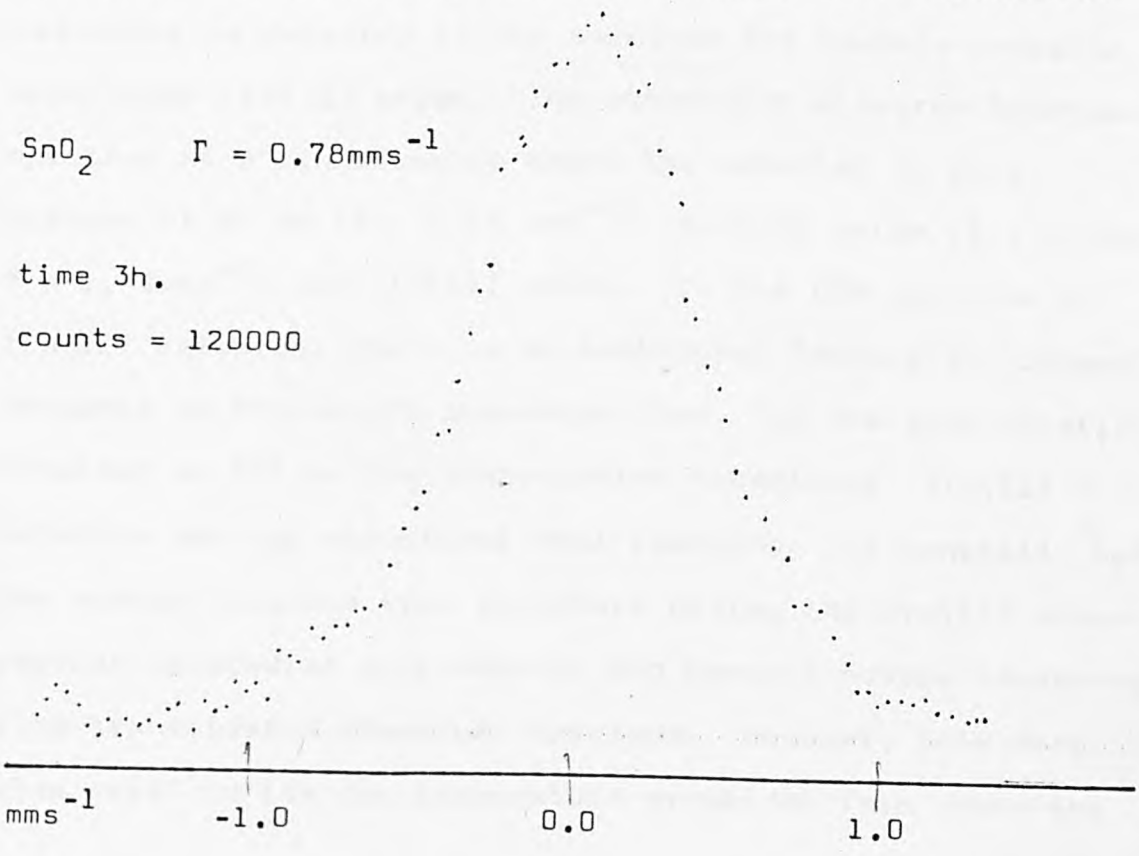

The tin(II) compounds studied include red and blue black tin(II) oxide, tin(II) sulphide, selenide and fluoride. In addition, a tin suboxide was examined. For all the tin(II) compounds, except the selenide, the CEM chemical shift data are similar to those obtained by transmission techniques, whilst for some, their quadrupole splittings are actually less than those measured in the transmission mode. This is surprising since it is expected that the tin sites at the surface would be more distorted. It is not possible at this stage to decide whether the smaller quadrupole coupling constants are due to surface properties or to differences in the fitting of the spectra. It has always been assumed that tin(II) compounds are metastable and that surface oxidation is likely to be a major feature of their chemistry. Of the compounds studied, small amounts of tin(IV) are detected for red SnO and SnS, (Figure 4.3), but no tin(IV) resonance is detected in the spectrum for freshly prepared blue black tin(II) oxide. The conversion electron Mössbauer spectrum of a tin suboxide shows the material to be a mixture of β- Sn (δ = 2.64 mms^{-1}), tin(II) oxide (δ = 2.73mms^{-1}, Δ = 1.43mms^{-1}) and tin(IV) oxide. In the CEM spectrum of tin(II) selenide, there is an additional feature at 3.00mms^{-1} compared to the single resonance line, for the bulk material, obtained at 80K by the transmission technique. Tin(II) selenide has two structural modifications. It generally has the sodium chloride type structure giving the tin(II) atom a regular octahedral environment, and hence a narrow resonance line transmission Mössbauer spectrum. However, SnSe does also exist in its low temperature pyramidal form where the

tin atom is in a distorted lone pair environment. It is clear that the CEM spectrum is that of a distorted tin site suggesting that distorted sites exist on the surface of SnSe at room temperature.

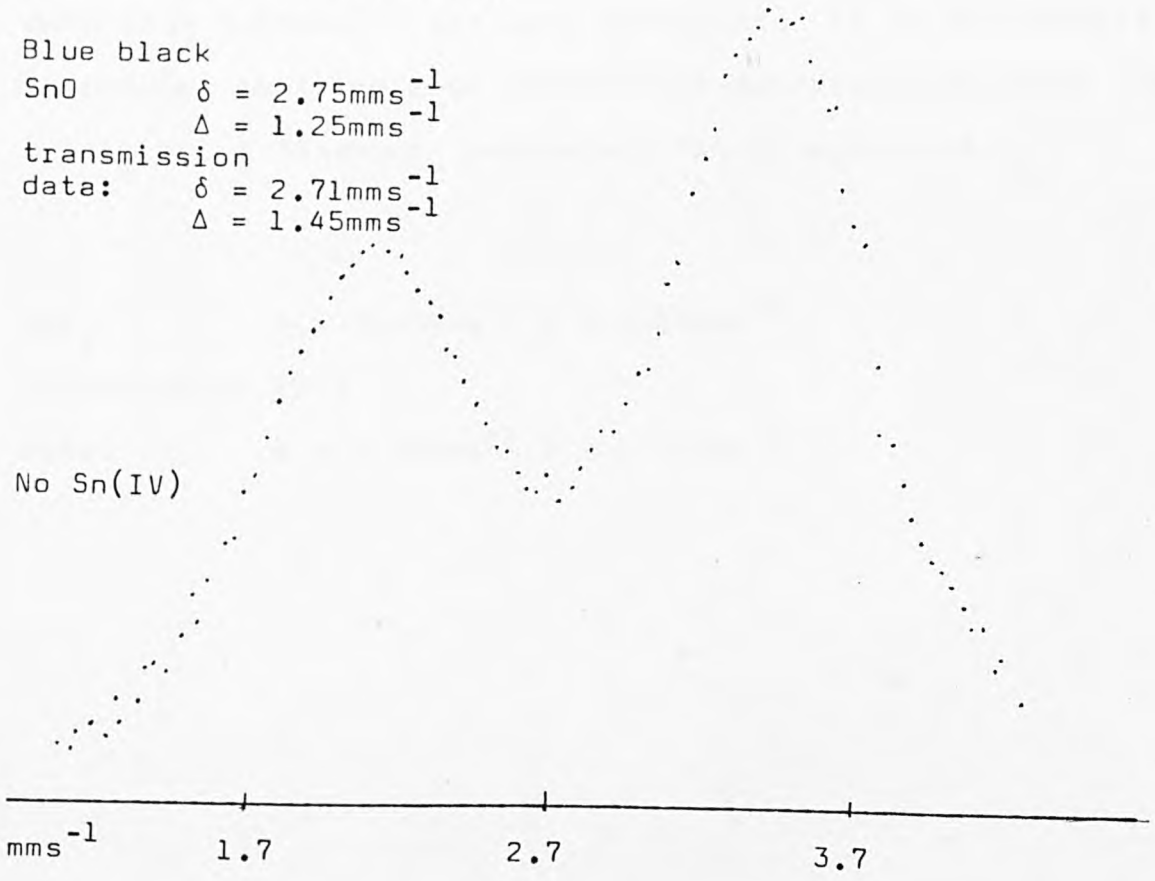

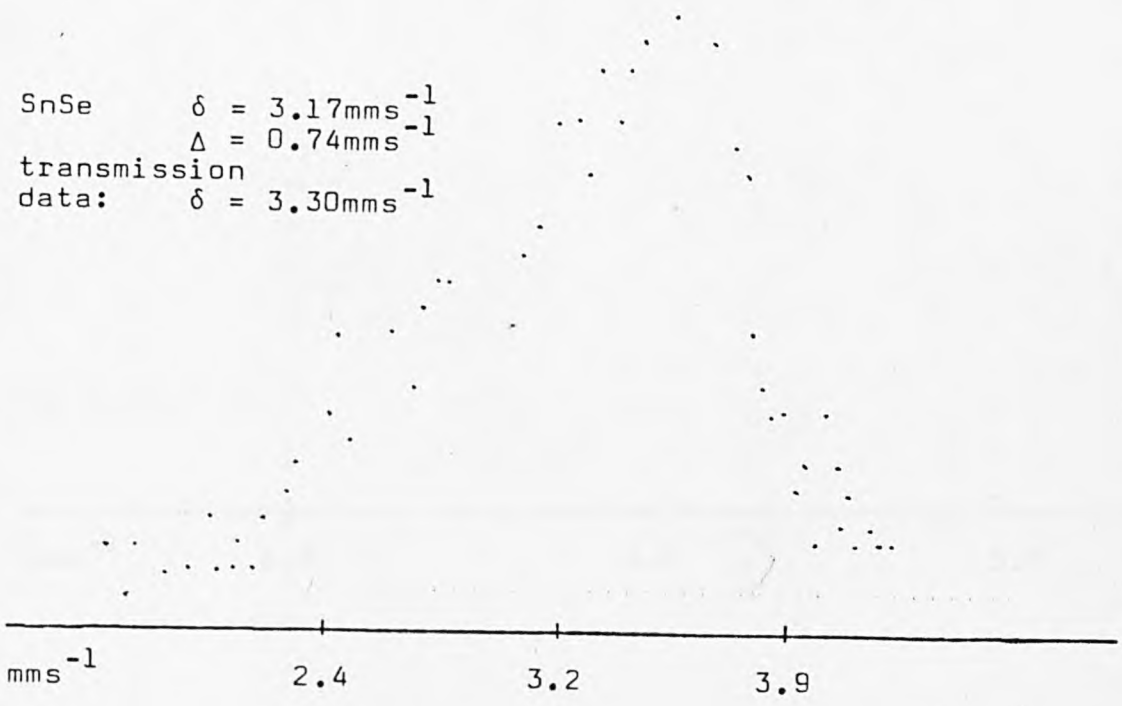

For all the compounds studied except tin(II) fluoride there is little difference between room temperature and 80K transmission chemical shift data. For tin(II) fluoride, however the room temperature data (δ = 3.38mms^{-1}) and 80K transmission data (δ = 3.65mms^{-1}) are very different. It is not surprising therefore, that the room temperature conversion electron and transmission Mössbauer parameters are in agreement.

SnF_2 δ = 3.40mms^{-1} Δ = 1.56mms^{-1}

transmission (RT)

data: δ = 3.38mms^{-1} Δ = 1.51mms^{-1}

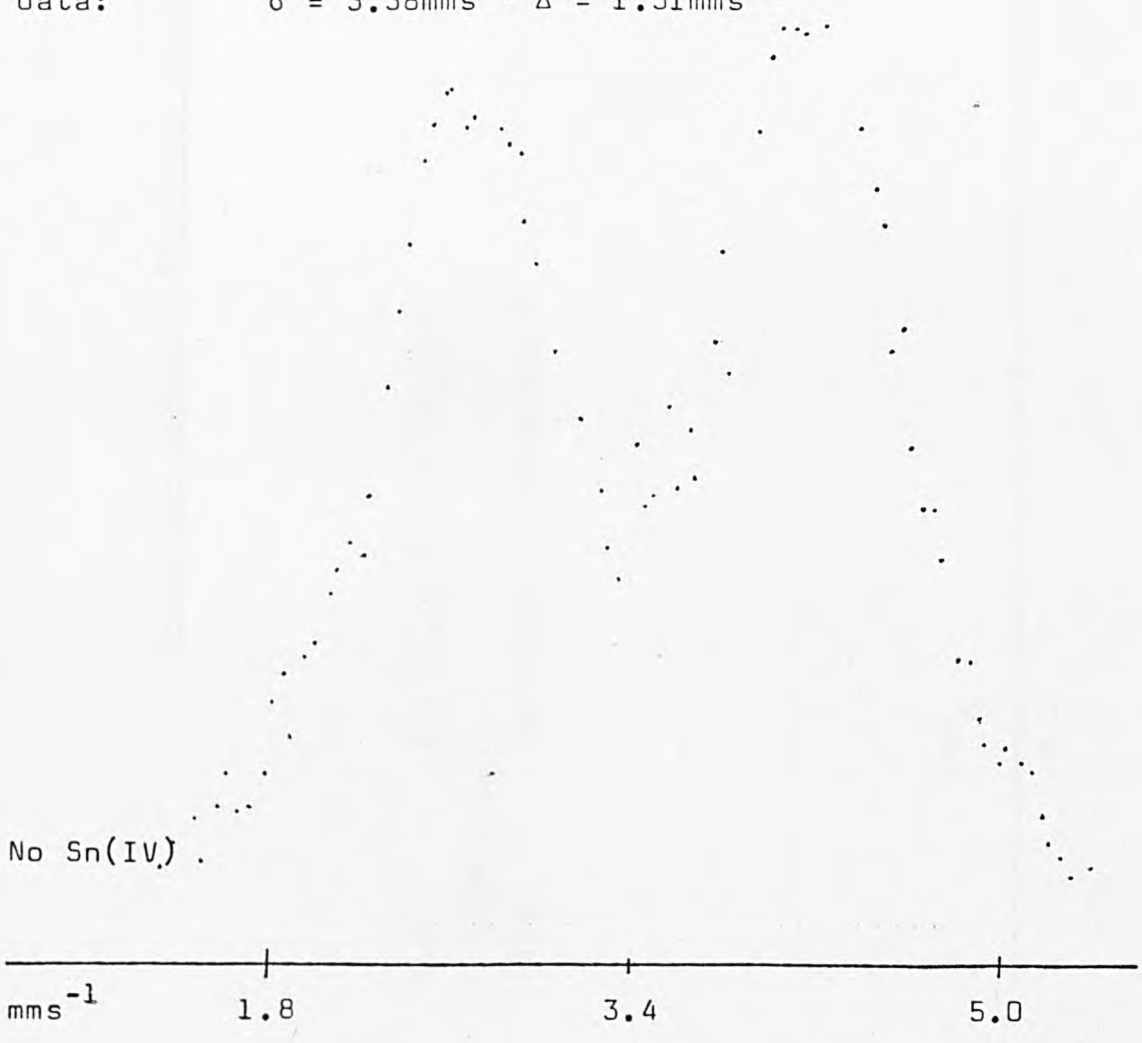

Conversion Electron Mössbauer Spectrum of Red Tin(II) Oxide

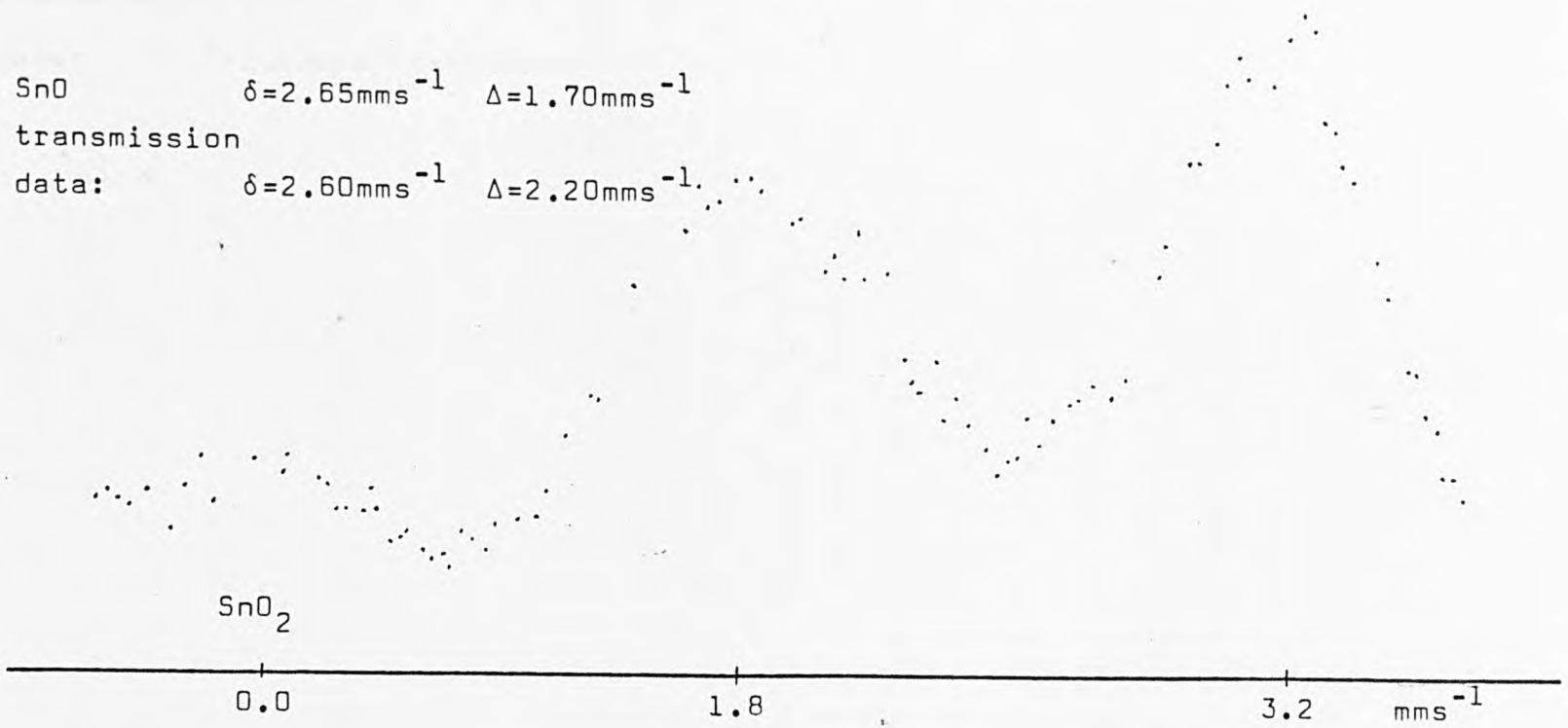

Figure 4.3

Conversion Electron Mössbauer Spectrum of Tin(II) Sulphide

SnS $\delta=3.32 mms^{-1} \Delta=0.64 mms^{-1}$

transmission (RT)

data: $\delta=3.23 mms^{-1} \Delta=0.86 mms^{-1}$

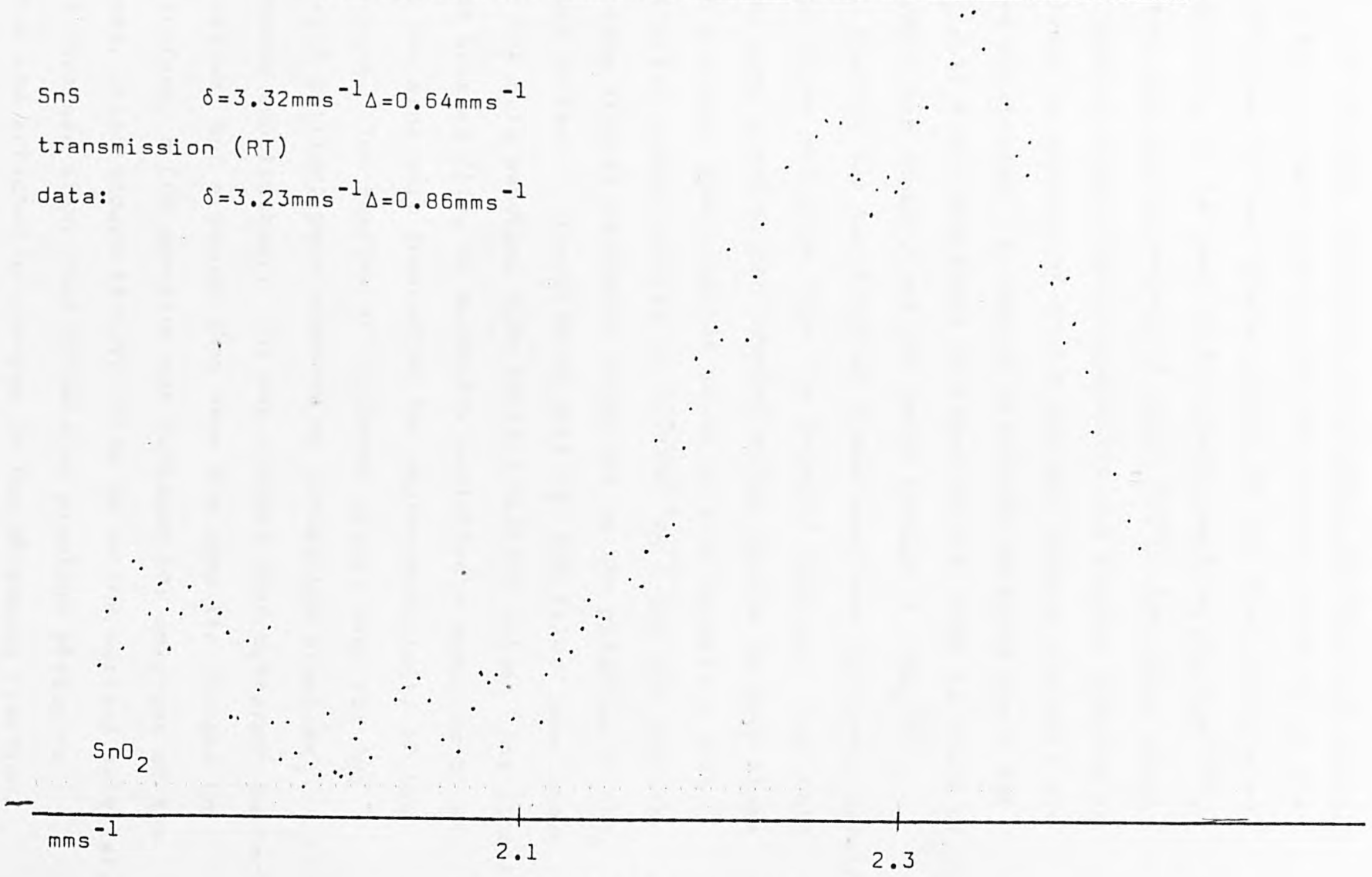

Figure 4.3(continued)

(2) Surface reactions on glasses, ceramics and fabrics

An important application for stannic oxide is in the manufacture of lead glass, where, in the form of sintered electrodes, it is used in the electromelting process[58]. At temperatures in excess of about 800°C, the glass melts and becomes electrically conductive and further heating is achieved by passage of a high current through the melt via these electrodes. A typical electrode contains about 98% SnO_2 with small additions of other oxides, such as those of antimony and copper, and can weigh between 5 -50kg[59].

Spectra for two types of glass have been obtained, namely ohmic films and glass from 'no deposit' bottles. The ohmic films were glass slides treated either on one or both sides with antimony doped stannic oxide to give materials with electrical conductivities of $50/500\Omega^{-1}cm^{-1}$. The CEM spectra all show singlet resonance lines due to the presence of SnO_2 at the surface. Transmission data for the films have shown that the bulk material also contain tin(IV) oxide. The single sided treated film, as expected, exhibited a spectrum of SnO_2 from one side only indicating the depth-sensitivity of the technique. Two samples of toughened glass, used for 'no deposit' bottles, were examined by conversion electron Mössbauer spectroscopy. The two glasses have different surface properties, but although they have the same tin content on the surface, a CEM spectrum was achieved for only one of the glasses, which showed tin(IV) oxide to be the surface material. It is therfore clear that conversion electron Mössbauer spectra are affected by changes in the Mössbauer fraction, and that such changes can be used for diagnostic purposes.

The rutile-type structure of stannic oxide is able to accommodate transition metal colourant ions in the lattice and these form the basis of the commercial pigments for ceramic tiles and pottery. The photoacoustic spectra for some of these pigments have already been recorded, as part of this work, and details are given in Chapter 3, section 3.4.2. In the course of the present work, the surface properties of some glazes on tiles were examined. The pigments used in the glazes are metal(IV) metastannates ($MSnO_3$), all of which exhibit single line conversion electron and transmission Mössbauer spectra of stannic oxide. It is not surprising therefore, that for both the green and blue tile glazes containing $NiSnO_3$ and $SbSnO_3$ respectively, singlet tin(IV) oxide peaks are obtained.

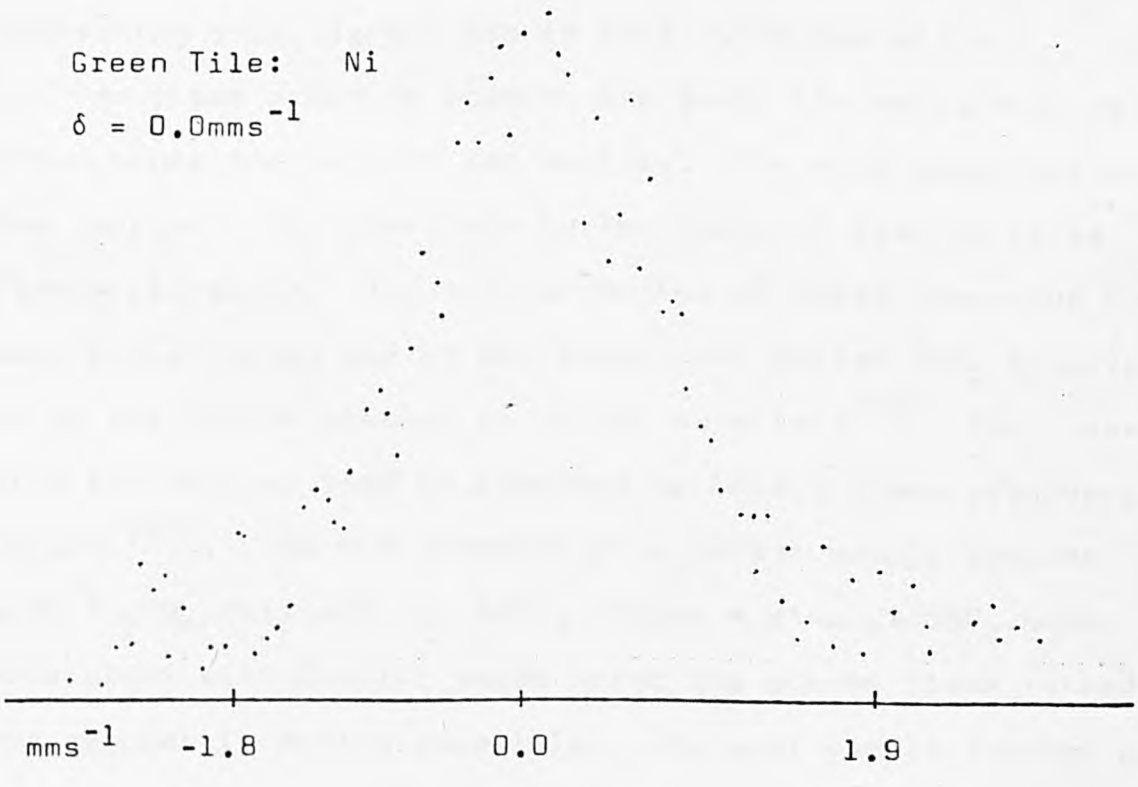

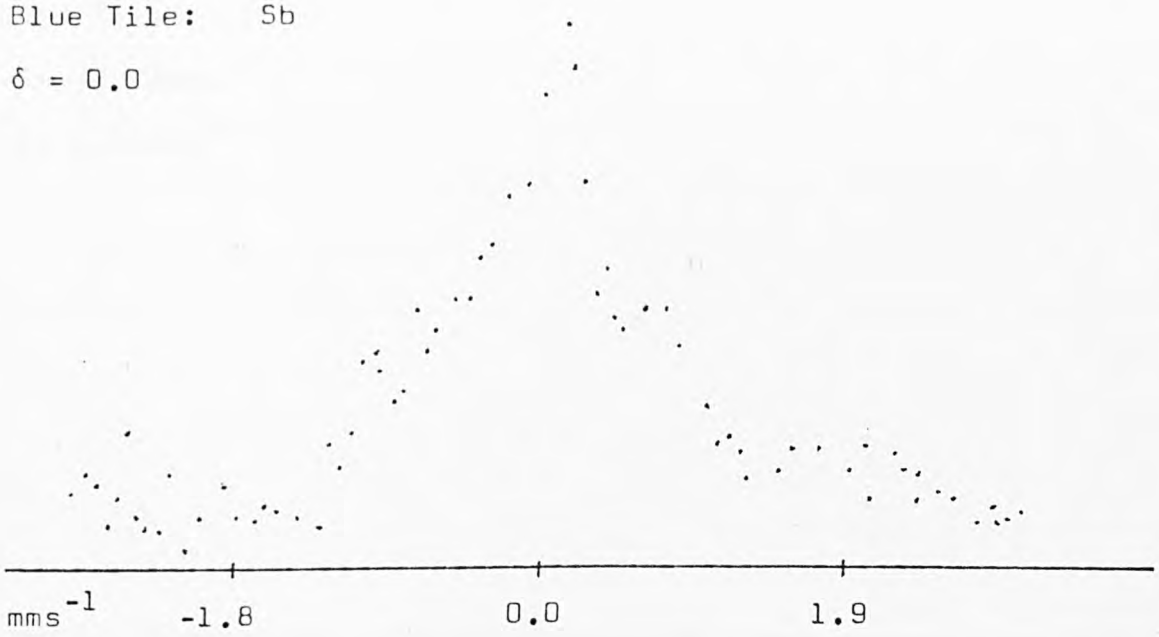

For the red tile, containing a $CrSnO_3$ pigment, however, a quadrupole split doublet, with a shift of $-0.13 mms^{-1}$, is obtained, with no evidence of SnO_2 at the surface. It must therefore be concluded that the tin atoms at the surface glaze containing this pigment are in very distorted sites.

As flame proofing agents, inorganic tin salts have been known since the turn of the century. The most important outlet for inorganic tin chemicals in the field of fabrics is as flame-retardants. The mode of action of these compounds has been investigated and it was found that whilst SnO_2 appears to be the active species in cotton materials[60], the presence of a tin-halogen bond is required to impart flame-retardancy to wool[61]. The CEM spectrum of a cotton sample treated with Na_2WO_4 followed by $SnCl_4$, shows a singlet SnO_2 peak, consistent with tin(IV) oxide being the active flame retardant species in cotton materials. The wool sample treated with

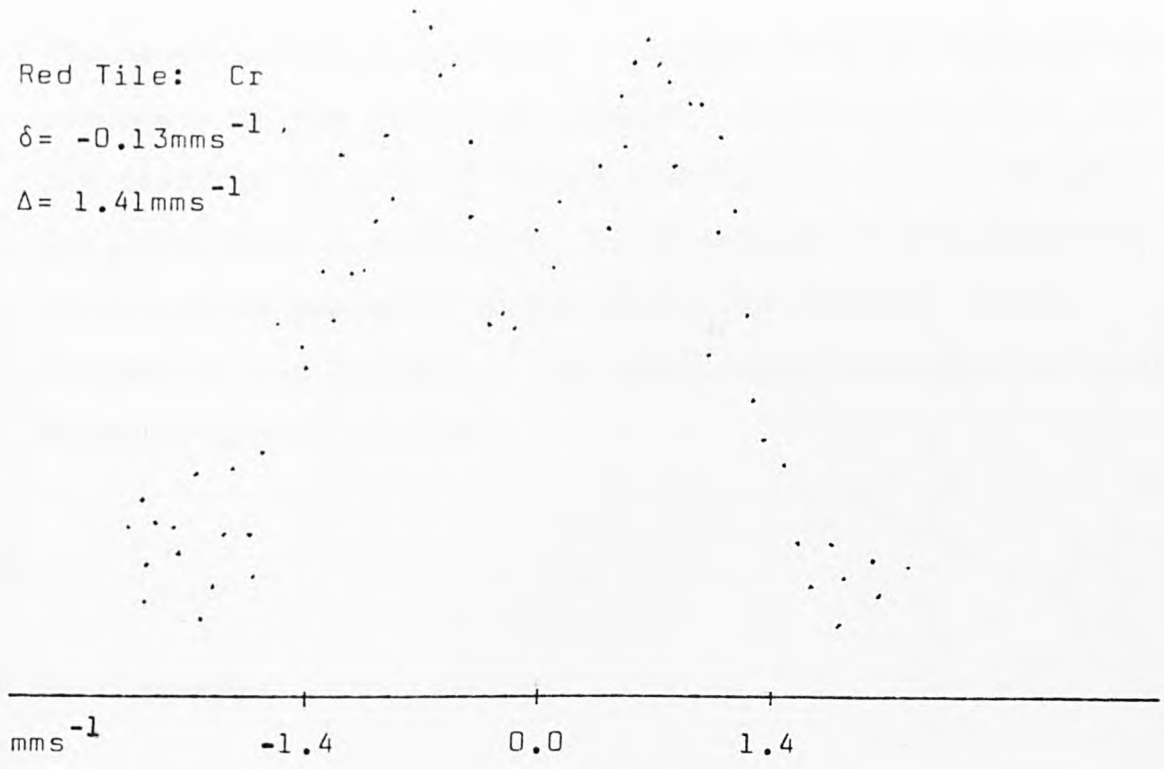

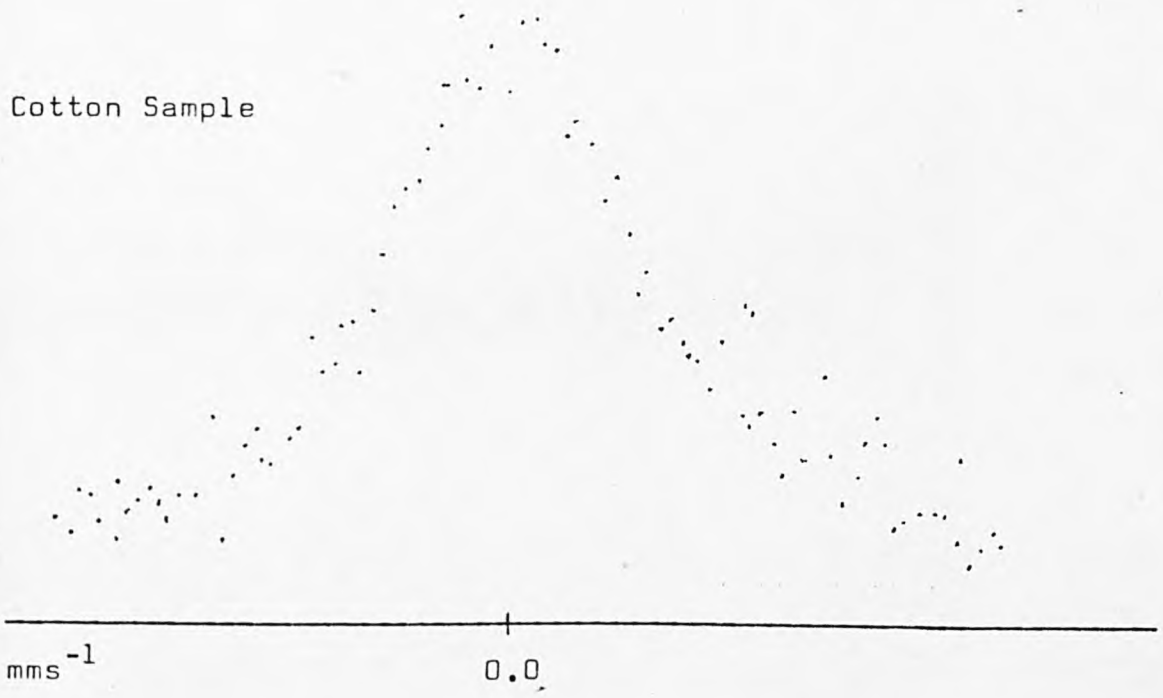

$SnCl_4 . NH_4HF_2$ solution was reported [61] to contain the active species $[SnF_5OH]^{2-}$ (resulting from hydrolysis of the SnF_6^{2-} anions in solution) before washing, this was then hydrolysed to the ineffective SnO_2 when the treated wool was subjected to a standard washing procedure. The transmission

Mössbauer spectrum exhibited a singlet SnO_2 as the main tin component of the bulk wool sample. On the other hand, the CEM spectrum is very different showing not only a singlet SnO_2, but also a quadrupole split doublet (δ = 0.03mms^{-1}), which can be assigned to the fluorostannate(IV) moiety present at the surface of the wool, which provides the active flame retardant species.

Wool Sample

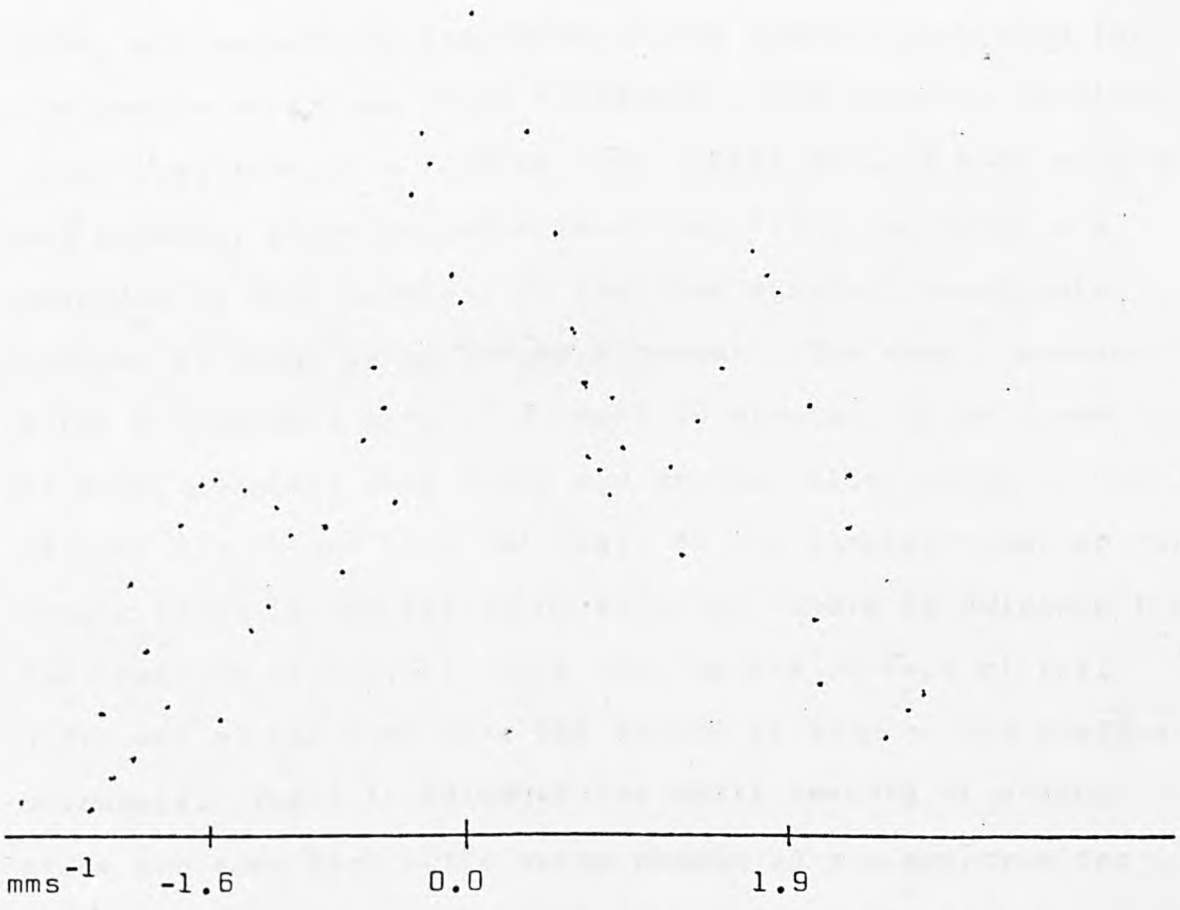

(3) Application in some Detinning and Desoldering Projects

In a sequence study of detinning tin-plate[62], samples of plate were removed at various time intervals from a refluxing solution of sodium hydroxide and sodium nitrite ($150gNaOH + 25gNaNO_2/L$). Conversion electron Mössbauer spectroscopy was used to follow this detinning process and the following results were achieved (Figure 4.4).

The singlet spectrum of β-Sn($\delta = 2.60mms^{-1}$) on the surface of tin-plate appears as the only surface material present after treatment of one hour. The spectral components arising from β-Sn and a quadrupole split doublet of $FeSn_2$ are separately indicated in the spectrum achieved for the sample after two hours treatment. The spectrum obtained after treatment of a further hour, still shows a β-Sn singlet and an alloy phase probably involving $FeSn_2$, although the spectrum is more complex, in that the distinct quadrupole doublet of $FeSn_2$ is no longer apparent. The sample removed after a treatment time of 3 hours 20 minutes, gives a spectrum of β-Sn, possibly some $FeSn_2$ and another alloy phase of FeSn, or just tin in the iron lattice. As the samples remained for longer times in the refluxing solution, there is evidence for the presence of tin(IV) oxide coating the surface of the plate and at the same time the amount of β-Sn on the surface decreases. There is evidence for small amounts of stannic oxide and some iron : tin oxide phases in the spectrum for the sample treated for 3 hours 40 minutes. Finally no spectrum was obtained for the four hour treated sample, indicating all tin phases have been removed by this time.

Detinning Studies

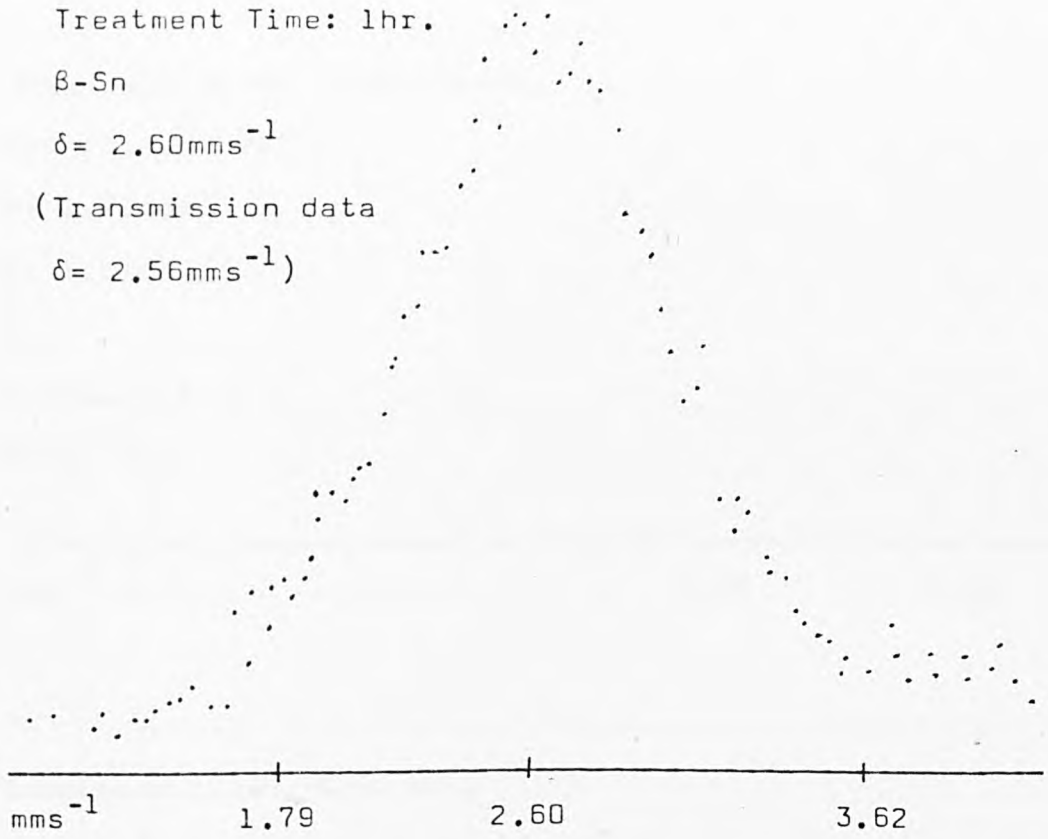

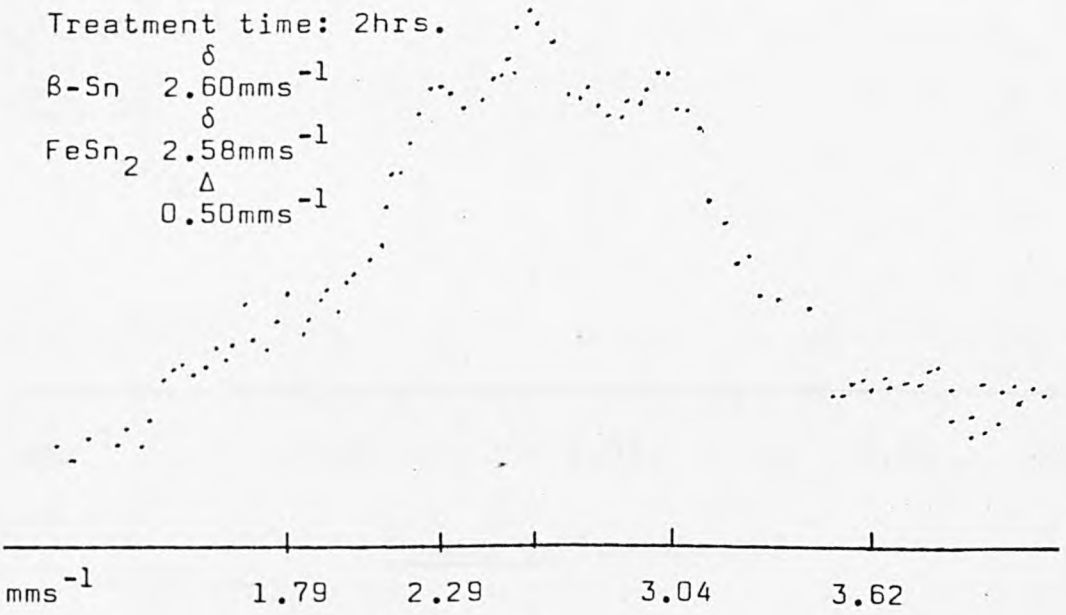

Figure 4.4

Detinning Studies

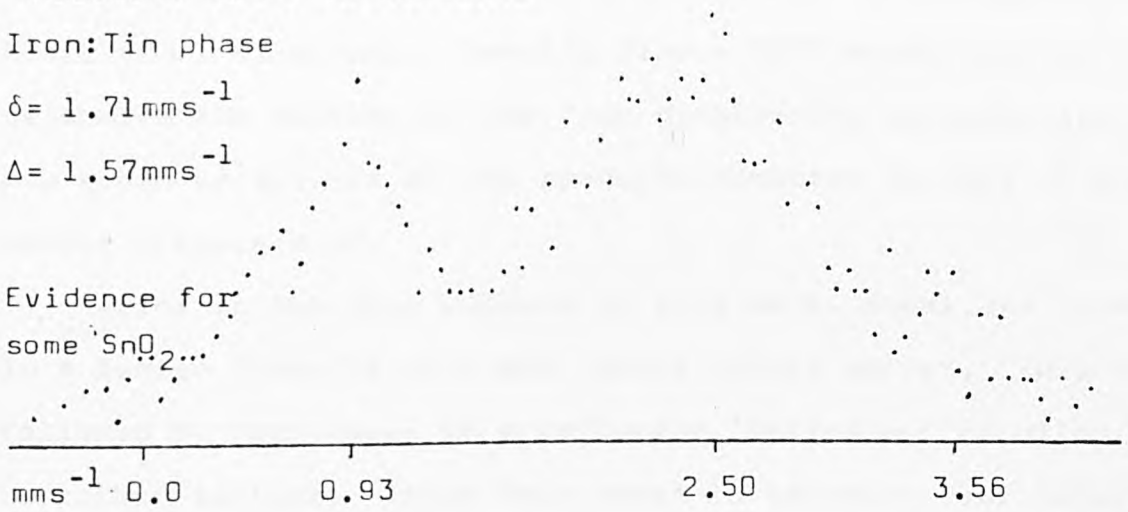

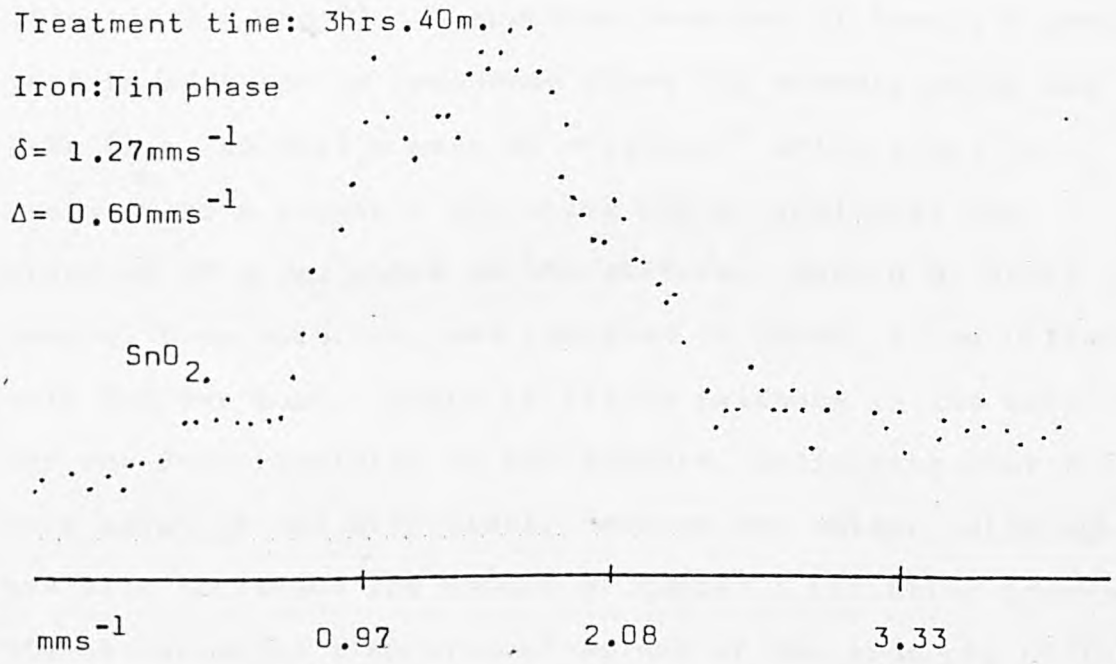

Figure 4.4(continued)

In a metal recovery project undertaken at City University[62], four attempts were made to remove a lead : tin solder which had been used to bind sheets of an alloyed metal MONEL (Cu : Ni alloy). Results from a CEMS study used to determine the success of the four desoldering methods, are now given as spectra of the products compared to that of the solder (Figure 4.5).

Prior to the four methods of treatment, monel was treated in a bunsen flame to melt and remove excess solder. This was followed by four hours in a refluxing 'detinning' solution described earlier. After four hours in solution four samples were removed, one of which remained untreated (Sample A), whilst the other three were subjected to further treatment, (Samples B,C and D). A spectrum recorded of Sample A shows that in addition to resonance lines for stannic oxide and β-Sn (i.e. solder) a peak at $\simeq 1.6 mms^{-1}$ which could be assigned to a copper : tin alloy phase, indicates the presence of a new phase on the surface. Sample B, after removal from solution, was immersed in $2MHNO_3$ in an ultrasonic bath for one hour. There is little evidence in its spectrum for any β-Sn remaining on the surface, indicating that the acid solution has effectively removed the solder, although it has also increased the amount of copper : tin alloy present. Stannic oxide is also present as one of the products of this surface reaction. Similar results are obtained for Sample C immersed in 2MHCl, the resonance peak heights for the two surface products SnO_2 and the copper : tin alloy are now almost equal indicating an increased production of SnO_2 at the surface. A final attempt to remove the solder involved an immersion of

Desoldering Studies

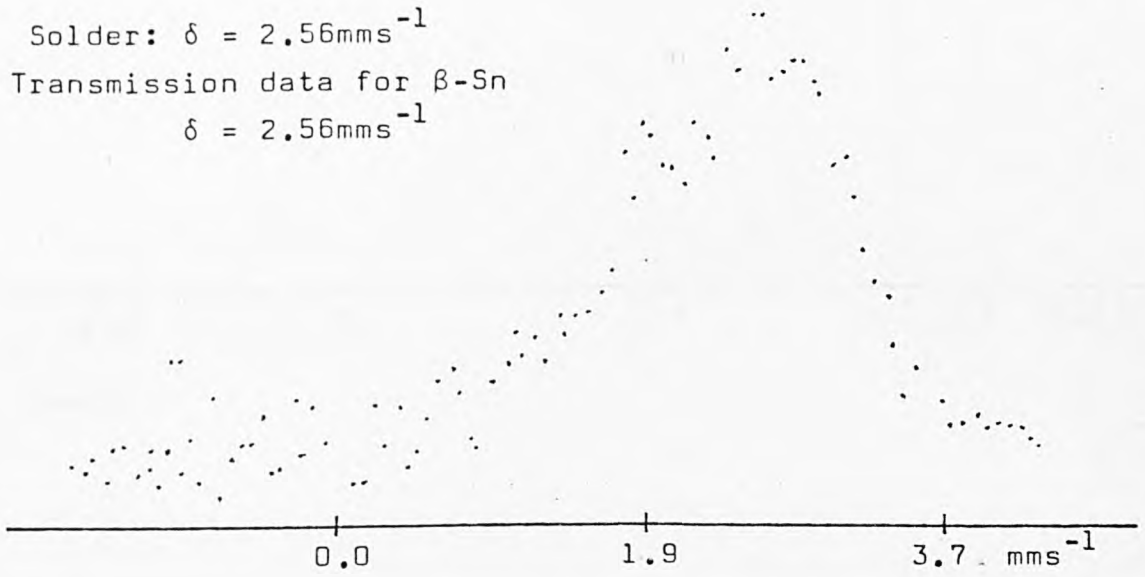

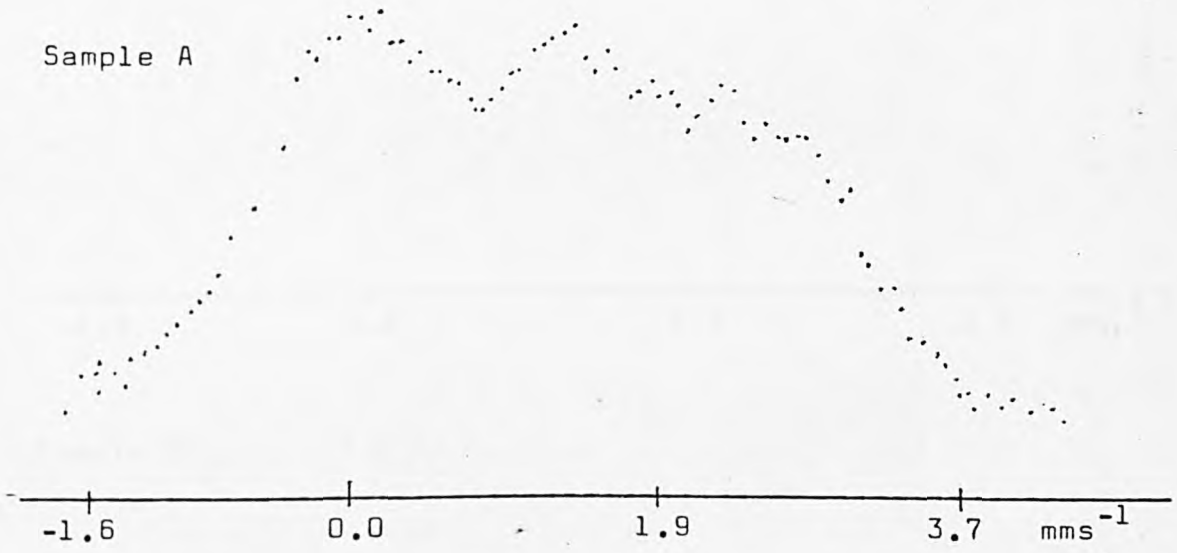

Figure 4.5

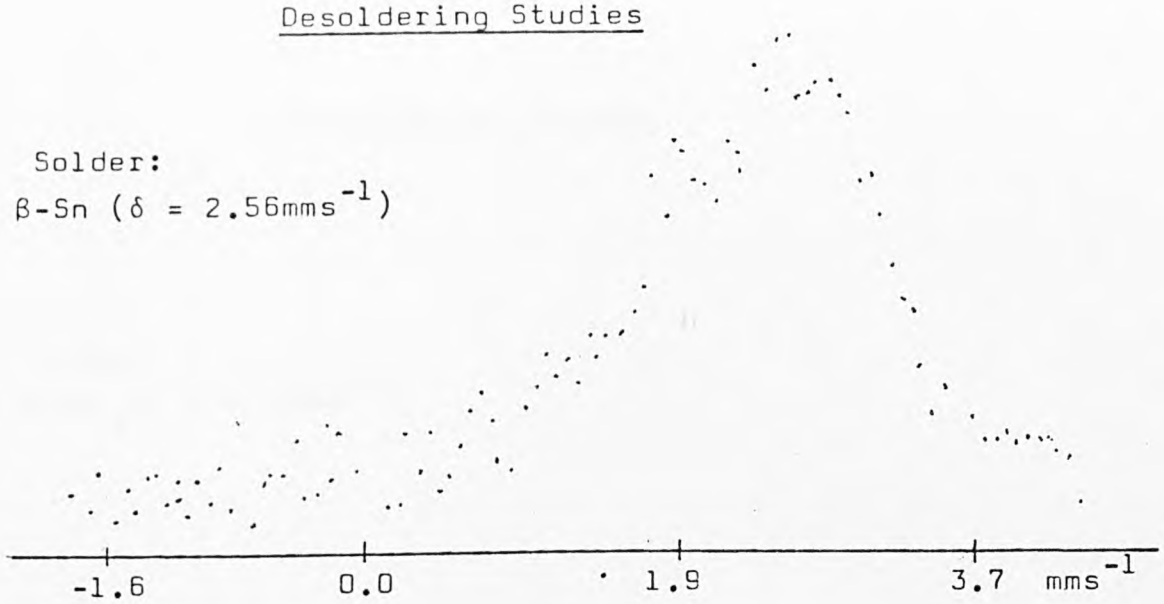

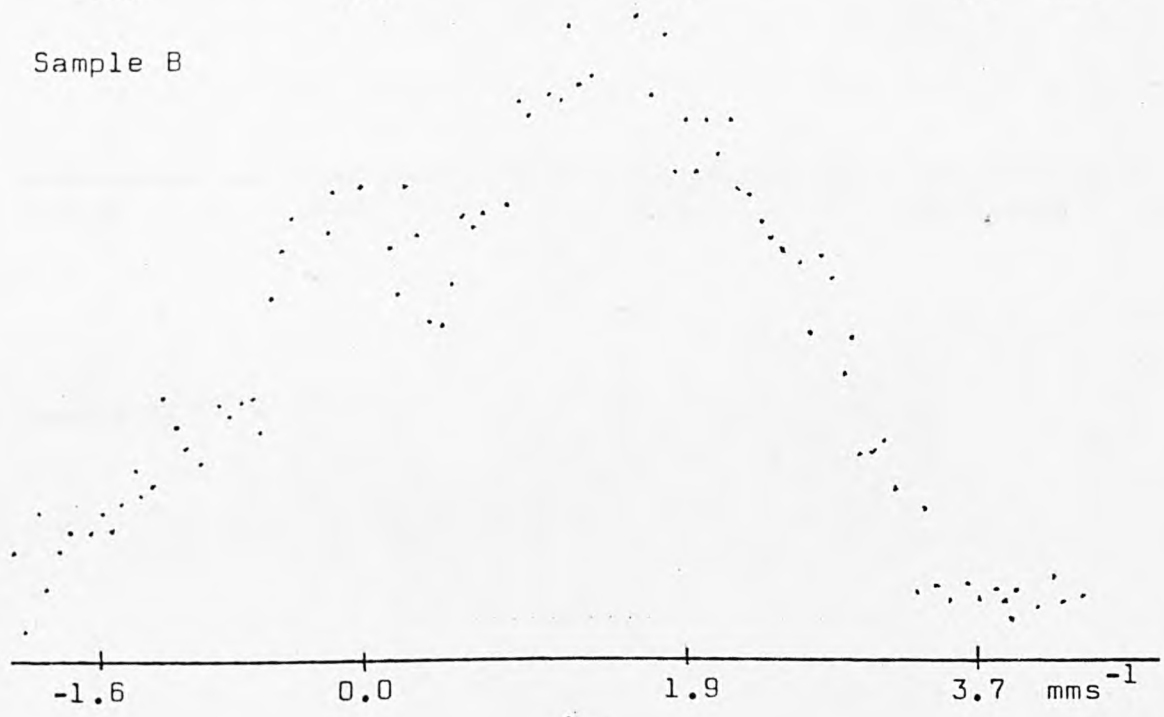

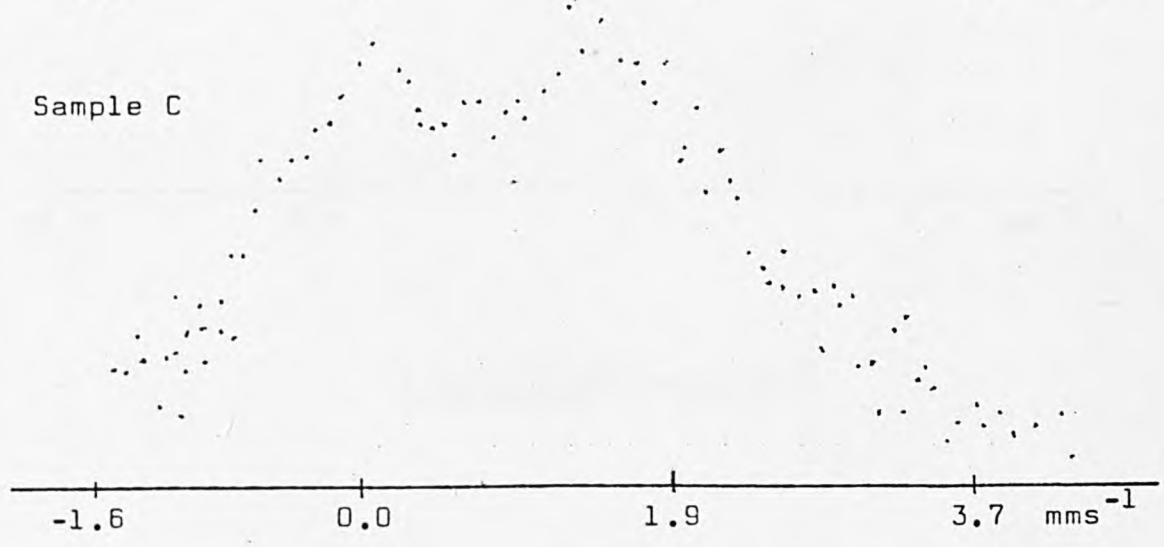

Figure 4.5(continued)

Desoldering Studies

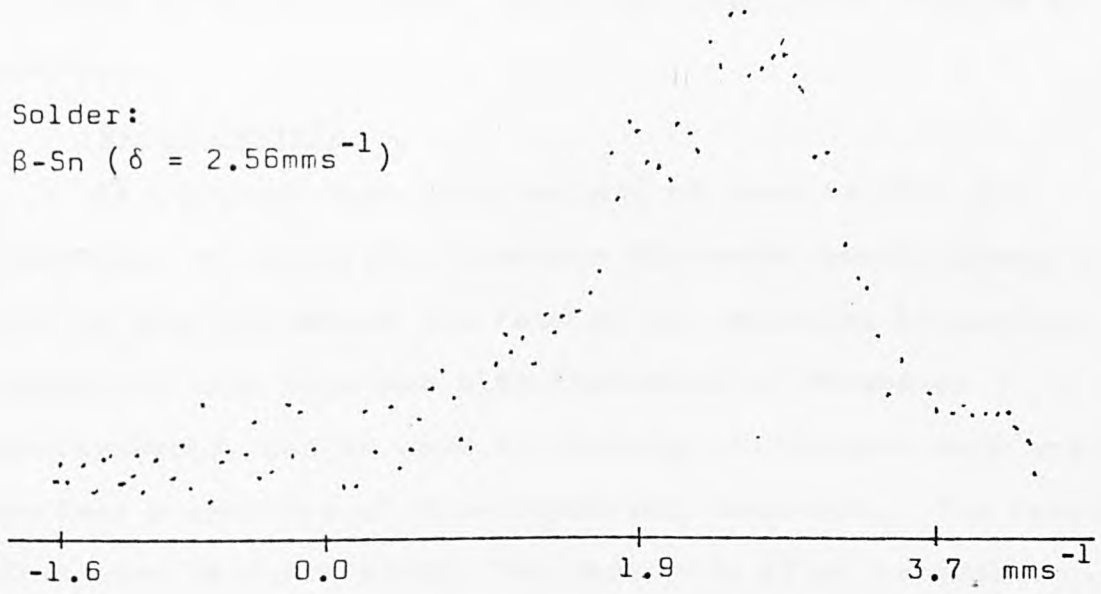

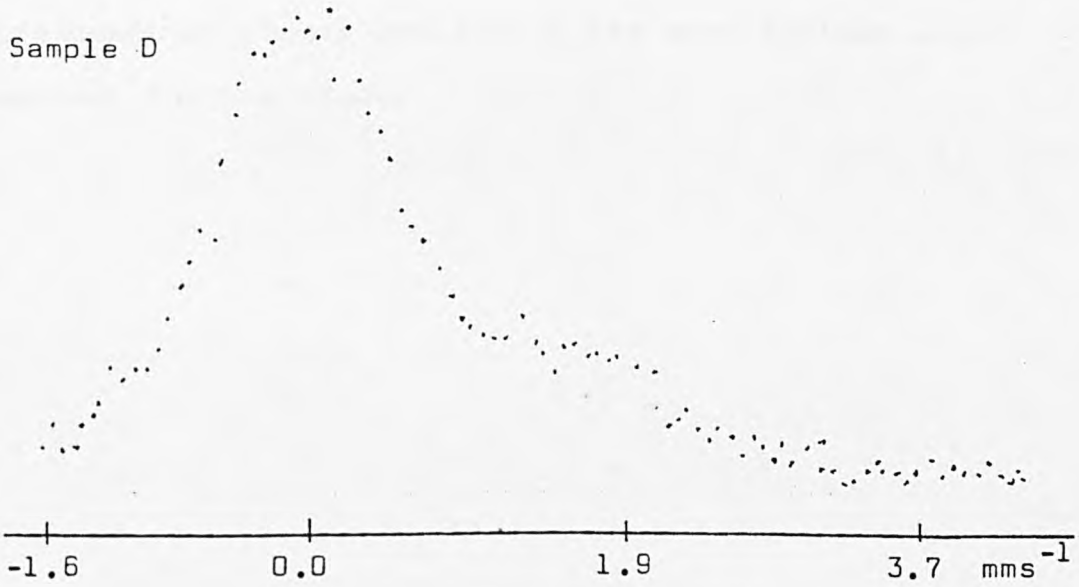

Figure 4.5(continued)

Sample D in water in an ultrasonic bath for one hour. The spectrum of Sample D provides evidence for the complete removal of the solder, leaving tin(IV) oxide as the only surface material present, which can readily be removed by washing.

4.1.5 Summary

It is clear from this variety of results that the technique of conversion electron Mössbauer spectroscopy can be used to detect the fate of tin moieties in surface reactions and, together with transmission Mössbauer spectroscopy, can be used to distinguish between bulk and surface properties of tin-containing compounds. The results presented here are simply the beginning of an extensive study of tin-containing surface reactions. Examinations of alloyed materials, laminated surfaces and fungicidal treatment of plants are just a few such systems which warrant further study.

4.2 ^{119}Sn Transmission Mössbauer Spectroscopy

4.2.1 Introduction

A survey of the literature on the known crystal structures of tin(II) compounds was carried out as part of this research and is contained in the microfiche at the end of this thesis. The survey confirmed that the tin atoms are nearly always in low symmetry environments. The most common tin(II) environment consists of a trigonal pyramidal arrangement of three nearest- neighbour tin-ligand bonds with three longer essentially non-bonding contacts completing a distorted octahedral coordination about the tin. The longer contacts arise because close approach of the ligands to the tin is prevented by the lone-pair orbitals. Tin(II) compounds in which this type of environment is found are listed together with details of bond distances and angles in Table 4.3. In Table 4.4 the data are given for those compounds which have tin in a distorted square pyramidal environment. The main structural feature found in all four coordinate tin environments is the existence of two bonds of considerably greater length than those normally found in tin(II) compounds.

The survey was discussed in three parts. In the first part crystal structure data were used to provide evidence for the extent of lone-pair distortion in tin(II) compounds. In the second part the results of ^{119}Sn Mössbauer spectroscopic studies on tin(II) compounds were described, and this was followed in the third part by a critical discussion of all the theories so far used to explain lone-pair effects and a theory was proposed to account for all aspects of lone pairs in tin(II) chemistry.

The theoretical background to the technique of Mössbauer

Bond Lengths, Next Nearest Bond Lengths and Bond Angles in Tin(II) Compounds of Structural Type SnX_3

Compound	Sn-X	Bond Lengths in Å				Next nearest Sn-X	Bond Angles In (°)
		1	2	3	next nearest		
$Ca[Sn(CH_3CO_2)_3]$	Sn-O	2.14	2.14	2.14	2.93	Sn-O	83.5 83.5 83.5
$K[Sn(HCO_2)_3]$	Sn-O	2.14	2.17	2.18	2.89	Sn-O	78.4 83.2 82.9
β-$SnWO_4$	Sn-O	2.21	2.21	2.21	2.81	Sn-O	
$K[Sn(CH_2ClCO_2)_3]$	Sn-O	2.14	2.18	2.18	2.92	Sn-O	78.6 83.3 88.0
$K_2[Sn_2(CH_2C_2O_4)_3]$-H_2O	Sn1-O	2.18	2.20	2.18	2.91	Sn-O	83.6 84.0 74.6
	Sn2-O	2.24	2.21	2.16	2.72	Sn-O	83.3 73.2 78.2
$SnSO_4$	Sn-O	2.25	2.27	2.27	2.95	Sn-O	79.0 77.1 77.1
$SnPO_3F$	Sn-O	2.15	2.15	2.15	3.13	Sn-O	all ≈ 90.0
$[Sn_2(OH)][PO_4]$	Sn1-O	2.08	2.15	2.18	3.01	Sn-O	Range
	Sn2-O	2.10	2.13	2.15	2.92	Sn-O	84.3 to 88.2
$[Sn_3O(OH)_2][SO_4]$	Sn1-O	2.06	2.14	2.18	2.95	Sn-O	86.5 88.9 93.5

Table 4.3

Bond Lengths, Next Nearest Bond Lengths and Bond Angles in Tin(II) Compounds of Structural Type SnX_3

Compound	Sn-X	Bond Lengths in Å					Bond Angles In(°)		
		1	2	3	next nearest	Next nearest Sn-X			
$Sr[Sn(CH_2ClCO_2)_3]_2$	Sn1-O	2.13	2.14	2.13	a.v. = 3.05	Sn-O	86.0	80.8	85.7
	Sn2-O	2.14	2.14	2.14		Sn-O	80.4	80.1	90.9
$Sn_3(PO_4)_2$	Sn1-O	2.12	2.12	2.12	2.96	Sn-O	Range		
	Sn2-O	2.08	2.09	2.12	3.05	Sn-O	69.6	to	94.2
	Sn3-O	2.15	2.23	2.32	2.86	Sn-O			
$K_2Sn_2O_3$	Sn1-O	1.96	1.96	1.96					
	Sn2-O	2.09	2.09	2.09					
$Sn_{10}W_{16}O_{46}$	Sn1-O	2.16	2.16	2.16			92.0	92.0	92.0
$SnHPO_4$	Sn-O	2.15	2.29	2.36	2.61	Sn-O	83.2	78.8	74.8
$SnHPO_3$	Sn-O	2.15	2.14	2.22	2.90	Sn-O	80.9	87.7	84.5
$[Sn_3(O)(OH)][PO_4]$	Sn1-O	2.12	2.14	2.15	2.67	Sn-O	Range		
	Sn2-O	2.06	2.16	2.26	2.74	Sn-O	72.8	to	91.2

Table 4.3 (continued)

Bond Lengths, Next Nearest Bond Lengths and Bond Angles in Tin(II) Compounds of Structural Type SnX_3

Compound	Sn-X	Bond Lengths in Å				Next nearest Sn-X	Bond Angles In (°)		
		1	2	3	next nearest				
Sn(edaa)	Sn-O	2.08	2.10	2.20					
	Sn-N	2.23	2.28	2.29					
$[MeB(NSiMe_3)_2Sn]_2$	Sn-N	2.25	2.23	2.10			82.3	66.9	94.6
$[Me_2Si(N^tBu_2)_2Sn]_2$	Sn-N	2.24	2.10	2.39			103.7	82.8	73.1
SnS	Sn-S	2.68	2.62	2.62	3.27	Sn-S	88.0	88.0	88.0
Sn_2S_3	Sn-S	2.74	2.64	2.64	3.15	Sn-S	83.5	90.2	83.5
$SnGeS_3$	Sn-S	2.63	2.94	2.86					
$BaSnS_2$	Sn-S	2.52	2.58	2.61	3.59	Sn-S	93.5	96.2	95.3
SnSe(orthorhombic)	Sn-Se	2.77	2.82	2.82	3.35	Sn-Se	89.0	89.0	96.0
Sn_2ClF_3	Sn1-F	2.18	2.19	2.20	3.51	Sn-F	80.0	78.5	78.7
	Sn2-F	2.11	2.10	2.11	3.38	Sn-F	81.4	80.9	81.9
NH_4SnF_3	Sn-F	2.08	2.08	2.08	2.87	Sn-F	82.4	82.4	82.4

Table 4.3 (continued)

Bond Lengths, Next Nearest Bond Lengths and Bond Angles in Tin(II) Compounds of Structural Type SnX_3

Compound	Sn-X	Bond Lengths in Å				Next nearest Sn-X	Bond Angles In (°)
		1	2	3	next nearest		
Sn_3BrF_5	Sn1-F	2.15	2.12	1.99	2.55	Sn-F	Range
	Sn2-F	2.21	2.15	2.21	2.80	Sn-F	75.0 to 88.4
	Sn3-F	2.21	2.11	2.16			
$NaSn_2F_5$	Sn-F	2.08	2.07	2.22	2.53	Sn-F	89.3 81.2 84.1
$Na_4Sn_3F_{10}$	Sn1-F	1.99	2.11	2.15	2.49		
SnF_2(monoclinic)	Sn1-F	2.07	2.10	2.15	2.67	Sn-F	78.6 83.9 87.3
	Sn2-F	2.03	2.20	2.27	2.40	Sn-F	88.8 76.6 83.2
Sn_3F_8	Sn-F	2.10	2.17	2.25	2.55	Sn-F	77.8 85.5 81.9
$SnCl_2$	Sn-Cl	2.78	2.78	2.67	3.06	Sn-Cl	80.0 80.0 105
$KCl.KSnCl_3.H_2O$	Sn-Cl	2.54	2.63	2.54			87.7 90.8 87.7
$CsSnCl_3$(monoclinic)	Sn-Cl	2.50	2.52	2.55	3.21	Sn-Cl	
$Sr(SnCl_3)_2.5H_2O$	Sn-Cl	2.58	2.61	2.63	3.22	Sn-Cl	87.1 86.2 93.9

Table 4.3 (continued)

Bond Lengths, Next Nearest Bond Lengths and Bond Angles in Tin(II) Compounds of Structural Type SnX_3

Compound	Sn-X	Bond Lengths in Å				Next nearest Sn-X	Bond Angles In (°)		
		1	2	3	next nearest				
$[(NH_4)_5CoS(O)_2C_6H_5]$-$[Cl_3SnOClO_3]$	Sn-Cl	2.49	2.52	2.57	2.91	Sn-O	89.1	92.3	91.9
$[Co^{II}(en)_3](SnCl_3)Cl$	Sn-Cl	2.49	2.49	2.48	>4.0	Sn-Cl	91.8	94.8	91.7
$[Co(dpe)_2Cl]SnCl_3$	Sn-Cl	2.44	2.44	2.45			94.8	93.9	94.6
$[Co(dpe)_2Cl]SnCl_3$.-n-C_6H_5Cl	Sn-Cl	2.44	2.43	2.43			91.4	96.2	93.5
$Co^{III}(NH_3)_6(SnCl_3)Cl_2$	Sn-Cl	2.53	2.47	2.67	3.00	Sn-Cl	90.8	87.5	89.9

Table 4.3 (continued)

Bond Lengths, Next Nearest Bond Lengths and Bond Angles of Tin(II) Compounds of Structural Type SnX_2Y

Compound	Sn-X	Sn-Y	Bond Lengths in Å			next nearest	Next Nearest Sn-X(Y)	Bond Angles in(°)		
			Sn-X	Sn-X	Sn-Y					
$(Sn_2O_2F_4)Sn_2$	Sn(1)-F	Sn(1)-O	2.14	2.14	2.04	2.80	Sn-F			
$Sn_3F_3PO_4$	Sn-F	Sn-O	2.08	2.26	2.12	2.54	Sn-O	88.5	84.1	81.8
$SnCl_2.2H_2O$	Sn-Cl	Sn-O	2.50	2.56	2.32	3.21	Sn-Cl	85.0	87.9	86.9
$Sn(NCS)_2$	Sn-N	Sn-S	2.20	2.27	2.84	3.11	Sn-S	73.5	85.6	84.0
$SnCl_2Me_3Si(N\text{-}Bu)_2Sn.SnO_2$	Sn-Cl	Sn-O			2.07					
	Sn-N	Sn-O	2.31	2.31	2.09					
$Sn_2Br_{0.65}Cl_{3.35}.3H_2O$	Sn(1)-O	Sn(1)-Cl/Br	2.32	2.34	2.62			76.6	79.6	84.0
	Sn(2)-Cl	Sn(2)-Cl/Br	2.64	2.58	2.71			81.2	82.5	97.4
$SnCl(H_2PO_2)$	Sn-O	Sn-Cl	2.16	2.16	2.57			85.8	85.8	86.7

Table 4.3 (continued)

Bond Lengths, Next Nearest Bond Lengths and Bond Angles in Tin(II) Compounds of Structural Type SnX_4

Compound	Sn-X	Bond Lengths in Å				Next nearest		Bond Angles (°)
		1	2	3	4	next nearest	Sn-X	
$Sn[O_4C_4H_2].H_2O$	Sn-O	2.17	2.19	2.44	2.31	2.82	Sn-O	77.6- 158.6
$[Sn_3O(OH)_2]SO_4$	Sn2-O	2.06	2.16	2.38	2.48	3.22	Sn-O	75.7- 139.9
	Sn3-O	2.09	2.15	2.40	2.47	3.34	Sn-O	73.4- 142.2
$[Sn_3O(OH)][PO_4]$	Sn3-O	2.07	2.17	2.28	2.46			
α-$SnWO_3$	Sn-O	2.18	2.18	2.39	2.39	2.83	Sn-O	
SnO	Sn-O	2.21	2.21	2.21	2.21			
$K_2Sn(C_2O_4)_2.H_2O$	Sn-O	2.14	2.20	2.36	2.30			
SnC_2O_4	Sn-O	2.23	2.23	2.39	2.39	2.87	Sn-O	
$Sn(HCO_2)_2$	Sn1-O	2.13	2.14	2.36	2.36			
	Sn2-O	2.20	2.20	2.36	2.37			
$Sn[H_2PO_4]_2$	Sn-O	2.21	2.21	2.47	2.47	2.92	Sn-O	
Bis(1-PhButane 1.3 dionato) tin	Sn-O	2.13	2.13	2.29	2.29			

Table 4.4

Bond Lengths, Next Nearest Bond Lengths and Bond Angles In Tin(II) Compounds of Structural Type SnX_4

Compound	Sn-X	Bond Lengths in Å				Next nearest		Bond Angles (°)
		1	2	3	4	next nearest	Sn-X	
Bis(1.4-diPhPropane 1.3 dionato) tin	Sn-O	2.17	2.15	2.35	2.26	2.98	Sn-O	81.2-150.0
$Na_2[Sn(C_2O_4)_2]$	Sn-O	2.25	2.25	2.36	2.36	2.91	Sn-O	
Bis(N.N.diEt.thio-carbamato) tin	Sn-S	2.57	2.59	2.76	2.82			65.9- 67.9
Tin(II)bis(O.Medi-thiocarbonate)	Sn-S	2.60	2.64	2.81	2.80	>3.4	Sn-S	
$Sn[S_2P(OC_6H_5)_2]_2$	Sn-S	2.62	2.83	3.02	3.39	3.65	Sn-S	
Tin(II)Phthalocyanine	Sn-N	2.25	2.24	2.25	2.27			
$KSnF_3 \cdot \frac{1}{2}H_2O$	Sn-F	2.04	2.01	2.27	2.27			
Sn_2F_3I	Sn-F	2.19	2.23	2.38	2.38	2.53	Sn-I	67.7-133.5
$Na_4Sn_3F_{10}$	Sn2-F	2.04	2.04	2.26	2.26			75.7-84.8

Table 4.4 (continued)

Bond Lengths, Next Nearest Bond Lengths and Bond Angles in Tin(II) Compounds of Structural Type SnX_4

Compound	Sn-X	Bond Lengths in Å				Next nearest	Next nearest Sn-X	Bond Angles (°)
		1	2	3	4			
$SnF_2.AsF_5$	Sn-F	2.09	2.09	2.59	2.59	2.85	Sn-F	74.2-136.0
$Sn_5Br_4F_6$	Sn1-Br	2.67	2.98	2.98	3.02			
	Sn2-F	2.29	2.34	2.40	2.40			
	Sn3-F	2.29	2.34	2.55	2.55			
	Sn4-F	2.01	2.03	2.33	2.33			
	Sn5-F	2.04	2.44	2.47	2.47			
Sn_4OF_6	Sn1-F	2.06	2.10	2.29	2.31			77.4-150.0

Table 4.4 (continued)

Bond Lengths, Next Nearest Bond Lengths and Bond Angles in Tin(II) Compounds of Structural Type SnX_3Y

Compound	Sn-X	Sn-Y	Bond Lengths in Å						Bond Angles In (°)
			Sn-X	Sn-X	Sn-X	Sn-Y	next nearest	Next nearest Sn-X(Y)	
Sn(NCS)F	Sn-F	Sn-N	2.22	2.40	2.40	2.24			67.4- 130.0
SnClF	Sn-F	Sn-Cl	2.18	2.39	2.39	2.52	3.28	Sn-Cl	
Sn_4OF_6	Sn2-F	Sn2-O	2.10	2.39	2.21	2.09			74.6- 156.5
	Sn3-F	Sn3-O	2.12	2.13	2.57	2.06			68.1- 103.1
	Sn4-F	Sn4-O	2.25	2.14	2.39	2.04			76.5- 153.4

Table 4.4 (continued)

Bond Lengths, Next Nearest Bond Lengths and Bond Angles : Tin(II) Compounds of Structural Type SnX_2Y_2

Compound	Sn-X	Sn-Y	Bond Lengths in Å					Next nearest Sn-X(Y)	Bond Angles In (°)
			Sn-X	Sn-X	Sn-Y	Sn-Y	next nearest		
$SnCl_2$.-									
1.4 dioxan	Sn-Cl	Sn-O	2.47	2.47	2.53	2.53	3.45	Sn-Cl	
$SnBr_2$.-									
1.4 dioxan	Sn-Br	Sn-O	2.64	2.64	2.55	2.55	3.51	Sn-Br	
$[Sn_2O_2F_4]Sn_2$	Sn-F	Sn-O	2.39	2.39	2.11	2.11			
$Sn(tu)_2SO_4$	Sn-O	Sn-S	2.41	2.24	2.62	2.86			76.2- 157.3
Sn(edaa)	Sn-O	Sn-N	2.09	2.20	2.26	2.28			

Table 4.4 (continued)

spectroscopy has already been discussed in Chapter 1. The value of the results obtained from ^{119}Sn Mössbauer studies in describing the bonding and structural properties of tin compounds has also been implied.

In discussion of individual compounds, it has often been suggested that there could be a relationship between crystal structure data and Mössbauer parameters. This has often consisted of comments on the relationship between non- spherical crystallographic environments and the Mössbauer splitting parameter. Less frequently comments have been made on possible connections between shift data and bond lengths. In this section of the thesis, a detailed comparison of shifts with bond length data is carried out for tin(II) compounds. A knowledge of any relationship between these data is particularly important because of the low symmetry environments found for lone pair distorted tin(II) compounds.

4.2.2 Relationship between Crystal Structures and Mössbauer data

The relationship between the Mössbauer parameters and X-ray crystal structures of tin(II) compounds can be discussed under two headings:- (1) the general relationship between the main features of the X-ray structure and Mössbauer parameters and (2) a specific relationship between Mössbauer chemical shifts and bond lengths. The 80K ^{119}Sn Mössbauer parameters for some tin(II) compounds that are of known crystal structure are listed in Table 4.5.

(1) The General Relationship Between the Main Features of the X-ray Structure and Mossbauer Parameters:

Mössbauer spectroscopy was, for example, used in studies of

^{119}Sn Mössbauer for Tin(II) Compounds with Tin in Trigonal Pyramidal Sites

Compound	≈80K.		Average of three nearest Sn-Ligand Bonds	
	δmms^{-1}	Δmms^{-1}		
Sn_2ClF_3	3.35	1.29	Sn1-F	2.19
			Sn2-F	2.11
Sn_3BrF_5	3.69	1.18	Sn1-F	2.08
			Sn2-F	2.19
			Sn3-F	2.16
NH_4SnF_3	3.25	1.88	Sn-F	2.08
$NaSn_2F_5$	3.32	1.86	Sn-F	2.12
SnF_2(monoclinic)	3.62	1.77	Sn1-F	2.10
			Sn2-F	2.16
Sn_3F_8	3.82	1.34	Sn-F	2.15
$SnCl_2$	4.12	c.a.0	Sn-Cl	2.74
$KCl.KSnCl_3.H_2O$	3.70	0.70	Sn-Cl	2.57
$CsSnCl_3$(monoclinic)	3.64	0.90	Sn-Cl	2.52

Table 4.5

^{119}Sn Mössbauer for Tin(II) Compounds with Tin in Trigonal Pyramidal Sites

Compound	≈80K.		Average of three nearest Sn-Ligand Bonds	
	δmms^{-1}	Δmms^{-1}		
$[(NH_3)_5CoS(O)_2-C_6H_5][Cl_3SnOClO_3]-H_2O$	3.52	1.14	Sn-Cl	2.53
$[Co(dpe)_2Cl]SnCl_3$	3.10		Sn-Cl	2.44
$[Co(dpe)_2Cl]SnCl_3$-n-C_6H_5Cl	3.08		Sn-Cl	2.43
$SnCl_2.2H_2O$	3.63	1.21	Sn-Cl	2.32
			Sn-O	2.53
$KSn[HCO_2]_3$	3.08	1.95	Sn-O	2.16
$KSn(CH_2ClCO_2)_3$	2.96		Sn-O	2.16
$SnSO_4$	3.95	1.00	Sn-O	2.26
$Sn_3(PO_4)_2$	3.07	1.90	Sn1-O	2.12
			Sn2-O	2.09

Table 4.5 (continued)

^{119}Sn Mössbauer for Tin(II) Compounds with Tin in Trigonal Pyramidal Sites

Compound	≃ 80K.		Average of three nearest Sn-Ligand bonds	
	δmms^{-1}	Δmms^{-1}		
$SnHPO_4$	3.25	1.74	Sn-O	2.26
$SnHPO_3$	3.15	1.60	Sn-O	2.17
SnS	3.29	0.93	Sn-S	2.64
$Sn[S_2P(OC_6H_5)_2]_2$	3.78	1.06	Sn-S	2.82
$Sn(NCS)_2$	3.47	0	Sn-S	2.84
			Sn-N	2.23
SnSe(orthorhombic)	3.34	0.83	Sn-Se	2.80
Sn_2S_3	3.49	0.90	Sn-S	2.67

Table 4.5 (continued)

^{119}Sn Mössbauer Data for Tin(II) Compounds with Tin in Square Pyramidal Sites

Compound	≃ 80K.		Average of four nearest Sn-Ligand bonds	
	δmms^{-1}	Δmms^{-1}		(Å)
$KSnF_3.\frac{1}{2}H_2O$	3.07	1.92	Sn-F	2.15
Sn_2F_3I	3.57	1.34	Sn-F	2.26
SnClF	3.73	1.10	Sn-F	2.32
			Sn-Cl	2.52
$SnCl_2.$(1.4 dioxan)	3.71	1.61	Sn-Cl	2.47
			Sn-O	2.53
$SnBr_2.$(1.4 dioxan)	3.71	1.60	Sn-Br	2.64
			Sn-O	2.55
SnC_2O_4	3.75	1.52	Sn-O	2.31
$Sn(tu)_2SO_4$	3.25		Sn-O	2.32
			Sn-S	2.74
$Sn(HCO_2)_2$	3.33	1.70	Sn-O	2.23
$K_2Sn(C_2O_4)_2.H_2O$	3.19		Sn-O	2.25

Table 4.5 continued

tenary tin(II) halides, to show the necessity of carrying out complete X-ray crystal structure determinations. The Mössbauer spectra (Table 4.5) for the ternary halides $SnXX'$, Sn_2XX_3' and Sn_3XX_5' show no evidence for the presence of SnX and SnX' sites, and although it is possible to devise an $SnCl_2$-type structure, with only one tin site, for $SnXX'$ and Sn_2XX_3' the same cannot be done for Sn_3XX_5'. The crystal structure determination of Sn_3BrF_5 was carried out [63] to explain these observations in the Mössbauer spectrum. Its structure is consistent with the Mössbauer data in that it is built up from a polymeric Sn-F anionic network with Br^- ions, not bonded to the tin, occupying spaces in the lattice to balance the charge. The tin sites in the ternary structure are not identical crystallographically but are sufficiently alike to give similar Mössbauer resonance which appear as a quadrupole-split doublet. The crystal structure of Sn_2ClF_3 was also determined[63] and again shown to consist of $(Sn_2F_3)_n^{n+}$ Cl_n^{n-} with no Sn-Cl bonds, in agreement with the Mössbauer data.

The Mössbauer isomer shift for $Sn[CH(SiMe_3)_2]_2$(δ=2.11mms^{-1} Δ=-2.31mms^{-1}) lies just above the value for α-tin, the borderline between Sn(II) and Sn(IV). The crystal structure and Mössbauer data for this compound distinguish it from formally similar compounds, $Sn(Cp)_2$,(δ=3.69mms^{-1},Δ=-0.86mms^{-1}) and $Sn(Bu_2^n)n$, (δ=1.45mms^{-1},Δc.a0). The Cp compound has no Sn-Sn bonding and its isomer shift value which is only just below that for $SnCl_2$,(4.12mms^{-1}) is characteristic for tin(II) compounds with a non-bonding electron pair on each tin atom. The compound $Sn(Bu_2^n)n$ is polymeric with strong Sn-Sn interactions, therefore the formally non-bonding pairs on the tin

atoms in the structure are used in polymerization. The zero quadrupole splitting is indicative of a compound containing both Sn-C and Sn-Sn bonds. The Mössbauer parameters for $Sn[CH(SiMe_3)_2]_2$ lie between those for $Sn(Cp)_2$ where there is no Sn-Sn interaction and $Sn(Bu^n_2)_n$ where the Sn-Sn interaction is weak. Although the shift for $Sn[CH(SiMe_3)_2]_2$ is on the borderline between tin(II) and tin(IV) the value of the quadrupole splitting is not consistent with the formation of Sn-Sn interactions to give a Sn(IV) polymer. The quadrupole splitting value is $-2.31 mms^{-1}$. The negative sign means that there is a deficiency of electrons in the direction of the major component of the field gradient. This in turn means that the z direction of the field is in the direction of an empty or nearly empty p-type orbital and not in the direction of a lone-pair. These observations would be consistent with a tin(II) formulation for the compound (A) but in the Cr compound which has an empty p-orbital of the type (B)

A

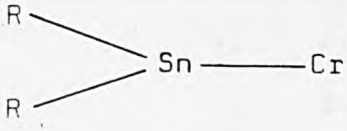

B

the quadrupole splitting is $-4.43 mms^{-1}$. The reduction in the value of the quadrupole splitting from $4.43 mms^{-1}$ to $2.31 mms^{-1}$ can only arise because of weak Sn-Sn interactions between neighbouring R_2Sn moieties. This overlap between the lone pair on each tin atom and the empty p-orbital of the neighbouring tin atom would give the dimeric structure $(R_2Sn)_2$[64]. On each tin atom there is a direction in which any electron density on the tin must arise from the weak interaction with the lone pair

on the neighbouring tin atom and this produces the field gradient.

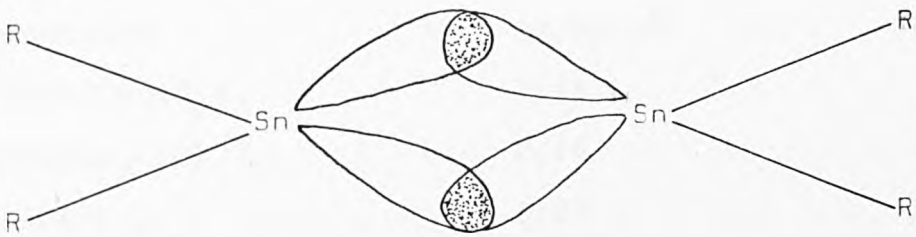

The crystal structure of $[CH(SiMe_3)_2]_2Sn$ shows that the material consists of R_2Sn dimers with weak Sn-Sn interactions of 2.76Å.

(2) A Specific Relationship Between Mössbauer Chemical Shifts and Bond Lengths: For those tin(II) compounds with the tin in trigonal pyramidal SnL_3 sites with Sn-L bonds to the same ligand L there is a close connection between the Mössbauer chemical isomer shift and the Sn-L bond distances.

For tin-fluorine compounds with single SnF_3 sites there is an increase in shift with increasing average bond length, that is, with increasing electrostatic character.

Compound	Average b.l(Å)	$\delta(mms^{-1})$
NH_4SnF_3	2.08	3.25
$NaSn_2F_5$	2.12	3.32
Sn_3F_8	2.17	3.82

The shifts for tin-fluorine compounds with more than one tin site are not included in the comparison because they must have shift values that are the averages of the shifts for the individual sites. For SnF_2, for example, the shift of $3.65mms^{-1}$ must arise because of overlap of a resonance line of lower shift arising from the site with three short bonds viz. 2.03Å, 2.20Å and 2.20Å.

The relationship between shifts and average bond

distances also holds for tin-oxygen containing species with single SnO_3 sites.

Compound	Average b.l.Å	δmms^{-1}
$CaSn(CH_3CO_2)_3$	2.14	2.90
$KSn(CH_2ClCO_2)_3$	2.16	2.96
$KSn(HCO_2)_3$	2.16	3.08
$SnHPO_3$	2.17	3.15
$SnSO_4$	2.26	3.95

The data for $SnHPO_4$ (δ = 3.25mms^{-1}, average bond length = 2.26Å) are interesting and confirm that the fourth nearest neighbour bond in this compound, of 2.61Å, is short enough to make it intermediate between trigonal and four pyramidal coordination.

Crystals of $Sn_6O_4(OMe)_4$ have been shown[65] to consist of two crystallographically non-interacting $Sn_6O_4(OMe)_4$ units with a central adamantane-like Sn_6O_4 core. The chemical shift value of 2.78mms^{-1} is consistent with tin being in the tin(II) oxidation state. The Sn-O bonds within the Sn_6O_4 skeleton are very short (2.05-2.08Å) which probably explains why the shift is so low.

Of those known sulphides it is still clear that with an increase in Sn-S bond length there is a corresponding increase in the chemical shift values.

Compound	Average b.l. (Å)	δmms^{-1}
SnS	2.64	3.29
Sn_2S_3	2.67	3.49

The sulphur-containing tin(II) compound $Sn[S_2P(OC_6H_5)_2]_2$, has a chemical shift value (δ = 3.78mms^{-1}) which is considerably larger than that of its parent compound SnS[66]. This large

increase in s-electron density on the tin, is reflected in the longer Sn-S bond length, and is possibly due to the π-C_6H_5 interaction with the tin which is characteristic of this compound.

Those compounds only containing Sn-Cl bonds as nearest and next nearest neighbours and with pyramidal $SnCl_3$ groups include:

Compound	Average b.l.Å	δmms^{-1}
$Co(dpe)_2ClSnCl_3.nC_6H_5Cl$	2.43	3.08
$Co(dpe)_2ClSnCl_3$	2.44	3.10
$CsSnCl_3$(monoclinic)	2.52	3.64
$KCl.KSnCl_3.H_2O$	2.57	3.70
$SnCl_2$	2.74	4.12

These compounds clearly follow the trend showing the close relationship between the average bond length and the chemical isomer shifts. The similarity in the data between $CsSnCl_3$ and $[(NH_4)_5CoS(O_2)C_6H_5]$ $[Cl_3SnOClO_3]H_2O$[67] (δ = 3.52mms^{-1}, average bond length = 2.52Å) show that the next nearest bond in the perchlorate complex, the Sn-O bond of 2.91Å is producing at the most a very weak perturbation of the tin electron density.

A knowledge of the existence of the relationship between chemical shift and bond length for the trigonal pyramidal tin sites provides a starting point for discussion of other data.

The dihydrate $SnCl_2.2H_2O$ has a chemical shift value of 3.63mms^{-1}, less than that for $SnCl_2$ (4.12mms^{-1}) as would be expected for complex formation, and similar to those for some trichlorostannates(II).

The combination of two Sn-Cl bonds of 2.50Å and 2.56Å with one Sn-O bond of 2.32Å appears to produce a similar total bonding effect to that for the three Sn-Cl bonds in KCl. $KSnCl_3.H_2O$ and $CsSnCl_3$. This can be rationalised in terms of sp usage.

Fewer tin(II) compounds with tin in a square pyramidal environment are of known structure. Of those known there is a small number whose Mössbauer data have been recorded. These compounds include tin(II) oxalate and its complex derivative $K_2Sn(C_2O_4)_2.H_2O$ which provide a good example of a change (i.e. a decrease) in chemical shift on complex formation. The difference in chemical shift value for $Sn(tu)_2SO_4$ is clearly due to reduction in the s-electron density on the tin as a result of complexation.

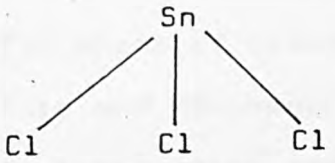

$KCl.KSnCl_3.H_2O(3.70mms^{-1})$

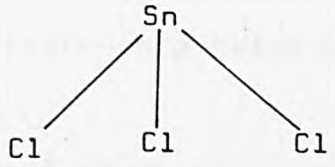

$CsSnCl_3$(monoclinic)$(3.64mms^{-1})$

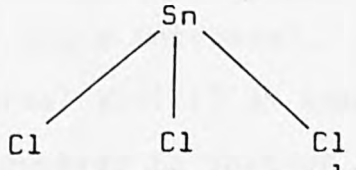

$SnCl_2.2H_2O(3.63mms^{-1})$

Comparisons made in this section have been of room temperature crystallographic data and 80K Mössbauer data. To check the validity of the results arising from such comparisons a series of room temperature Mössbauer measurements have

been carried out and the data in the following table show negligible difference in the room temperature and 80K Mössbauer parameters.

Compound	RT Mössbauer δ (mms^{-1})	80K Mössbauer δ (mms^{-1})
α-$SnHPO_4$	3.33	3.25
$KSn(CH_2ClCO_2)_3$	3.03	2.96
$SnSO_4$	3.92	3.95
SnS	3.23	3.29
Sn_2S_3	3.38	3.49

4.2.3 Relationship between Crystal Structure and Mössbauer Parameters for Compounds of the type SnX_2L_2 where L is a neutral donor ligand

Anomalies in ^{119}Sn Mössbauer parameters can be used to identify unusual aspects of tin(II) bonding and to provide fruitful areas of research on the relationship between crystal structure and Mössbauer parameters.

An interesting series of compounds whose structure and bonding may be discussed on the basis of their Mössbauer data (Table 4.6) is the following: $SnSO_4$.2tu, Sn(acetate)$_2$. 2tu and Sn_2Br_4.5tu.$2H_2O$. (tu = thiourea). The crystal structure of sulphatobis(thiourea) tin(II) is known[68]. Its reduced isomer shift value compared to that of tin(II) sulphate must be associated with the formation of one short Sn-S bond (2.62Å) and it is therefore tempting to interpret complex formation in all thiourea complexes of tin(II) compounds in the same way. However, provided the compounds Sn(acetate)$_2$.2tu and Sn_2Br_4.5tu.$2H_2O$ have similar structures to $SnSO_4$.2tu only the Mössbauer data for the bromide can be interpreted in the

^{119}Sn Mössbauer Data for some Thiourea Complexes of Tin(II) Compounds

Compound	*δmms^{-1}	Δmmm^{-1}
$SnSO_4$	3.95	1.00
$SnSO_4.2tu$	3.25	0
$Sn(CH_3CO_2)_2$	3.26	1.77
$Sn(CH_3CO_2)_2.2tu$	3.35	0
$SnBr_2$	3.98	0
$Sn_2Br_4.5tu.2H_2O$	3.67	0

tu = thiourea,

*80K Mössbauer data relative to $BaSnO_3$

Table 4.6

same way, as there is a reduction in its shift value on complex formation compared to the parent tin(II) bromide. As a result the crystal structure determinations of both $Sn(acetate)_2.2tu$ and $Sn_2Br_4.5tu.2H_2O$ have been carried out in this work.

Crystal Structure Determinations of the Two Thiourea Complexes

The complexes were prepared[69] by adding the appropriate molar quantity of thiourea to a solution of the tin(II) compound in the parent acid. The crystal data were obtained from Weissenberg and single crystal precession data, and refined on the basis of the powder diffraction patterns. Single crystal intensity data were collected at the University of Padua. Details of the cell data for $Sn(acetate)_2.2tu$ and $Sn_2Br_4.5tu.2H_2O$ are given in Tables 4.7 and 4.8 respectively.

On the basis of its systematic absences, the crystal of $Sn(acetate)_2.2tu$ was assigned to the monoclinic space group Pc which has a 2-fold general position (No. 7 in the International Tables of X-ray crystallography[70]). In the same way the crystal of $Sn_2Br_4.5tu.2H_2O$ was assigned to the orthorhombic space group Pnma which has an eight-fold set of general positions and three sets of four-fold special positions (No. 62 in the International Tables of X-ray crystallography[70]).

Location of Atomic Positions

The X-ray crystallographic programs used throughout the crystal structure determinations are described in Chapter 1. The atomic positions were located as a result of a heavy atom

$Sn(acetate)_2 . 2tu$

Cell data: $\underline{a}$ = 11.93Å, $\underline{b}$ = 10.94Å, $\underline{c}$ = 21.92Å.

$\alpha = 90^o$, $\beta = 96.5^o$, $\gamma = 90^o$.

V = 2841.7 cm^3. F(000) = 1536. M = 388.7g

Monoclinic Space Group Pc

2 - fold general position

X, Y, Z: X, $\bar{Y}$, 1/2+Z.

Patterson Map

	Height	X/A	Y/B	Z/C
1	999	0.0000	0.0000	0.0000
2	469	0.4934	0.0000	0.2482
3	454	0.0000	0.5832	0.5000
4	267	0.7586	0.0000	-0.0000
5	230	0.0063	0.0715	0.2385
6	226	0.2720	0.0000	0.2183
7	202	0.2686	0.8805	0.4886
8	168	0.2399	0.5000	0.2417
9	168	0.7681	0.1014	0.2577
10	144	0.2395	0.1068	0.2778
11	134	0.8171	0.0000	0.4711
12	131	0.6472	0.5000	0.5035
13	116	0.4875	0.2400	0.4117

Table 4.7

$Sn_2Br_4.5tu.2H_2O$

Cell data : $\underline{a} = 27.63\text{Å}$, $\underline{b} = 16.13\text{Å}$ $\underline{c} = 6.11\text{Å}$

$\alpha = 90^o$ $\beta = 90^o$ $\gamma = 90^o$

$V = 2724.4cm^3$ $F(000) = 1456$ $M = 973_g$

Orthorhombic Space Group Pnma (centrosymmetric)

8-fold general position

$X, Y, Z; \frac{1}{2} + X, \frac{1}{2} - Y, \frac{1}{2} - Z; \bar{X}, \frac{1}{2} + Y, \bar{Z}; \frac{1}{2} - X, \bar{Y}, \frac{1}{2} + Z;$

$\bar{X}, \bar{Y}, \bar{Z}; \frac{1}{2} - X, \frac{1}{2} + Y, \frac{1}{2} + Z; X, \frac{1}{2} - Y, Z; \frac{1}{2} + X, Y, \frac{1}{2} - Z;$

4-fold special position

$X, \frac{1}{4}, Z; \bar{X}, \frac{3}{4}, \bar{Z}; \frac{1}{2} - X, \frac{3}{4}, \frac{1}{2} + Z; \frac{1}{2} + X, \frac{1}{4}, \frac{1}{2} - Z;$

4-fold special position

$0, 0, \frac{1}{2}; \quad 0, \frac{1}{2}, \frac{1}{2}; \quad \frac{1}{2}, 0, 0; \quad \frac{1}{2}, \frac{1}{2}, 0;$

4-fold special position

$0, 0, 0; \quad 0, \frac{1}{2}, 0; \quad \frac{1}{2}, 0, \frac{1}{2}; \quad \frac{1}{2}, \frac{1}{2}, \frac{1}{2};$

The 8-fold general positions generate the following set of equivalent positions:

$2X ; 2Y; 2Z;$

$\frac{1}{2}, 2Y-\frac{1}{2}, 2Z -\frac{1}{2};$

$2X-\frac{1}{2}; \frac{1}{2}; \frac{1}{2};$

$2X ; \frac{1}{2}; 2Z$

$0 ; 2Y-\frac{1}{2};0$

$2X-\frac{1}{2}; 2Y; \frac{1}{2}$

$\frac{1}{2} ; 0; 2Z-\frac{1}{2}$

Table 4.8

$Sn_2Br_4.5tu.2H_2O$

Patterson Map

	Height	X/A	Y/B	Z/C	S.O.F.
1.	999	0.0000	0.0000	0.0000	0.1250
2.	361	0.0000	0.5000	0.5000	0.1250
3.	331	0.6406	0.0000	0.1954	0.5000
4.	270	0.0000	0.0000	0.4341	0.2500
5.	240	0.5000	0.0000	0.5000	0.1250
6.	212	0.5000	0.0000	0.0509	0.2500
7.	206	0.5000	0.5000	0.0000	0.1250
8.	200	0.0000	0.5000	0.0644	0.2500
9.	195	0.3612	0.5000	0.3073	0.5000
10.	191	0.3551	0.5000	0.5000	0.2500
11.	188	0.1558	0.5000	0.4446	0.5000
12.	184	0.9182	0.1260	0.0000	0.5000
13.	150	0.1607	0.0000	0.0991	0.5000
14.	149	0.8763	0.5000	0.1864	0.5000
15.	134	0.1453	0.0000	0.3250	0.5000
16.	133	0.0000	0.2454	0.0000	0.2500
17.	128	0.3598	0.5000	0.1116	0.5000
18.	127	0.5000	0.5000	0.3999	0.2500
19.	123	0.0793	0.3767	0.4123	1.0000
20.	122	0.0751	0.1237	0.5000	0.5000
21.	113	0.2705	0.1214	0.1180	1.0000
22.	111	0.2749	0.5000	0.0813	0.5000
23.	104	0.4344	0.3753	0.5000	0.5000
24.	99	0.0000	0.5000	0.3015	0.2500
25.	98	0.9187	0.3791	0.0000	0.5000

Table 4.8(continued)

Patterson synthesis and refinement by the Fourier synthesis using four cycles of full matrix least squares, by the method described previously in Sections 2.4.2 and 3.1.1 of this thesis. On location of all the atomic positions for the two structures, a final residual of 0.0601 and 0.0768 for $Sn(acetate)_2$. 2tu and Sn_2Br_4.5tu.$2H_2O$ respectively was obtained. Details of the final atomic positions are given in Table 4.9.

Tin Environments in $Sn(acetate)_2$. 2tu and Sn_2Br_4. 5tu.$2H_2O$

Although full structure determinations of $Sn(acetate)_2$. 2tu and Sn_2Br_4.5tu.$2H_2O$, have been carried out as part of this work, only brief descriptions of the tin environments in the two structures, sufficient to interpret the Mössbauer data, are given here. Full details of bond distances and angles and structure factors are in the microfiche at the end of this thesis.

In $Sn(acetate)_2$.2tu the tin atom lies in a square pyramidal environment bonded to the two sulphur atoms of the thiourea moieties and to two unidentate acetate groups via the oxygen atoms. The two bonds to the carboxylate oxygens are slightly longer than average at 2.18Å compared to 2.14Å, whilst the Sn-S bonds of 2.85Å are long compared to the average Sn-S bond of 2.67Å. Two longer tin-oxygen bonds (2.80, 3.09Å) to oxygen atoms from surrounding acetate groups, complete a distorted octahedral environment about the tin atom (Figure 4.6).

Final Atomic Positions for $Sn(acetate)_2.2tu$

Sn	0.2491	0.2084	0.1227
S1	0.4869	0.1760	0.1573
S2	0.0137	0.1635	0.1150
O1	0.2395	0.0410	0.0676
O2	0.3475	0.1269	0.0044
O3	0.2608	0.0618	0.1907
O4	0.2184	0.2190	0.2473
N1	0.5002	0.3183	0.0588
N2	0.6375	0.3433	0.1379
N3	0.0130	0.4030	0.0924
N4	0.0855	0.3444	0.1708
C1	0.2895	0.0408	0.0180
C2	0.2744	0.9277	0.9798
C3	0.5462	0.2860	0.1149
C4	0.2385	0.1069	0.2422
C5	0.9785	0.3121	0.1265
C6	0.2313	0.0180	0.2936

The hydrogen atoms have also been located. Their atomic positions are not included in this table but are given in the microfiche at the end of this thesis.

Table 4.9

Final Atomic Positions

for $Sn_2Br_4.5tu.2H_2O$

Sn1	0.1013	0.2500	0.6144
Sn2	0.2473	0.2500	0.7101
Br1	0.2587	0.2500	0.2750
Br2	0.1221	0.2500	0.0375
Br3	0.3285	0.1290	0.7581
S1	0.0367	0.1311	0.7067
S2	0.1830	0.1100	0.5767
S3	0.4723	0.2500	0.3787
N1	0.0510	0.0862	0.2893
N2	0.0684	0.9906	0.5531
N3	0.1964	0.9616	0.7583
N4	0.1905	0.0678	0.0085
N5	0.3784	0.2500	0.2539
N6	0.4307	0.2500	0.9742
C1	0.0512	0.0666	0.4996
C2	0.1951	0.0450	0.7917
C3	0.4219	0.2500	0.2048
OH	0.9274	0.4399	0.9787

Table 4.9 (continued)

Structure of $Sn(acetate)_2.2tu$

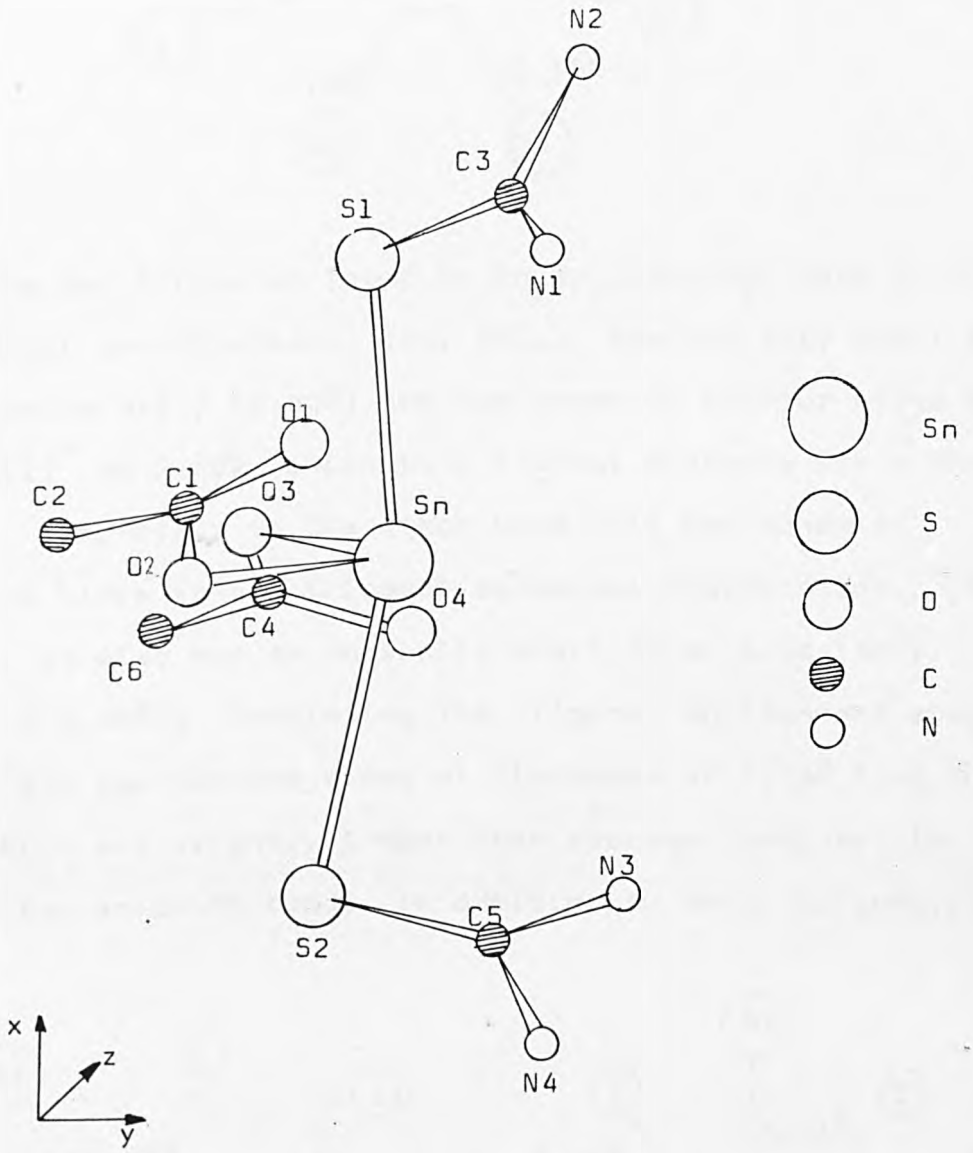

Figure 4.6

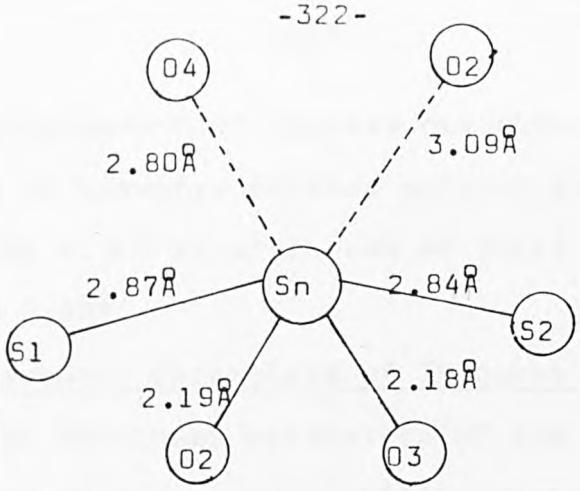

The two tin sites found in $Sn_2Br_4.5tu.2H_2O$ have trigonal pyramidal coordination. Tin, Sn(1), has one very short bond to bromine Br(2) (2.65Å) and two bonds to sulphur atoms S(1) and S(1)′ at 2.68Å, which is a typical distance for a Sn-S bond. Tin, Sn(2), on the other hand only has bonds to bromine atoms in its trigonal pyramidal coordination. Like Sn(1), it also has an unusually short Sn-Br bond (Sn(2) - Br(1) : 2.68Å). Completing the trigonal environment about Sn(2) are two bromine atoms at distances of 2.98Å from the tin, which are slightly longer than average, compared to 2.83Å for an Sn-Br bond. In addition to their trigonal

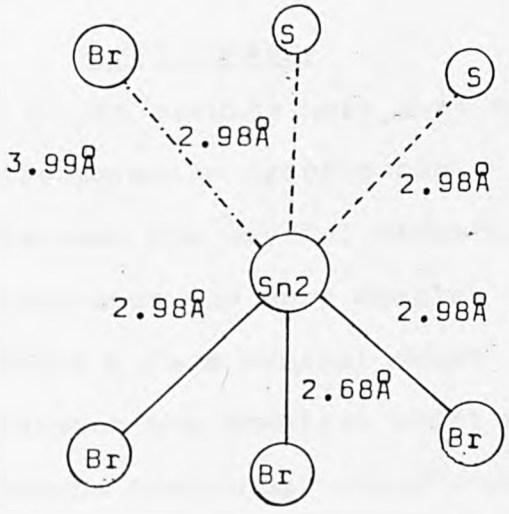

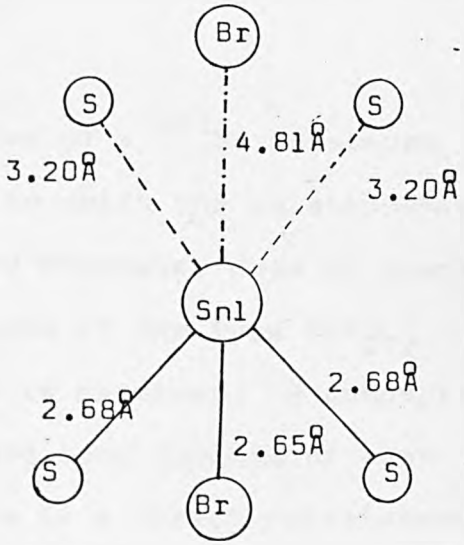

pyramidal arrangement of nearest neighbours the tin atoms are bridged by symmetry related sulphur atoms S(2) and S(2)′ (Figure 4.7) at distances of Sn(1) - S = 3.20Å and Sn(2) - S = 2.98Å.

Mössbauer parameters of Thiourea Complexes

The ^{119}Sn Mössbauer parameters of the thioureatin(II) complexes and of the parent tin(II) compounds are in Table 4.6. The reduced isomer shift for $SnSO_4.2tu$ compared to that of tin(II) sulphate is interpreted as being associated with the formation of one short Sn-S bond (2.62Å). The slight increase in chemical shift for the acetate complex from that of its parent compound, is consistent with the fact that there is no shortening of the Sn-O bonds to the acetate moiety, or formation of short Sn-S bonds to the thiourea ligands, on complex formation. The singlet resonance line ($3.67 mms^{-1}$) observed for the $Sn_2Br_4.5tu.2H_2O$ complex is surprising since there are two tin sites with apparently different environments. However, the lowering in shift from that of tin(II) bromide must be due to the shortening of Sn-Br bonds.

4.2.4 Summary

The results have been presented of a ^{119}Sn Mössbauer transmission spectroscopic study in which the relationship between the crystal structures and Mössbauer data of simple compounds and more complex compounds of the type SnX_2L_2 where L is a neutral donor ligand is examined. A comparison between the chemical shift data and bond lengths of some simple compounds, shows that there is a direct relationship in that with increasing bond lengths there is an increase

Structure of $Sn_2Br_4.5tu.2H_2O$

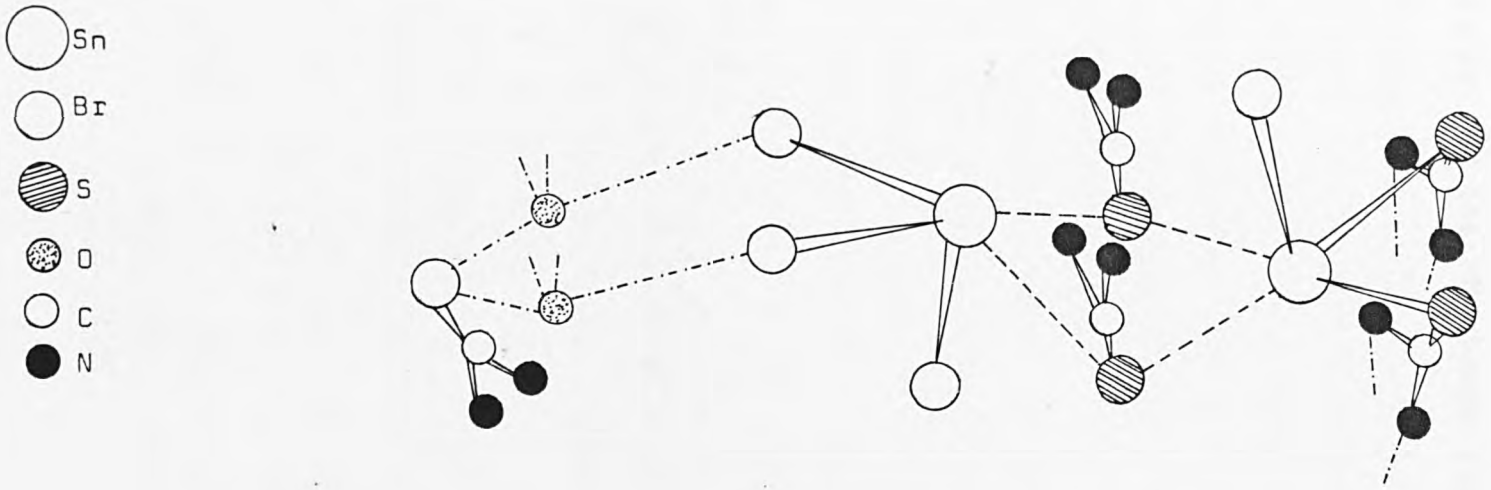

— — — — Sn-Ligand contacts

═══ Bonds

—·—·—·— Contact distances not involving bonds to tin

Figure 4.7

in the s-electron density on the tin atom, recorded as an increase in the shift value. Such a direct relationship does not appear to hold for more complex tin(II) compounds of the type $SnX_2.2L$ because, although there is compatibility between the X-ray and the Mössbauer data, the relationship is not simple.

References

1. M.J.Tricker, "Surface and Defect Properties of Solids", A Chemical Society Specialist Periodical Report, London. U.K., 1977, 6, 106.

2. F.J.Berry, Trans Met.Chem., 1979, 4, 209.

3. B.Mahieu, Rev. Quest. Sci., 1979, 150, 187.

4. J.D.Donaldson, S.J.Clark and S.M.Grimes, "Mössbauer Spectroscopy", A Chemical Society Annual Report in press.

5. J.D.Donaldson, S.J.Clark and S.M.Grimes, "Mössbauer Spectroscopy", A Chemical Society Specialist Periodical Report in press.

6. "Mössbauer Spectroscopy and Its Chemical Applications", Advances in Chem. Series, (194).

7. N.N.Greenwood and T.C.Gibb, "Mössbauer Spectroscopy". Chapman and Hall, 1971.

8. K.R.Swanson and J.J.Spijkerman, J.Appl. Phys., 1970, 41, 3155

9. M.J.Tricker, A.G.Freeman, A.P.Winterbottom and J.M.Thomas, Nucl. Instr. Methods, 1976, 135, 117.

10. M.J.Tricker, J.M.Thomas and A.P.Winterbottom, "Surface Science", 1974, 45, 601.

11. L.J.Swartzendruber and L.H.Bennett, Scripta Met., 1972, 6, 737.

12. J.Stanek, J.A.Sawicki and B.D.Sawicka, Nucl. Instr. Methods, 1975, 130, 613.

13. B.D.Sawicka, J.A.Sawicki and J.Stanek, J.Physics Letters, 1976, 59A, 59.

14. J.A.Sawicki, B.D.Sawicka, J.Stanek and J.Kowalski, Phys.Status Solidi(B), 1976, 77, K1.

15. J.A.Sawicki, B.D.Sawicka, A.Lazarski, E.Maydell and E.M.Ondrusz, Phys.Status Solidi(B), 1973, 57, K143.

16. J.A.Sawicki, B.D.Sawicka, A.Lazarski and E.M.Ondrusz, Phys.Status Solidi(B), 1973, 18, 85.

17. B.D.Sawicka, M.Orwiega and J.A.Sawicki, Hyperfine Interactions, 1978, 5, 147.

18. M.J.Tricker, R.K.Thorpe, J.H.Freeman and G.A.Gard, Phys.Status Solidi(A), 1976, 33, K97.

19. H.Onodera, H.Yamamoto, H.Watanabi and H.Ebiko, Japan J.Appl.Phys., 1972, 11, 1380.

20. G.W.Simmons, E.Kellerman and H.Leidheiser, Corrosion, 1973, 29, 227.

21. J.M.Thomas, M.J.Tricker and A.P.Winterbottom, J.C.S.Faraday II, 1975, 71, 1708.

22. A.Sette-Camara and W.Keune, Corrosion Science, 1975, 15, 441.

23. D.W.Forester,Proc.4th Lunar Sci.Conf.Suppl.4. Geochem.Cosmochim. Acta, 1973, 3, 2697.

24. M.Petreva, U.Gonser, U.Hasmann, W.Keune and J.Lauer, J.Phys.Colloq. 1976, C6, 295.

25. M.J.Tricker, L.A.Ash and T.E.Cranshaw, Nucl.Instr.Methods, 1977, 143, 307.

26. D.Liljequist, T.Ehdahl and U.Bäverstam, Nucl.Instr. Methods, 1978, 155, 529.

27. P.J.McCarthy and F.A.Deeney, Nucl.Instr.Methods, 1979, 159, 381.

28. M.J.Tricker, L.A.Ash and W.Jones, Surface Science, 1979, 79, L333.

29. Z.W.Bonchev, A.Jordanov and A.Minkova, Nucl. Instr. Methods, 1969, 70, 36.

30. C.H.Yagnik, R.A.Mazak and R.L.Collins, Nucl. Instr. Methods, 1974, 114, 1.

31. Ts.Bonchev, A.Minkova and M.Grozdanov, Nucl. Instr. Methods, 1977, 147, 481.

32. M.Grozdanov, Ts.Bonchev and A.Likov, Nucl. Instr. Methods, 1979, 165, 231.

33. Ts.Bonchev, M.Grozdanov and L.Shev, Nucl.Instr. Methods, 1979, 165, 237.

34. K.Endo, K.Shilbuya and H.Sano, Radiochem. Radioanal. Letts. 1977, 28, 363.

35. K.Shilbuya, K.Endo and H.Sano, Bull.Chem.Soc. Japan, 1978, 51, 1363.

36. G.P.Huffman and G.R.Dunmyre, J.Electrochem.Soc. 1978, 125, 1652.

37. C.L.Lau and G.K.Wertheim, J.Vac.Sci. Technol,1978, 622.

38. J.P.Schunk, J.M.Friedt and Y.Llabador, Rev.Phys.Appl. 1975, 10, 121.

39. G.L.Zhang, W.-X.Hu and W.-N.Zhou, Yuan Tzu Heh Wu Li, 1980, 2, 59.

40. K.D.Duneva, S.K.Peneva, E.A.Tsukeva and I.Batov, Thin Solid Films, 1980, 67, 371.

41. J.W.Petersen, J.U.Andersen, S.Damgaard, F.Q.Lu, I.Stensgaard, J.Y.Tang,G.Weyer and Z.H.Zhang, Hyperfine Interactions, 1981, 10, 989.

42. S.Damgaard, H.Andreasen, V.I.Nevolin, J.W.Petersen and G.Weyer, Nucl. Phys. Meths.Mat.Res., 1980, 432

43. A.Kato, K.Endo and H.Sano, Bunseki Kagaku, 1980, 29, 708.

44. I.J.R.Baumvol, G.Longworth, L.W.Becker and R.E.J.Watkins, Hyperfine Interactions, 1981, 10, 1123.

45. W.J.J.Spijkervet, F.Pleiter and H.De Waard, Hyperfine Interactions, 1980, 8 173.

46. A.K.Konovalov and V.S.Shashkin, Fiz.Khim.Stekia, 1981, 7, 249.

47. J.Fenger, Nucl.Instr.Methods, 1973, 106, 203.

48. J.J.Spijkermann, "Mössbauer Effect Methodology", Plenum Press, N.Y., 1971, 8, 85.

49. M.Takafuchi, Y.Isozumi and R.Katano, Bull.Inst.Chem. Res.,Kyoto Univ., 1973, 51, 13.

50. Y.Isozumi, D.I.Lee and I.Kadar, Nucl.Instr.Methods, 1974,120, 23.

51. D.Salomon, P.J.West and G.Weyer, Hyperfine Interact. 1977, 5, 61.

52. W.Jones, J.M.Thomas, R.K.Thorpe and M.J.Tricker, Appl. Surf. Sci., 1978, 1, 388.

53. O.Massenet, J.Phys.Colloq., 1979, C1, 26.

54. M.Carbucicchio, Nucl. Inst. Methods, 1977, 144, 225.

55. M.Inaba, H.Nakagawa and Y.Ujihira, Nucl. Inst. Methods, 1981, 180, 131.

56. Y.Isozumi, M.Kurakado and R.Katano, Rev. Sci. Instrum., 1981, 52, 413.

57. J.A.Sawicki, ref. 164 in Chemical Society SPR Vol.15.

58. W.B.Hampshire and C.J.Evans, Tin Its Uses, 1978, 118, 3.

59. M.J.Fuller, Tin Its Uses, 1975, 103, 3.

60. P.A.Cusack and P.J.Smith, Private Communication.

61. P.A.Cusack, P.J.Smith, J.S.Brooks and R.Smith, J.Text. Inst., 1979, 70, 308.

62. A.F.Le C.Holding, Private Communication.

63. J.D.Donaldson, D.R.Laughlin and D.C.Puxley, J.C.S.Dalton, 1977, 865.

64. J.D.Cotton, P.J.Davidson, M.F.Lappert, J.D.Donaldson and J.Silver, J.C.S.Dalton, 1976, 2286.

65. P.G.Harrison, B.J.Haylett and T.J.King, J.C.S.Chem. Comm., 1978, 112.

66. J.L.Lefferts, M.B.Hossain, K.C.Molloy, D.Van der Helm and J.J.Zuckerman, Angew.Chem.Int. Ed.Engl. 1980, 19, 309.

67. R.C.Elder, M.J.Heeg and E.Deutsch, Inorg. Chem., 1978, 17, 427.

68. J.D.Donaldson, D.G.Nicholson, D.C.Puxley and R.A.Howie, J.C.S.Dalton, 1973, 1810.

69. J.E.Cassidy, W.Moser, J.D.Donaldson, A.Jelen and D.G.Nicholson, J.Chem.Soc.(A)., 1970, 173.

70. "International Tables for X-ray Crystallography", Birmingham, Kynoch Press, 1962.

Chapter 5

Conclusion

CHAPTER 5

Conclusion

The work described in this thesis involved a study of the fate of tin moieties in a variety of chemical reactions in both solution and solid state systems. The techniques used to identify the fate of tin in such reactions include electrical, optical and thermal measurements, X-ray crystallography and ^{119}Sn conversion electron and transmission Mössbauer spectroscopy. The results are reported in Chapters 2, 3 and 4 that deal respectively with reactions of tin species in solution, solid state reactions involving tin, and the use of the ^{119}Sn Mössbauer effect to study bulk and surface properties of tin-containing materials.

As each of the three chapters contains separate conclusions in which the major results of the subsections within the chapter are described, discussion in this summary is confined to a general conclusion of this work followed by a critical assessment of the theoretical descriptions of bonding in tin(II) chemistry.

5.1 General Conclusions

The conclusions of this work are summarized under the following headings, *viz*. Preparative work, Thermal Analysis, ^{119}Sn Mössbauer spectroscopy, Optical and Electrical Measurements and X-ray Crystal Structure Determination.

5.1.1 Preparative Work

The compounds prepared in the course of the present work include:

(i) Formation of a normal tin(II) compound $ClSn(C_4H_7N_2O_3)$, as well as the adduct $SnCl_2.2(C_4H_8N_2O_3)$ from the $SnCl_2$:

glycylglycine system.

(ii) Formation of adducts of the type $SnCl_2.L.\ CH_3OH$ (L = adenosine, cytidine and inosine) and $SnCl_2.L_2CH_3OH$ (L = adenine and cytosine) from the system $SnCl_2$; purine and pyrimidine bases and nucleosides.

(iii) Formation of halostannate(II) species in products such as $CsSn_3BrF_6$, $CsSn_2BrF_4$, $CsSnBrF_2.CsBr$ and $CsSnBrF_2$ from both the aqueous and molten SnF_2; CsBr system.

(iv) Formation of fluorostannates(II) and chloro-stannates(II) of $In(SnF_3)_3$; $In(Sn_2F_5)_3$ and $In(SnCl_3)_3$; $In(Sn_2Cl_5)_3$ from the SnF_2 : InF_3 and $SnCl_2$: $InCl_3$ systems respectively.

(v) Formation of tin(II) complexes containing nitrogen, oxygen and sulphur donor atoms in which there is more than one ligand per tin atom.

(vi) Formation of the mixed anion compounds $K_3Sn_2(SO_4)_3Cl$ and $K_3Sn_2(SO_4)_3Br$ from the K : Sn : SO_4 : X system (where X = Cl, Br).

(vii) Formation of $Pd_2I_2(SnCl_3)_4$ and $Pd_2I_2(SnI_3)_4$ in which tin(II) has used its lone pair electrons in bonding to give a formally tin(IV) species from the Pd : Sn : Cl : I system.

(viii) Formation of compounds with both low and high symmetry tin(II) sites in the $CsSnBr_3$: $CsPbBr_3$ and $CsSnBr_3$; $CsSnCl_3$ systems.

(ix) Formation of caesium tin bromide phases containing both tin(II) and tin(IV) in the lattice.

(x) Formation of mixed halide : sulphide phases of the type $Sn_7Br_{10}S_2$, $Sn_6CdBr_{12}S$ and Sn_4PbBr_8S for example from

molten $SnBr_2$: M(II)S systems.

(xi) Formation of tin(IV) complexes of type R_2SnCl_2. glycylglycine (R = Me, Bu, Oct, Ph) and $RSnCl_3$. glycylglycine (R = Bu, Oct, Ph) from a reaction of organotin(IV) halides and glycylglycine.

The products obtained from the systems studied give some indication of the fate of the tin moiety during chemical reaction, for example, in the formation of adducts and halostannate(II) ions, in the use of the lone pair to form palladium : tin bonds and in the formation of high symmetry compounds with optical colouration. However, more detail on the exact nature of the fate of the tin moiety on reaction is to be found in the following sections that describe the general conclusions obtained from various physical measurements.

5.1.2 Thermal Analysis

The purpose of using thermal analysis as a method for studying the fate of tin in chemical reactions is threefold, to identify and characterise new compounds, to study the fate of tin during thermal reaction and to construct a phase diagram of some solid state systems. These three uses are discussed separately.

Thermal analysis of a series of products obtained from reaction of tin compounds with glycylglycine provided a means of comparison of materials formed under differing reaction conditions. For example, the thermal decomposition of $SnCl_2 . 2(C_4H_8N_2O_3)$ which showed the loss of NH_3 at an early stage, was consistent with the existence of weak Sn-N interactions in the complex. The first decomposition stage of

$ClSn(C_4H_7N_2O_3)$, however, accounted for the decomposition of the glycylglycine in such a way that some of the carboxylate oxygens remained bonded to the tin. Another example stems from the work on organotin(IV) adducts of glycylglycine in which the aim was to identify and assign the stages involved in the decomposition processes of two different types of glycylglycine complex viz. monoorganotin(IV) derivatives and diorganotin(IV) derivatives. The diorganotin derivatives decomposed thermally by one of the following two processes: (1) in which the decomposition of the complex was similar to that of a mixture of the organotin compound and the ligand, and (2) in which the decomposition of the complex differed from that of the mixture. The pyrolysis of the monoorganotin derivatives was more complicated. The final tin containing product of the thermal decomposition of a series of organotin sugar derivatives was shown to depend upon the nature of the sugar. The aldoses, in general, gave tin(II) oxide as a product, whilst, in general the ketoses did not reduce the tin(IV) to tin(II) but gave tin(IV) oxide as a product.

Since tin(II) molecules should be essentially mono-functional acceptors a thermal study was carried out to obtain information on the bonding of the second ligand to tin(II) in materials of type $SnX_2.2L$. Examples of tin(II) chloride species containing molecules of water, pyridine, DMSO and piperidine provided sufficient information to detect a difference in the mode of bonding between tin and the two ligands of type L in $SnCl_2.2L$. The loss of one ligand molecule at low temperature strongly suggested that this ligand made no contribution to the bonding to tin, but

was present for lattice packing purposes only. The thermal decomposition of the thiourea tin(II) complexes involved one of three possible mechanisms, viz. (1) in which the tin-ligand bond is weak and the material decomposes by loss of a second ligand and subsequent decomposition of normal tin(II) compounds, eg. the tin carboxylate and bromide derivatives of thiourea, (2) in which the Sn-L bond is relatively strong and the ligand reacts with the tin moiety to give a new tin(II) species, eg. the formation of SnS in the decomposition of $SnCl_2$.tu and $Sn_2Cl_4$5tu.$2H_2O$), and finally, (3) in which the Sn-L bond is relatively strong and there is reaction between the tin(II) moiety and the ligand to give a tin(IV) species, eg. formation of SnS_2 in the pyrolysis of tin sulphate derivatives of thiourea.

Finally, in most of the solid state reaction studies, thermal analysis was used as a method of constructing phase diagrams with a view to isolating new phases from molten solution. The systems studied in this way included:-

(1) Tin(II) bromide : Metal (II) sulphide

(2) Tin(II) fluoride : Caesium bromide

(3) Mixed tin(II) : tin(IV) system ($CsSnBr_3$: Cs_2SnBr_6)

Thermal analysis was used to obtain information on the fate of tin moieties in chemical reaction by providing evidence for the formation of new compounds, the nature of thermal decomposition of tin containing materials and the strength of tin-ligand bonds. Additional confirmatory evidence for the information suggested from thermal studies is contained in the following subsections.

5.1.3 ^{119}Sn Mössbauer Spectroscopy

The conclusions arising from ^{119}Sn Mössbauer studies are discussed under three headings: transmission data, the relationship between Mössbauer parameters and tin to ligand bond lengths, and conversion electron data. Transmission Mössbauer data were recorded to identify changes in the use of tin bonding electrons in chemical reactions. In the case of complex formation in tin(II) species there is generally a lowering of the chemical isomer shift from the value for the parent tin(II) compound, because of the formation of covalent tin-ligand bonds. The difference in the shift between the parent compound and the complex generally provides some indication of the strength of the tin-ligand bond. In the case of complex formation in tin(IV) species there is also a decrease in the chemical isomer shift in comparison with that of the parent compound, but in this case, the increase represents a movement to a more electrostatic compound because of an increase in coordination number to six. Mössbauer spectroscopy also provides a very rapid and effective means of confirming that an oxidation- reduction reaction has taken place, for example, in the formation of tin(II) oxide from the aldose phases and in the formation of stannic sulphide during the pyrolysis of tin(II) sulphate thiourea complexes. The very narrow resonance lines obtained for the compounds in which tin(II) is in a high symmetry site, generally have a much lower chemical isomer shift than would be expected, because of the loss of non-bonding tin s-electrons to the solid state band structure.

Mössbauer spectroscopy was also used to determine the extent of competition between ligands for the use of tin bonding electrons and between tin and other metal ions for the use of ligand bonding electrons. For example, Mössbauer parameters show (1) that the products from the tin(II) fluoride : caesium bromide system have tin more strongly bonded to fluorine than to bromine, and (2) that indium(III) competes with tin(II) to form strong metal-fluorine and metal-chlorine bonds in the In : Sn : X systems.

Comparisons between Mössbauer data obtained at 80K and room temperature crystallographic data have been made, in the past, without reference to possible changes arising from the differences in the temperatures at which the data were obtained. It has now been shown in the present work, that there is a valid relationship between room temperature Mössbauer data and crystallographic tin-ligand bond lengths for simple tin(II) compounds. For more complicated systems a relationship still exists between the Mössbauer data and the bond distances between tin and its nearest neighbours, but, it is clear that in these more complicated systems the relationship is only apparent when the crystal structure is known, and that structural predictions based on Mössbauer parameters alone could lead to wrong assumptions being made.

Conversion electron Mössbauer spectroscopy provides a means of studying the reactions of tin species at surfaces. Comparison of the results with transmission data enables differences between surface and bulk reactions of tin moieties to be identified. Results have been presented in this thesis to show the fate of tin in surface reactions, in

the following systems:-

(i) Normal tin compounds

(ii) Glasses, ceramics and fabrics

(iii) Tinplate and soldered MONEL.

5.1.4 Optical and Electrical Measurements

Tin(II) compounds should under normal circumstances, be insulators and show only atomic absorption and luminescence effects in the uv region. In compounds where the distorting effects of the lone pair can be diminished by the population of delocalised solid state bands, band to band optical absorption and luminescence effects in the visible region are found.

Both luminescence and reflectance measurements have been made on some of the cooled melts from the $SnBr_2$: M(II)S systems, whilst only reflectance measurements were made for the cooled melts from the SnF_2 : CsBr system. The results from the systems $SnBr_2$: M(II)S ; SnF_2 : CsBr and $CsSn(II)Br_3$: $Cs_2Sn(IV)Br_6$ are consistent with band to band transitions.

As part of this work a comparison was also made of data obtained by photoacoustic spectroscopy with data previously obtained by optical absorption measurements. The photoacoustic spectra of a number of tin(II) and tin(IV) containing materials were recorded. A direct comparison has been made between the positions of the edges in the photoacoustic spectra of both the mixed metal ($CsSnBr_3$: $CsPbBr_3$) and mixed halide ($CsSnBr_3$: $CsSnCl_3$) systems and their relevant optical spectra, and good agreement was found. The spectral data are consistent with band to band transitions and these differed from

the spectra obtained as a result of atomic transitions of the transition metal ions in the stannates(IV) and hydroxostannates(IV).

Optical electronic spectra were also used to study the reactions in the palladium : tin : mixed halide system.

Presence of electrons in solid state bands in high symmetry tin(II) compounds should lead to electrical conductivity and for this reason measurements of electrical conductivity were made on compounds prepared in this work that had high optical colouration. A general relationship was found between the position of the optical edge, Mössbauer data and electrical conductivity in compounds of this type. There are some cases, eg. $Sn_7Br_{10}S_2$ and related compounds where their conductivity, optical colouration and Mössbauer data cannot be explained in terms of direct population of the solid state bands, but must be associated with impurity levels in the lattice.

5.1.5 X-ray Crystal Structure Determination

The crystal structures were determined for five materials, $K_3Sn_2(SO_4)_3Cl$, $K_3Sn_2(SO_4)_3Br$, $Sn_7Br_{10}S_2$, $Sn(acetate)_2.2tu$ and $Sn_2Br_4.5tu.\ 2H_2O$. The crystal structure determinations were carried out because the preparative and Mössbauer data did not give a clear indication of the nature of the bonding of the tin in their lattices. The structures were therefore determined to provide information on the fate of the tin moiety in the chemical reactions leading to their crystallization. In all five cases, it is unlikely that the nature of the final tin species could have been predicted without knowledge of the crystal structures.

The two complexes $K_3Sn_2(SO_4)_3Cl$ and $K_3Sn_2(SO_4)_3Br$ were found to be isostructural. Their structure is made up of a three dimensional network of tin atoms and bridging sulphate groups, with discrete potassium and halide ions sited within the holes of the tin-sulphate network. The allocation of positions in the two structures was unusual as the tin atoms did not occupy two sets of twofold special positions as expected, but instead occupied only four sixths of a sixfold general position, with the remaining two sixths being taken up by two sixths of the available potassium atoms. The remaining potassium and halogen atoms were found to be in special positions, as discrete ions. The tin-oxygen and tin-halide bond distances in the two structures are relatively long. The Sn-O bonds are in the range 2.44 - 2.93Å whilst the tin-halogen distances are in the region 2.97 - 3.41Å. The Mössbauer parameters for $K_3Sn_2(SO_4)_3Cl$ (δ = 3.76mms^{-1}) and $K_3Sn_2(SO_4)_3Br$ (δ = 3.86mms^{-1}) gave no indication as to whether tin was bonded to oxygen or halogen or both, but did suggest that a complex had been formed involving tin(II) and one or both of these ligands.

It had previously been reported[1] that $Sn_7Br_{10}S_2$ was isostructural with $Pb_7Br_{10}S_2$ and hence would be likely to have a structure closely related to that of Th_7S_{12}[2]. To test the validity of this assumption a full determination based on the atomic positions for Th_7S_{12} was carried out, but the high residual obtained from even the best fit of the data cast doubts on this assumption. The structure was therefore redetermined following a Patterson and Fourier synthesis. The crystal structure was shown to contain an

unusual set of disordered atomic positions. It was not surprising that the total of twelve anions in the hexagonal cell were well accommodated in two complete sets of six-fold positions, although it was found that random distribution of bromide and sulphide ions within the structure was confined to only one of the two sets of six-fold positions, whilst the second set of six positions was occupied by Br^- ions only. Three tin sites are found, two of which have environments typical of many tin(II) compounds; the third tin site, however, is most unusual, with an extremely short Sn-L bond of 2.19Å which is considered to be a Sn-S rather than Sn-Br bond. This distance together with six tin-ligand distances (3.04 - 3.52Å) gives an irregular coordination about the tin atom Sn(3).

Determination of the structures of the two thiourea tin(II) complexes, $Sn(acetate)_2.2tu$ and $Sn_2Br_4.5tu.2H_2O$, was carried out, and proved that discussion of their bonding on the basis of Mössbauer data alone was insufficient to predict correctly the fate of the tin in the formation of such complexes. In $Sn(acetate)_2.2tu$ the tin atom lies in a square pyramidal environment bonded to the two sulphur atoms of the thiourea moieties (Sn-S ≃ 2.85Å) and to two unidentate acetate groups via the oxygen atoms (Sn-O ≃ 2.18Å). The two tin sites in $Sn_2Br_4.5tu.2H_2O$ have trigonal pyramidal coordination, and are bridged by symmetry related sulphur atoms. Characteristic of these two tin sites are the unusually short Sn-Br bonds(≃2.65Å). The two structures show that the nature of the tin-thiourea complex is different in the two compounds and both structures differ from that found for the sulphato-

bis tin(II) thiourea complex which had previously been determined[3].

X-ray single crystal structure determination has been used in this work to show details of the tin(II) environments in compounds which contain tin in unusual bonding situations.

Since most of the work in this thesis has been concerned with tin(II), it became necessary to consider the theories that have been used to describe bonding in these compounds.

5.2 Theoretical Description of Bonding in Tin(II) Compounds

The discussion which now follows is a shortened version of a review carried out as part of this work, and full details on the theoretical description of non-bonding electron pairs applied to tin(II) are given in the microfiche at the end of this thesis.

A number of theoretical approaches have been used to explain the distorting effects of the non-bonding electrons as lone pairs, but, no single approach successfully describes all aspects of the bonding in these compounds. To date, all review articles on bonding have been concerned with a more general discussion of the group of related ns^2 elements and have not dealt solely with tin. Various aspects of the bonding in tin(II) compounds can be explained in terms of either covalent or electrostatic effects although the covalent approach that effectively defines a volume for the non-bonding electrons as a lone pair is more commonly adopted.

The covalent descriptions of tin(II) bonding are all based on the Nyholm and Gillespie concepts of orbital mixing and the valence shell electron pair repulsion theory. The

less common electrostatic approach depends upon the results of the crystal field effects on the ns^2 ion described by Orgel.

In 1957 Gillespie and Nyholm showed that the simple concept of electron-pair repulsion[4] could not only be justified in terms of quantum-mechanics but could also, when refined to take into account differences between the repulsions between lone-pair and bonding pairs of electrons, provide a satisfactory explanation of the stereochemistry of inorganic molecules. They found[5] that in almost every case electron-pair repulsion predicts the correct molecular shape of any molecule AX_n simply from the number of bonding and non-bonding electron pairs in the valency shell of the central atom indicating that in almost every case lone pairs appear to be stereochemically active. The main disadvantage of the VSEPR ideas is, however, that they are strictly applicable to molecular structure. To use these concepts in discussing solid state structures it is necessary to pick out the environment of an atom from the structure and to consider it as if it were a molecule. To a first approximation this provides a reasonable description of the immediate environment of tin(II) atoms in stannous compounds in that the common trigonal pyramidal and distorted four pyramidal sites could be regarded as being based on sp^3 and sp^3d hybridisation of the tin orbitals including a non-bonding lone pair. The theory however neglects possible intermolecular and solid state interactions and cannot explain effects such as the distortion normally found in the trigonal arrangement of bonds to tin even when all bonds are

to the same ligand or the fact that the X-Sn-X angles in trigonal SnX_3 coordinations are usually less than 90^o. Consideration of the crystal structures of even the compounds like $SnCl_2$ shows that solid state and intermolecular effects are important. In the solid state, $SnCl_2$ can no longer be described in terms of sp^2 hybridisation as in the vapour state, but instead the tin environment has to be described in terms of a distorted sp^3 hybrid involving a Cl atom from a neighbouring molecule. Electron pair repulsion ideas seem to provide a very convenient pictorial representation of the lone pair distorted environment of tin in its II+ oxidation state compounds but they fall far short of providing an adequate description of the details of the use of the tin valence electrons in bonding in the solid state.

Brown[6] has extended the Nyholm and Gillespie concept by describing the stereochemistry of oxygen and fluorine complexes of the atoms Sn(II), Sb(III), Te(IV), I(V) and Xe(VI) which show very irregular coordination in their crystalline compounds. He has suggested that this approach provides a method of understanding the stereochemistry of the main group atoms and of describing the long, as well as the short atom to ligand distances. The inclusion of long bonds in the arguments is important and has tended to have been overlooked by other authors. His model assumes that the coordination polyhedron of the main group ns^2 elements is based on an octahedron which has been distorted by the lengthening of some of the bonds in such a way that weak bonds occur opposite strong bonds and that bonds of intermediate strength occur opposite each other. The importance of this

model for the bonding in tin(II) compounds is that it recognizes the presence of strong, intermediate and weak interactions. The importance of long contacts between elements including Sn(II) and surrounding ligands has also been stressed by Alcock[7]. The Brown model however seems simply to provide a descriptive statement to explain the types of environment found in tin(II) chemistry. Given the crystal structure, the model defines the type of environment found, but in the absence of structural data it has no predictive powers. Moreover the model does not provide any insight into the reasons for the distortion of the octahedron in the first place.

Another extension of Gillespie and Nyholm's ideas was used by Galy et al[8] and by Andersson and Åström[9] basing their evidence for the stereochemical activity of the lone pair on a comparison of the volume of the anion in compact structures and in structures containing a lone pair (E). One of the problems associated with the Galy and Andersson model is that although they give the lone pair a spherical volume similar to that for O^{2-} and F^{-} they have to effectively reduce this volume by moving the central atom towards the lone pair in considering the known structures. The Galy et al model of non-bonding electron pairs is essentially geometrical in origin and result. It starts with the knowledge of distorted environments for tin(II) and similar atoms and allocates volume to the lone pair from the known amount of distortion. The consistency obtained in their calculations shows that the concept of the non-bonding electron pair having a volume is a good one, but in

emphasising this geometrical aspect of the chemistry, their model does not and cannot explain why the lone pairs should be stereochemically active in the first place other than involving the Nyholm and Gillespie concept.

The less common electrostatic approach is used by Orgel in considering the distortion of the environment of ns^2 species such as tin(II)[10]. He showed that a careful study of crystal field effects on the occupation of the available energy levels of the stannous ion also leads to the prediction of a distorted environment for the ion. The theory put forward by Orgel predicts fluorides and oxides as the most distorted of tin(II) structures, which is consistent with the known structural data of tin(II) compounds. The anomalously low Mössbauer chemical shift value for fluorides can be accounted for by the loss of s-electrons by electrostatic crystal field s-p mixing in addition to loss by covalent s-p mixing. The short bonds in the fluorides must however involve some covalency, as the average bond length is closest to the sum of the covalent radii, Orgel, in his argument does not take account of this.

It is interesting that Hall[11,12] has also pointed out the ns-np separations play an important role in determining bond angles in main group compounds. He claims that this has been neglected in VSEPR and that it is not always obvious in M.O. treatments. He uses extended Huckel arguments to suggest that the stereochemical activity of a lone pair arises from the desire of the system to lower its total energy through maximum population of the lower energy valence s-orbital. The results of these calculations are however

only strictly applicable to the vapour phase molecules formed by relatively light atoms.

One of the problems associated with the description of bonding in tin(II) compounds is the difficulty of including in any model those derivatives that have tin(II) in undistorted regular octahedral sites and have unusual solid state properties. The covalent models have to assume that the non-bonding electrons are in stereochemically inactive orbitals, that is that they behave essentially as a $5s^2$ pair in these compounds. An alternative suggestion[13] that can be applied to the bonding in octahedrally coordinated tin(II) halide moieties is that, since the ns orbital (a_1g) of the central atom plays little part in the bonding, the extra pair of electrons can be accommodated in the a_1g antibonding molecular orbital, without distorting the Oh symmetry. None of the models based on covalency can, however, explain why non-bonding orbitals can be stereochemically active in one site and inactive in a similar site in another compound. More importantly none of these approaches account for the unusual optical and electrical solid state properties associated with high symmetry tin(II) environments. The electrostatic arguments of Orgel, on the other hand, do predict that distortion will be greatest for tin(II) bonding to light atoms and least for tin(II) bonding to heavy atoms. This is consistent with the observation that regular octahedral structures are never found with oxide and fluorides and that the few examples of regular octahedral tin(II) sites known are found in heavy halide or chalcogenide lattices. Orgel's approach, however suffers from the same disadvantage

as the covalent approach, in so far as localisation of the description to crystal field effects on the tin atom alone means that the model cannot explain any three-dimensional solid-state effects.

It seems that all of the models described above (covalent and electrostatic) suffer from the same draw back in that they concentrate on the tin atoms and fail to take account of the energies and bonding characteristics of the ligand orbitals as well as the tin(II) orbitals. The aim of the present chapter is to provide an explanation for the differences observed in the stereochemical activity of the lone pairs in tin(II) compounds, by considering the energy levels of the bonding orbitals of both tin and its ligands. Consideration of the overall symmetry of the lattice then enables one to extend the arguments used to account for the solid state effects in some high symmetry tin(II) compounds. The approach described in this section is an extension of the method used by Donaldson and Tricker[14] to provide a preliminary explanation of the bonding in SnX_3^- species with a C_{3v} symmetry. If these compounds contained perfectly spherical Sn^{2+} ions their structures would be based on the postulates of close packing of large anions with metal ions occupying suitable high symmetry interstices with little or no distortion of the anion lattice. Many of the $MSnX_3$ compounds, however, in common with the majority of tin(II) compounds, have distorted tin(II) environments because of the presence of a stereochemically active lone-pair of electrons on Sn(II).. One of the simplest distortions to envisage is a trigonal distortion of an octahedral ligand

environment around the central tin(II) ion brought about by the presence of a lone pair of electrons directed along a three-fold axis thus, in effect, preventing the close approach of three ligands. In practice it is found that electronegative ligands such as fluorine give rise to the more distorted tin environments whilst less electronegative ligands such as iodine give rise to more regular environments. The electronic implication is that the lone-pair in $MSnX_3$ fluorides is highly directional and hence stereochemically active and contains high tin 5p character but the lone-pair in, for example, the iodides, contain high tin 5s character and therfore has less directional character. For the formation of a strong bond in the LCAO approximation the atomic orbitals involved should, a) be of the correct symmetry, and b) be of similar energy. In fact the strongest bond should be formed when energies of the component atomic orbitals are equal.

Figure 5.1 shows how these general structural observations together with the trends in the Sn-119 Mössbauer parameters of $MSnX_3$ compounds may be rationalized by the simple concept of orbital energy matching arising from criteria (b) above. It is expected that in order to form a strong a_1 bond, tin 5s and $5p_z$ orbitals will premix such that the energy of the hybrid orbital so formed will match that of the halogen np orbital. The binding energies of the tin 5s and 5p and halogen np orbitals show that in order to obtain a good energy match with the appropriate halogen group orbital the tin a_1 bonding orbital should contain high 5s character when bound to fluorine but high $5p_z$ character

Relative Binding Energies of valence shell p-orbitals of halogens and chalcogens and of the 5s and 5p orbitalsof Sn

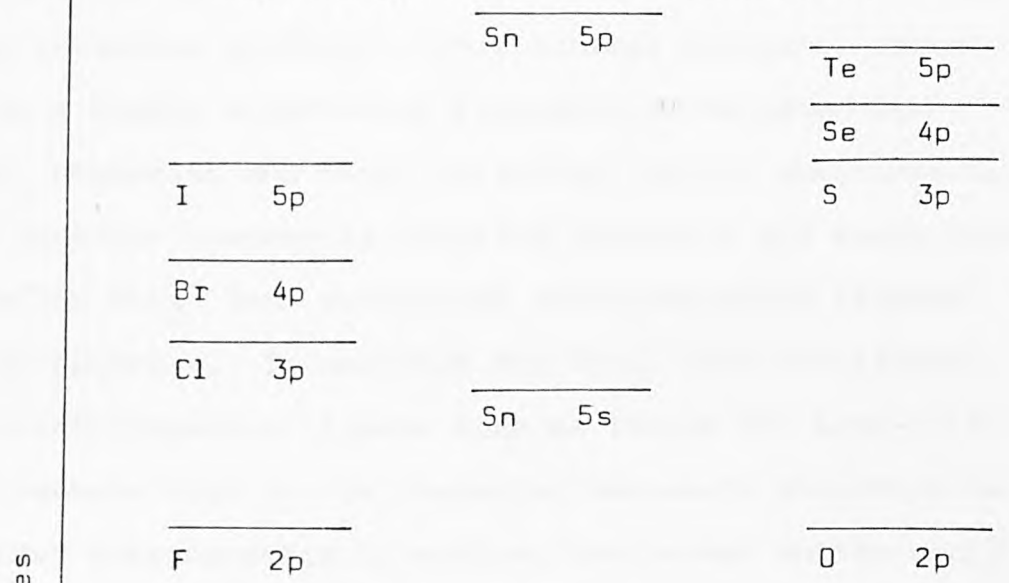

Figure 5.1

Formation of Bands before premixing Chalcogen and Halogen(np) and Tin(5s,5p) Orbitals

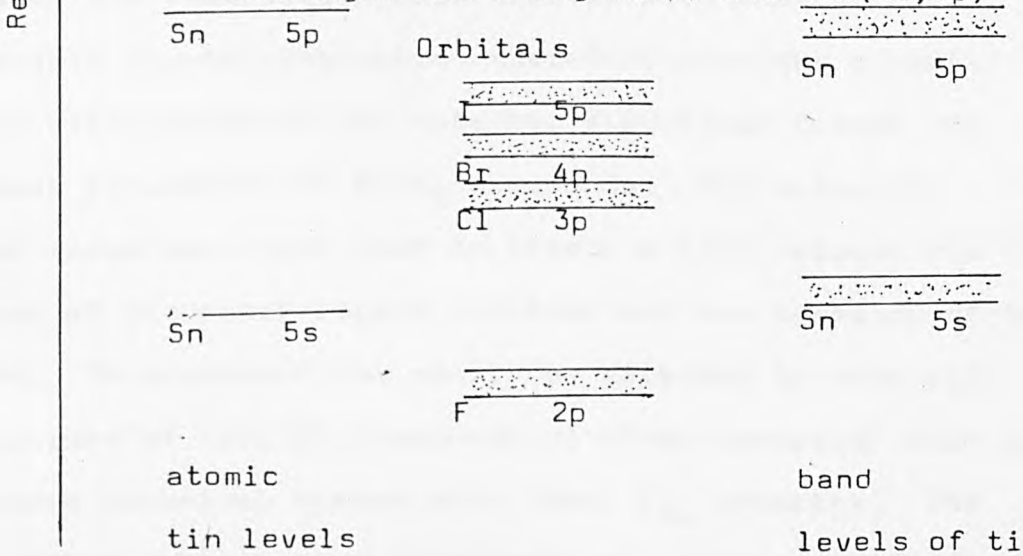

Figure 5.2

when bound to iodine. The non-bonding orbital(because of orthogonality requirements) thus contains high tin $5p_z$ and low 5s character in SnF_3^-. This orbital occupancy would lead to a highly directional lone-pair containing high tin $5p_z$ character and hence distorted tin(II) environments, large negative quadrupole coupling constants and small isomer shifts for SnX_3^- ions containing electronegative ligands such as fluorine. In contrast for SnX_3^- ions containing less electronegative ligands such as iodine the lone-pair would contain high tin 5s character and would therefore be much less stereochemically active, the isomer shifts would be large and the quadrupole coupling constants small. These predictions concur with the general observations on the structure of tin(II) derivatives and the observed trends in the experimental Mössbauer data.

This simple molecular orbital picture which postulates that the tin 5s, $5p_z$ mixing varies in order to equalise the energy of the resulting hybrid orbital with that of the appropriate ligand combination therefore provides a qualitative explanation of the observed structural trends and Mössbauer parameters of $MSnX_3$ compounds. The molecular orbital terms have been used to create a link between the energies of the metal-ligand orbitals and the symmetry of the lattice. This concept can easily be extended to cope with descriptions of tin(II) compounds of other symmetry, such as the square pyramidal system with ideal C_{4v} symmetry. The group ligand orbitals can form bonds of symmetry a_1, b_1 and e with the tin atomic orbitals s, px, py and dx^2-y^2. This will leave a non bonding orbital of symmetry a_1 (p_z) for the

extra electron pair on the tin. Again, to form a strong a_1 bond, 5s and $5p_z$ orbitals on the tin will premix such that the energy of the hybrid orbital so formed will match the halogen np orbitals leading to the same conclusions as those obtained for C_{3v} symmetry.

Lowering the symmetry from C_{3v} to C_s or C_1 affects the molecular orbital description of the bonds formed making it difficult to assign definite tin orbital character to the bonds. In C_s symmetry, for example, the orbitals available for bonding and non bonding electrons are three of symmetry a′ and one of symmetry a′′. In this case the lone pair cannot lie in the z-direction of the point group. The tin 5s orbitals will mix with both px and py to give two strong a′ bonds and one a′ non bonding orbital with s, px and py. character. In C_1 symmetry all orbitals must transform as a so that the premixing to form a strong a bond will involve different amounts of s, px, py and pz character leaving the non bonding pairs with the residual s, px, py and pz character. Similar arguments apply to the reduction in C_{4v} symmetry. The complications in the molecular orbital description for the systems of lower symmetry do not however alter the requirement of orbital mixing to maximise the energy match. The overall conclusion must therefore still be that tin will tend to use more s-electron density in bonding orbitals to fluorine than in bonding to iodine. In the same way, comments, such as these, can be made about tin(II) bonds to oxygen, sulphur, selenium and tellurium based on the orbital energy diagram shown in Figure 5.1. Although the relative atomic binding energies used in the figure cannot

be taken as the exact values in a bonding situation the trends with the halogen and chalcogen group will remain the same. To extend the arguments further, assessments have to made of the likely differences between for example an oxygen bonding orbital in the formation of a bond between tin and an oxygen atom and tin to an acetato oxygen atom. Tin in a mixed ligand environment will give rise to different orbital matching parameters due to the different energies of the different ligands.

Whatever the symmetry of the final tin(II) environment however, the concept of orbital energy matching will produce similar trends to those found for $MSnX_3$. Moreover, by considering terminal and bridging chlorine atoms as having slightly different binding energies in the bonding situation and therefore requiring slightly different use of the tin bonding orbitals, the model describes simple solid state effects such as the formation of chlorine bridges in $SnCl_2$ to give a trigonal pyramidal tin(II) coordination.

One of the strengths of the orbital matching model is the ease with which it can be extended to describe the bonding and the properties of the tin(II) compounds with high symmetry structures.

The increase in the tin 5s character of the non-bonding pair in going from fluorides to iodides is paralleled by a decrease in distortion. As the distortion decreases it becomes possible to remove the distorting effects of the non-bonding electron pair by solid-state effects as well as by direct alteration in the p-character of the electrons in the orbital. The removal of distortion by solid state

effects can be explained in terms of direct population of empty delocalised bands by the non-bonding electrons. Extension of the molecular orbital theory to account for such effects in the solid state would involve the merging of the atomic energy levels of the tin 5s and 5p, and the halogen and chalcogen np orbitals to form bands before premixing: Figure 5.2. In this way the tin which has a large amount of s-electron density in high symmetry environments, will readily accommodate some of this density in the bands. Effects such as these will lead to a similar conclusion to that obtained in the orbital matching concept defined for tin(II) in low symmetry environments. This phenomenon is best illustrated by discussion of the undistorted perovskite $CsSnBr_3$ which is a black solid with a metallic lustre, which acts as a pseudo-metallic conductor over a wide temperature range and which shows interesting photoluminescent effects.

Calculation of the size of the $5s^2$ orbital on the tin atom has led to the conclusion that there will be an overlap between the $5s^2$ orbital and the empty bromine 4d- orbitals, thus making it possible for the distortive effects of the non-bonding orbital to be reduced by the direct population of the solid state band with the non-bonding tin electrons.

The concept of direct population of solid state bands can explain all of the apparently anomalous properties of $CsSnBr_3$ *viz.* its undistorted perovskite lattice, its ^{119}Sn Mössbauer data (δ = 3.97mms^{-1} Δ ca 0mms^{-1}), its electrical conductivity (9.00 x 10^{-4} $\Omega^{-1}cm^{-1}$), its colour and optical absorption and emission spectra.

The undistorted perovskite structure must arise because

the mutual overlaps of the Br 4d orbitals would be at a maximum in such a structure and this in turn would permit maximum transfer of electron density from the potentially distorting non-bonding tin orbital.

A band model has been proposed[15] which explains the observed electrical and optical properties of $CsSnBr_3$ as well as its Mössbauer data (see p. 170 Chapter 3), this model shows the Sn 5s orbitals form a narrow band which overlaps with an empty band formed by the Br 4d orbitals in the forbidden energy region, allowing direct population of the empty band by the Sn 5s electrons.

The high symmetry solid state environment for tin in its lower oxidation state is only found for those compounds in which the distorting effect of the lone pair orbitals can be reduced by causing the electrons to populate a low energy delocalised band in the structure. Regular octahedral Sn(II) environments are found in SnSe[16], SnTe[16] and SnI_2[16] as well as in $CsSnBr_3$, $CsSnBr_{3-x}Cl_x$, $CsSn_{1-x}Pb_xBr_3$ and related halides. This model can be extended to explain colour in tetragonal SnO and other materials which have relatively short metal-metal contacts because, in these cases, the ns^2 element is not only supplying the donor electrons but also forming the band by mutual overlap of its empty d-orbitals.

5.3 Summary

The fate of tin moieties in chemical reactions has been studied in this work by a number of techniques. Most of the examples reported have been concerned with tin in its (II) + oxidation state. Various types of lone pair distorted tin environments and high symmetry tin(II) sites are found in

the wide range of products from the reactions studied.

The concept of orbital energy matching between tin(II) bonding orbitals and the bonding orbitals of ligands is shown to explain the amount of distortion to be expected for any tin(II) ligand environment in the solid state. The model has the advantage of retaining the best features of previous models in that 1) it explains why tin(II) sites in oxide and fluoride lattices are more distorted than in the heavier chalcogenide and halide lattices 2) it results in the concept of directional lone-pair orbitals having volume which can prevent the close approach of ligands in the directions in which these lone pair orbitals point 3) by considering both tin(II) and ligand orbital energies it can explain differences between tin-terminal ligand and tin-bridging ligand bonds and this is capable of extension to cope with the presence of Sn-ligand bonds of different lengths 4) it can be extended to account for solid-state effects and in particular to a description of the bonding situations in compounds that have tin(II) in undistorted octahedral sites.

References

1. J.D.Donaldson, D.R.Laughlin and J.Silver, J.C.S.Dalton, 1977, 996.
2. W.H.Zachiariasen, Acta Cryst., 1949, 2, 288.
3. J.D.Donaldson, D.G.Nicholson, D.C.Puxley and R.A.Howie, J.C.S.Dalton, 1973, 1810.
4. R.J.Gillespie and R.S.Nyholm, Quart. Rev., 1957, 11, 339.
5. R.J.Gillespie, J.Chem.Education, 1970, 47, 18.
6. I.D.Brown, J.Solid State Chem., 1974, 11, 214.
7. N.W.Alcock, Adv. Inorg.Chem. Radiochem., 1972, 15, 1.
8. J.Galy, G.Meunier, S.Andersson and A.Åström, J.Solid State Chem., 1975, 13, 142.
9. S.Andersson and A.Åström, Solid State Chemistry Proceedings of the 5th Mat.Reseach Symposium, 1972, Pub.No. 364, p.3.
10. L.E.Orgel, J.Chem. Soc., 1959, 3815.
11. M.B.Hall, Inorg. Chem., 1978, 17, 2261.
12. M.B.Hall, J.Amer.Chem.Soc., 1978, 100, 6333.
13. D.G.Urch, J.Chem.Soc., 1964, 5775.
14. M.J.Tricker and J.D.Donaldson, Inorg. Chim.Acta Letters, 1978, 31, 445L.
15. S.J.Clark, C.D.Flint and J.D.Donaldson, J.Phys.Chem.Solids, 1981, 42, 133.
16. J.D.Donaldson, Progress in Inorganic Chemistry, 1967, 8, 287.